Intercalated Injection, Target Model Construction and H_2 Performance of Retrospective Cost Adaptive Control

by

Yousaf Rahman

A dissertation submitted in partial fulfillment
of the requirements for the degree of
Doctor of Philosophy
(Aerospace Engineering)
in The University of Michigan
2017

Doctoral Committee:

Professor Dennis S. Bernstein, Chair
Assistant Professor Kira L. Barton
Associate Professor Anouck R. Girard
Assistant Professor Dimitra Panagou
Mario A. Santillo, Ford Motor Company

Verily, with hardship comes relief – Quran 94:6

For Pakistan

ACKNOWLEDGEMENTS

I would like to begin by thanking my advisor, Professor Dennis S. Bernstein for all of his guidance, encouragement, and support during the past five and a half years. His persistence to finding solutions and attention to detail are some of the most important lessons I have learned in my time in Michigan. Also, I would like to thank my committee members Professor Kira Barton, Professor Anouck Girard, Professor Dimitra Panagou, and Mario Santillo for their helpful comments and suggestions, which greatly improved this work. I'd also like to thank Professor Ilya V. Kolmanovsky, who also contributed to this dissertation. I am grateful for all the hard work the professors at the University of Michigan helping me along the way in graduate school.

I'd also like to appreciate my friends and colleagues at the University of Michigan: Syed Fahad Naeem, Osama Khan, Burhan Sadiq, Arjang Talattof, Syed Yasir Ahmed, Mehdi Saligane, Akbar Ali, Farhan ul Haque, Erol D. Sumer, Khaled F. Aljanaideh, Sweewarman Balachandran, Asad A. Ali, Jin Yan, Ray Yu, Jiapeng Zhong, Frant Sobolic, Ahmad Ansari, Ankit Goel, Syed Aseem Islam. I'd like to hank Antai Xie for helping me with the intercalated injection and target model construction in Chapter 4 of this dissertation.

Finally, I would like to thank my family. To my parents Saif and Farzana, for their love, support, and excellent example. My wife Saadia for her love, patience while I worked long hours during her pregnancy, and my son Zakaria, whose presence has helped relieve much of the stress involved with research work. My sisters Aysha, Amina and Zainab, my nieces Khadija and Rania, and my nephews Isa, Abu Bakr, Adam, Saleh, Murtaza, Hussain, and Yahya. It was very difficult to spend six years away from you all and I am very grateful for the love that you all have given me.

TABLE OF CONTENTS

LIST OF FIGURES

Figure

LIST OF TABLES

Table

LIST OF APPENDICES

Appendix

ABSTRACT

Intercalated Injection, Target Model Construction and H_2 Performance of Retrospective Cost Adaptive Control

by

Yousaf Rahman

Chair: Dennis S. Bernstein

This dissertation extends retrospective cost adaptive control (RCAC) by developing a novel interpretation of RCAC, wherein the retrospective cost minimization uses intercalated injection between the controller numerator and denominator to fit a specific closed-loop transfer function to a target model. The target model thus incorporates the modeling information required by RCAC. To demonstrate the effect of the target model on closed-loop performance, RCAC is applied to a collection of problems that demonstrate adaptive pole placement, where the target model is used to place closed-loop poles; adaptive PID control, where RCAC adaptively tunes PID gains; and LQG cost minimization, where the optimality and closed-loop frequency response of RCAC is compared with the performance of discrete-time LQG controllers.

Next, RCAC is applied to plants that are difficult to control using fixed gain controllers, including an aircraft lateral dynamics model that has an unknown transition from minimum-phase to nonminimum-phase (NMP) dynamics, as well as plants with severely limited achievable gain and delay margin.

Methods are developed to control NMP plants without knowledge of the NMP zero. Specifically, a decentralized feedback-feedforward architecture as well as quasi-FIR controllers are considered, where the FIR controller operates in parallel with an internal model controller in order to follow commands for NMP plants without knowledge of the NMP zeros.

Next, the following question is considered: Are all full-order dynamic compensators observer-based? It is shown that the only case where a dynamic compensator is not observer-based is the case where n is odd and the closed-loop spectrum has no real eigenvalues. Since this is the case, such controllers are necessarily suboptimal in the sense of LQG. This question is relevant to understanding the closed-loop pole locations arising from full-order RCAC compensators.

Finally, retrospective cost model refinement (RCMR) is used to estimate parameters in a mass-spring-damper system and an aircraft lateral dynamics model. RCMR is compared to the extended Kalman filter (EKF) and the unscented Kalman filter (UKF), and the ability to estimate parameters without knowledge of the noise characteristics using RCMR is demonstrated. RCMR is then paired with a forward-propagating Riccati-based controller for indirect adaptive control of the aircraft lateral dynamics model considered earlier.

CHAPTER 1

Introduction

1.1 Motivation for Adaptive Control

The development and implementation of model-based feedback control systems requires an accurate model of the physical process being controlled, actuators capable of producing the required control effort, and reliable sensors that provide accurate measurements. The aircraft fly-by-wire system shown in Figure 1.1 is an example of a feedback control system, where navigation computers and other sensors provide measurements of position, airspeed, altitude, and angular velocity to a controller designed using a model of the aircraft dynamics. The controller requests the required control inputs from the engines and aerodynamic control surfaces based on the desired trajectory, which is provided by either the pilot or autopilot, as well as the disturbances affecting the vehicle. Control research is typically focused on applications for which accurate models, precise sensing, and effective actuators are available, and the goal is to use this technology reliably and efficiently in order to develop control algorithms to achieve stabilization, command following, and disturbance rejection objectives.

Despite the wide-scale use of model-based feedback control design, many applications remain beyond the reach of modern tools and techniques. These applications may be highly under-sensed and under-actuated relative to the order of their dynamics; they may be required to perform in hostile environments, where obtaining

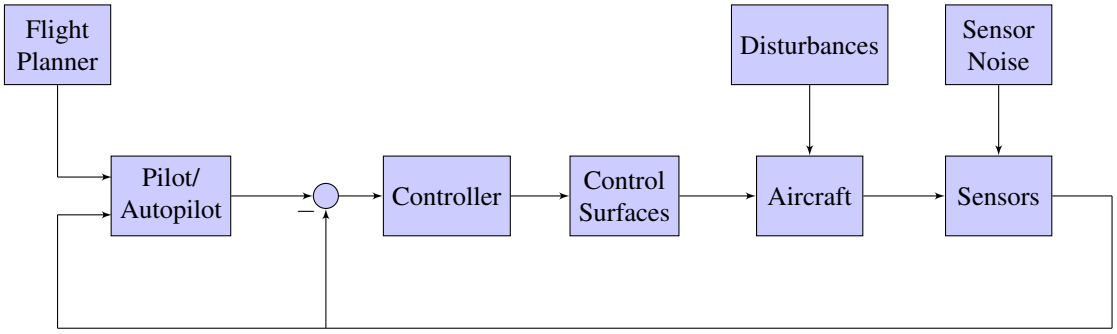

Figure 1.1: Aircraft fly-by-wire control architecture

accurate measurements is difficult or unpredictable disturbances may be present; and they may be subject to complex, unknown, or unpredictably changing physics. These applications may also require reliable high-performance control systems that must be engineered within restricted budgets, and tight deadlines that leave limited time for modeling, simulation, and verification.

These reasons motivate the desire to develop *adaptive* control algorithms that are able to learn about the physics underlying the plant, actuator constraints, sensor failures, and other obstacles to achieving a desired performance objective. We now consider two such examples, where designing a traditional fixed-gain feedback controller that is robust to uncertainties is difficult or even infeasible.

Example 1.1. Plants with limited achievable margins. Consider the unstable, minimum-phase, continuous-time plant from [1] given by

$$A = \begin{bmatrix} 1 & 1 \\ 0 & 1 \end{bmatrix}, \quad B = \begin{bmatrix} 0 \\ 1 \end{bmatrix}, \quad D_1 = \begin{bmatrix} 1 \\ 1 \end{bmatrix}, \tag{1.1}$$

$$C = E_1 = \begin{bmatrix} 1 & 1 \end{bmatrix}, \quad D_2 = 1. \tag{1.2}$$

It is shown in [1] that there are no guaranteed margins for this plant using an LQG controller. Although LQG controllers are optimal in the H_2 sense, they often yield

unstable controllers that result in feedback loops with low gain and phase margin, particularly in the high-authority case. This raises the question of whether there may exist an adaptive method that can yield near-optimal controllers, and also adapt to changes in the plant dynamics that may destabilize the system.

As another example, consider the unstable, minimum-phase, continuous-time plant given by [2]

$$A = \begin{bmatrix} -0.08 & -0.03 & 0.2 \\ 0.2 & -0.04 & -0.005 \\ -0.06 & 0.2 & -0.07 \end{bmatrix}, \quad B = D_1 = \begin{bmatrix} -0.1 \\ -0.2 \\ 0.1 \end{bmatrix}, \tag{1.3}$$

$$C = E_1 = \begin{bmatrix} 0 & -1 & 0 \end{bmatrix}, \quad D_2 = 0. \tag{1.4}$$

This plant has an unstable pole at 0.1081. It is shown in [2] that the maximum achievable delay margin for this plant is 18.51 sec. Such plants may be problematic for fixed-gain controllers. As shown in this dissertation, a controller designed to yield the achievable delay margin delivers poor transient response, and is also unable to stabilize the system in the presence of destabilizing delays. Adaptive control may provide a viable alternative to fixed-gain controllers for the difficult cases considered here. We consider both plants in this example in Chapter 5. ■

Example 1.2. Plant with unmodeled time-varying dynamics. Consider the

aircraft lateral dynamics model

$$A_0 = \begin{bmatrix} -0.0771 & 0.269 & -0.9631 & 0.0397 \\ -25.60 & 0.0218 & 0.0995 & 0 \\ 0.6160 & 0.0376 & -0.2687 & 0 \\ 0 & 1 & -0.4202 & 0.0058 \end{bmatrix}, \quad B_0 = \begin{bmatrix} -0.0002 \\ 2.519 \\ -0.0222 \\ 0 \end{bmatrix}, \tag{1.5}$$

$$A_1 = \begin{bmatrix} -0.0771 & 0.269 & -0.9631 & 0.0397 \\ -108.8 & 0.0218 & 0.0995 & 0 \\ 0.4107 & 0.0376 & -0.2687 & 0 \\ 0 & 1 & -0.4202 & 0.0058 \end{bmatrix}, \quad B_1 = \begin{bmatrix} -0.0002 \\ 2.519 \\ -0.0665 \\ 0 \end{bmatrix}, \tag{1.6}$$

where A_0 and B_0 represent the nominal plant dynamics and A_1 and B_1 represent the off-nominal dynamics. With the feedback $y = x_4$, the off-nominal dynamics have a NMP zero at 1.274. The change from nominal to off-nominal dynamics is witnessed by an effect similar to roll reversal, and represents a challenge for fixed-gain controllers. We consider this example in Chapters 3 and 8. ■

These examples show that fixed-gain control laws may suffer from extreme sensitivity to modeling information. Consequently, these examples motivate the need for adaptive control, where online adaptation can potentially account for changing dynamics.

Adaptive control techniques typically use one of the following two architectures, namely, *indirect adaptive control*, where parameter estimates are used to update a model-based controller online at each data assimilation step, or *direct adaptive control*, where the controller itself is adjusted based on a performance measure. In most cases, direct adaptive control is used to fit the closed-loop system to a *reference model*, that is, *model reference adaptive control* (MRAC). Another application is to use an adaptive controller in conjunction with a model-based controller in order to

prevent unpredictable perturbations or unmodeled dynamics from destabilizing the closed-loop system.

Adaptive control differs from robust control, which also accounts for uncertainty. In particular, robust control considers uncertainty as static and seeks to trade performance for robustness to the assumed level of uncertainty. In contrast, adaptive controllers attempt to learn about the plant during operation, in order to overcome prior uncertainty or unexpected changes in the dynamics. Consequently, by tuning itself to the actual plant, an adaptive controller may be able to avoid the performance/robustness tradeoff inherent to robust control at the possible expense of undesirable transient performance as the controller adapts to the uncertainty.

The underlying motivation for research in adaptive control is to develop algorithms that can accommodate sensor and actuator limitations, communication constraints, account for complex, uncertain, unmodeled, and time-varying dynamics, and also be robust to matched and unmatched disturbances, sensor noise, and sensor/actuator failure. The promise of adaptive control is the ability to account for all of these effects with minimal prior modeling, tuning, and analysis for applications that are beyond the applicability of fixed-gain and fixed-logic model-based control design.

Adaptive control algorithms for continuous-time plants are developed in [3–11] and for discrete-time plants in [12–23]. For discrete-time plants, the ability to handle plants with nonminimum-phase (NMP) zeros, that is, zeros outside of the open unit disk, is demonstrated in [13–16]. We now consider a plant with an unmodeled NMP zero, which may be a difficult case even for adaptive control techniques.

Example 1.3. Plant with unmodeled NMP sampling zero. Consider the asymptotically stable, continuous-time plant $T(s) = \Lambda(s)T_0(s)$, where

$$\Lambda(s) = \frac{229}{(s - 15 + 2\jmath)(s - 15 - 2\jmath)}, \quad T_0(s) = \frac{2}{s + 1}, \tag{1.7}$$

where $\Lambda(s)$ represents unmodeled high-frequency dynamics [24]. Since the relative degree of $T_0(s)$ is 1, the discrete-time sampled-data plant $G_0(\mathbf{z})$ obtained by discretizing $T_0(s)$ does not yield any sampling zeros [25]. However, since the relative degree of $T(s)$ is 3, the discrete-time sampled-data plant $G(\mathbf{z})$ obtained by discretizing $T(s)$ possesses two sampling zeros due to $\Lambda(s)$. It can be shown that, if the sampling period $h \lesssim 0.2$, then one of the sampling zeros is NMP. This plant may be particularly difficult to control, because the nature of the zeros depends on the sampling rate. Therefore it may be difficult to predict if the plant is minimum phase or NMP.■

This dissertation focuses on retrospective cost adaptive control (RCAC). RCAC is a discrete-time, direct adaptive control algorithm, that may be used for stabilization, command following and disturbance rejection applications.

RCAC was initally based on the concept of *retrospectively optimized control* [26], where past controller coefficients used to generate past control inputs are *re-optimized* in the sense that *if* the re-optimized coefficients had been used over a previous window of operation, then the performance would have been better. However, unlike signal processing applications such as estimation and identification, it is impossible to change past control inputs, and thus the re-optimized controller coefficients are used only to generate the next control input. Since RCAC depends heavily on data for the controller update, this technique is similar to data-driven control [27–32]. Some elements of RCAC appear in [16].

Although RCAC has been developed and applied to many systems [26, 33–58], much work remains to be done. Firstly, the role of the filter G_{f} and the modeling information required for RCAC is not well understood. Also, the H_2 optimality of the controllers produced by RCAC has not been investigated. Thus, the goals of this dissertation are

- *Determine the role of the filter G_{f} and use this understanding to present the minimal modeling information required by RCAC.*

- *Compare the optimality and closed-loop response of RCAC with discrete-time LQG control.*

- *Develop techniques for the application of RCAC in cases where the required modeling information is erroneous or unavailable.*

1.2 Development of RCAC

RCAC was originally developed within the context of active noise control experiments [26]. The algorithm used in [26] is gradient-based, where the gradient direction and step size are based on different cost functions. In subsequent work [36], the gradient algorithm was replaced by batch least-squares optimization. In both [26] and [36], the modeling information is given by Markov parameters (impulse response coefficients) of the open-loop transfer function G_{zu} from the control input u to the performance variable z.

More recently, in [37], a recursive least squares algorithm was used, along with knowledge of the NMP zeros of G_{zu}. The approaches in [26, 36] and [37] are closely related in the sense that all of the NMP zeros outside of the spectral radius of G_{zu} are approximate zeros of a polynomial whose coefficients are Markov parameters of G_{zu}. RCAC uses a filter G_{f} to define the retrospective cost by filtering the difference between the actual past control inputs and the re-optimized control inputs. To construct G_{f}, Markov parameters are used in [26, 36], and NMP zeros are used in [37].

The theoretical development of RCAC includes gradient optimization with Markov parameters [26], batch optimization with Markov parameters for NMP plants [36], and RLS optimization using the NMP zeros in G_{f} [37]. RCAC was applied to the Rohrs

counterexamples in [38] and demonstrated for broadband disturbance rejection in [39]. Application of RCAC to Hammerstein plants with monotonic input nonlinearities is considered in [40]. Extensions to MIMO systems was considered in [41], where it is shown that RCAC squares non-square plants, which may introduce NMP squaring zeros.

RCAC has been implemented in both simulation and laboratory experiments. Numerical simulation studies are given in [42, 43] for flow control; in [44] for noncolocated control of a linkage; in [39, 45–47] for vibration control; in [48] for engine control; in [49–53] for aircraft control; in [54] for spacecraft control; in [55] for quadrotor control; in [56] for missile control; in [57] for scramjet control; and in [58] for control of systems with hysteresis. Laboratory experiments are reported in [26, 33, 34] for noise control; in [35] for ducted flame control; and in [59] for 6DOF motion control.

In addition to adaptive control, the retrospective cost optimization used by RCAC may also be used for model refinement. We call this application retrospective cost model refinement (RCMR) [60–65]. RCMR can be used to estimate the dynamics of a possibly dynamic subsystem in feedback interconnection with a main subsystem; the unknown subsystem is assumed to be inaccessible in the sense that its inputs and outputs are not measured. A special case of an inaccessible subsystem occurs when the unknown subsystem is static; in this case, inaccessible subsystem identification is equivalent to parameter estimation. We compare RCMR to other parameter estimation techniques in Chapter 8, and use RCMR for indirect adaptive control of the aircraft lateral dynamics model from Example 1.2.

1.3 Contributions

The major contributions of this dissertation are listed below.

- We apply RCAC on systems with unknown transitions to NMP dynamics, and using system identification techniques, we show that RCAC can adapt to a transition from minimum phase to NMP dynamics.

- We demonstrate the modeling information required by RCAC, as incorporated in the filter G_{f}, and we develop the *target model* interpretation of G_{f}.

- We use the target model for adaptive pole placement using RCAC, develop the connections of RCAC with discrete-time LQG, and compare the H_2 cost and closed-loop frequency response of RCAC with LQG.

- We apply RCAC on plants that are practically impossible to control by fixed-gain control laws due to limited gain margin and delay margin, and demonstrate the ability of RCAC to re-adapt and restabilize the closed-loop system following destabilizing perturbations.

- We answer the question: Are all full-order dynamic compensators observer-based? We show that the only case where a dynamic compensator is not observer based is the case where the order of the plant n is odd and the closed-loop spectrum has no real eigenvalues.

- We apply RCMR on plants with unknown subsystem dynamics, and compare RCMR to established techniques for parameter estimation. We pair RCMR with a Riccati-based controller for indirect adaptive control of an aircraft with an unknown transition to NMP dynamics.

1.3.1 Publications

The following is a list of publications relevant to the research presented in this dissertation.

- Y. Rahman, A. Xie, D. S. Bernstein, "Retrospective Cost Adaptive Control: Pole Placement, Frequency Response and Connections with LQG Control," *IEEE Contr. Sys. Mag.* (Accepted)

- Y. Rahman and D. S. Bernstein, "Are All Full-Order Dynamic Compensators Observer-Based?," *IEEE Contr. Sys. Mag.*, vol. 37, no. 1

- Y. Rahman, and D. S. Bernstein, "Adaptive Control of Plants That Are Practically Impossible to Control by Fixed-Gain Control Laws," in *Proc. Conf. Dec. Contr.*, Las Vegas, NV, Dec 2016, pp. 371–376

- Y. Rahman, A. Xie, J. B. Hoagg, D. S. Bernstein, "A Tutorial and Overview of Retrospective Cost Adaptive Control," in *Proc. Amer. Contr. Conf.*, Boston, MA, July 2016, pp. 3386–3409

- Y. Rahman, K. Aljanaideh, E. D. Sumer, D. S. Bernstein, "Adaptive Control of Aircraft Lateral Motion with an Unknown Transition to Nonminimum-phase Dynamics," in *Proc. Amer. Contr. Conf.*, Portland, OR, June 2014, pp. 2359-2364

- Y. Rahman, J. Zhong, A. Morozov, D. S. Bernstein, "On the Accuracy of State Estimators for Constant and Time-varying Parameter Estimation," in *Proc. AIAA Guid. Nav. Contr. Conf.*, Boston, MA. 2013.

1.4 Dissertation Outline

This dissertation is organized as follows.

Chapter 2 Summary

In Chapter 2, we present the RCAC algorithm, and apply RCAC to several examples, including step command-following and disturbance rejection, harmonic command following and disturbance rejection. We demonstrate the ability of RCAC to automatically develop internal models. Next, we apply RCAC on adaptive PID control, and use RCAC to adaptively tune PID controllers and avoid integrator windup. Finally we apply RCAC with feedforward for adaptive control of NMP plants without knowledge of the NMP zero.

Chapter 3 Summary

In Chapter 3, we apply RCAC to linearized aircraft lateral dynamics with an unknown transition to NMP dynamics. We extend the use of RCAC to command following for cases where the dynamics transition from minimum-phase to NMP. We use system identification techniques to identify the NMP zero, and use this information to construct the target model. We consider both full-state feedback and output feedback, and in both cases we follow step commands with transitioning dynamics. We first consider the case where RCAC is unaware of the change and NMP zero identification is unavailable to RCAC. In this case, we show that RCAC does not cause the closed-loop system to become unstable as the plant becomes nonminimum phase. We then assume that NMP-zero information is available to RCAC from system identification, and show that RCAC is able to re-adapt to the transitioning dynamics and follow step commands.

Chapter 4 Summary

Chapter 4 contains the main contributions of this dissertation. This contribution concerns the modeling data used by RCAC as incorporated in G_{f}. In particular, we show that G_{f} serves as a target model for a closed-loop transfer function $\widetilde{G}_{z\tilde{u},k}$ whose zeros include the zeros of G_{zu}. The special closed-loop transfer function $\widetilde{G}_{z\tilde{u},k}$ arises from the way in which RCAC updates the controller coefficients. This controller

update can be interpreted as a virtual external control perturbation $\tilde{u}$ that is injected internally to the control update. We call this *intercalated injection*.

We show that the intercalated injection of $\tilde{u}$ gives rise to the closed-loop transfer function $\widetilde{G}_{z\tilde{u},k}$, and minimization of the retrospective cost updates the controller coefficients so as to fit $\widetilde{G}_{z\tilde{u},k}$ to the target model G_{f}. We then use these insights to show that RCAC requires knowledge of the relative degree, leading numerator coefficient, and NMP zeros of G_{zu}.

Chapter 5 Summary

In Chapter 5, we consider LTI plants that are practically impossible to control due to extremely small gain and phase margins. These plants tend to be either unstable or nonminimum phase or both. Since practical control of these plants using fixed-gain controllers is not feasible, it is of interest to determine whether adaptive control can overcome these difficulties. To investigate this question, we apply RCAC to a collection of plants that are practically impossible to control from an LTI perspective. For each plant, we introduce a destabilizing perturbation in order to determine whether or not RCAC can re-adapt in such a way as to compensate for the loss of margin and restabilize the closed-loop system without manual retuning. Since these plants are inherently difficult to control, it is of interest to determine whether or not restabilization is possible and, if so, assess the severity of the transient response.

Chapter 6 Summary

Chapter 6 considers plants that are stabilizable by asymptotically stable controllers but result in unstable LQG controllers, and we apply RCAC to these plants. We ensure controller stability by using quasi-FIR compensators, where most of the controller poles are confined to the origin. We define quasi-FIR controllers as containing a high-order FIR component and a low-order IIR component. We apply a reflection technique to enforce stability of the IIR component of the compensator. We then compare the H_2 cost and the closed-loop frequency response of the RCAC

controller to the unstable LQG controller. Next, we use an FIR controller in parallel with an internal model controller for step-command following for Lyapunov stable, NMP plants without knowledge of the NMP zero.

Chapter 7 Summary

In Chapter 7, we focus on the state observer followed by state-estimate feedback. We answer the question posed in the title of the chapter, namely, Are All Full-Order Dynamic Compensators Observer-Based? It turns out that the answer to the question posed in the title of the chapter is "no." To see that this is the case, consider a plant of odd order n controlled by a compensator such that none of the $2n$ closed-loop eigenvalues are real. Since the closed-loop spectrum arising from an observer-based compensator must be the union of the spectra of two real matrices of odd order, it follows that the closed-loop system must have at least two real eigenvalues. However, we demonstrate that this is the only case where full-order dynamic compensators are not observer based. Since the LQG controller is based on the separation principle, it follows that, in the case where n is odd, there exists a set of full-order compensators that are never quadratically optimal.

Chapter 8 Summary

In Chapter 8, we compare RCMR with nonlinear estimation techniques that are often used for parameter estimation. We use illustrative examples to compare the accuracy of two estimation techniques (the extended Kalman filter and the unscented Kalman filter) with RCMR. Both constant and time-varying examples are considered. Each algorithm is tuned to illustrate its capabilities for the given examples. Next, we use RCMR to provide parameter estimates to forward-propagating Riccati-based control, which is applicable to time-varying systems with dynamics that are known at the present time but not in the future. Both full-state-feedback and output-feedback architectures are considered, where the goal is to follow roll commands for the aircraft lateral dynamics model with a transition to NMP behavior from Chapter 3. We show

that RCMR is able to provide parameter estimates sufficient for stabilization, despite the lack of persistent excitation.

Finally, we present conclusions and explore possible extensions to this research in Chapter 9.

CHAPTER 2

Retrospective Cost Adaptive Control

2.1 Introduction

RCAC is a direct, digital adaptive control algorithm, that has been in development since 1999 [26]. In the original interpretation, RCAC was based on using past data to retrospectively optimize the controller to find the optimal controller for the past data. The rationale was that if the optimized controller had been used, the performance would have been better. However, in Chapter 4, we show that RCAC minimizes the residual between the performance variable z, and the difference between the actual control input and the optimal control input, passed through the filter G_{f}.

RCAC can be applied to stable or unstable systems, minimum phase or NMP systems, linear or nonlinear systems, on stabilization, command following or disturbance rejection problems. In this dissertation, we extend RCAC for applications such as adaptive pole placement, adaptive PID control, and we compare RCAC to discrete-time LQG.

In this chapter, we present the development of the RCAC algorithm and define the filter G_{f}. Next, we apply RCAC for step and harmonic command following and disturbance rejection, adaptive PID control, and we present a feedforward architecture for command following for NMP systems and investigate the effect of sensor noise on RCAC.

Although all examples in this dissertation use a cumulative cost function and an RLS minimization, we may also implement RCAC with either an instantaneous cost function, a sliding window batch cost function, or use gradient based optimization. For numerical examples, we use either the adaptive standard problem or the adaptive servo problem, described below.

2.2 Standard Problem

Consider the standard problem consisting of the discrete-time, linear time-invariant plant

$$x(k+1) = Ax(k) + Bu(k) + D_1 w(k), \tag{2.1}$$

$$y(k) = Cx(k) + D_0 u(k) + D_2 w(k), \tag{2.2}$$

$$z(k) = E_1 x(k) + E_2 u(k) + E_0 w(k), \tag{2.3}$$

where $x(k) \in \mathbb{R}^n$ is the state, $y(k) \in \mathbb{R}^{l_y}$ is the measurement, $u(k) \in \mathbb{R}^{l_u}$ is the control input, $w(k) \in \mathbb{R}^{l_w}$ is the exogenous input, and $z(k) \in \mathbb{R}^{l_z}$ is the performance variable. The plant (2.1)–(2.3) may represent a continuous-time, linear time-invariant plant sampled at a fixed rate. The goal is to develop a feedback or feedforward controller that operates on y to minimize z in the presence of the exogenous signal w. The components of w can represent either a command signal r to be followed, an external disturbance d to be rejected, or sensor noise v that corrupts the measurement as determined by the choice of D_1, D_2, and E_0. Depending on the application, components of w may or may not be measured, and, for feedforward control, the measured components of w can be included in y by suitable choice of C and D_2. For fixed-gain control, z need not be measured. For adaptive control, however, z is assumed to be measured.

Using the forward shift operator $\mathbf{q}$, we can rewrite (2.1)–(2.3) as

$$z(k) = G_{zw}(\mathbf{q})w(k) + G_{zu}(\mathbf{q})u(k), \tag{2.4}$$

$$y(k) = G_{yw}(\mathbf{q})w(k) + G_{yu}(\mathbf{q})u(k), \tag{2.5}$$

where

$$G_{zw}(\mathbf{q}) \triangleq E_1(\mathbf{q}I - A)^{-1}D_1 + E_0, \quad G_{zu}(\mathbf{q}) \triangleq E_1(\mathbf{q}I - A)^{-1}B + E_2, \tag{2.6}$$

$$G_{yw}(\mathbf{q}) \triangleq C(\mathbf{q}I - A)^{-1}D_1 + D_2, \quad G_{yu}(\mathbf{q}) \triangleq C(\mathbf{q}I - A)^{-1}B + D_0. \tag{2.7}$$

Furthermore, the discrete-time, linear time-invariant controller has the form

$$u(k) = G_{\mathrm{c}}(\mathbf{q})y(k). \tag{2.8}$$

Note that $\mathbf{q}$ is a time-domain operator that accounts for initial conditions, and, although (2.6) and (2.7) are written as transfer functions, these expressions are convenient representations of time-domain dynamics. For pole-zero analysis, $\mathbf{q}$ can be replaced by the Z-transform complex variable $\mathbf{z}$, in which case (2.4), (2.5), and (2.8) do not account for the initial conditions. Figures 2.1 and 2.2 illustrate (2.4)–(2.8).

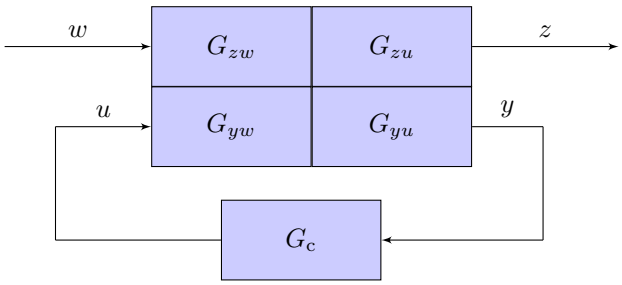

Figure 2.1: Transfer function representation of the standard problem.

The closed-loop transfer function from the exogenous signal w to the performance

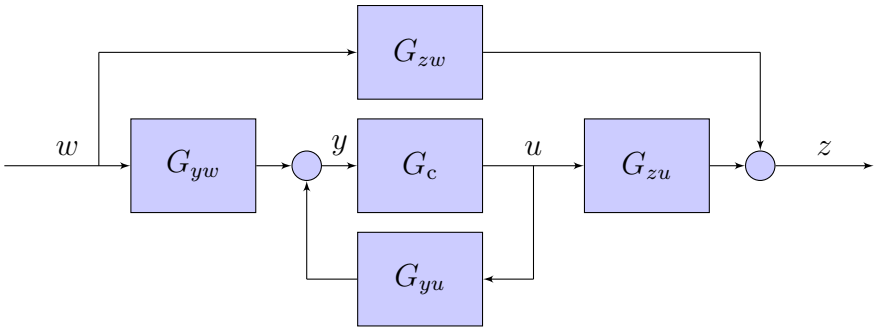

Figure 2.2: Equivalent transfer function representation of the standard problem.

variable z is given by

$$\widetilde{G}_{zw} \triangleq G_{zw} + G_{zu}G_{\mathrm{c}}(I - G_{yu}G_{\mathrm{c}})^{-1}G_{yw}. \tag{2.9}$$

We refer to the poles of $\widetilde{G}_{zw}$ as the closed-loop poles, and the transmission zeros of $\widetilde{G}_{zw}$ as the closed-loop zeros. In the case where y, z, u, and w are scalar signals, (2.6)–(2.7) and (2.9) can be written as

$$G_{zw} = \frac{N_{zw}}{D}, \quad G_{zu} = \frac{N_{zu}}{D}, \quad G_{yw} = \frac{N_{yw}}{D}, \quad G_{yu} = \frac{N_{yu}}{D}, \tag{2.10}$$

$$\widetilde{G}_{zw} = \frac{\widetilde{N}_{zw}}{\widetilde{D}_{zw}} = \frac{N_{zu}N_{yw}N_{\mathrm{c}} + N_{zw}(DD_{\mathrm{c}} - N_{yu}N_{\mathrm{c}})}{D(DD_{\mathrm{c}} - N_{yu}N_{\mathrm{c}})}, \tag{2.11}$$

where

$$G_{\mathrm{c}} = \frac{N_{\mathrm{c}}}{D_{\mathrm{c}}}. \tag{2.12}$$

We assume that D and D_{c} are monic. In the case where $y = z$, that is, $C = E_1$, $D_0 = E_2$, and $D_2 = E_0$, (2.10) and (2.11) can be written as

$$G_{zw} = G_{yw} = \frac{N_w}{D}, \quad G_{zu} = G_{yu} = \frac{N_u}{D}, \quad \widetilde{G}_{zw} = \frac{N_w D_{\mathrm{c}}}{DD_{\mathrm{c}} - N_u N_{\mathrm{c}}}. \tag{2.13}$$

In the case where w is matched with u, that is, $B = D_1$, $E_0 = E_2$, and $D_0 = D_2$,

(2.10) and (2.11) can be written as

$$G_{zw} = G_{zu} = \frac{N_z}{D}, \quad G_{yw} = G_{yu} = \frac{N_y}{D}, \quad \widetilde{G}_{zw} = \frac{N_z D_{\mathrm{c}}}{D D_{\mathrm{c}} - N_y N_{\mathrm{c}}}. \tag{2.14}$$

In the case where $y = z$ and w is matched with u, (2.10) and (2.11) can be written as

$$G \triangleq G_{zw} = G_{yw} = G_{zu} = G_{yu} = \frac{N}{D}, \quad \widetilde{G}_{zw} = \frac{N D_{\mathrm{c}}}{D D_{\mathrm{c}} - N N_{\mathrm{c}}}. \tag{2.15}$$

For examples where $y = z$ and w is matched with u, we use G to define the plant (2.1)–(2.3); otherwise, we use the state space representation.

2.2.1 Servo Problem

As a special case of the standard problem, we consider the discrete-time, linear time-invariant plant

$$x(k+1) = Ax(k) + Bu(k) + \bar{D}_1 d(k), \tag{2.16}$$

$$y_0(k) = \bar{C}x(k) + \bar{D}_0 u(k), \tag{2.17}$$

$$y_{\mathrm{n}}(k) = y_0(k) + v(k), \tag{2.18}$$

$$e_0(k) = r(k) - y_0(k), \tag{2.19}$$

$$e_{\mathrm{n}}(k) = r(k) - y_{\mathrm{n}}(k), \tag{2.20}$$

where $x(k) \in \mathbb{R}^n$ is the state, $y_{\mathrm{n}}(k) \in \mathbb{R}^{l_y}$ is the measurement, $u(k) \in \mathbb{R}^{l_u}$ is the control input, $d(k) \in \mathbb{R}^{l_d}$ is the disturbance, $r(k) \in \mathbb{R}^{l_y}$ is the command, $v(k) \in \mathbb{R}^{l_y}$ is the sensor noise, and $e_{\mathrm{n}}(k) \in \mathbb{R}^{l_y}$ is the performance variable. We can rewrite (2.17) in terms of $\mathbf{q}$ as

$$y_0(k) = G_u(\mathbf{q})u(k) + G_d(\mathbf{q})d(k), \tag{2.21}$$

where

$$G_u(\mathbf{q}) \triangleq \bar{C}(\mathbf{q}I - A)^{-1}B + \bar{D}_0, \quad G_d(\mathbf{q}) \triangleq \bar{C}(\mathbf{q}I - A)^{-1}\bar{D}_1. \tag{2.22}$$

Furthermore, the linear time-invariant controller has the form

$$u(k) = G_{\mathrm{c}}(\mathbf{q})e_{\mathrm{n}}(k). \tag{2.23}$$

The measured error signal e_{n} is the difference between the command r and the measurement y_{n}, which may be corrupted by noise. Since only the measured error is available for feedback, it serves as the performance variable within RCAC. However, the true error signal e_0, which is the difference between the command r and the plant output y_0, provides a true measure of the command-following performance. Since this signal is not available for feedback, it is used only as a diagnostic. If, however, sensor noise is absent, then e_{n} and e_0 are identical. Figure 2.3 illustrates (2.21)–(2.23).

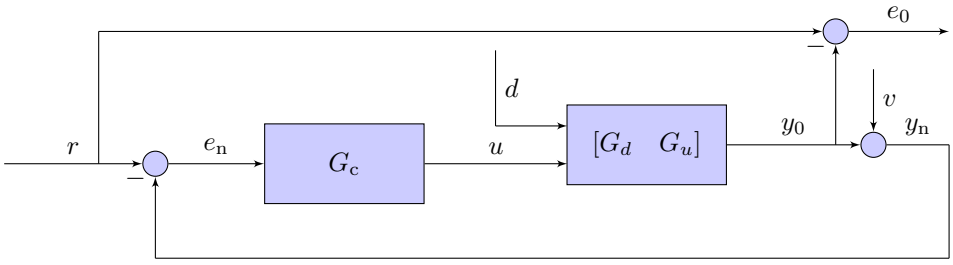

Figure 2.3: Transfer function representation of the servo problem.

In the notation of the standard problem,

$$w = \begin{bmatrix} r \\ d \\ v \end{bmatrix}, \quad y = e_{\mathrm{n}}, \quad z = e_{\mathrm{n}}. \tag{2.24}$$

The servo problem is a special case of the standard problem with

$$D_1 = [0 \quad \bar{D}_1 \quad 0], \quad C = E_1 = -\bar{C}, \quad D_0 = E_2 = -\bar{D}_0, \tag{2.25}$$

$$D_2 = [I_{l_y} \quad 0 \quad -I_{l_y}], \quad E_0 = [I_{l_y} \quad 0 \quad 0], \tag{2.26}$$

$$G_{zw} = [I_{l_y} \quad -G_d \quad 0], \quad G_{zu} = -G_u, \quad G_{yw} = [I_{l_y} \quad -G_d \quad -I_{l_y}], \quad G_{yu} = -G_u. \tag{2.27}$$

In the case where d and u are colocated, it follows that $\bar{D}_1 = B$ and $\bar{D}_0 = 0$, and thus $G_d = G_u$. In this case, we define $G \triangleq G_d = G_u$. However, w is not necessarily matched with u. Moreover, if $r = v = 0$, and d and u are colocated, then w is matched with u. For examples where d and u are colocated, we use G to define the plant (2.16)–(2.20); otherwise, we use the state space representation.

2.3 Retrospective Cost Adaptive Control Algorithm

2.3.1 Adaptive Standard Problem and Adaptive Servo Problem

Figure 2.4 shows the adaptive standard problem, which is the standard problem with an adaptive controller, while Figure 2.5 shows the adaptive servo problem, which is the servo problem with an adaptive controller. Note that, for the adaptive servo problem, it is desirable to minimize the true error e_0. However, since e_0 is not available, RCAC minimizes the measured error e_{n}, which may be corrupted by noise, as shown in Figure 2.3. In terms of the adaptive standard problem, $z = e_{\mathrm{n}}$.

2.3.2 Controller Structure

Define the dynamic compensator

$$u(k) = \sum_{i=1}^{n_{\mathrm{c}}} P_i(k)u(k-i) + \sum_{i=k_{\mathrm{c}}}^{n_{\mathrm{c}}} Q_i(k)y(k-i), \tag{2.28}$$

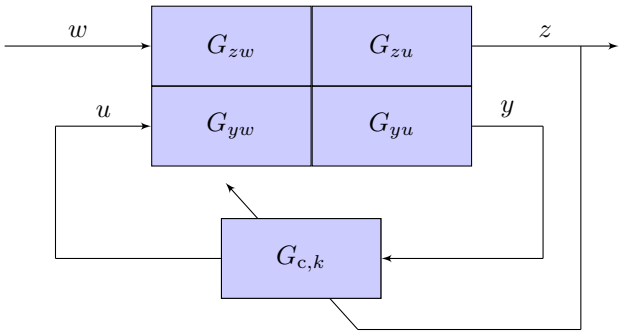

Figure 2.4: Transfer function representation of the adaptive standard problem with the adaptive controller $G_{c,k}$.

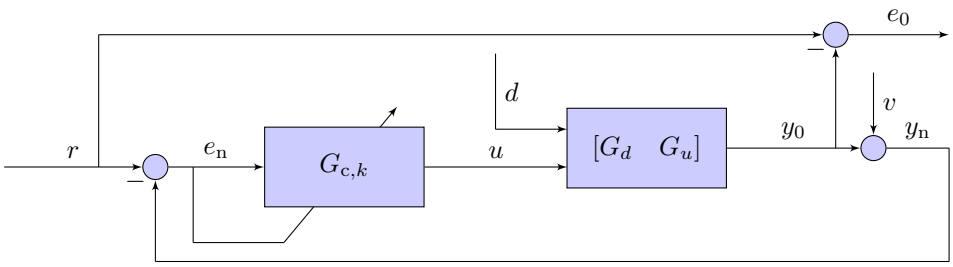

Figure 2.5: Transfer function representation of the adaptive servo problem with the adaptive controller $G_{c,k}$.

where $P_i(k) \in \mathbb{R}^{l_u \times l_u}$ and $Q_i(k) \in \mathbb{R}^{l_u \times l_y}$ are the controller coefficient matrices, and $k_c \geq 0$. For controller startup, we implement (2.28) as

$$u(k) = \begin{cases} 0, & k < k_w, \\ \Phi(k)\theta(k), & k \geq k_w, \end{cases} \tag{2.29}$$

where the regressor matrix $\Phi(k)$ is defined by

$$\Phi(k) \triangleq \begin{bmatrix} u(k-1) \\ \vdots \\ u(k-n_{\mathrm{c}}) \\ y(k-k_{\mathrm{c}}) \\ \vdots \\ y(k-n_{\mathrm{c}}) \end{bmatrix}^{\mathrm{T}} \otimes I_{l_u} \in \mathbb{R}^{l_u \times l_\theta}, \tag{2.30}$$

$k_{\mathrm{w}} \geq n_{\mathrm{c}}$ is an initial waiting period during which $\Phi(k)$ is populated with data, and the controller coefficient vector $\theta(k)$ is defined by

$$\theta(k) \triangleq \mathrm{vec} \begin{bmatrix} P_1(k) & \cdots & P_{n_{\mathrm{c}}}(k) & Q_{k_{\mathrm{c}}}(k) & \cdots & Q_{n_{\mathrm{c}}}(k) \end{bmatrix}^{\mathrm{T}} \in \mathbb{R}^{l_\theta}, \tag{2.31}$$

$l_\theta \triangleq l_u^2 n_{\mathrm{c}} + l_u l_y (n_{\mathrm{c}} + 1 - k_{\mathrm{c}})$, "$\otimes$" is the Kronecker product, and "vec" is the column-stacking operator. Note that $k_{\mathrm{c}} = 0$ allows an exactly proper controller, whereas $k_{\mathrm{c}} \geq 1$ yields a strictly proper controller of relative degree of at least k_{c}. In all examples in this dissertation, we use $k_{\mathrm{c}} = 1$, and, unless specified otherwise, we use $k_{\mathrm{w}} = n_{\mathrm{c}}$. In terms of $\mathbf{q}$, the time-domain transfer function of the controller from y to u is given by

$$G_{\mathrm{c},k}(\mathbf{q}) = \left(\mathbf{q}^{n_{\mathrm{c}}} I_{l_u} - \mathbf{q}^{n_{\mathrm{c}}-1} P_1(k) - \cdots - P_{n_{\mathrm{c}}}(k)\right)^{-1} \left(\mathbf{q}^{n_{\mathrm{c}}-k_{\mathrm{c}}} Q_{k_{\mathrm{c}}}(k) + \cdots + Q_{n_{\mathrm{c}}}(k)\right). \tag{2.32}$$

Note that the coefficients of $G_{\mathrm{c},k}$ are given by the components of $\theta(k)$, which are time-dependent, and thus $G_{\mathrm{c},k}$ is a linear, time-varying controller. Also, note that (2.32) is expressed in terms of the forward-shift operator $\mathbf{q}$ rather than the Z-transform variable $\mathbf{z}$. Consequently, although (2.32) is written as a transfer function, this expression is merely a convenient representation of the time-domain operator represented by (2.28).

If y and u are scalar signals, then $G_{c,k}$ is SISO and (2.32) can be written as

$$G_{c,k}(\mathbf{q}) = \frac{\mathbf{q}^{n_c-k_c}Q_{k_c}(k) + \cdots + Q_{n_c}(k)}{\mathbf{q}^{n_c} - \mathbf{q}^{n_c-1}P_1(k) - \cdots - P_{n_c}(k)}. \tag{2.33}$$

Note that (2.32) is an infinite impulse response (IIR) controller. By removing $u(k-1), \ldots, u(k-n_c)$ from (2.28) and $\Phi(k)$, and by modifying the structure of θ, we can enforce a finite impulse response (FIR) controller structure, where

$$u(k) = \sum_{i=k_c}^{n_c} Q_i(k)y(k-i). \tag{2.34}$$

In this case (2.32) becomes

$$G_{c,k}(\mathbf{q}) = \frac{1}{\mathbf{q}^{n_c}}\left(\mathbf{q}^{n_c-k_c}Q_{k_c}(k) + \cdots + Q_{n_c}(k)\right). \tag{2.35}$$

2.3.3 Retrospective Performance Variable

We define the retrospective performance variable as

$$\hat{z}(k,\hat{\theta}) \stackrel{\triangle}{=} z(k) + G_f(\mathbf{q})[\Phi(k)\hat{\theta} - u(k)], \tag{2.36}$$

where $\hat{\theta} \in \mathbb{R}^{l_\theta}$ and G_f is an $n_z \times n_u$ filter specified below. The rationale underlying (2.36) is to replace the control $u(k)$ with $\Phi(k)\hat{\theta}^*$, where $\hat{\theta}^*$ is the retrospectively optimized controller coefficient vector obtained by optimization below. The updated controller thus has coefficients $\theta(k+1) = \hat{\theta}^*$. Consequently, the implemented control at step $k+1$ is given by

$$u(k+1) = \Phi(k+1)\theta(k+1). \tag{2.37}$$

The filter G_{f} is constructed based on the required modeling information. This filter has the form

$$G_{\mathrm{f}} \triangleq D_{\mathrm{f}}^{-1} N_{\mathrm{f}}, \tag{2.38}$$

where D_{f} is an $l_z \times l_z$ polynomial matrix with leading coefficient I_{l_z}, and N_{f} is an $l_z \times l_u$ polynomial matrix. For reasons given in Chapter 4, we refer to G_{f} as the *target model*. By defining the filtered versions $\Phi_{\mathrm{f}}(k) \in \mathbb{R}^{l_z \times l_\theta}$ and $u_{\mathrm{f}}(k) \in \mathbb{R}^{l_z}$ of $\Phi(k)$ and $u(k)$, respectively, (2.36) can be written as

$$\hat{z}(k, \hat{\theta}) = z(k) + \Phi_{\mathrm{f}}(k)\hat{\theta} - u_{\mathrm{f}}(k), \tag{2.39}$$

where

$$\Phi_{\mathrm{f}}(k) \triangleq G_{\mathrm{f}}(\mathbf{q})\Phi(k), \quad u_{\mathrm{f}}(k) \triangleq G_{\mathrm{f}}(\mathbf{q})u(k). \tag{2.40}$$

Note that implementation requires $k_{\mathrm{w}} \geq \max(n_{\mathrm{c}}, n_{\mathrm{f}})$, where n_{f} is the McMillan degree of G_{f}.

2.3.4 Retrospective Cost

Using the retrospective performance variable $\hat{z}(k, \hat{\theta})$ defined by (2.36), we define the cumulative retrospective cost function

$$\begin{aligned} J(k, \hat{\theta}) \triangleq \sum_{i=1}^{k} \lambda^{k-i} [\hat{z}^{\mathrm{T}}(i, \hat{\theta}) R_z(i) \hat{z}(i, \hat{\theta}) + (G_{\mathrm{f}}(\Phi(i)\hat{\theta}))^{\mathrm{T}} R_u(i) G_{\mathrm{f}}(\Phi(i)\hat{\theta})] \\ + \lambda^k (\hat{\theta} - \theta(0))^{\mathrm{T}} R_\theta (\hat{\theta} - \theta(0)), \end{aligned} \tag{2.41}$$

where $\lambda \in (0, 1]$ is the forgetting factor, $R_\theta \in \mathbb{R}^{l_\theta \times l_\theta}$ is positive definite, and, for all $i \geq 1$, $R_z(i) \in \mathbb{R}^{l_z \times l_z}$ is positive definite and $R_u(i) \in \mathbb{R}^{l_z \times l_z}$ is positive semidefinite.

The performance-variable and control-input weighting matrices $R_z(i)$ and $R_u(i)$ are time-dependent and thus may depend on present and past values of y, z, and u. For example, choosing $R_u(i)$ to be a function of $z(i)^{\mathrm{T}}z(i)$ can help prevent unstable pole-zero cancellation in the case of unmodeled NMP zeros [66]. Recursive minimization of (2.41) is used to update the controller coefficient vector $\hat{\theta}$. The following result uses recursive least squares to obtain the minimizer of (2.41).

Proposition: Let $P(0) = R_\theta^{-1}$, and, for all $k \geq 1$, let $\hat{\theta}^*$ be the unique global minimizer of the retrospective cost function (2.41). Then, $\hat{\theta}^*$ is given by

$$\hat{\theta}^* = \theta(k) - P(k)\Phi_{\mathrm{f}}^{\mathrm{T}}(k)\Upsilon^{-1}(k)\big[\Phi_{\mathrm{f}}(k)\theta(k) + (R_z(k) + R_u(k))^{-1} R_z(k)(z(k) - u_{\mathrm{f}}(k))\big], \tag{2.42}$$

$$P(k+1) = \frac{1}{\lambda}P(k) - \frac{1}{\lambda}P(k)\Phi_{\mathrm{f}}^{\mathrm{T}}(k)\Upsilon^{-1}(k)\Phi_{\mathrm{f}}(k)P(k), \tag{2.43}$$

where

$$\Upsilon(k) \triangleq \lambda(R_z(k) + R_u(k))^{-1} + \Phi_{\mathrm{f}}(k)P(k)\Phi_{\mathrm{f}}^{\mathrm{T}}(k). \tag{2.44}$$

Setting $\theta(k+1) = \hat{\theta}^*$, (2.42) yields the recursive controller coefficient update equation

$$\theta(k+1) = \theta(k) - P(k)\Phi_{\mathrm{f}}^{\mathrm{T}}(k)\Upsilon^{-1}(k)\big[\Phi_{\mathrm{f}}(k)\theta(k) + (R_z(k) + R_u(k))^{-1} R_z(k)(z(k) - u_{\mathrm{f}}(k))\big]. \tag{2.45}$$

Note that, if $\lambda = 1$, then the covariance $P(k)$ decreases monotonically, and thus the rate of adaptation decreases. To maintain adaptation in cases where the plant or exogenous signals are changing, the covariance can be reset using suitable logic. Al-

ternatively, choosing the forgetting factor $\lambda < 1$ prevents monotonic decrease of $P(k)$, but can lead to instability in the presence of noise and in the absence of persistency [67, 68]. An alternative approach is to include an additional positive-semidefinite term $Q(k)$ on the right-hand side of (2.43) of the form

$$P(k+1) = P(k) - P(k)\Phi_{\mathrm{f}}^{\mathrm{T}}(k)\Upsilon^{-1}(k)\Phi_{\mathrm{f}}(k)P(k) + Q(k), \tag{2.46}$$

where $\lambda = 1$ in (2.44). Note that (2.46) is the discrete-time Kalman predictor Riccati error-covariance update equation with the dynamics matrix $A = I_{l_\theta}$, output matrix $C(k) = \Phi_{\mathrm{f}}(k)$, and process-noise covariance $Q(k)$ [69]. Consequently, persistency in (2.46) is determined by the observability of the time-varying pair $(I_{l_\theta}, \Phi_{\mathrm{f}})$, and the corresponding state-estimate update is given by (2.42). Alternatively, we can also use the discrete-time Kalman filter Riccati error-covariance update equation

$$P(k+1) = P(k) - P(k)\Phi_{\mathrm{f}}^{\mathrm{T}}(k+1)\Upsilon^{-1}(k)\Phi_{\mathrm{f}}(k+1)P(k) + Q(k), \tag{2.47}$$

where the corresponding state-estimate update is given by

$$\begin{aligned}\theta(k+1) = \theta(k) &- P(k)\Phi_{\mathrm{f}}^{\mathrm{T}}(k+1)\Upsilon^{-1}(k+1) \\ &\cdot \left[\Phi_{\mathrm{f}}(k+1)\theta(k) + \left(R_z(k) + R_u(k)\right)^{-1} R_z(k)\left(z(k+1) - u_{\mathrm{f}}(k+1)\right)\right].\end{aligned} \tag{2.48}$$

Note that in (2.48), the estimate $\theta(k+1)$ depends on $z(k+1)$. Therefore, implementation of (2.48) requires instantaneuous update of the controller coefficient vector. In contrast, in (2.45), $\theta(k+1)$ depends on $z(k)$, and thus (2.45) is implementable.

For all examples in this dissertation, we initialize $\theta(0) = 0$ in order to reflect the absence of additional prior modeling information. Furthermore, for all $i \geq 1$, we use $R_z(i) = I_{l_z}$. Note that RCAC may use batch least squares optimization instead of

recursive minimization.

2.4 Modeling Information Required for G_{f}

In this section we specify the modeling information required by RCAC. For the standard problem, this information includes the relative degree, the first nonzero Markov parameter, and all of the NMP zeros of G_{zu}. For the servo problem, it follows from (2.27) that this information is obtained from $G_u = -G_{zu}$. All of the modeling information required by RCAC is used to construct the filter G_{f}. The discussion in this section is confined to the case where z and u are scalar signals. Note, however, that y may be a vector signal, and thus the controllers based on G_{f} as specified below may be multiple-input, single-output.

2.4.1 First Nonzero Markov Parameter

The first nonzero Markov parameter $H_{\mathrm{d}_{zu}}$ of G_{zu} is equal to the leading numerator coefficient of G_{zu}. We choose the leading numerator coefficient of G_{f} to be equal to the leading numerator coefficient of G_{zu}, and thus RCAC requires knowledge of the first nonzero Markov parameter $H_{\mathrm{d}_{zu}}$ of G_{zu} [37]. This choice is explained in Chapter 4.

2.4.2 Relative Degree

We choose the relative degree of G_{f} to be equal to the relative degree of G_{zu}, and thus RCAC requires knowledge of the relative degree d_{zu} of G_{zu} [37]. This choice is explained in Chapter 4.

2.4.3 NMP Zeros

We choose to include all of the NMP zeros of G_{zu} in N_{f}, and this RCAC requires knowledge of the NMP zeros of G_{zu}. This choice is explained in Chapter 4.

2.4.4 FIR G_{f}

In the case where G_{zu} is minimum phase, we define the FIR filter

$$G_{\mathrm{f}}(\mathbf{q}) \triangleq \frac{H_{\mathrm{d}_{zu}}}{\mathbf{q}^{\mathrm{d}_{zu}}}. \tag{2.49}$$

This choice of G_{f} requires knowledge of the relative degree d_{zu} of G_{zu} and the first nonzero Markov parameter $H_{\mathrm{d}_{zu}}$ of G_{zu}. Note that, for the adaptive servo problem, since $G_{zu} = -G_u$, it follows that $H_{\mathrm{d}_{zu}} = -H_{\mathrm{d}_u}$, where H_{d_u} is the first nonzero Markov parameter of G_u.

In the case where G_{zu} is NMP, we define the FIR filter

$$G_{\mathrm{f}}(\mathbf{q}) \triangleq \frac{H_{\mathrm{d}_{zu}} N_{zu,\mathrm{u}}(\mathbf{q})}{\mathbf{q}^{\mathrm{d}_{zu}+\deg(N_{zu,\mathrm{u}})}}, \tag{2.50}$$

where the roots of the monic polynomial $N_{zu,\mathrm{u}}$ are the NMP zeros of G_{zu}. This choice of G_{f} requires knowledge of the relative degree d_{zu} of G_{zu}, the first nonzero Markov parameter $H_{\mathrm{d}_{zu}}$ of G_{zu}, and the NMP zeros of G_{zu}. In both cases, the relative degree of G_{f} is equal to the relative degree of G_{zu}.

2.4.5 Markov Parameters

In [26, 36], G_{f} is based on the Markov parameters of G_{zu}. In particular, for each complex number $\mathbf{z}$ whose absolute value is greater than the spectral radius of A, it follows that G_{zu} has the Laurent expansion

$$G_{zu}(\mathbf{z}) = E_1(\mathbf{z}I - A)^{-1}B = \sum_{i=\mathrm{d}_{zu}}^{\infty} \frac{H_i}{\mathbf{z}^i}, \tag{2.51}$$

where $H_0 \triangleq E_2$ and, for all $i \geq 1$, the i^{th} Markov parameter of G_{zu} is given by

$$H_i \triangleq E_1 A^{i-1} B. \tag{2.52}$$

As shown in [36], a sufficiently large number $\bar{n} > \mathrm{d}_{zu}$ of Markov parameters in a truncation of (2.51) yields an FIR target model $G_{\mathrm{f}}(\mathbf{z}) = \sum_{i=\mathrm{d}_{zu}}^{\bar{n}} \frac{H_i}{\mathbf{z}^i}$ whose zeros approximate the NMP zeros of G_{zu} with absolute value greater than the spectral radius of A. In addition, every truncation of (2.51) with $\bar{n} \geq \mathrm{d}_{zu}$ has the correct relative degree, that is, the relative degree of G_{zu}. Note that, since $G_{zu} = \frac{N_{zu}}{D}$ and D is monic, $H_{\mathrm{d}_{zu}}$ is the leading numerator coefficient of G_{zu}.

2.5 Step Command Following and Disturbance Rejection

Example 2.1. Effect of R_θ on command-following performance for a step command. Consider the asymptotically stable, minimum-phase plant

$$G(\mathbf{q}) = \frac{\mathbf{q} - 0.85}{(\mathbf{q} - 0.8)(\mathbf{q} - 0.9)}. \tag{2.53}$$

Let r be a unit-height step command, and let $d = v = 0$. We use the FIR target model (2.49), and set $n_{\mathrm{c}} = 3$. Figure 2.6 shows the command-following performance for $R_\theta = 20 I_{l_\theta}$ and $R_\theta = 0.2 I_{l_\theta}$. For $R_\theta = 20 I_{l_\theta}$, RCAC follows the step command in about 2000 time steps, whereas, for $R_\theta = 0.2 I_{l_\theta}$, RCAC follows the step command in about 200 time steps. For both values of R_θ, the converged controllers have integrators, as shown by the controller poles at 1. ■

Example 2.2. Step disturbance rejection for the adaptive servo problem

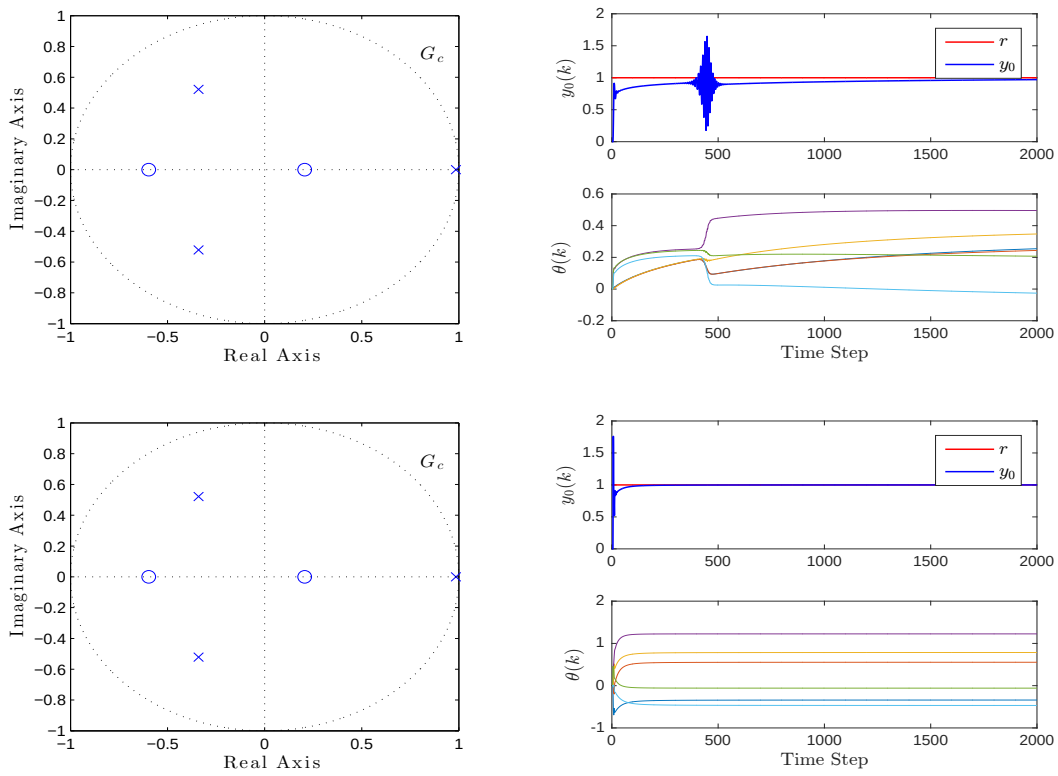

Figure 2.6: Example 2.1: Effect of R_θ on command-following performance for a step command for (2.53). For $R_\theta = 20I_{l_\theta}$ (upper plots), RCAC follows the step command in about 2000 time steps, whereas, for $R_\theta = 0.2I_{l_\theta}$ (lower plots), RCAC follows the step command in about 200 time steps. For both values of R_θ, the converged controllers have integrators, as shown by the poles at 1.

Consider the asymptotically stable, minimum-phase plant

$$G(\mathbf{q}) = \frac{\mathbf{q}^2 - 1.44\mathbf{q} + 0.81}{(\mathbf{q} - 0.9)(\mathbf{q}^2 - 1.71\mathbf{q} + 0.903)}. \tag{2.54}$$

Let $r = v = 0$ and let d be a unit-height step disturbance. We use the FIR target model (2.49), and set $R_\theta = 10^{-10}I_{l_\theta}$ and $n_c = 4$. RCAC rejects the step disturbance, as shown in Figure 2.7. ■

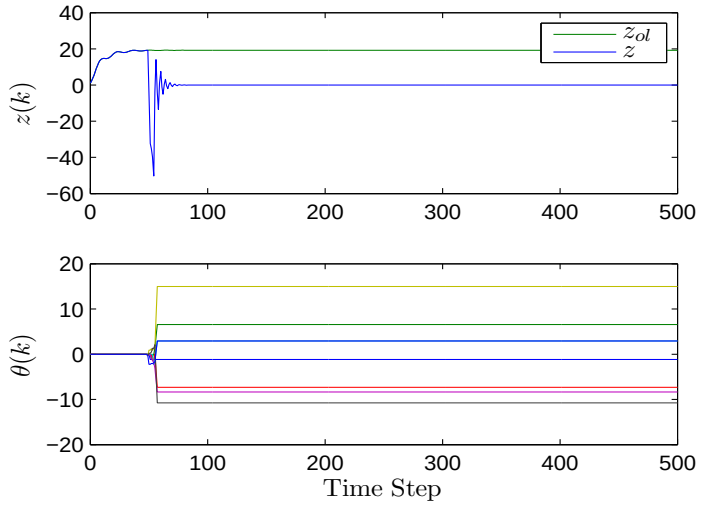

Figure 2.7: Example 2.2: Step disturbance rejection. RCAC rejects the step disturbance.

2.6 Adaptive Harmonic Command Following and Disturbance Rejection

In this section, we demonstrate the ability of RCAC to develop internal models of harmonic commands and disturbances by considering two examples of adaptive harmonic command following and disturbance rejection. In the first example, we use RCAC to follow harmonic commands with an IIR feedback controller as well as with combined feedback-feedforward control. Next, for harmonic disturbance rejection, we investigate the ability of RCAC to readapt to changing disturbance frequencies.

Example 2.3. Harmonic command following for the adaptive servo problem. Consider the asymptotically stable, minimum-phase plant

$$G(\mathbf{q}) = \frac{\mathbf{q} - 0.8}{(\mathbf{q} - 0.95)(\mathbf{q} - 0.99)}. \tag{2.55}$$

Let r be the harmonic command $r(k) = \cos \omega k$, where $\omega = 0.5$ rad/sample, and let $d = v = 0$. We apply RCAC with $R_\theta = 0.2I_{l_\theta}$, $R_u = 0$, and $n_c = 5$, and we use the FIR target model (2.49). We restrict $G_{c,k}$ to be an FIR controller (2.34), (2.35). Since

RCAC cannot develop an internal model of the command due to the FIR structure of $G_{c,k}$, the command-following performance is severely restricted, as shown in Figure 2.8. The closed-loop system is instantaneously unstable at most time steps up to $k = 500$.

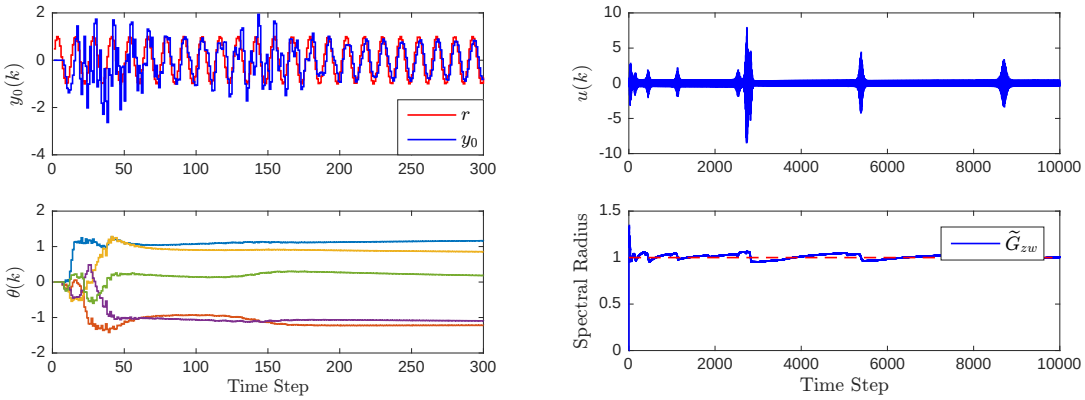

Figure 2.8: Example 2.3: Harmonic command following for the adaptive servo problem using an FIR controller. Since RCAC cannot develop an internal model of the command due to the FIR structure of $G_{c,k}$, the command-following performance is severely restricted. Note that the controller coefficients do not converge, and the closed-loop system alternates between asymptotic stability and instability.

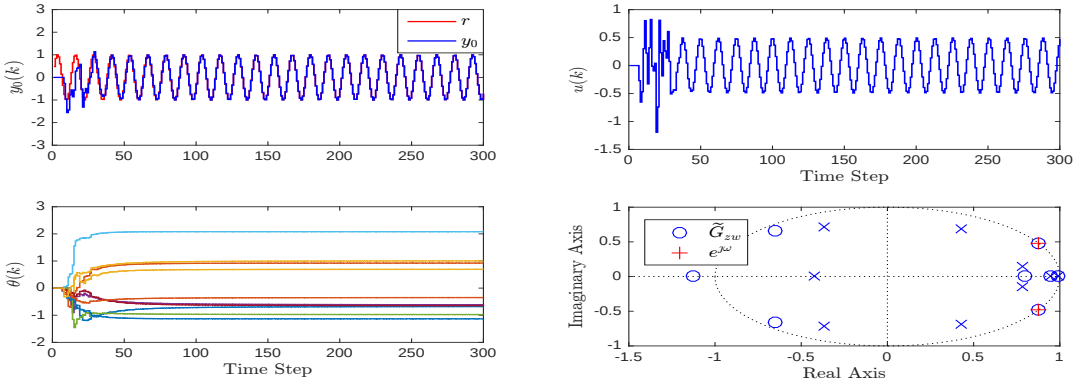

Figure 2.9: Example 2.3: Harmonic command following for the adaptive servo problem. RCAC achieves an internal model of the harmonic command signal by placing controller poles on the unit circle at the command frequency. The internal model poles of the controller are evident in the form of two closed-loop zeros on the unit circle at the command frequency, which are shown by the red plus signs. The closed-loop poles and zeros are shown at step $k = 300$.

Next, we allow $G_{c,k}$ to be IIR. In this case, RCAC asymptotically follows the harmonic command and develops an internal model in the form of controller poles

located on the unit circle at the command frequency ω, as shown in Figure 2.9. ■

Example 2.4. Two-tone harmonic disturbance rejection for the adaptive servo problem using an IIR controller. Consider the asymptotically stable plant

$$A = \begin{bmatrix} 0.9 & -0.5625 & 0 \\ 1 & 0 & 0 \\ 0 & 1 & 0 \end{bmatrix}, \quad B = \begin{bmatrix} 1 \\ 0 \\ 0 \end{bmatrix}, \quad \bar{D}_1 = \begin{bmatrix} 0 & 0 \\ 1 & 0 \\ 0 & 1 \end{bmatrix}, \tag{2.56}$$

$$\bar{C} = [0.78 \quad -1.18 \quad 1], \quad \bar{D}_0 = 0, \tag{2.57}$$

where G_u is NMP. Let $r = v = 0$ and $d(k) = [\cos\omega_1 k \quad \cos\omega_2 k]^{\mathrm{T}}$, where $\omega_1 = \frac{\pi}{8}$ rad/sample and $\omega_2 = \frac{\pi}{12}$ rad/sample. We apply RCAC with $k_{\mathrm{w}} = 50$, $R_\theta = 0.01 I_{l_\theta}$, $R_u = 0$, and $n_{\mathrm{c}} = 12$, and we use the FIR target model (2.50) with an IIR controller. RCAC rejects the harmonic disturbance and develops an internal model, as shown in Figure 2.10.

Next, let $r(k) = \cos\omega_1 k$, $v = 0$, and $d(k) = [\cos\omega_2 k \quad 1]^{\mathrm{T}}$, where $\omega_1 = \frac{\pi}{15}$ rad/sample and $\omega_2 = \frac{\pi}{5}$ rad/sample for $1 \leq k \leq 2000$, and where $\omega_2 = \frac{\pi}{8}$ rad/sample for $2000 < k \leq 4000$. RCAC asymptotically follows the harmonic command, rejects the step and harmonic disturbances, and develops internal models of the command and disturbance, as shown in Figure 2.11. Note that, after the disturbance frequency changes at step $k = 2000$, RCAC adapts to the change and rejects the disturbance. ■

2.7 Adaptive PID Control

Proportional-integral-derivative (PID) control is likely the most widely used feedback control technique [70–72]. Adaptive PID control is considered in [73]. In this

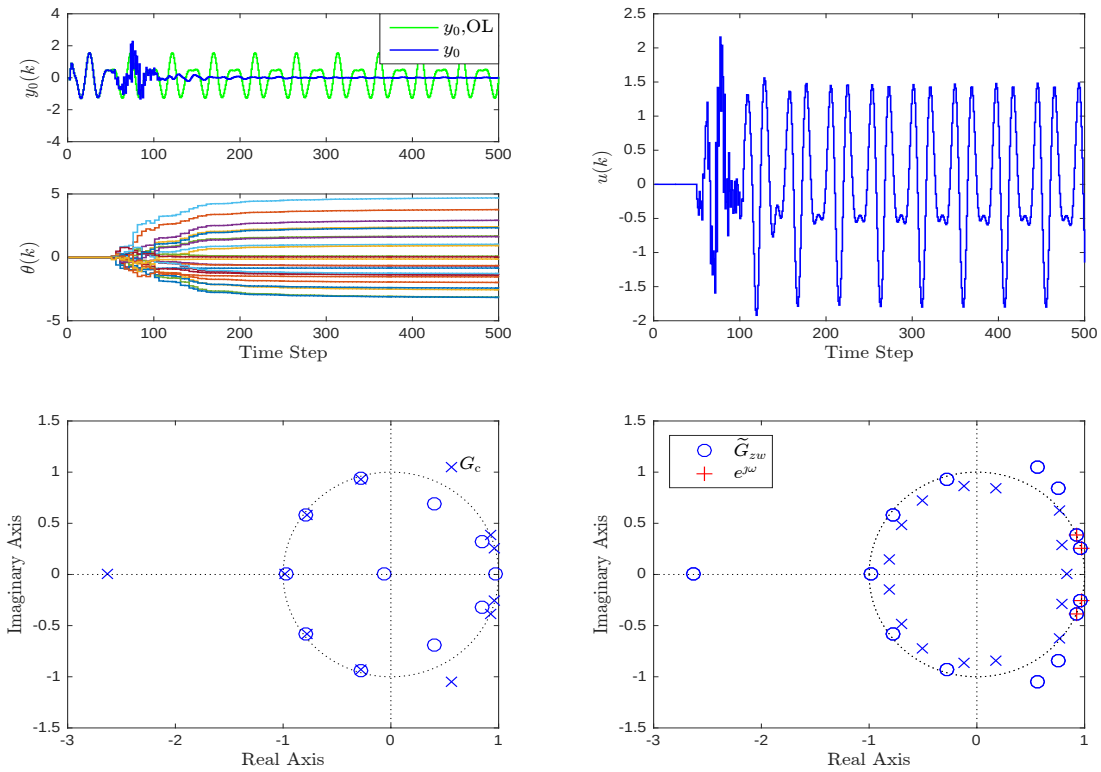

Figure 2.10: Example 2.4: Two-tone harmonic disturbance rejection for the adaptive servo problem using an IIR controller. y_0,OL indicates the open-loop response. RCAC achieves an internal model of the harmonic disturbance by placing controller poles at the two disturbance frequencies. The internal model poles of the controller are evident in the form of four closed-loop zeros on the unit circle at the disturbance frequencies , which are shown by the red plus signs. The closed-loop poles and zeros are shown at step $k = 10^4$.

section, we consider the discrete-time PID controller structure

$$u(k) = u_{\mathrm{P}}(k) + u_{\mathrm{I}}(k) + u_{\mathrm{D}}(k), \tag{2.58}$$

where

$$u_{\mathrm{P}}(k) = K_{\mathrm{P}}(k)e_{\mathrm{n}}(k-1), \tag{2.59}$$

$$u_{\mathrm{I}}(k) = K_{\mathrm{I}}(k)\gamma(k-1), \tag{2.60}$$

$$u_{\mathrm{D}}(k) = K_{\mathrm{D}}(k)[e_{\mathrm{n}}(k-1) - e_{\mathrm{n}}(k-2)], \tag{2.61}$$

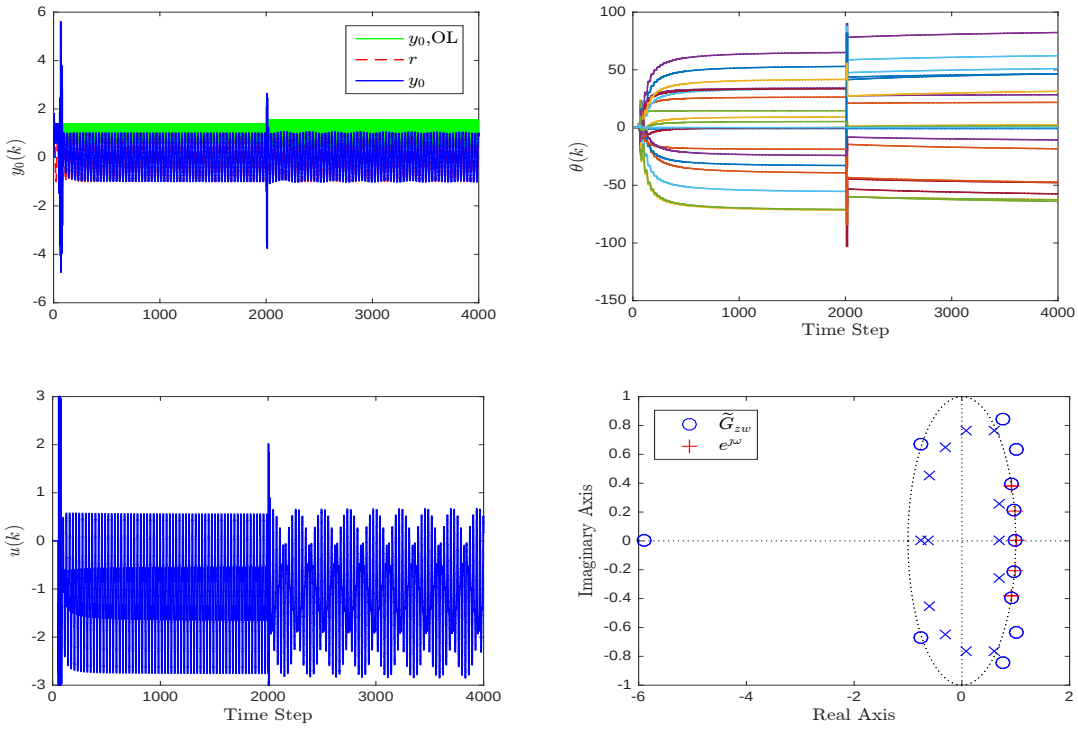

Figure 2.11: Example 2.4: Harmonic command following and step-plus-harmonic disturbance rejection for the adaptive servo problem. Note that, after the disturbance frequency changes at step $k = 2000$, RCAC readapts and rejects the disturbance. RCAC achieves an internal model of the command and disturbance signals by placing controller poles on the unit circle at the command frequency and at the two disturbance frequencies. The internal model poles of the controller are evident in the form of five closed-loop zeros on the unit circle at the command and disturbance frequencies, which are shown by the red plus signs. The closed-loop poles and zeros are shown at step $k = 10^5$.

and the integrator state γ satisfies

$$\gamma(k) = \gamma(k-1) + e_{\mathrm{n}}(k-1). \tag{2.62}$$

Note that the PID controller (2.58)–(6.5) is strictly proper. We use RCAC to adaptively tune K_{P}, K_{I}, and K_{D}.

Example 2.5. Step command following for the adaptive servo problem using adaptive PID control. Consider the asymptotically stable, NMP plant

$$G(\mathbf{q}) = \frac{(\mathbf{q}-0.975)(\mathbf{q}-1.2)}{(\mathbf{q}-0.99)(\mathbf{q}^2-1.6\mathbf{q}+0.965)}, \tag{2.63}$$

let r be a step command with height 2, let d be a step disturbance with height -1.1, and let $v = 0$. We apply RCAC to the adaptive PID controller (2.58)–(2.62), with $R_\theta = 10^4 I_{l_\theta}$ and $R_u = 0$. RCAC rejects the step disturbance and asymptotically follows the step command, as shown in Figure 2.12. ■

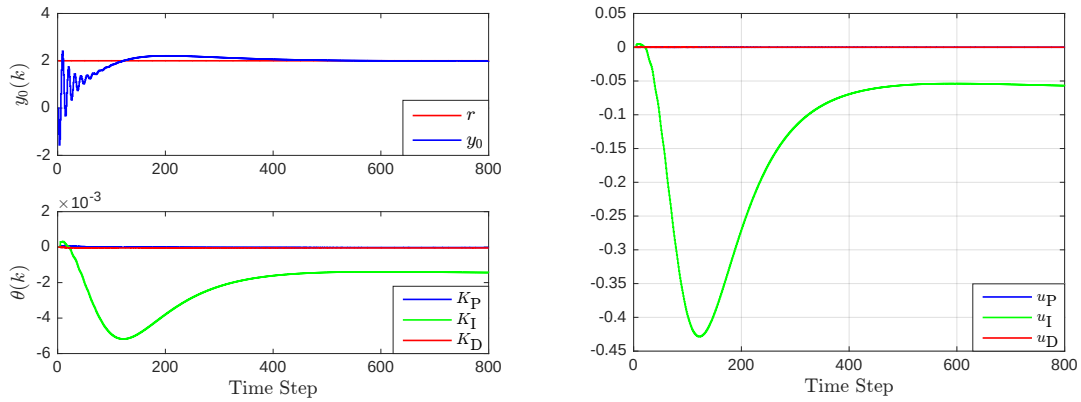

Figure 2.12: Example 2.5: Step command following for the adaptive servo problem using adaptive PID control. RCAC rejects the disturbance and asymptotically follows the step command.

2.7.1 Application to Anti-Windup

The most common nonlinearity encountered in practice is control saturation, which can lead to integrator windup and possibly instability. Since control magnitude and rate saturation affect all real-world control systems, it is not surprising that an extensive literature is devoted to this problem [74–77].

We now investigate the performance of RCAC in the presence of control magnitude and rate saturation, as shown in Figure 2.13. The output of RCAC is the requested control $u(k)$, and the input to the plant is the actual control $u_\mathrm{a}(k)$. In all examples, the regressor $\Phi(k)$ contains $u_\mathrm{a}(k)$. This means that either the nonlinearity is known or its output is measured. The case where the nonlinearity is unknown and its output is not measured is considered in [40].

Example 2.6. Control magnitude saturation for the adaptive servo problem with adaptive PID control. Consider the asymptotically stable, minimum-phase

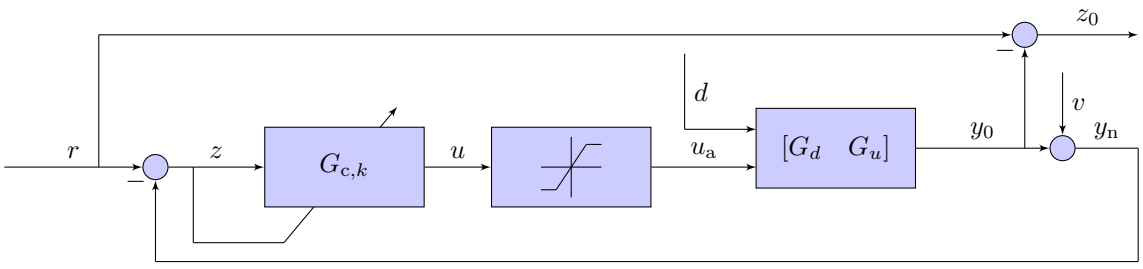

Figure 2.13: Adaptive servo problem with control magnitude and rate saturation.

plant

$$G(\mathbf{q}) = \frac{(\mathbf{q} - 0.09)(\mathbf{q} - 0.8)}{(\mathbf{q}^2 - \mathbf{q} + 0.5)(\mathbf{q} - 0.9)}. \tag{2.64}$$

Let r be a sequence of step commands with heights ± 0.4 and ± 1, and let $d = v = 0$. We use the PID controller structure (2.58), and set $R_\theta = 0.1 I_{l_\theta}$ and $R_u = 0$. The control u is saturated at ± 0.2. This saturation level allows the controller to follow step commands with height ± 0.4, but not with height ± 1. Figure 2.14 shows the response of the adaptive PID controller. For step commands with height ± 0.4, the adaptive PID controller uses integral action to follow the step command. However, for step commands with height ± 1, the adaptive PID controller drives the integral gain K_I to zero. The reduction in K_I allows RCAC to avoid integrator windup. ■

2.8 Adaptive Feedforward Control

In this section we consider extensions of the adaptive servo problem to include feedforward control. The first feedforward architecture uses centralized adaptation, as shown in Figure 2.15.

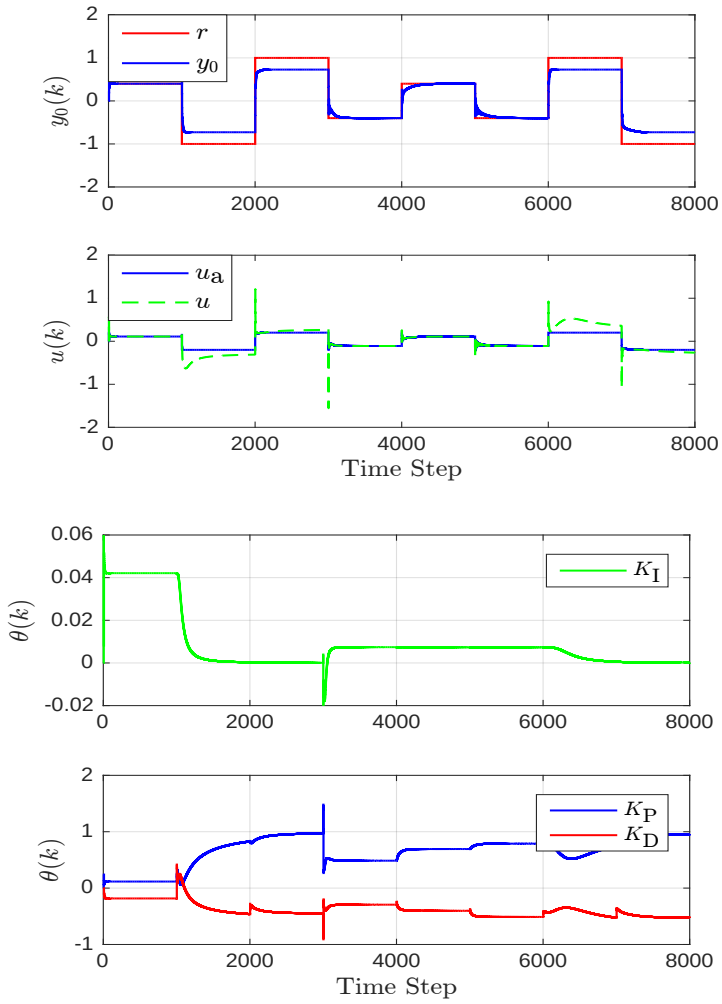

Figure 2.14: Example 2.6: Control magnitude saturation for the adaptive servo problem with adaptive PID control. For step commands with height ± 0.4, the adaptive PID controller uses integral action to follow the step command. However, for step commands with height ± 1, which cannot be followed due to the magnitude saturation, the adaptive PID controller reduces the integral gain K_I to zero, and thus avoids integrator windup.

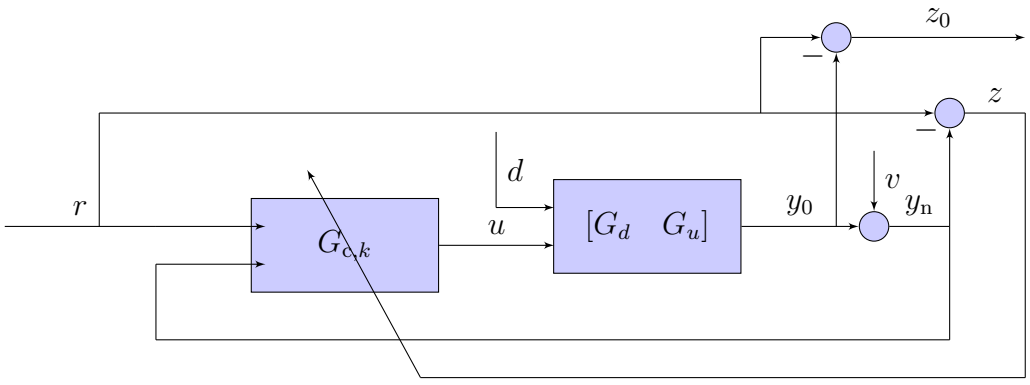

Figure 2.15: Transfer function representation of centralized feedback-feedforward control for the adaptive servo problem.

Alternatively, RCAC may use a decentralized feedback and feedforward architecture that allows for decentralized adaptation, as shown in Figure 2.16. In this case, the feedback controller $G_{\mathrm{fb},k}$ may have poles that are different from those of the feedforward controller $G_{\mathrm{ff},k}$, which is not possible with centralized feedback-feedforward control. Moreover, we may choose the feedback controller to be FIR.

We use feedforward architectures for two reasons. Firstly, as shown in [78], it may sometimes be difficult for RCAC to obtain an internal model for plants with high spectral radius. By using a feedforward controller, RCAC is able to follow commands without the need of an internal model. Secondly, we demonstrate that by using decentralized feedback-feedforward control, RCAC may perform command following for NMP plants without knowledge of the NMP zeros.

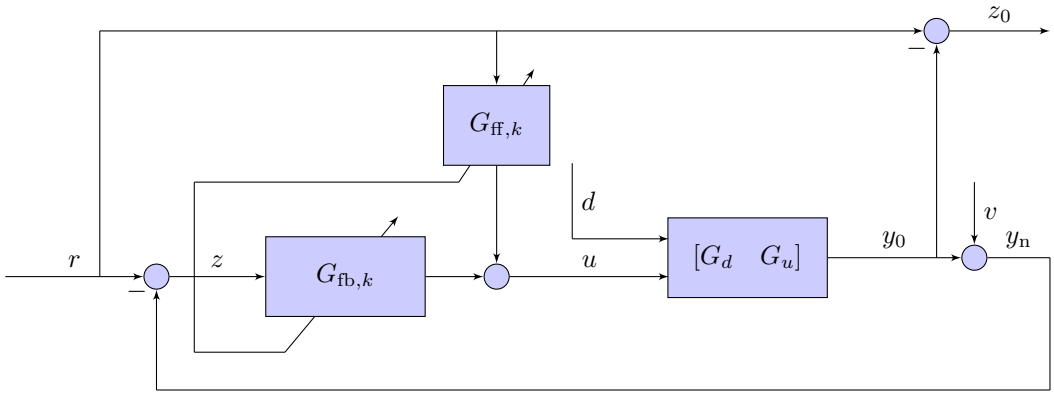

Figure 2.16: Transfer function representation of combined feedback-feedforward control with decentralized adaptation for the adaptive servo problem.

Example 2.7. Command following using centralized feedback-feedforward control for the adaptive servo problem. Consider the asymptotically stable, NMP plant

$$G(\mathbf{q}) = \frac{(\mathbf{q}-1.2)(\mathbf{q}^2-1.8\mathbf{q}+0.85)}{(\mathbf{q}-0.9)(\mathbf{q}-0.95)(\mathbf{q}^2-1.4\mathbf{q}+0.74)}. \tag{2.65}$$

Let r be the harmonic command $r(k) = \cos \omega k$, where $\omega = 0.4$ rad/sample, and let $d = v = 0$. We apply the centralized feedback-feedforward control architecture shown

in Figure 2.15 with $R_\theta = 10I_{l_\theta}$, $R_u = 0$, and $n_c = 8$, and we use the FIR target model (2.50). Figure 2.17 shows the command-following performance for combined feedforward and feedback control. RCAC follows the harmonic command without developing an internal model. ■

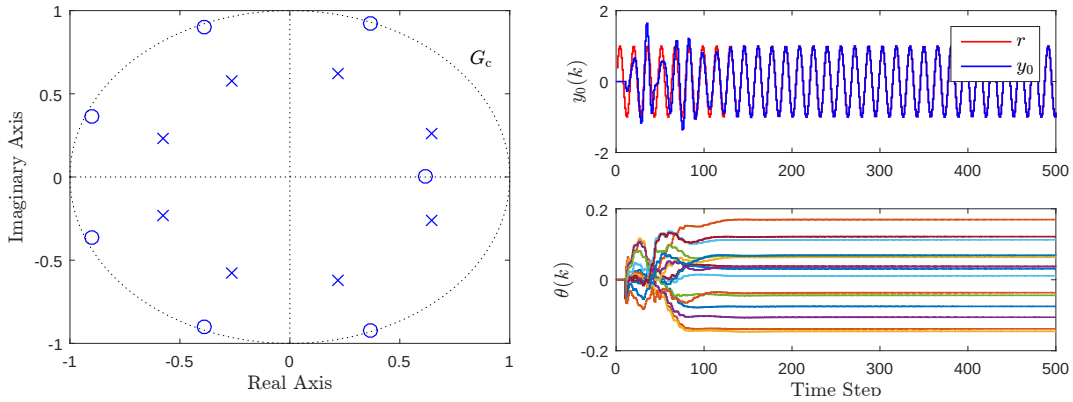

Figure 2.17: Example 2.7: Centralized feedforward and feedback control. RCAC follows the harmonic command without developing an internal model.

Example 2.8. Command following using decentralized feedback-feedforward control for the adaptive servo problem. Consider the asymptotically stable, NMP plant

$$G(\mathbf{q}) = \frac{(\mathbf{q} - 0.9)(\mathbf{q} - 1.1)}{(\mathbf{q} - 0.99)(\mathbf{q}^2 - 1.9\mathbf{z} + 0.9925)}. \tag{2.66}$$

Let r be a unit-height step command, and let $d = v = 0$. We apply the decentralized feedback-feedforward control architecture shown in Figure 2.16, and for both controllers we set $R_\theta = 10^5 I_{l_\theta}$, $R_u = 0$, and $n_c = 10$, and we use the FIR target model (2.49). We restrict G_{fb} to be an FIR controller. Figure 2.18 shows the command-following performance. Note that, since the feedback controller is FIR, RCAC cannot develop an internal model of the command. However, RCAC adapts G_{ff} so that the command is followed. In this example, we demonstrate step command following for NMP plants using RCAC, without knowledge of the NMP zero. Since the feedback

controller is FIR, it cannot cancel NMP zeros. Therefore, we may use RCAC without knowledge of the NMP zero in the target model. ■

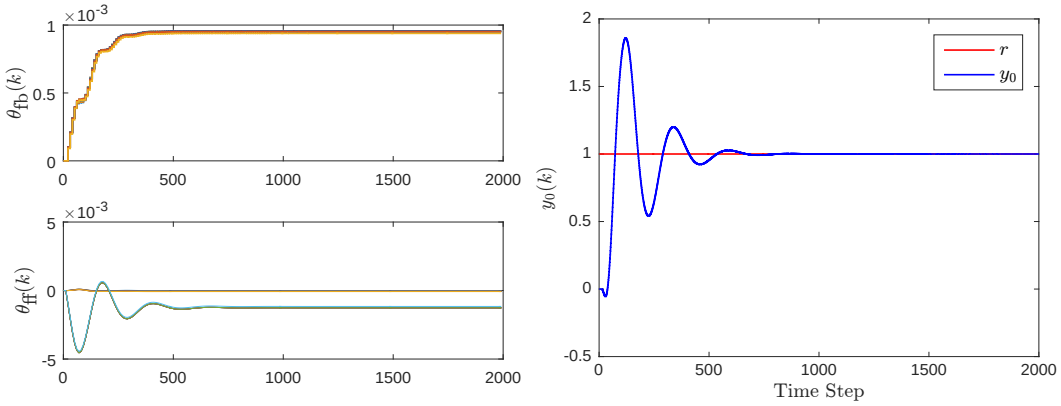

Figure 2.18: Example 2.8: Command following using decentralized feedback-feedforward control for the adaptive servo problem. Since the feedback controller is FIR, RCAC cannot develop an internal model of the command. However, RCAC adapts G_{ff} so that the command is followed. In this example, we demonstrate step command following for NMP plants using RCAC, without knowledge of the NMP zero. Since the feedback controller is FIR, it cannot cancel NMP zeros. Therefore, we may use RCAC without knowledge of the NMP zero in the target model.

2.9 Conclusions

This chapter developed the formulation of the RCAC algorithm, and used numerical examples to illustrate properties of RCAC. The examples in this chapter show that, for harmonic command following and disturbance rejection, RCAC has the ability to develop an internal model of the command and disturbance without knowledge of the spectrum of the exogenous dynamics.

Next, two contributions of this dissertation, namely Adaptive PID Control and Adaptive Feedforward Control for NMP plants were presented. First, we applied RCAC to step-command following using an adaptively tuned PID controller, and demonstrated anti-windup using adaptively tuned PID control, whereby the integral gain K_{I} is reduced to zero when the actuator is saturated. Next, we used a combined feedback-feedforward control architectures to perform step command following with-

out developing an internal model, as well as for NMP plants without knowledge of the NMP zero.

In the subsequent chapters, we apply RCAC to adaptive control of aircaft lateral motion with NMP dynamics, develop the role of the filter G_{f}, and we apply RCAC to stochastic disturbance rejection and compare the performance of RCAC with discrete-time LQG.

CHAPTER 3

Adaptive Control of Aircraft Lateral Motion with an Unknown Transition to Nonminimum-Phase Dynamics

3.1 Introduction

The performance limitations due to NMP zeros are inherent to fixed-gain feedback control [79–81]. Within the context of adaptive control, NMP zeros pose an additional challenge, namely, the tendency of the adaptive controller to cancel NMP zeros. This issue can be overcome with full-state feedback, but in many cases full state measurements are not available. Traditional output feedback model reference adaptive control is typically based on positive real conditions, which cannot be met for NMP systems [82–84]. In applications, however, such as aircraft flight control, robotics, and active vibration control [85–88], NMP zeros arise due to sensor/actuator noncolocation. In these applications, NMP zeros are unavoidable, and developing techniques that can address this problem remains a research challenge.

To at least a limited extent, adaptive control laws have been developed to address the challenge of NMP zeros. For example, RCAC has been shown to be effective for NMP systems with known NMP zeros [89]. For systems with unknown NMP zeros, a constrained optimization approach is used in [90] to prevent unstable pole-zero

cancellation. However, it is clear that much remains to be done to address the effect of NMP zeros within adaptive control.

With this motivation in mind, the goal of this chapter is to consider the lateral dynamics of a flight vehicle under conditions of uncertainty that motivate the use of adaptive control. In particular, the lateral dynamics are assumed to transition from minimum phase to nonminimum phase. This scenario is reminiscent of the dynamics of a hypersonic vehicle in glide phase with unknown thermal effects [91–93]. The ultimate goal is to achieve reliable command following under the assumption that the transition occurs over an interval of time whose onset and duration are unknown and, in addition, the final NMP dynamics are also uncertain. As an intermediate step in addressing this problem, we consider the case where the details of the transition and the final NMP dynamics are known, provided by simultaneous identification. RCMR has been used for model refinement of a lateral dynamics model with erroneous modeling information in the presence of noisy and biased measurements [64]. Nevertheless, this objective is nontrivial since the adaptive control law must account for the transition from minimum-phase to NMP dynamics.

In this chapter we address this problem by applying RCAC in several ways, with the objective of ascertaining how this problem can best be addressed. After presenting the aircraft model in Section 3.2, we proceed in Section 3.4 to consider the case of full-state feedback. In Section 3.5, we consider the output feedback case where only ϕ is available for feedback. Finally, in Section 3.6 we consider NMP zero identification.

3.2 Aircraft Model

We consider the lateral dynamics of an aircraft with a transition to NMP dynamics. We present the transition as follows. The dynamics are first expressed in terms of a nominal plant. Then, at an unknown time and in an unknown manner,

the plant parameters transition from stable, minimum phase to stable, but NMP. We call the stable and minimum phase plant the *nominal* plant and the NMP plant the *off-nominal* plant.

The *nominal continuous-time* plant is given by

$$A_0 = \begin{bmatrix} -0.0771 & 0.269 & -0.9631 & 0.0397 \\ -25.60 & 0.0218 & 0.0995 & 0 \\ 0.6160 & 0.0376 & -0.2687 & 0 \\ 0 & 1 & -0.4202 & 0.0058 \end{bmatrix}, \quad B_0 = \begin{bmatrix} -0.0002 \\ 2.519 \\ -0.0222 \\ 0 \end{bmatrix}, \qquad (3.1)$$

and the *off-nominal continuous-time* plant is given by

$$A_1 = \begin{bmatrix} -0.0771 & 0.269 & -0.9631 & 0.0397 \\ -108.8 & 0.0218 & 0.0995 & 0 \\ 0.4107 & 0.0376 & -0.2687 & 0 \\ 0 & 1 & -0.4202 & 0.0058 \end{bmatrix}, \quad B_1 = \begin{bmatrix} -0.0002 \\ 2.519 \\ -0.0665 \\ 0 \end{bmatrix}, \qquad (3.2)$$

where $x = \begin{bmatrix} \beta & P & R & \phi \end{bmatrix}^{\mathrm{T}}$, that is, sideslip angle, roll rate, yaw rate, and roll angle.

Note that there are two parameter changes in A and one parameter change in B, and both plants are open-loop stable. Step commands are specified for the roll angle ϕ. Therefore, we consider two approaches, namely,

1. Full-state feedback with dummy commands for β, P, and R; and

2. Output feedback with only ϕ available for feedback.

3.2.1 Euler Discretization

We discretize the nominal and off-nominal plants with sampling period $h = 0.1$ sec using Euler discretization. The discretized nominal and off-nominal plants are

$$A_{\mathrm{D0}} = \begin{bmatrix} 0.9553 & 0.0265 & -0.0934 & 0.0039 \\ -2.5210 & 0.9680 & 0.1310 & -0.0050 \\ 0.0551 & 0.0045 & 0.9708 & 0.0001 \\ -0.1282 & 0.0989 & -0.0369 & 1.0004 \end{bmatrix}, \quad B_{\mathrm{D0}} = \begin{bmatrix} 0.0034 \\ 0.2492 \\ -0.0017 \\ 0.0126 \end{bmatrix}, \quad (3.3)$$

$$A_{\mathrm{D1}} = \begin{bmatrix} 0.9482 & 0.0255 & -0.0900 & 0.0038 \\ -10.3212 & 0.9595 & 0.5152 & -0.0210 \\ 0.0186 & 0.0041 & 0.9723 & 0.0001 \\ -0.5304 & 0.0953 & -0.0239 & 0.9999 \end{bmatrix}, \quad B_{\mathrm{D1}} = \begin{bmatrix} 0.0036 \\ 0.2390 \\ -0.0061 \\ 0.0124 \end{bmatrix}. \quad (3.4)$$

All examples in this chapter use these discretized plant dynamics. Unless stated otherwise, we assume that the plant transition occurs at $t = 250$ sec and that it takes 10 sec to transition from the nominal plant to the off-nominal plant. We assume that all parameters vary simultaneously with a linear transition.

3.3 NMP-Zero-Based Construction of G_{f}

We construct the target model G_{f} such that the numerator N_{f} is equivalent to $H_{\mathrm{d}}N_{\mathrm{osz,u}}(\mathbf{q})$ for the full-state feedback case and $H_{\mathrm{d}}N_{zu,\mathrm{u}}(\mathbf{q})$ for the output feedback case, where the roots of the monic polynomial $N_{\mathrm{osz,u}}$ are the NMP output subspace zeros, and the roots of the monic polynomial $N_{zu,\mathrm{u}}$ are the NMP zeros of G_{zu}. We explain output subspace zeros in the next section.

3.4 Full-State Feedback

We now apply a full-state feedback control law where we command all four states. The advantage of using full-state feedback is the lack of nonminimum-phase zeros in the transfer function G_{zu}. However, as shown below, output subspace zeros arise due to the nonsquare nature of the dynamics [41], and the plant may exhibit NMP behavior. The drawback of using full-state feedback is the need to provide commands for the three additional states, which is not straightforward in the presence of uncertain dynamics. To overcome this problem, we specify dummy commands for the states x_1, x_2, and x_3 given by

$$r_1(k) = x_1(k-1), \tag{3.5}$$

$$r_2(k) = x_2(k-1), \tag{3.6}$$

$$r_3(k) = x_3(k-1), \tag{3.7}$$

where $r_i(k)$ denotes the command for state x_i at step k.

3.4.1 Output-Subspace Zeros

A plant is nonsquare if $l_u \neq l_y$. In the case of the aircraft when using full state feedback, the plant is nonsquare. Since in this case, $l_y > l_u$, the plant is "tall". As shown in [41], RCAC implicitly squares the plant. We thus consider the notion of output-subspace zeros, which for the servo problem are the zeros from the control input to the scaled performance variable $H_i^{\mathrm{T}} z$, which drives the update of $\theta(k)$, where H_i is the Markov parameter used by RCAC [41]. If G_{zu} is square or wide and has full rank, then $\mathcal{N}(H_i^{\mathrm{T}}) = \{0\}$. Therefore, $H_i^{\mathrm{T}} z = 0$ if and only if $z = 0$. In this case, it is reasonable to expect that the zeros from u to z and zeros from u to $H_i^{\mathrm{T}} z$ are identical. However, in the case where G_{zu} is tall, $\mathcal{N}(H_i^{\mathrm{T}})$ is a proper subspace of $\mathbb{R}^{l_z}$,

and thus $H_i^{\mathrm{T}} z$ may be zero with nonzero z. In this case, the output-subspace zeros and the transmission zeros of G_{zu} may be distinct. In fact, in the full state feedback case, there are no transmission zeros but there may be output-subspace zeros. If the output-subspace zeros are NMP, then NMP behavior arises despite the use of full-state feedback.

Example 3.1. Step command following using full-state feedback. Let r_4 be a step command with height 0.15, and let $d = v = 0$. We apply RCAC with full-state feedback, and with $n_c = 6$, $R_u = 50e_0^2(k)$, $\lambda = 1$ and $R_\theta = I_{l_\theta}$. Figure 3.1 shows command following when the NMP dynamics are unmodeled. Notice that in this case RCAC does not destabilize the closed-loop system.

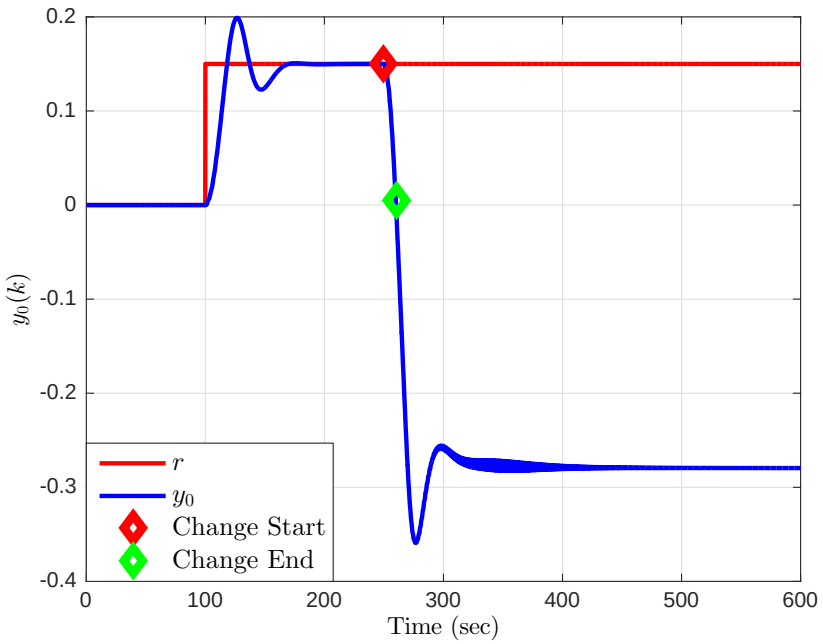

Figure 3.1: Example 3.1: Step command following using full-state feedback. We assume the NMP dynamics are unmodeled. RCAC is able to follow the command until the transition to NMP behavior. After the transition, RCAC does not cause instability, but there is a large steady state error.

Next, we assume that NMP information is known throughout the flight. We apply RCAC with full-state feedback, and with $n_c = 40$, $R_u = 350e_0^2(k)$, $\lambda = 0.9997$ and $R_\theta = 1.1I_{l_\theta}$. Figure 3.2 shows command following assuming NMP information

is known throughout the flight. RCAC is able to follow the command despite having poor transient performance during and immediately after the transition to NMP dynamics. The adaptation is slower and a penalty is added to the control input at the expense of performance before the transition. Figure 3.3 shows the controller coefficients θ. The controller converges before the transition, adapts and converges to different controller coefficients after the transition. ■

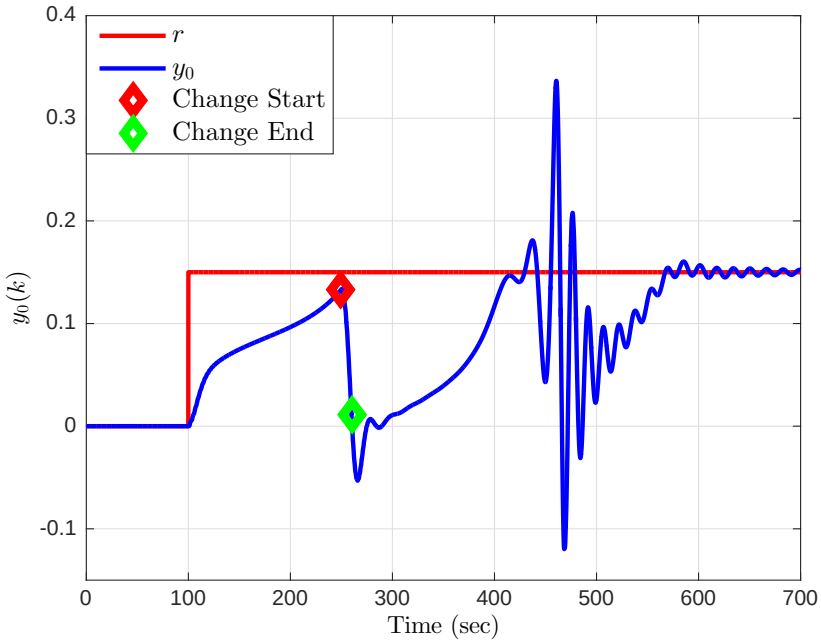

Figure 3.2: Example 3.1: Step command following using full-state feedback. We assume RCAC uses the NMP zero information. RCAC is able to follow the command throughout, despite poor transients and slow response before transition to NMP dynamics.

3.5 Output Feedback

We now consider output feedback, where measurements of only ϕ are available for feedback. We follow step commands for ϕ. The nominal plant has one real zero at -0.9959 and two complex zeros at $0.9818 \pm 0.0556j$. Figure 3.4 shows the transition of the two complex zeros as the system transitions from minimum phase to NMP.

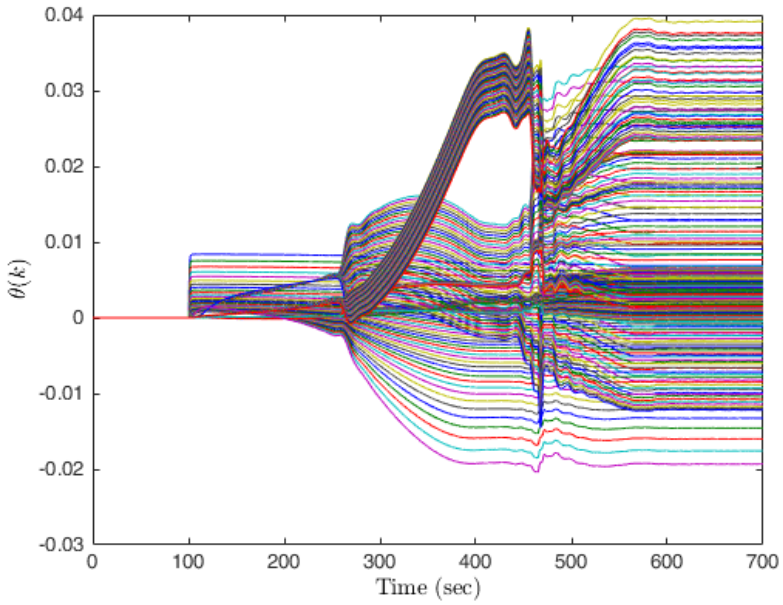

Figure 3.3: Example 3.1: Step command following using full-state feedback. We assume RCAC uses the NMP zero information. The controller coefficients converge before the transition, adapt and converge to different controller coefficients after the transition.

The two complex conjugate zeros become real and diverge along the real line. At the end of the transition, the plant has two NMP zeros at -1.0027 and 1.1369. Figure 3.5 shows the magnitude of the zeros as a function of time.

Example 3.2. Step command following using output feedback. Let r_4 be a step command with height 0.15, and let $d = v = 0$. We apply RCAC with output feedback, and with $n_c = 15$, $\lambda = 1$, $R_u = 50e_0^2(k)$, and $R_\theta = 2I_{l_\theta}$. Figure 3.6 shows step command following with unmodeled NMP dynamics. Notice that in this case RCAC does not destabilize the closed-loop system.

Next, we assume that NMP information is known throughout the flight. We apply RCAC with with $n_c = 15$, $\lambda = 1$, $R_u = 0$, and $R_\theta = 2I_{l_\theta}$. Figure 3.7 shows step command following performance in this case. After a transient, RCAC follows the command despite the transition to NMP dynamics. Figure 3.8 shows the con-

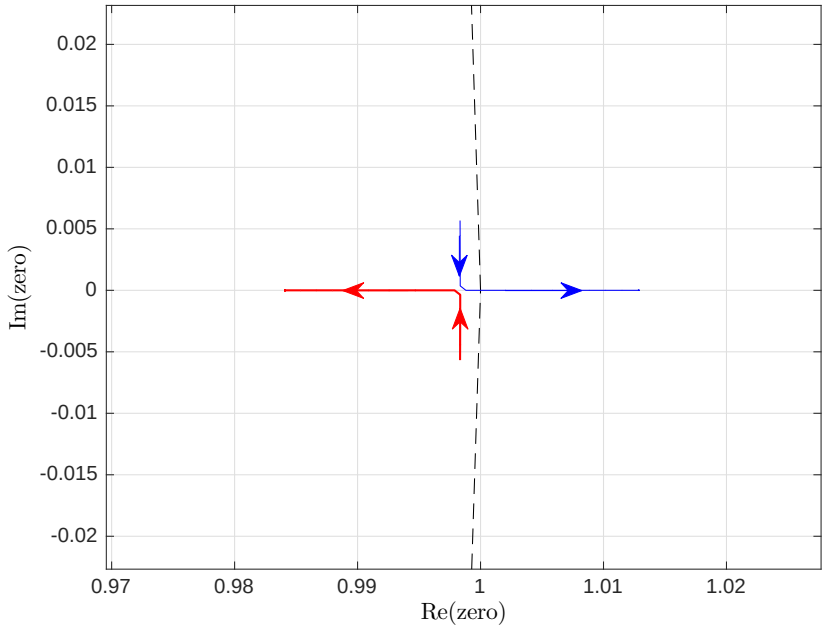

Figure 3.4: Zero Locations. The two complex conjugate zeros become real and diverge along the real line. The transition to NMP dynamics occurs as the real zero crosses the unit circle.

troller coefficients θ. The controller converges before the transition, and adapts and converges to different controller coefficients after the transition. The identified zeros are shown in Figure 3.9. Note that the transition to NMP dynamics takes place over 1 sec, instead of 10 sec. RCAC performs better when using only output feedback, because the zeros of G_{zu} better describe the system than the output subspace zeros.■

3.6 NMP Zero Identification

To perform the identification process we use the μ-Markov model. For all $k \geq 0$, $\mu \geq 1$, and each model order $n_{\text{mod}} \geq n$, the input $u(k)$ and the output $y(k)$ satisfy

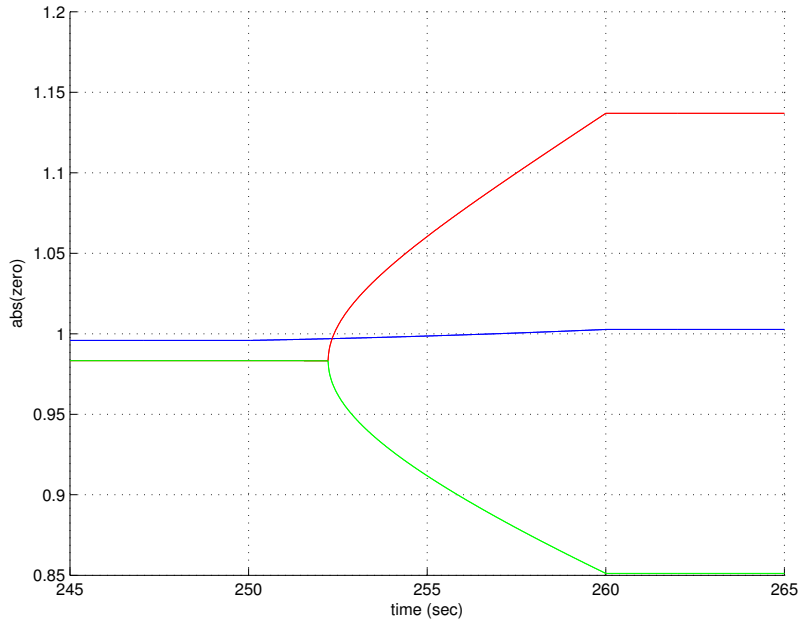

Figure 3.5: Zero Magnitudes. The system becomes NMP at approximately $t = 252$ sec. The zero transitions to 1.1369 in 10 sec.

the μ-Markov model

$$y(k) = \sum_{j=0}^{\mu-1} H_j u(k-j) + \sum_{j=\mu}^{n_{\text{mod}}+\mu-1} b_j u(k-j) - \sum_{j=\mu}^{n_{\text{mod}}+\mu-1} a_j y(k-j), \tag{3.8}$$

where $H_0, \ldots, H_{\mu-1}$ are Markov parameters of the system, that is, if the outputs $y(k-j)$ for all $j \in \{\mu, \ldots, n_{\text{mod}} + \mu - 1\}$ are zero and the input is the impulse $u(0) = 1, u(k) = 0$ for all $k > 0$, then the first μ outputs of (3.8) are the Markov parameters $H_1, \ldots, H_\mu$ of the system. Models of the form (3.8) are of interest because consistent estimation of $H_1, \ldots, H_\mu$ is possible in the presence of arbitrary output noise using standard least squares [94, 95] when the input u is white.

The μ-Markov model (3.8) can be expressed as

$$y(k) = \theta_\mu \phi_\mu(k) + \theta_u \phi_u(k) - \theta_y \phi_y(k), \tag{3.9}$$

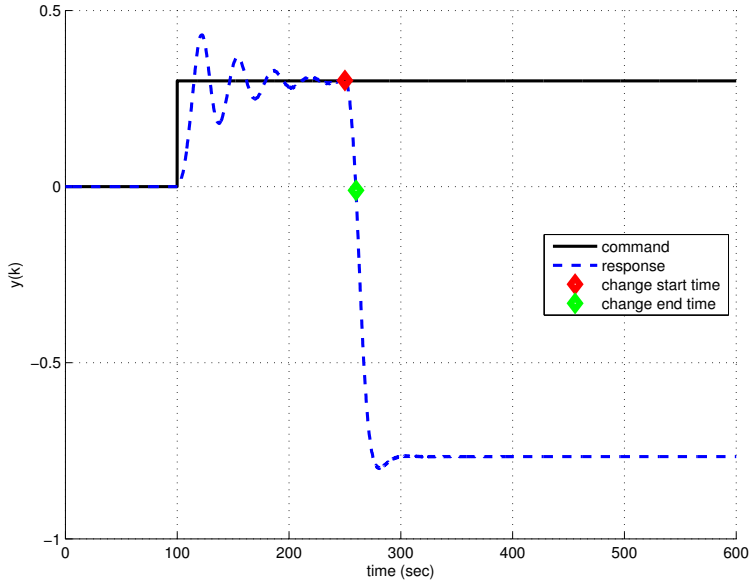

Figure 3.6: Example 3.2: Step command following using output feedback. We assume the NMP dynamics are unmodeled. RCAC is able to follow the command until the transition to NMP behavior. After the transition, RCAC does not cause instability, but there is a large steady state error.

where

$$
\begin{aligned}
\theta_\mu &\triangleq \begin{bmatrix} H_0 & \cdots & H_{\mu-1} \end{bmatrix}, \\
\theta_u &\triangleq \begin{bmatrix} b_\mu & \cdots & b_{n_{\rm mod}+\mu-1} \end{bmatrix}, \\
\theta_y &\triangleq \begin{bmatrix} a_\mu & \cdots & a_{n_{\rm mod}+\mu-1} \end{bmatrix}, \\
\phi_\mu(k) &\triangleq \begin{bmatrix} u(k) & \cdots & u(k-\mu+1) \end{bmatrix}^{\rm T}, \\
\phi_u(k) &\triangleq \begin{bmatrix} u(k-\mu) & \cdots & u(k-n_{\rm mod}-\mu+1) \end{bmatrix}^{\rm T}, \\
\phi_y(k) &\triangleq \begin{bmatrix} y(k-\mu) & \cdots & y(k-n_{\rm mod}-\mu+1) \end{bmatrix}^{\rm T}.
\end{aligned}
$$

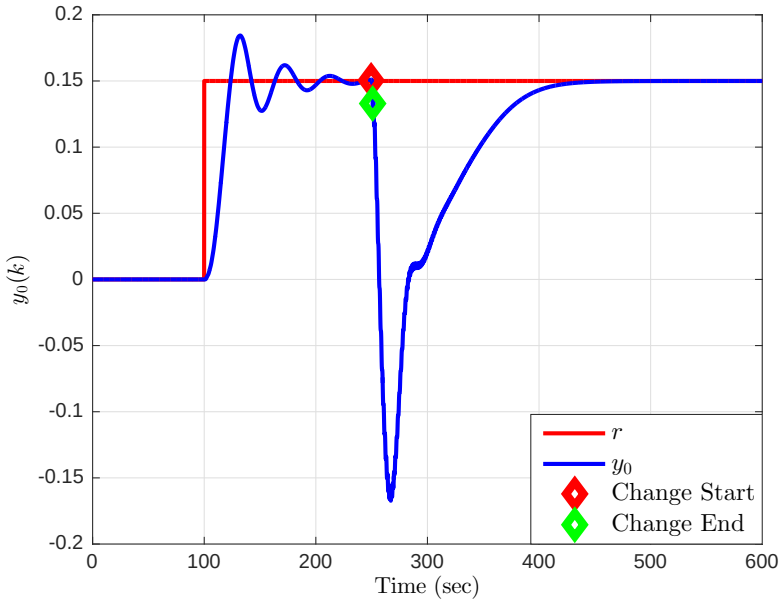

Figure 3.7: Example 3.2: Step command following using output feedback. We assume RCAC uses the NMP zero information. RCAC is able to follow the command throughout, and yields better performance than the full-state feedback case, with better minimum phase performance and quicker adaptation to NMP dynamics.

The least squares estimates $\hat{\theta}_{\mu,\ell}$, $\hat{\theta}_{u,\ell}$, $\hat{\theta}_{y,\ell}$ of θ_μ, θ_u, θ_y are given by

$$\begin{bmatrix} \hat{\theta}_{\mu,\ell} & \hat{\theta}_{u,\ell} & \hat{\theta}_{y,\ell} \end{bmatrix} = \underset{[\,\bar{\theta}_\mu \;\bar{\theta}_u \;\bar{\theta}_y\,]}{\operatorname{argmin}} \left\| \Psi_{y,\ell} - \bar{\theta}_\mu \Phi_{\mu,\ell} - \bar{\theta}_u \Phi_{u,\ell} + \bar{\theta}_y \Phi_{y,\ell} \right\|_{\mathrm{F}}, \tag{3.10}$$

where $\bar{\theta}_\mu, \bar{\theta}_u, \bar{\theta}_y$ are variables of appropriate size, $||\,.\,||_{\mathrm{F}}$ denotes the Frobenius norm,

$$\begin{aligned}
\Psi_{y,\ell} &\triangleq \begin{bmatrix} y(n_{\mathrm{mod}}+\mu-1) & \cdots & y(\ell) \end{bmatrix}, \\
\Phi_{\mu,\ell} &\triangleq \begin{bmatrix} \phi_\mu(n_{\mathrm{mod}}+\mu-1) & \cdots & \phi_\mu(\ell) \end{bmatrix}, \\
\Phi_{u,\ell} &\triangleq \begin{bmatrix} \phi_u(n_{\mathrm{mod}}+\mu-1) & \cdots & \phi_u(\ell) \end{bmatrix}, \\
\Phi_{y,\ell} &\triangleq \begin{bmatrix} \phi_y(n_{\mathrm{mod}}+\mu-1) & \cdots & \phi_y(\ell) \end{bmatrix},
\end{aligned}$$

and ℓ is the number of samples. Since the system is time-varying, in order to track the

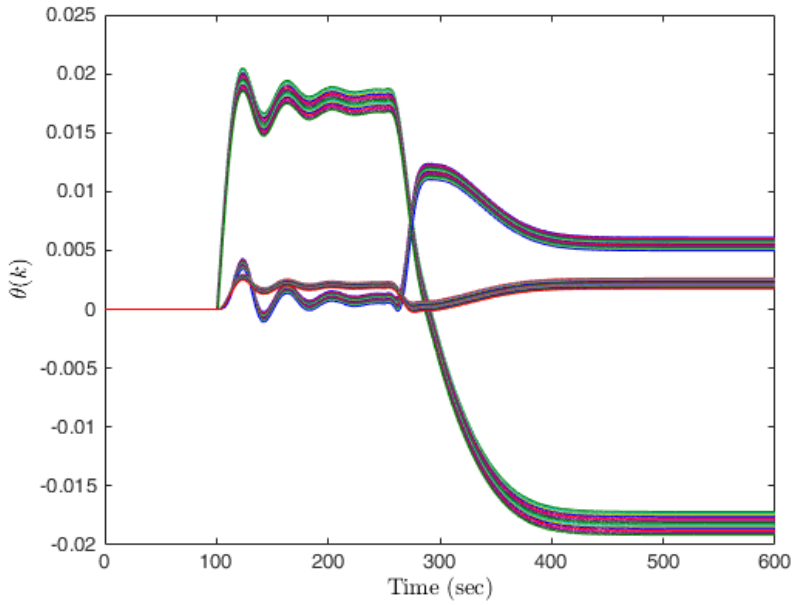

Figure 3.8: Example 3.2: Step command following using output feedback. We assume RCAC uses the NMP zero information. The controller coefficients converge before the transition, adapt and converge to different controller coefficients after the transition.

change in the parameters, a sliding window of 70 data points moving 70 steps at a time is used to obtain estimates of the Markov parameters. Once the Markov parameter estimates are obtained for a specific window, the eigensystem realization algorithm (ERA) [96] is applied to reconstruct the system from its Markov parameters. The ERA provides a state space realization, from which a transfer function representation is constructed to find the zeros of the system. Figure 3.9 shows a plot of the modulus of all zeros of the system versus time. Note that before $t = 250$ sec the lateral dynamics have three minimum phase zeros while after $t = 265$ sec the lateral dynamics have two NMP zeros, one of which is a sampling zero.

3.7 Conclusions

In this chapter, we used RCAC together with system identification to control aircraft lateral motion with an unknown transition to NMP dynamics. We considered

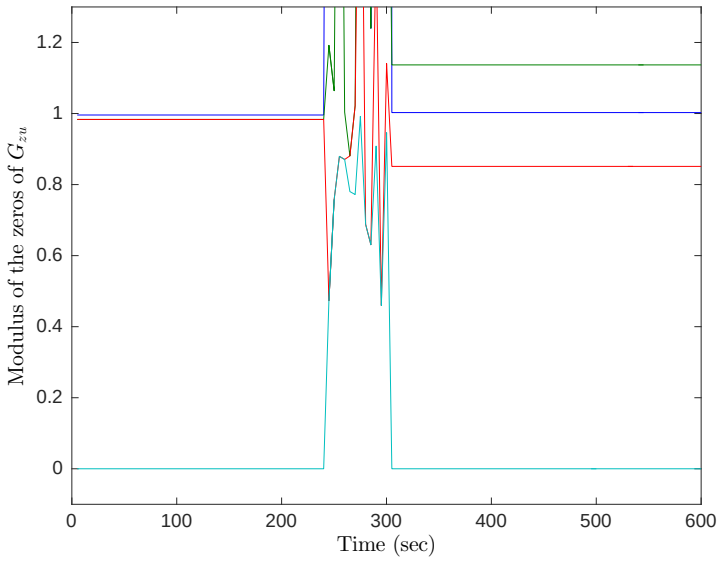

Figure 3.9: Modulus of the zeros of the identified system. A window of width of 7 seconds and moving 7 seconds at a time is used to perform the identification process. Note that before $t = 250$ sec the lateral dynamics have three minimum phase zeros while after approximately $t = 265$ sec the lateral dynamics have two NMP zeros. Note the abrupt change in the modulus of the identified zeros between $t = 250$ sec and $t = 265$ sec as the transition data enter the identification process.

both the full-state-feedback case with output-subspace zeros and the output feedback case with NMP zeros. Even in the case where NMP zeros exist and are unmodeled, RCAC did not cause instability. A μ-Markov model along with standard least squares was used to identify the Markov parameters of the system given input-output data obtained using a moving window of a specific size. Then, the ERA was used to obtain a realization of the system from its Markov parameters, and the NMP zero information was be used by RCAC. Future work will consist of improving the response and identification during the transition from minimum phase to nonminimum phase behavior.

3.8 Acknowledgment

I'd like to thank John Burken and Tim Cox for providing the lateral aircraft dynamics model and helpful discussions.

CHAPTER 4

Intercalated Injection and Target Model Construction

4.1 Introduction

The contents of this chapter and the following two chapters represent the key contributions of this dissertation. In its early development, RCAC was viewed as an optimization of a dynamic compensator, using past data to optimize the control effort to achieve an objective such as command following and/or disturbance rejection. To this effect, the filter G_{f} was viewed as a model of the open-loop system, representing the required modeling information. This chapter shows that in fact, RCAC updates the controller coefficient vector θ to minimize the residual between z and the output of G_{f} with input $\tilde{u}$. This added insight leads to the naming of G_{f} as the *target model*. This chapter and the following chapters discuss the construction of the target model G_{f}, and the modeling information required for the construction of the target model.

In addition, in this chapter, we also compare RCAC with discrete-time high-authority LQG, comparing the closed-loop frequency response and also the H_2 cost of RCAC and high-authority LQG. In particular, we show that by constructing the target model with the closed-loop denominator of high-authority LQG, RCAC can approximate the closed-loop frequency response and H_2 cost of LQG. However, note

that constructing the target model with this denominator requires knowledge of the open-loop poles and zeros. However, we also show that by using $n_c >> n$, RCAC approximates the closed-loop frequency response and H_2 cost of discrete-time LQG with minimal modeling information. Discrete-time high-authority LQG is discussed separately in Appendix A.

We illustrate these properties through eight examples. First, we use RCAC to approximate high-authority LQG for the adaptive standard problem with stochastic w. Next, for the adaptive servo problem, we use RCAC for command following and stochastic disturbance rejection, and show that RCAC approximates the closed-loop frequency response of high-authority LQG, apart from at the command frequency, where RCAC places an internal model. Next, we investigate the effect of sensor noise, and compare the performance and frequency response of RCAC to LQG in the case where sensor noise is present. Finally, we develop the IIR target model for pole placement, and use RCAC for adaptive pole placement for command following and disturbance rejection problems.

We use the developments of the intercalated transfer function and the IIR target model for pole placement in Chapter 5 for adaptive control of plants that are either difficult or even impossible to control using fixed gain control methods, and in Chapter 6 to enforce stability of the adaptive controller $G_{c,k}$ using Quasi-FIR controller structures, particularly in cases where high-authority LQG yields unstable controller designs. We also present a method for step command following for NMP plants, without knowledge of the NMP zeros.

4.2 Virtual External Control Perturbation

The target model G_f is a key feature of RCAC. In [36], G_f is viewed as a model of G_{zu} that captures the sign of the leading coefficient of N_{zu} along with the NMP zeros of G_{zu}. In [37], the analysis of RCAC involves an ideal filter $\bar{G}_f$, which is a closed-loop

transfer function involving an ideal feedback controller $\bar{G}_{\mathrm{c}}$. These insights lead to an alternative interpretation of G_{f} as a target model for a specific closed-loop transfer function. These properties are demonstrated below.

Using (2.29), the retrospective performance variable (2.36) can be written as

$$\hat{z}(k,\hat{\theta}) = z(k) - G_{\mathrm{f}}(\mathbf{q})[u(k) - \Phi(k)\hat{\theta}]. \tag{4.1}$$

It can be seen from (4.1) that minimizing the cumulative retrospective cost function (2.41) determines the controller coefficient vector $\hat{\theta}$ that best fits $G_{\mathrm{f}}(\mathbf{q})[u(k) - \Phi(k)\hat{\theta}]$ to the performance data $z(k)$. In terms of the optimal controller coefficient vector $\hat{\theta}^*$, (4.1) can be written as

$$\hat{z}(k,\hat{\theta}^*) = z(k) - G_{\mathrm{f}}(\mathbf{q})[u(k) - \Phi(k)\hat{\theta}^*]. \tag{4.2}$$

For convenience, we define

$$u^*(k) \triangleq \Phi(k)\hat{\theta}^*, \tag{4.3}$$

$$\tilde{u}(k) \triangleq u(k) - u^*(k), \tag{4.4}$$

so that

$$u(k) = u^*(k) + \tilde{u}(k). \tag{4.5}$$

With this notation, (4.2) can be written as

$$\hat{z}(k,\hat{\theta}^*) = z(k) - G_{\mathrm{f}}(\mathbf{q})\tilde{u}(k). \tag{4.6}$$

Using (4.5) to replace u in Φ by $u^* + \tilde{u}$, it follows from (2.28)–(2.30) and (4.3) that

u^* satisfies

$$u^*(k) = \sum_{i=1}^{n_c} P_i^* u^*(k-i) + \sum_{i=1}^{n_c} P_i^* \tilde{u}(k-i) + \sum_{i=k_c}^{n_c} Q_i^* y(k-i). \tag{4.7}$$

Note that the actual input to the plant at step k is $u(k)$. However, in (4.5), $u(k)$ is written as the sum of the *pseudo control input* $u^*(k)$ and the *virtual external control perturbation* $\tilde{u}(k)$. Note that the signals u^* and $\tilde{u}$ are not explicitly used by RCAC. From (4.7) it follows that

$$u^*(k) = D_c^{*-1}(\mathbf{q})[(\mathbf{q}^{n_c} I_{l_u} - D_c^*(\mathbf{q}))\tilde{u}(k) + N_c^*(\mathbf{q})y(k)], \tag{4.8}$$

where

$$D_c^*(\mathbf{q}) \triangleq \mathbf{q}^{n_c} I_{l_u} - \mathbf{q}^{n_c-1} P_1^* - \cdots - P_{n_c}^*, \tag{4.9}$$

$$N_c^*(\mathbf{q}) \triangleq \mathbf{q}^{n_c-k_c} Q_{k_c}^* + \cdots + Q_{n_c}^*, \tag{4.10}$$

$$G_c^* \triangleq D_c^{*-1} N_c^*. \tag{4.11}$$

Figures 4.1 and 4.2 are equivalent transfer function representations of (4.5) and (4.8) with $\tilde{u}$ represented as an external input. Figure 4.1 illustrates the intercalated injection of $\tilde{u}$ inside the control update.

It follows from (2.4), (2.5), (4.5), and (4.8) that

$$z(k) = G_{zw}(\mathbf{q})w(k) + G_{zu}(\mathbf{q})[D_c^{*-1}(\mathbf{q})[(\mathbf{q}^{n_c} I_{l_u} - D_c^*(\mathbf{q}))\tilde{u}(k) + N_c^*(\mathbf{q})y(k)] + \tilde{u}(k)], \tag{4.12}$$

$$y(k) = G_{yw}(\mathbf{q})w(k) + G_{yu}(\mathbf{q})[D_c^{*-1}(\mathbf{q})[(\mathbf{q}^{n_c} I_{l_u} - D_c^*(\mathbf{q}))\tilde{u}(k) + N_c^*(\mathbf{q})y(k)] + \tilde{u}(k)]. \tag{4.13}$$

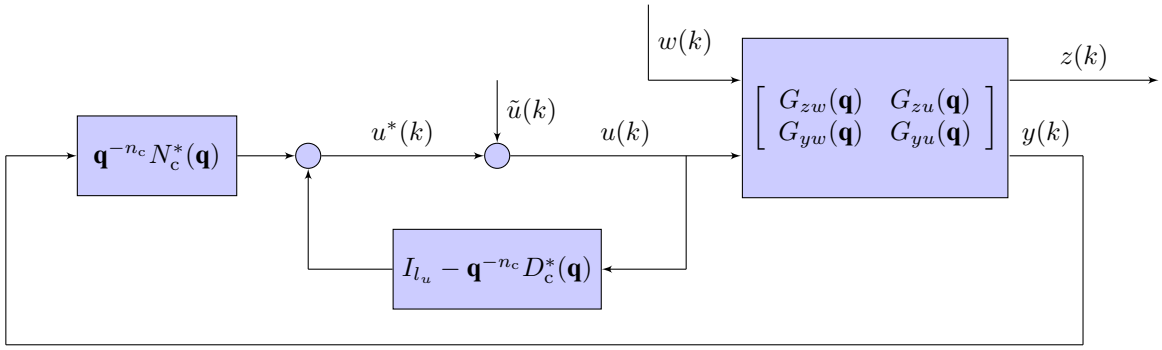

Figure 4.1: Transfer function representation of (4.5) and (4.8) with the virtual external control perturbation $\tilde{u}$ represented as an external input. The inner feedback loop represents (4.8) and illustrates the intercalated injection of $\tilde{u}$ inside the control update.

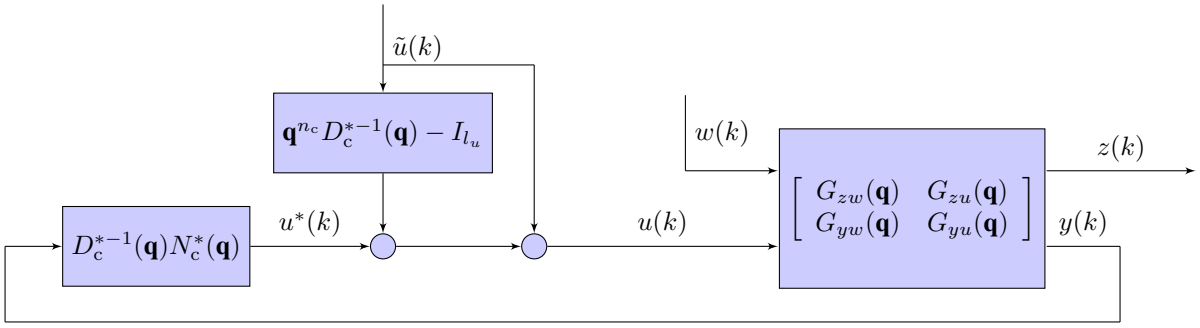

Figure 4.2: Equivalent transfer function representation of (4.5) and (4.8) with $\tilde{u}$ represented as an external input. In this representation, the inner feedback loop in Figure 4.1 is replaced by an equivalent prefilter.

Solving (4.13) for $y(k)$ and substituting $y(k)$ into (4.12) yields

$$z(k) = \widetilde{G}^*_{zw}(\mathbf{q})w(k) + \widetilde{G}^*_{z\tilde{u}}(\mathbf{q})\tilde{u}(k), \tag{4.14}$$

where $\widetilde{G}^*_{zw}$ is given by (2.9) with G_c replaced by G_c^*, that is,

$$\widetilde{G}^*_{zw} \triangleq G_{zw} + G_{zu}G_c^*(I - G_{yu}G_c^*)^{-1}G_{yw}, \tag{4.15}$$

and where

$$\widetilde{G}^*_{z\tilde{u}}(\mathbf{q}) \triangleq \mathbf{q}^{n_c}G_{zu}(\mathbf{q})[D_c^{*-1}(\mathbf{q}) + G_c^*(\mathbf{q})[I_{l_y} - G_{yu}(\mathbf{q})G_{c,}^*(\mathbf{q})]^{-1}G_{yu}(\mathbf{q})D_c^{*-1}(\mathbf{q})]. \tag{4.16}$$

Now assume that y, z, and u are scalar signals. Using the notation in (2.10), (4.16) can be written as

$$\widetilde{G}^*_{z\tilde{u}}(\mathbf{q}) = \frac{N_{zu}(\mathbf{q})\mathbf{q}^{n_c}}{D(\mathbf{q})D^*_c(\mathbf{q})} + \frac{N_{zu}(\mathbf{q})N^*_c(\mathbf{q})N_{yu}(\mathbf{q})\mathbf{q}^{n_c}}{D(\mathbf{q})D^*_c(\mathbf{q})[D(\mathbf{q})D^*_c(\mathbf{q}) - N_{yu}(\mathbf{q})N^*_c(\mathbf{q})]} \tag{4.17}$$

$$= \frac{N_{zu}(\mathbf{q})\mathbf{q}^{n_c}}{D(\mathbf{q})D^*_c(\mathbf{q}) - N_{yu}(\mathbf{q})N^*_c(\mathbf{q})}. \tag{4.18}$$

It can be seen from (4.6) that $\hat{z}(k, \hat{\theta}^*) = z(k) - G_f(\mathbf{q})\tilde{u}(k)$ is the residual of the fit between z and the output of the target model G_f with input $\tilde{u}$. However, it follows from (4.14) that $\widetilde{G}^*_{z\tilde{u}}$, whose coefficients are given by $\hat{\theta}^*$, is the actual transfer function from $\tilde{u}(k)$ to $z(k)$. Therefore, minimizing the retrospective cost function (2.41) yields the value $\theta(k+1) = \hat{\theta}^*$ of $\hat{\theta}$ and thus the controller $G_{c,k+1}$ that provides the best fit of $G_f(\mathbf{q})$ by the transfer function $\widetilde{G}_{z\tilde{u},k+1}$ from $\tilde{u}(k, \theta(k+1))$ to $z(k)$. In other words, RCAC determines $G_{c,k+1}$ so as to optimally fit $\widetilde{G}_{z\tilde{u},k+1}$ to $G_f(\mathbf{q})$.

The transfer function $\widetilde{G}_{z\tilde{u},k+1}$ is distinct from the transfer function $G_{z\bar{u},k}$ from an external control input perturbation $\bar{u}$ to the performance variable z with the loop closed, as shown in Figure 4.3. In the case where y, z, and u are scalar signals, this transfer function is given by

$$G_{z\bar{u},k} = \frac{N_{zu}D_{c,k}}{DD_{c,k} - N_{yu}N_{c,k}}. \tag{4.19}$$

The difference between (4.18) and (4.19) is the fact that (4.18) uses the fixed polynomial $\mathbf{q}^{n_c}$ in place of the time-varying polynomial $D_{c,k}$ in (4.19). This distinction implies that the only NMP zeros in (4.18) are those arising from G_{zu}, unlike (4.19), which includes "time-varying" zeros arising from $D_{c,k}$.

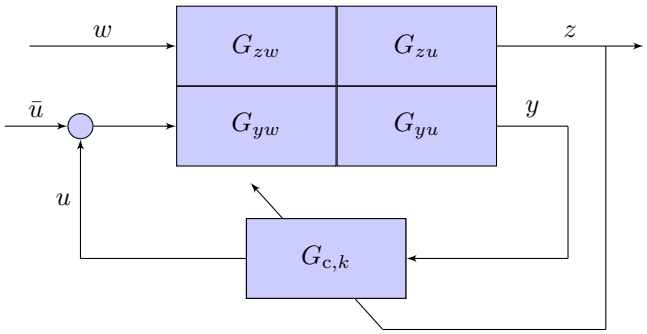

Figure 4.3: Adaptive standard problem with the external control perturbation $\bar{u}$ for defining $G_{z\bar{u},k}$.

4.3 Modeling Information Required for G_{f}

In this section, we use the development of the intercalated injection to present a rationale for the modeling information required by RCAC.

4.3.1 Relative Degree

Since $\widetilde{G}_{z\tilde{u},k+1}$ approximates G_{f}, it is advantageous to choose the relative degree of G_{f} to be equal to the relative degree of $\widetilde{G}_{z\tilde{u},k+1}$. It follows from (4.18) that the relative degree of $\widetilde{G}_{z\tilde{u},k+1}$ is equal to the relative degree of G_{zu}. We thus choose the relative degree of G_{f} to be equal to the relative degree of G_{zu}. This choice requires knowledge of the relative degree d_{zu} of G_{zu} [37].

4.3.2 NMP Zeros

In [37], the target model G_{f} is chosen such that the roots of N_{f} include the NMP zeros of G_{zu}. As can be seen from (4.18), a key feature of $\widetilde{G}_{z\tilde{u},k+1}$ is the factor N_{zu} in its numerator. This means that, since RCAC adapts $G_{\mathrm{c},k}$ so as to match $\widetilde{G}_{z\tilde{u},k+1}$ to G_{f}, RCAC may cancel NMP zeros of G_{zu} that are not included in the roots of N_{f} in order to remove them from $\widetilde{G}_{z\tilde{u},k+1}$. This observation motivates the need to include all of the roots of $N_{zu,\mathrm{u}}$ in N_{f}. As an aside, Example 4.6 shows that RCAC cancels all of the minimum-phase zeros of G_{zu} that are not included in the roots of N_{f} in order

to remove them from $\widetilde{G}_{z\tilde{u},k+1}$.

4.3.3 FIR Target Models

In the case where G_{zu} is minimum phase, we use the FIR target model (2.49). This choice of G_{f} requires knowledge of the relative degree d_{zu} of G_{zu} and the first nonzero Markov parameter $H_{\mathrm{d}_{zu}}$ of G_{zu}. Note that, for the adaptive servo problem, since $G_{zu} = -G_u$, it follows that $H_{\mathrm{d}_{zu}} = -H_{\mathrm{d}_u}$, where H_{d_u} is the first nonzero Markov parameter of G_u.

In the case where G_{zu} is NMP, we use FIR target model (2.50). This choice of G_{f} requires knowledge of the relative degree d_{zu} of G_{zu}, the first nonzero Markov parameter $H_{\mathrm{d}_{zu}}$ of G_{zu}, and the NMP zeros of G_{zu}. In both cases, the relative degree of G_{f} is equal to the relative degree of G_{zu}.

4.4 Adaptive Control with Stochastic w and d

We now apply RCAC to the adaptive standard problem in the case where the exogenous signal w is stochastic, as well as to the adaptive servo problem in the case where the disturbance d is stochastic. We also compare the closed-loop frequency response and the H_2 cost of RCAC with high-authority LQG, presented in the appendices.

4.4.1 H_2 Cost of Strictly Proper Controllers

For a plant (2.1)–(2.3), we can calculate the H_2 cost of an arbitrary stabilizing strictly proper controller $G_{\mathrm{c}} \sim \left[\begin{array}{c|c} A_{\mathrm{c}} & B_{\mathrm{c}} \\ \hline C_{\mathrm{c}} & 0 \end{array}\right]$ as follows. Defining

$$\widetilde{D} \triangleq \left[\begin{array}{c} D_1 \\ B_{\mathrm{c}} D_2 \end{array}\right], \quad \widetilde{V} = \widetilde{D}\widetilde{D}^{\mathrm{T}}, \tag{4.20}$$

the H_2 cost is given by

$$J(A_{\mathrm{c}}, B_{\mathrm{c}}, C_{\mathrm{c}}) = \mathrm{tr}(Q_1 R_1) + \mathrm{tr}(Q_2 C_{\mathrm{c}}^{\mathrm{T}} R_2 C_{\mathrm{c}}), \tag{4.21}$$

where $Q_1 \in \mathbb{R}^{n \times n}$, $Q_2 \in \mathbb{R}^{n_{\mathrm{c}} \times n_{\mathrm{c}}}$ satisfy

$$\widetilde{Q} = \left[\begin{array}{cc} Q_1 & Q_{12} \\ Q_{12}^{\mathrm{T}} & Q_2 \end{array} \right], \tag{4.22}$$

and $\widetilde{Q} \in \mathbb{R}^{n+n_{\mathrm{c}} \times n+n_{\mathrm{c}}}$ is the solution of the discrete-time Lyapunov equation

$$\widetilde{Q} = \widetilde{A} \widetilde{Q} \widetilde{A}^{\mathrm{T}} + \widetilde{V}, \tag{4.23}$$

where $\widetilde{A}$ is defined in (A.12).

4.4.2 High-Authority LQG Target Model

Since RCAC tends to match $\widetilde{G}_{z\tilde{u}}$ to G_{f}, we choose G_{f} with the numerator $N_{zu}(\mathbf{q})\mathbf{q}^{n_{\mathrm{c}}}$ and the closed-loop denominator of high-authority LQG $\widetilde{D}_{\mathrm{HA}}$ in order to construct the high-authority LQG target model

$$G_{\mathrm{f}}(\mathbf{q}) = \frac{N_{zu}(\mathbf{q})\mathbf{q}^{n_{\mathrm{c}}}}{\widetilde{D}_{\mathrm{HA}}(\mathbf{q})} = \frac{H_{\mathrm{d}_{zu}} \mathbf{q}^m N_{zu,\mathrm{u}}(\mathbf{q})}{N_{zu,\mathrm{u}}(\mathbf{q}^{-1}) N_{yw,\mathrm{s}}(\mathbf{q}) N_{yw,\mathrm{u}}(\mathbf{q}^{-1})}, \tag{4.24}$$

where $m \triangleq n_{\mathrm{c}} - \mathrm{d}_{zu} - \mathrm{d}_{yu}$. Note that m may be negative. The target model (4.24) is based on (A.17). By choosing (4.24), the goal is to compare the performance of RCAC with the performance of high-authority LQG in the case $n_{\mathrm{c}} = n$. Note that using (4.24) as the target model requires knowledge of $\widetilde{D}_{\mathrm{HA}}$ in addition to the modeling information required by (2.49) and (2.50). The use of (4.24) is thus only for conceptual illustration. Later, we use the FIR target models (2.49) and (2.50), but with $n_{\mathrm{c}} > n$.

4.4.3 Examples

In all examples in this section, unless specified otherwise, we set $R_\theta = 10^{-10} I_{l_\theta}$, $k_{\mathrm{w}} = 50$, and $R_u = 0$.

Example 4.1. Adaptive control with stochastic w for the adaptive standard problem. Consider the asymptotically stable plant

$$A = \begin{bmatrix} 0.855 & 1 & 0 & 0 & 0 \\ -0.1715 & 0.855 & -0.4266 & -0.3607 & 0.4952 \\ 0 & 0 & 0.5 & -0.5072 & 0.6964 \\ 0 & 0 & 0 & 0.6716 & 1 \\ 0 & 0 & 0 & -0.4514 & 0.6716 \end{bmatrix}, \tag{4.25}$$

$$B = \begin{bmatrix} 0 \\ 0 \\ 0 \\ 0 \\ 1 \end{bmatrix}, \quad D_1 = \begin{bmatrix} -0.6269 \\ 0.3985 \\ -0.3306 \\ 0.4415 \\ 0.3794 \end{bmatrix}, \tag{4.26}$$

$$C = [0.7298 \quad -0.3954 \quad -0.3605 \quad 0.4003 \quad 0.1447], \quad D_0 = 0, \quad D_2 = 0, \tag{4.27}$$

$$E_1 = [0.1717 \quad 0.3351 \quad -0.5294 \quad -0.4476 \quad 0.6145], \quad E_0 = 0, \quad E_2 = 0, \tag{4.28}$$

where G_{zu}, G_{zw}, G_{yu}, and G_{yw} are NMP. The H_2 cost of the LQG controller is 1.059. The exogenous signal w is zero-mean Gaussian white noise with standard deviation 0.1. We apply RCAC with $n_{\mathrm{c}} = n$, and we use the high-authority LQG target model (4.24). RCAC places the closed-loop poles near the high-authority LQG closed-loop poles and approximates the closed-loop frequency response of high-authority LQG, as shown in Figure 4.4. The H_2 cost of the RCAC controller is 1.0591.

Next, we show that, for sufficiently large $n_{\mathrm{c}} > n$, RCAC approximates the performance of the high-authority LQG controller using the FIR target model (2.50), which

uses knowledge of d_{zu}, $H_{\mathrm{d}_{zu}}$, and the NMP zeros of G_{zu}, but no other modeling data and no knowledge of $\widetilde{D}_{\mathrm{HA}}$. We apply RCAC with $n_{\mathrm{c}} = 4n = 20$. In this case RCAC approximates the closed-loop frequency response of high-authority LQG, as shown in Figure 4.5, and the H_2 cost of the RCAC controller is 1.061. ■

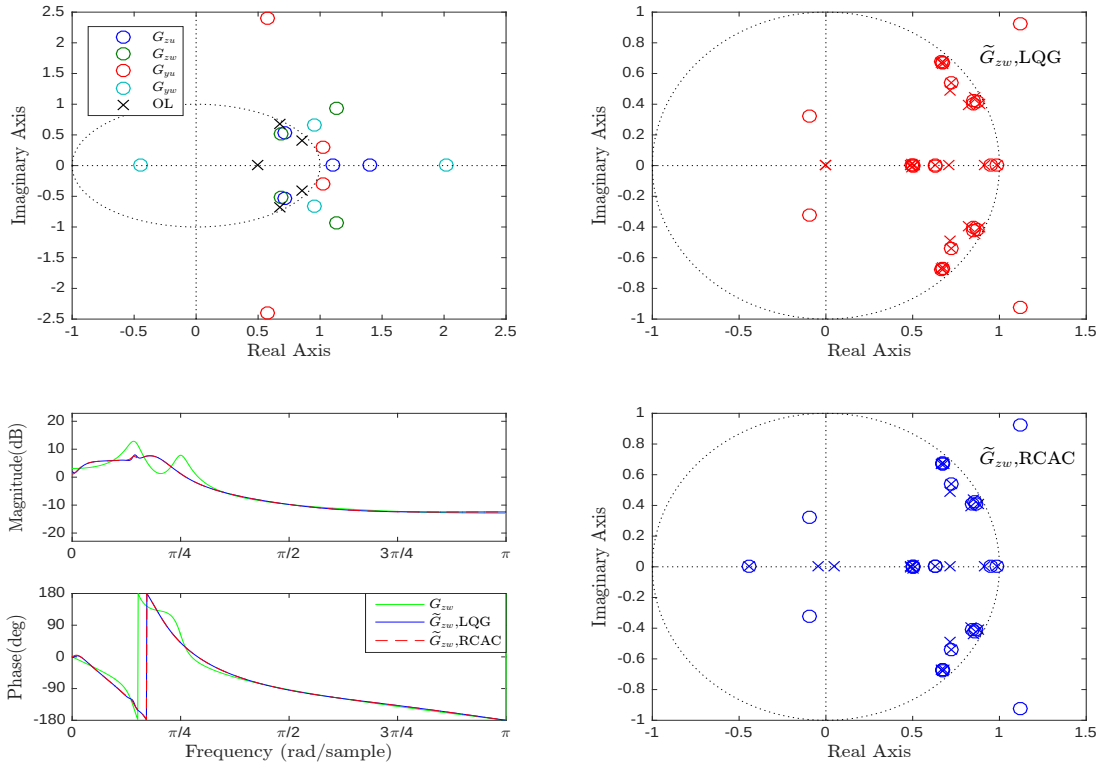

Figure 4.4: Example 4.1: Adaptive standard problem, with the high-authority LQG target model (4.24). RCAC places the closed-loop poles near the high-authority LQG closed-loop poles and approximates the closed-loop frequency response of high-authority LQG. The frequency-response plots and closed-loop poles and zeros are shown at step $k = 10^5$.

Example 4.2. Adaptive control with nonzero-mean, stochastic w for the adaptive standard problem. Consider the Lyapunov-stable, NMP plant

$$G(\mathbf{q}) = \frac{(\mathbf{q} - 0.5)(\mathbf{q}^2 - 1.92\mathbf{q} + 1.44)}{(\mathbf{q} - 1)(\mathbf{q} - 0.9)(\mathbf{q}^2 - 1.62\mathbf{q} + 0.81)}, \tag{4.29}$$

and let w be Gaussian white noise with mean 0.1 and standard deviation 0.05. The H_2 cost of the LQG controller is 28.96. We apply RCAC with $n_{\mathrm{c}} = 5n = 20$, and we use

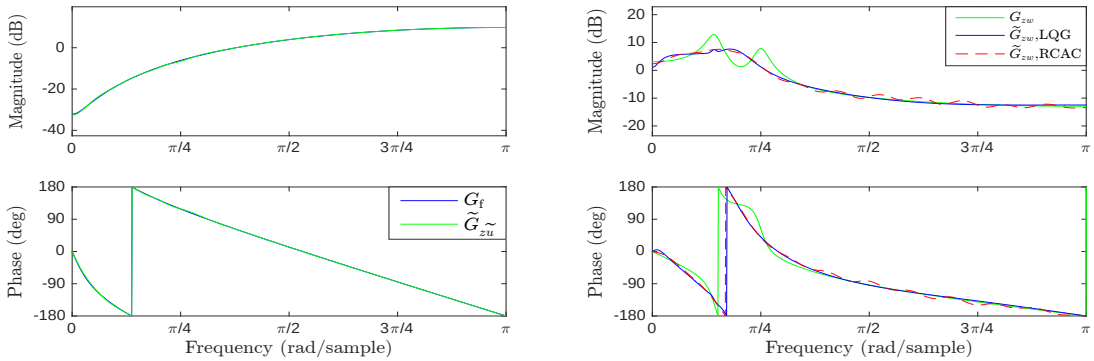

Figure 4.5: Example 4.1: Adaptive standard problem with $n_c = 20$. RCAC approximates the closed-loop frequency response of high-authority LQG. In addition, the frequency response of $\widetilde{G}_{z\tilde{u},k}$ approximates the frequency response of G_f. The frequency-response plots are shown at step $k = 10^5$.

the FIR target model (2.50), which uses no knowledge of $\widetilde{D}_{\mathrm{HA}}$. RCAC approximates the closed-loop frequency response of high-authority LQG except at DC due to the internal model needed to reject the nonzero-mean disturbance, which has the form of a notch at DC, as shown in Figure 4.6. Note that RCAC automatically develops the internal model in response to the disturbance bias. The H_2 cost of the RCAC controller is 35.79. ■

Example 4.3. Harmonic command following and stochastic disturbance rejection for the adaptive servo problem. Consider the asymptotically stable, minimum-phase plant

$$G(\mathbf{q}) = \frac{(\mathbf{q}^2 - 1.7\mathbf{q} + 0.785)(\mathbf{q}^2 - 1.4\mathbf{q} + 0.85)}{(\mathbf{q} - 0.5)(\mathbf{q}^2 - 1.8\mathbf{q} + 0.97)(\mathbf{q}^2 - 1.4\mathbf{q} + 0.98)}. \tag{4.30}$$

The H_2 cost of the LQG controller is 1.072. Let r be the harmonic command $r(k) = \cos \omega k$, where $\omega = 0.8$ rad/sample, let d be zero-mean Gaussian white noise with standard deviation 0.01, and let $v = 0$. We apply RCAC with $n_c = 8n = 40$, and we use the FIR target model (2.49), which uses no knowledge of $\widetilde{D}_{\mathrm{HA}}$. RCAC asymptotically follows the harmonic command and approximates the closed-loop frequency

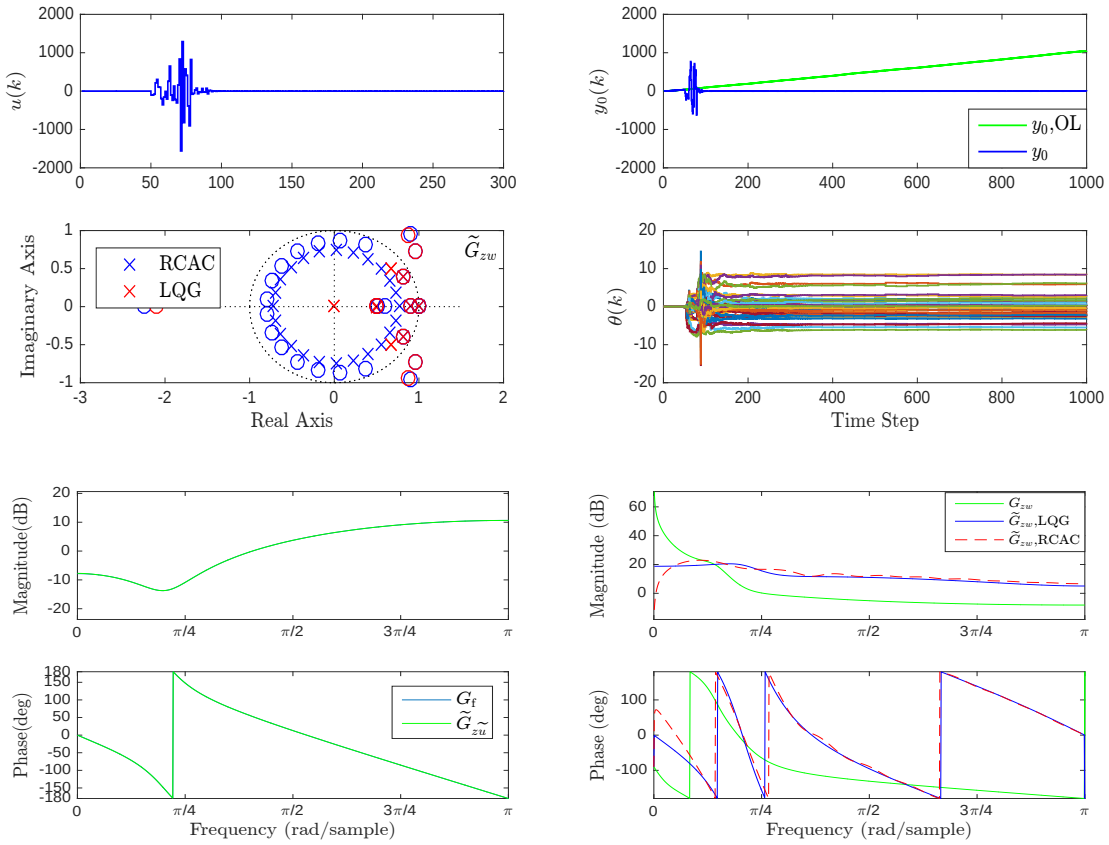

Figure 4.6: Example 4.2: Adaptive standard problem with $n_c = 5n = 20$. RCAC approximates the closed-loop frequency response of high-authority LQG except at DC due to the internal model needed to reject the step disturbance. The internal model has the form of a notch at DC corresponding to the closed-loop zero at 1. In addition, the frequency response of $\widetilde{G}_{z\tilde{u},k}$ approximates the frequency response of G_f. The frequency-response plots and closed-loop poles and zeros are shown at step $k = 10^5$.

response of high-authority LQG except at the command frequency due to the internal model of the command, which has the form of a notch at the command frequency, as shown in Figure 4.7. As in Example SD4.2, RCAC automatically develops an internal model in response to the harmonic command. The H_2 cost of the RCAC controller is 1.15. ■

Example 4.4. Stochastic disturbance rejection for the adaptive servo prob-

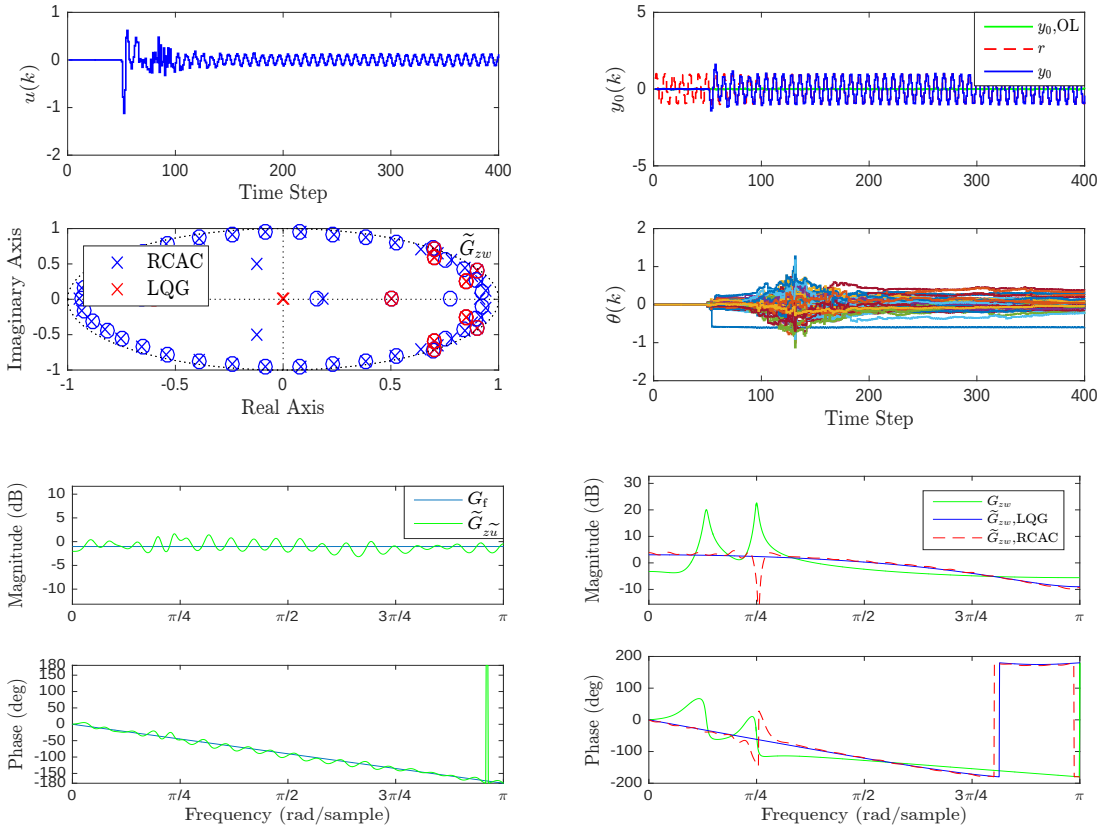

Figure 4.7: Example 4.3: Command following and stochastic disturbance rejection for the adaptive servo problem with $n_c = 8n = 40$. RCAC approximates the closed-loop frequency response of high-authority LQG except at the command frequency due to the internal model. The internal model has the form of a notch at the command frequency corresponding to the two closed-loop zeros on the unit circle. The frequency-response plots and closed-loop poles and zeros are shown at step $k = 10^5$.

lem with sensor noise. Consider the asymptotically stable, minimum-phase plant

$$A = \begin{bmatrix} 0.9 & 1 & 0 & 0 & 0 \\ 0 & 0.95 & -0.1507 & -0.1674 & 0.5189 \\ 0 & 0 & 0.65 & 1 & 0 \\ 0 & 0 & -0.4225 & 0.65 & 0.434 \\ 0 & 0 & 0 & 0 & 0.95 \end{bmatrix}, \quad B = D_1 = \begin{bmatrix} 0 \\ 0 \\ 0 \\ 0 \\ 1 \end{bmatrix}, \tag{4.31}$$

$$C = E_1 = [0.1596 \quad 0.3991 \quad -0.2405 \quad -0.2672 \quad 0.8283], \tag{4.32}$$

$$D_0 = E_0 = E_2 = 0, \quad D_2 = 1. \tag{4.33}$$

The H_2 cost of the LQG controller is 2.5437. Let d and v be zero-mean Gaussian white noise signals with standard deviation 1. We apply RCAC with $k_w = 50$, $R_\theta = 10^{-20} I_{l_\theta}$, $R_u = 0$, and $n_c = 4n = 20$, and we use the FIR target model (2.49). Instead of approximating the closed-loop frequency response of high-authority LQG, RCAC approximates the closed-loop frequency response of LQG in the presence of sensor noise, that is, the closed-loop frequency response of the LQG controller designed for the actual sensor noise level, namely, $V_2 = 1$, as shown in Figure 4.8. The H_2 cost of the RCAC controller is 2.5441. ■

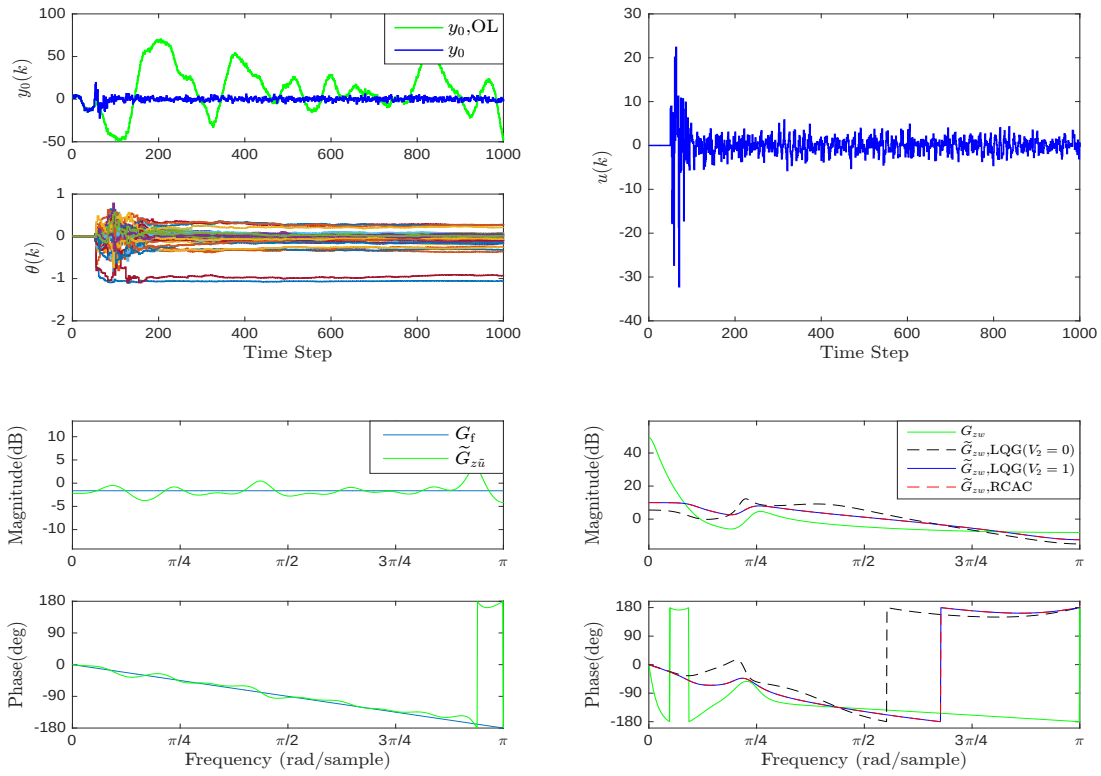

Figure 4.8: Example 4.4: Stochastic disturbance rejection for the adaptive servo problem with zero-mean Gaussian white sensor noise. RCAC approximates the closed-loop frequency response of LQG for $V_2 = 1$. In addition, the frequency response of $\widetilde{G}_{z\tilde{u},k}$ approximates the frequency response of G_f. The frequency-response plots are shown at step $k = 10^5$.

Example 4.5. Step command following and stochastic disturbance rejection for the adaptive servo problem with sensor noise. Consider the asymptotically

stable, minimum-phase plant

$$A = \begin{bmatrix} 0.8882 & 1 & 0 & 0 & 0 \\ -0.1715 & 0.8882 & -0.3624 & -0.3238 & 0.6679 \\ 0 & 0 & 0.693 & 1 & 0 \\ 0 & 0 & -0.4802 & 0.693 & 0.7276 \\ 0 & 0 & 0 & 0 & 0.5 \end{bmatrix}, \tag{4.34}$$

$$B = \begin{bmatrix} 0 \\ 0 \\ 0 \\ 0 \\ 1 \end{bmatrix}, \quad \bar{D}_1 = \begin{bmatrix} 0.5537 \\ 0.0603 \\ -0.5457 \\ 0.5596 \\ -0.2806 \end{bmatrix}, \tag{4.35}$$

$$\bar{C} = [0.2158 \quad 0.4234 \quad -0.3861 \quad -0.3449 \quad 0.7115]. \quad \bar{D}_0 = 0. \tag{4.36}$$

Let r be a unit step command, let d be zero-mean Gaussian white noise with standard deviation 0.05, and let v be zero-mean Gaussian white noise with standard deviation 0.025. In order to account for the standard deviation of the sensor noise, it follows from (2.26) that

$$V_2 = 0.025 D_2 D_2^{\mathrm{T}} = 0.025[1 \quad 0 \quad -1][1 \quad 0 \quad -1]^{\mathrm{T}} = 0.05. \tag{4.37}$$

We apply RCAC with $R_\theta = 10^{-10} I_{l_\theta}$, $R_u = 0$, and $n_{\mathrm{c}} = 8n = 40$, and we use the FIR target model (2.49). RCAC asymptotically follows the step command and approximates the closed-loop frequency response of LQG except at DC due to the internal model of the command, which has the form of a notch at DC, as shown in Figure 4.9. For this example, RCAC approximates the closed-loop frequency response of the LQG controller designed for the actual sensor noise level, namely, $V_2 = 0.05$.■

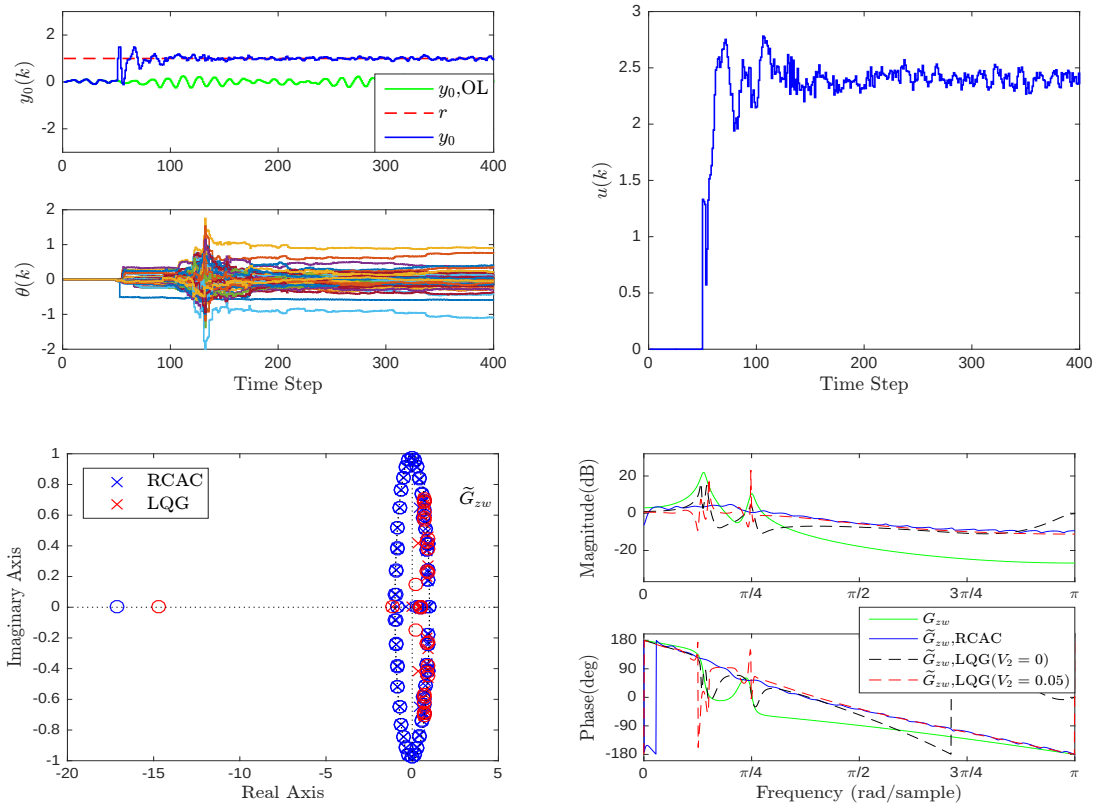

Figure 4.9: Example 4.5: Command following and stochastic disturbance rejection for the adaptive servo problem with zero-mean Gaussian white sensor noise. RCAC approximates the closed-loop frequency response of LQG for $V_2 = 2$ except at DC due to the internal model. The internal model has the form of a notch at DC corresponding to the closed-loop zero at 1. This example suggests that RCAC approximates the closed-loop frequency response of LQG in the presence of sensor noise. The frequency-response plots and closed-loop poles and zeros are shown at step $k = 10^5$.

The examples in this section show that, as $G_{\mathrm{c},k}$ adapts, the frequency response of $\widetilde{G}_{z\tilde{u}}$ tends to the frequency response of G_{f}. It is also shown that, for sufficiently large $n_{\mathrm{c}} > n$, the and H_2 cost of the RCAC controller approximates the H_2 cost of high-authority LQG, and the frequency response of the closed-loop transfer function $\widetilde{G}_{zw}$ obtained from RCAC with the FIR target models (2.49) and (2.50) approximates the closed-loop frequency response of high-authority LQG.

4.5 Adaptive Pole Placement

In this section, we consider adaptive pole placement for the adaptive standard problem and the adaptive servo problem using RCAC. We begin by defining IIR target models for pole placement.

4.5.1 IIR Target Model for Pole Placement

Since $\widetilde{G}_{z\tilde{u}}$ approximates G_{f}, RCAC attempts to place the poles of $\widetilde{G}_{z\tilde{u}}$ at the locations of the poles of G_{f}. It can be seen from (2.11) and (4.18) that the denominator of $\widetilde{G}_{z\tilde{u}}$ is equal to the denominator of the closed-loop transfer function $\widetilde{G}_{zw}$. Consequently, RCAC attempts to place the closed-loop poles at the locations of the poles of G_{f}. In order to use G_{f} for pole placement, let D_{p} be a monic polynomial of degree n_{p} whose roots are the desired closed-loop pole locations. Then, in the case where G_{zu} is minimum phase, we define the IIR target model

$$G_{\mathrm{f}}(\mathbf{q}) \triangleq \frac{H_{\mathrm{d}_{zu}}\mathbf{q}^{n_{\mathrm{p}}-\mathrm{d}_{zu}}}{D_{\mathrm{p}}(\mathbf{q})}, \tag{4.38}$$

and, in the case where G_{zu} is NMP, we define the IIR target model

$$G_{\mathrm{f}}(\mathbf{q}) \triangleq \frac{H_{\mathrm{d}_{zu}}\mathbf{q}^{n_{\mathrm{p}}-\mathrm{d}_{zu}-\deg(N_{zu,\mathrm{u}})}N_{zu,\mathrm{u}}(\mathbf{q})}{D_{\mathrm{p}}(\mathbf{q})}. \tag{4.39}$$

The target models (2.49) and (4.38) for minimum-phase G_{zu} along with the target models (2.50) and (4.39) for NMP G_{zu} represent the modeling information required by RCAC.

In the case where $n_{\mathrm{p}} < n + n_{\mathrm{c}}$, RCAC attempts to place n_{p} closed- loop poles at the locations of the poles of G_{f}. The remaining $n+n_{\mathrm{c}}-n_{\mathrm{p}}$ closed-loop poles are placed at either the locations of the minimum-phase zeros of G_{zu} that are not included in the roots of N_{f} or at zero.

Example 4.6. Pole placement for the adaptive servo problem. Consider the unstable, minimum-phase plant

$$G(\mathbf{q}) = \frac{\mathbf{q}^2 - 1.4\mathbf{q} + 0.85}{(\mathbf{q} - 1.05)(\mathbf{q}^2 - 1.6\mathbf{q} + 0.89)}. \tag{4.40}$$

Let r be a unit step command, and let $d = v = 0$. To place five closed-loop poles at $0.3, 0.4, 0.6$, and $\pm 0.1\jmath$, we use the IIR target model (4.38) with

$$D_{\mathrm{p}}(\mathbf{q}) = (\mathbf{q} - 0.3)(\mathbf{q} - 0.4)(\mathbf{q} - 0.6)(\mathbf{q}^2 + 0.01), \tag{4.41}$$

and set $R_\theta = 10^{-20} I_{l_\theta}$, $R_u = 0$, and $n_{\mathrm{c}} = 4$. RCAC asymptotically follows the step command and places five closed-loop poles near the locations of the roots of D_{p}, as shown in Figure 4.10. Note that the remaining two closed-loop poles cancel the minimum-phase zeros of G, which are not included in the target model (4.38).

Next, we set $R_\theta = 10^{-40} I_{l_\theta}$. Figure 4.11 shows the locations of the closed-loop poles. Note that RCAC places the closed-loop poles closer to the target locations as R_θ is decreased and thus $P(0)$ is increased. ■

Example 4.7. Pole placement for the adaptive standard problem with $y = z$ and with w matched with u. Consider the asymptotically stable, minimum-phase plant

$$G(\mathbf{q}) = \frac{\mathbf{q}^2 - 1.44\mathbf{q} + 0.81}{(\mathbf{q} - 0.9)(\mathbf{q}^2 - 1.71\mathbf{q} + 0.903)}. \tag{4.42}$$

Let w be a unit step. We apply RCAC with $k_{\mathrm{w}} = 50$, $R_\theta = 10^{-10} I_{l_\theta}$, $R_u = 0$, and $n_{\mathrm{c}} = 4$. To place four closed-loop poles at ± 0.5 and $\pm 0.8\jmath$, we use the IIR target

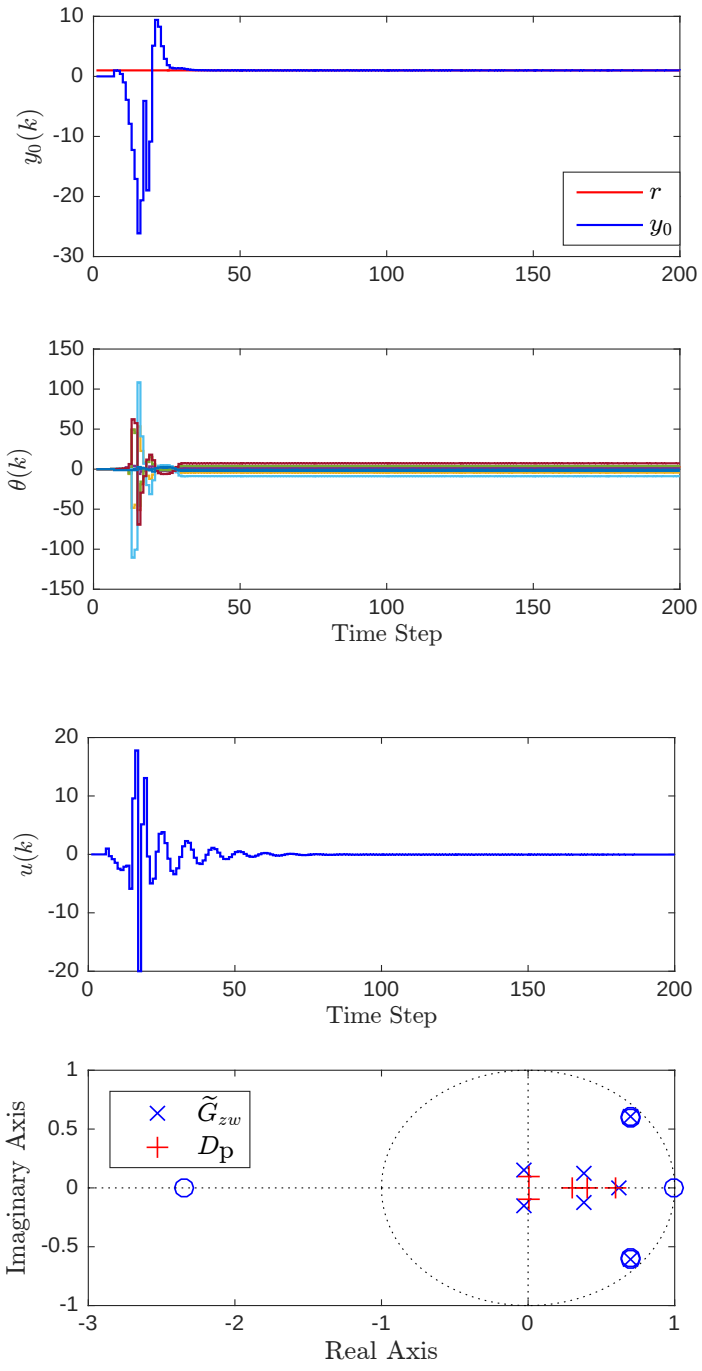

Figure 4.10: Example PP4.6: Pole placement for the adaptive servo problem. We apply RCAC with $R_\theta = 10^{-20} I_{l_\theta}$. RCAC places five closed-loop poles near the locations of the roots of $D_{\rm p}$. The closed-loop poles and zeros are shown at step $k = 100$.

model (4.38) with

$$D_{\rm p}(\mathbf{q}) = (\mathbf{q} - 0.5)(\mathbf{q} + 0.5)(\mathbf{q}^2 + 0.64). \tag{4.43}$$

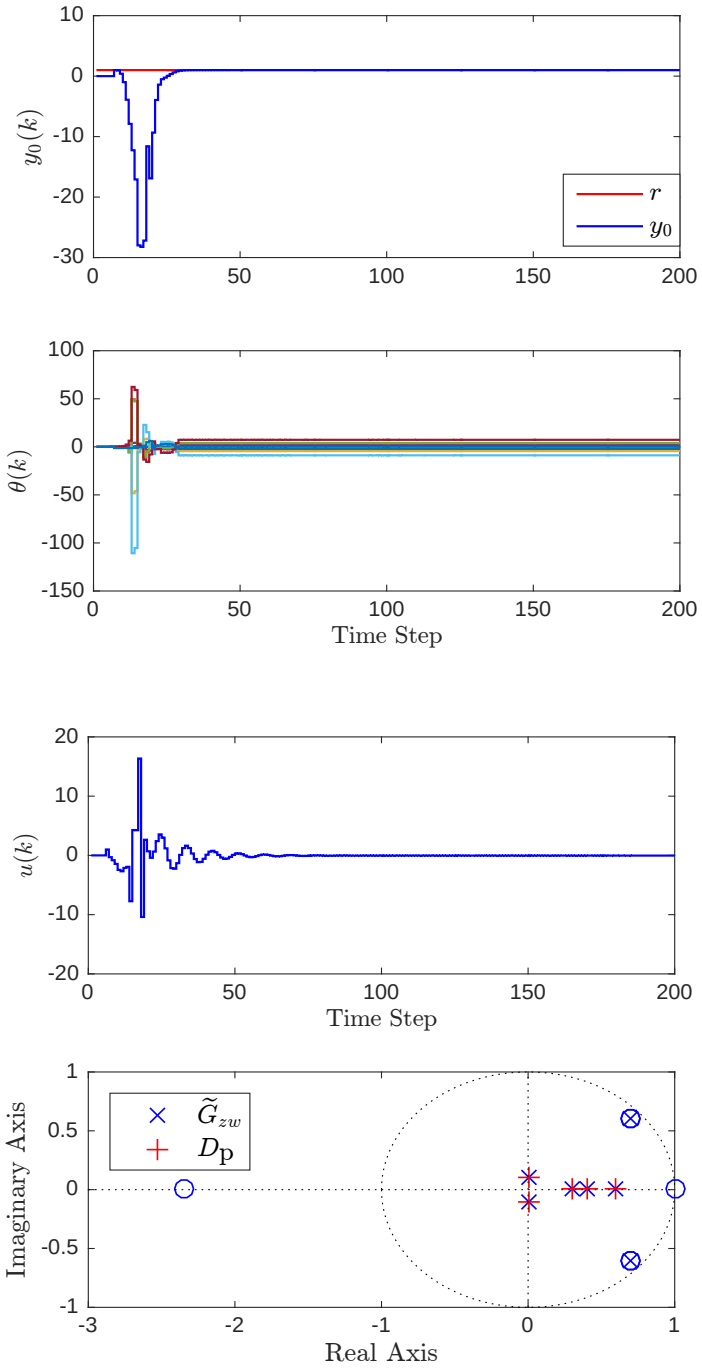

Figure 4.11: Example 4.6: Pole placement for the adaptive servo problem. We apply RCAC with $R_\theta = 10^{-40} I_{l_\theta}$. Note that RCAC places the closed-loop poles closer to the target locations as R_θ is decreased.

RCAC places four closed-loop poles near the locations of the roots of D_{p}, as shown in Figure 4.12. Note that two closed-loop two poles cancel the minimum-phase zeros of G, and the single unassigned closed-loop pole converges to 0. ■

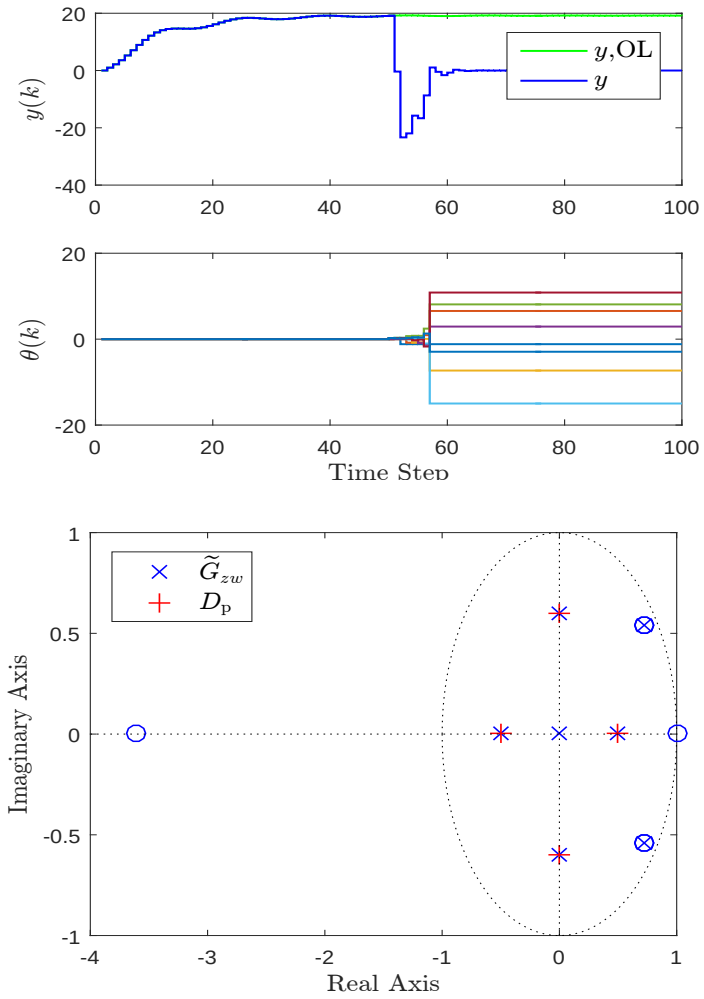

Figure 4.12: Example 4.7: Pole placement for the adaptive standard problem. RCAC places four closed-loop poles near the locations of the roots of D_{p}. The single unassigned closed-loop pole converges to 0. The closed-loop poles and zeros are shown at step $k = 100$.

Example 4.8. Pole placement for the adaptive standard problem. Consider the unstable, NMP plant

$$G(\mathbf{q}) = \frac{\mathbf{q} - 1.2}{(\mathbf{q} - 1.1)(\mathbf{q} - 2)}. \tag{4.44}$$

Let w be a unit step. We apply RCAC with $R_\theta = 10^{-40} I_{l_\theta}$, $R_u = 0$, and $n_{\mathrm{c}} = 3$. To place five closed-loop poles at $0.1, 0.3, 0.5$, and $\pm 0.3\jmath$, we use the IIR target model

(4.39) with

$$D_{\mathrm{p}}(\mathbf{q}) = (\mathbf{q} - 0.1)(\mathbf{q} - 0.3)(\mathbf{q} - 0.5)(\mathbf{q}^2 + 0.09). \tag{4.45}$$

Note that the unstable zero of (4.44) lies between the two unstable poles. It follows from root locus analysis and the parity interlacing property [97] that stabilization of (4.44) requires that the controller be unstable [14]. RCAC places five closed-loop poles near the locations of the roots of D_{p}, as shown in Figure 4.13. As expected, $G_{\mathrm{c},k}$ converges to an unstable controller. ■

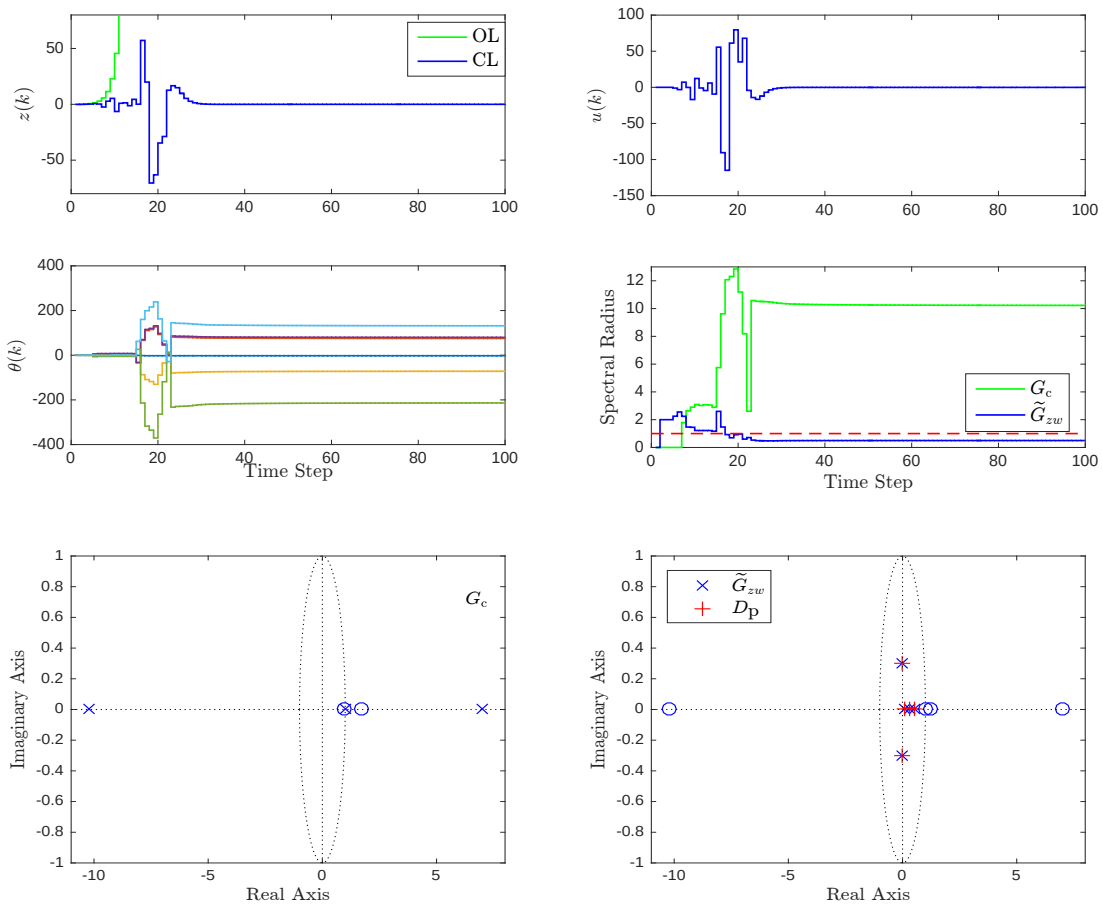

Figure 4.13: Example 4.8: Pole placement for the adaptive standard problem. RCAC places five closed-loop poles near the locations of the roots of D_{p}. Note that the controller becomes unstable after a few steps, and the closed-loop system is stabilized at step $k = 20$. The closed-loop poles and zeros are shown at step $k = 100$.

4.6 Conclusions

In this chapter, we demonstrated that retrospective cost optimization updates the controller coefficients so as to match the intercalated closed-loop transfer function $\widetilde{G}_{z\tilde{u},k}$ to a target model G_{f}. It was shown that $\widetilde{G}_{z\tilde{u},k}$ is the transfer function from the virtual external controller perturbation $\tilde{u}$ to the performance variable z. The special nature of $\widetilde{G}_{z\tilde{u},k}$ is due to the fact that $\tilde{u}$ enters the feedback loop through intercalated injection, which means that $\tilde{u}$ is injected internally to the controller as opposed to simply being added to the control input.

The target model G_{f} is selected by the user, and the choice of G_{f} is guided by its role in the controller adaptation. In particular, since RCAC tends to match $\widetilde{G}_{z\tilde{u},k}$ to the target model and, since the target model possesses the NMP zeros of G_{zu}, the NMP zeros must be reproduced in the target model; otherwise, RCAC may cancel them, resulting in a hidden instability. This modeling information, along with the relative degree of G_{zu} and its leading numerator coefficient, constitutes the basic modeling information required by RCAC. These statements apply to the case where G_{zu} is SISO.

The role of the target model was examined from various angles. First, it was shown that, in the absence of sensor noise and control weighting R_u, RCAC tends to match the closed-loop frequency response of the high-authority LQG controller. This connection is surprising in view of the fact that RCAC uses extremely limited modeling information relative to LQG. In effect, RCAC uses data to compensate for missing or erroneous modeling information. Next, it was shown that for command-following applications in the presence of stochastic disturbances, RCAC matches the closed-loop frequency response of LQG, except at the command frequency, where RCAC places an internal model. Finally, it was shown that in the presence of sensor noise, RCAC approximates the closed-loop frequency response of the LQG controller designed for the actual sensor noise level, without any knowledge of the noise characteristics.

In addition to matching closed-loop properties of the LQG controller, we show that RCAC can be used for adaptive pole placement by choosing the poles of the target model as the desired closed-loop spectrum. We show that in order to match $\widetilde{G}_{z\tilde{u},k}$ to G_{f}, RCAC places closed-loop poles at the locations of the poles of G_{f}.

CHAPTER 5

Adaptive Control of Plants That Are Practically Impossible to Control by Fixed-Gain Control Laws

5.1 Introduction

Feedback control presents numerous challenges due to dimensionality, uncertainty, nonlinearity, state and control constraints, MIMO coupling, delays, disturbances, and noise. Even in the SISO, LTI case, some plants are inherently difficult to control due to unstable open-loop poles, NMP zeros, high relative degree, and time delays. These properties limit the achievable gain and phase margins, thus undermining robust stability and performance [98]. For example, the analysis in [2] shows that the arrangement of the plant poles and zeros constrains the controller bandwidth and the achievable delay margin. These limitations severely limit the feasibility of implementing a feedback control law with the given sensors and actuators. Although robust and adaptive control can account for plant uncertainty, the above limitations apply to all LTI plants under LTI control.

For adaptive control, plants that are inherently difficult to control pose an especially troublesome challenge as explained in [99]:

> Control engineers grounded in classical control know it is possible to formulate control design problems which in practical terms are not possible to solve. An inverted pendulum with more than two rods is a well-known example; again, a plant with nonminimum phase zeros well inside the passband and unstable poles may be near impossible to control, unless additional inputs or outputs are used; another famous example was provided in [1] and so on. When the plant is initially known, as well as the control objective, it will generally become clear at some point in the design process, if not ab initio, that the control objective is impractical.
>
> Now what happens in adaptive control? The catch is that a full description of the plant is lacking. There may be no way to decide on the basis of the a priori information that the projected design task is or is not practical. So what will happen if an adaptive control algorithm is run in such a case? At the least, the algorithm will not converge. At worst, an unstable closed loop will be established.

This chapter is motivated by these concerns. In particular, we consider a collection of plants with severely limited achievable gain and phase margin. We apply RCAC to each plant, and then we allow the adaptive controller to converge. Once convergence is reached, we determine the gain and phase margin of the closed-loop system. We then introduce a destabilizing perturbation that exceeds either the gain margin or the phase margin. The objective is to determine whether or not RCAC can re-adapt in such a way as to compensate for the loss of margin and restabilize the closed-loop system without manual retuning. Since these plants are inherently difficult to control, it is of interest to determine whether or not restabilization is possible and, if so, assess the severity of the transient response.

We consider several examples. The first example entails an unmodeled change in the static gain, and the next two examples consider unmodeled time delays. Next, we consider a plant with an unmodeled change in the NMP zeros. Finally, we consider discrete-time versions of the well-known examples from [1] and [2].

5.2 Examples

Example 5.1. Unmodeled change in the static gain for the adaptive standard problem. Consider the asymptotically stable, NMP plant

$$G(\mathbf{q}) = \frac{(\mathbf{q}^2 - 1.7\mathbf{q} + 0.785)(\mathbf{q}^2 - 1.4\mathbf{q} + 0.85)}{(\mathbf{q} - 0.5)(\mathbf{q}^2 - 1.8\mathbf{q} + 0.97)(\mathbf{q}^2 - 1.4\mathbf{q} + 0.98)}, \tag{5.1}$$

and let w be zero-mean Gaussian white noise with standard deviation $\sigma = 0.01$. We set $n_{\mathrm{c}} = 10$, $R_\theta = 10^{-5} I_{l_\theta}$, and we use the FIR target model (2.50). Figure 5.1 shows that RCAC approximates the closed-loop frequency response of high-authority LQG. At step $k = 5000$, the closed-loop system has a gain margin of 1.81 at the phase crossover frequency $\omega_{\mathrm{pco}} = 0$ rad/sample. At step $k = 5000$, the nominal plant G is replaced by $2.9G$. If G_{c} is fixed to be $G_{\mathrm{c},5000}$, then the closed-loop system becomes unstable. However, under adaptation, the plant is restabilized, and RCAC approximates the closed-loop frequency response of LQG for the modified plant, as shown in Figure 5.1. ■

Example 5.2. Unmodeled time delay for the adaptive servo problem. Consider the asymptotically stable, minimum-phase plant $G = G_{\mathrm{TD}} G_0$, where

$$G_{\mathrm{TD}}(\mathbf{q}) \triangleq \mathbf{q}^{-k_{\mathrm{d}}}, \quad G_0(\mathbf{q}) = \frac{\mathbf{q} - 0.95}{(\mathbf{q} - 0.85)(\mathbf{q}^2 - 1.6\mathbf{q} + 0.89)}, \tag{5.2}$$

and G_{TD} represents an unmodeled time delay of k_{d} steps. Let r be the harmonic command $r(k) = \cos \omega k$, where $\omega = 0.35$ rad/sample, and let $d = v = 0$. We set $R_\theta = 0.03 I_{l_\theta}$, $R_u = e_0^2$, and $n_{\mathrm{c}} = 10$. Since G_{TD} is unmodeled, we use the FIR target model (2.49) based on G_0. Figure 5.2 shows the command-following error e_0 for $k_{\mathrm{d}} = 1$, $k_{\mathrm{d}} = 2$, $k_{\mathrm{d}} = 3$, and $k_{\mathrm{d}} = 4$. RCAC follows the harmonic command in each case, despite the unmodeled time delays. For this example, RCAC is robust to

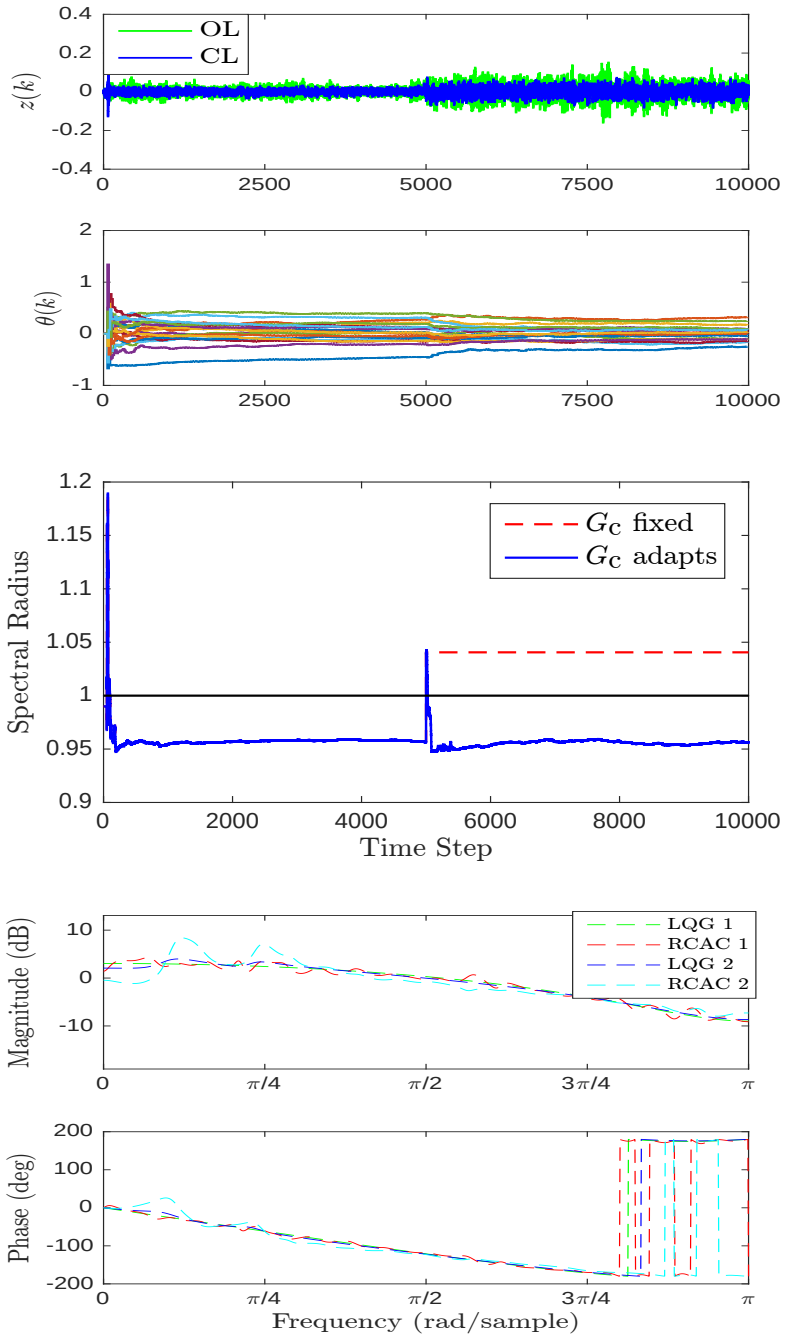

Figure 5.1: Example 5.1: Unmodeled change in the static gain for the adaptive standard problem. At step $k = 5000$, the gain margin is 1.81, and G is replaced by $2.9G$. If G_c is fixed to be $G_{c,5000}$, then the closed-loop system becomes unstable. However, under adaptation, the plant is restabilized.

unmodeled delays of upto 6 steps. In the next example, we consider unmodeled time delays during operation. ■

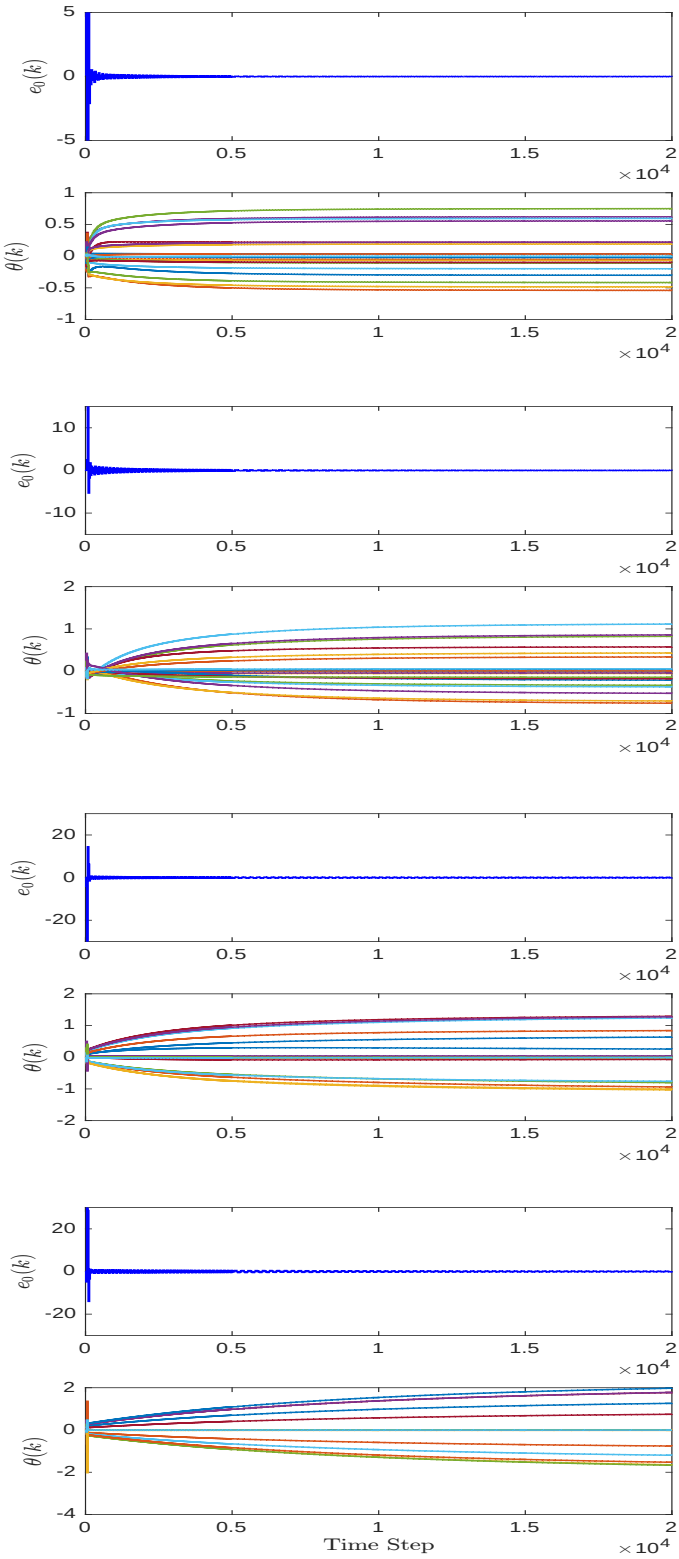

Figure 5.2: Example 5.2: Unmodeled time delay for the adaptive servo problem. For $k_\mathrm{d} = 1$ (top), $k_\mathrm{d} = 2$ (second), $k_\mathrm{d} = 3$ (third), and $k_\mathrm{d} = 4$ (bottom), RCAC follows the harmonic command, despite the unmodeled time delays.

Example 5.3. Unmodeled time-varying time delay for the adaptive servo problem. Consider the asymptotically stable, minimum-phase plant

$$G(\mathbf{q}) = \frac{\mathbf{q} - 0.9}{(\mathbf{q} - 0.95)(\mathbf{q}^2 - 1.6\mathbf{q} + 0.89)}. \tag{5.3}$$

Let r be the harmonic command $r(k) = \cos \omega k$, where $\omega = 0.5$ rad/sample, and let $d = v = 0$. We use the FIR target model (2.49), and set $n_c = 15$, $R_\theta = 0.1 I_{l_\theta}$, and $R_u = 0.1 e_0^2$. At step $k = 15000$, a 1-step delay is introduced into the closed-loop system. At step $k = 30000$, an additional 2-step delay is introduced, and at step $k = 60000$, an additional 6-step delay is introduced. Table 5.1 shows the magnitude crossover frequency ω_{mco}, the phase margin PM, and the delay margin DM prior to the insertion of additional delays. Note that each delay exceeds the delay margin. In each case, RCAC re-adapts and restabilizes the closed-loop system, as shown in Figure 5.3. After the third delay, RCAC restabilizes the system at step $k = 100000$ (not shown).■

k	ω_{mco} (rad/sample)	PM (deg)	DM (steps)
15000	1.8872	19.0799	0.1765
30000	1.4003	86.1123	1.0733
60000	0.5742	181.7065	5.5233

Table 5.1: Example 5.3: Unmodeled time-varying time delay for the adaptive servo problem. Magnitude crossover frequency, phase margin, and delay margin prior to inserting additional delays.

Example 5.4. Unmodeled change in NMP zeros for the adaptive standard problem. Consider the asymptotically stable, NMP plant

$$G(\mathbf{q}) = \frac{(\mathbf{q} - 0.5)(\mathbf{q}^2 - 1.92\mathbf{q} + 1.44)}{(\mathbf{q} - 0.35)(\mathbf{q} - 0.6)(\mathbf{q}^2 - 0.8\mathbf{q} + 0.32)}, \tag{5.4}$$

and let w be zero-mean Gaussian white noise with standard deviation $\sigma = 0.01$. We set $n_c = 4$, $R_\theta = 10^{-5} I_{l_\theta}$, $R_u = 0.1 z^2$, and we use the IIR target model (4.39)

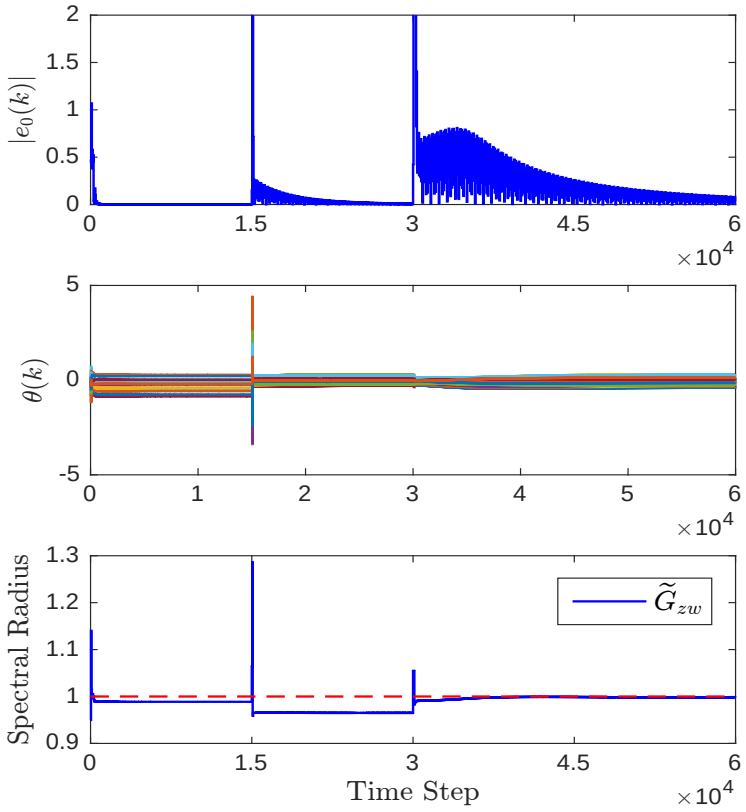

Figure 5.3: Example 5.3: Unmodeled time-varying time delay for the adaptive servo problem. At step $k = 15000$, a 1-step delay is introduced into the closed-loop system. At step $k = 30000$, an additional 2-step delay is introduced, and at step $k = 60000$, an additional 6-step delay is introduced. With G_c fixed, each delay is destabilizing. In each case, RCAC re-adapts and restabilizes the closed-loop system

with $D_p(\mathbf{q})$ chosen to contain the closed-loop poles of high-authority LQG. RCAC approximates the closed-loop frequency response of high-authority LQG. At step $k = 5000$, the NMP zeros move from $0.96 \pm 0.72\jmath$ to $0.99 \pm 1.38\jmath$. If G_c is fixed to be $G_{c,5000}$, then Figure 5.4 shows that the closed-loop system becomes unstable. However, under adaptation, the plant is restabilized, and RCAC approximates the closed-loop frequency response of LQG for the modified plant, as shown in Figure 5.4. ■

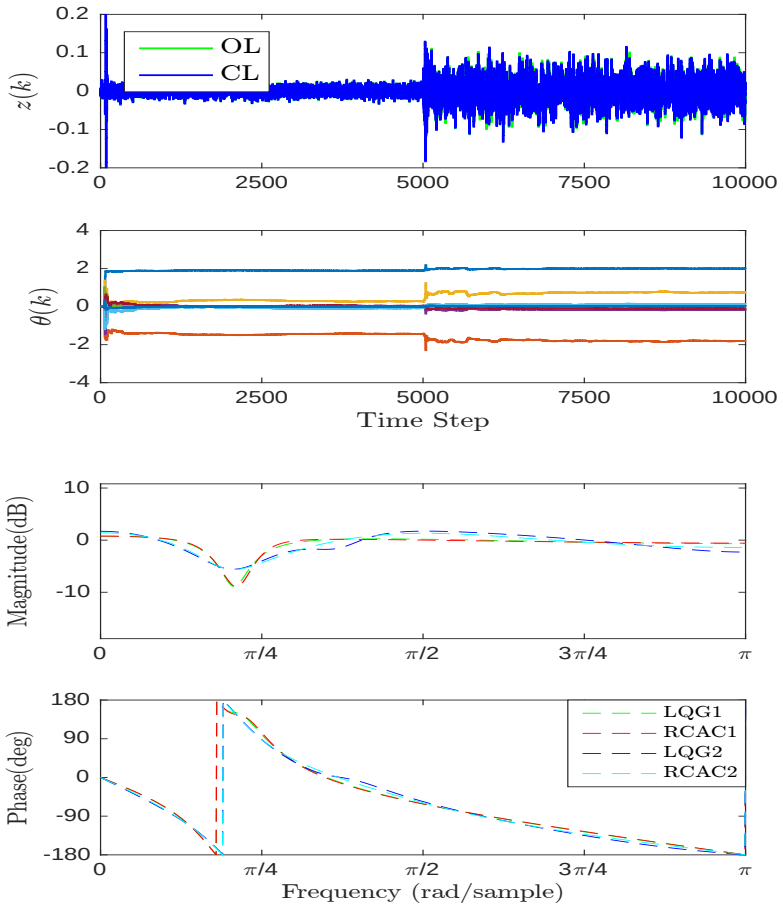

Figure 5.4: Example 5.4: Unmodeled change in NMP zeros for the adaptive standard problem. At step $k = 5000$, the NMP zeros move to $0.99 \pm 1.38\jmath$. If G_c is fixed to be $G_{c,5000}$, then the closed-loop system becomes unstable (not shown). However, under adaptation, the plant is restabilized.

Example 5.5. Severely limited gain margin for the adaptive standard problem. Consider the unstable, minimum-phase, continuous-time plant from [1] given by

$$A = \begin{bmatrix} 1 & 1 \\ 0 & 1 \end{bmatrix}, \quad B = \begin{bmatrix} 0 \\ 1 \end{bmatrix}, \quad D_1 = \begin{bmatrix} 1 \\ 1 \end{bmatrix}, \tag{5.5}$$

$$C = E_1 = \begin{bmatrix} 1 & 1 \end{bmatrix}, \quad D_2 = 1. \tag{5.6}$$

For the standard problem, we discretize (5.5) and (5.6) with a sampling period of 0.01 sec. Figure 5.5 shows that RCAC approximates the closed-loop frequency response of

high-authority LQG. The LQG controller yields a gain margin of 0.04, and the RCAC controller yields a gain margin of 0.0034. At step $k = 10000$, the nominal plant G is replaced by $1.1G$. If G_{c} is fixed to be $G_{\mathrm{c},10000}$, then the closed-loop system becomes unstable. However, under adaptation, the plant is restabilized, as shown by Figure 5.5. ■

Example 5.6. Limited delay margin for the adaptive standard problem. Consider the unstable, minimum-phase, continuous-time plant from [2] given by

$$A = \begin{bmatrix} -0.08 & -0.03 & 0.2 \\ 0.2 & -0.04 & -0.005 \\ -0.06 & 0.2 & -0.07 \end{bmatrix}, \tag{5.7}$$

$$B = \begin{bmatrix} -0.1 \\ -0.2 \\ 0.1 \end{bmatrix}, \quad C = E_1 = \begin{bmatrix} 0 & -1 & 0 \end{bmatrix}. \tag{5.8}$$

This plant has an unstable pole at 0.1081. It is shown in [2] that the maximum achievable delay margin for the plant is 18.51 sec. For the standard problem, we discretize (5.7) and (5.8) with a sampling period of 0.1 sec. Using the controller given by (23) in [2], and discretizing with a sampling period of 0.1 sec, the delay margin of the discrete-time closed-loop system is 6.07 steps.

Next, we use RCAC with the adaptive standard problem in order to stabilize (5.7) and (5.8). We apply RCAC with $R_\theta = 100I_{l_\theta}$, $R_u = 0.1z^2$, and $n_{\mathrm{c}} = 3$, and we use the FIR target model (2.49). The delay margin of the closed-loop system at step $k = 3000$ using RCAC is 0.31 steps, as shown by Table 5.2. Figure 5.6 shows the closed-loop responses for the initial condition $x(0) = [0.1\ 0.1\ 0.1]^{\mathrm{T}}$ for both the controller given by [2] and RCAC discretized with the sampling period $h = 0.1$ sec. Note that the controller given by [2], designed to achieve the maximum delay margin,

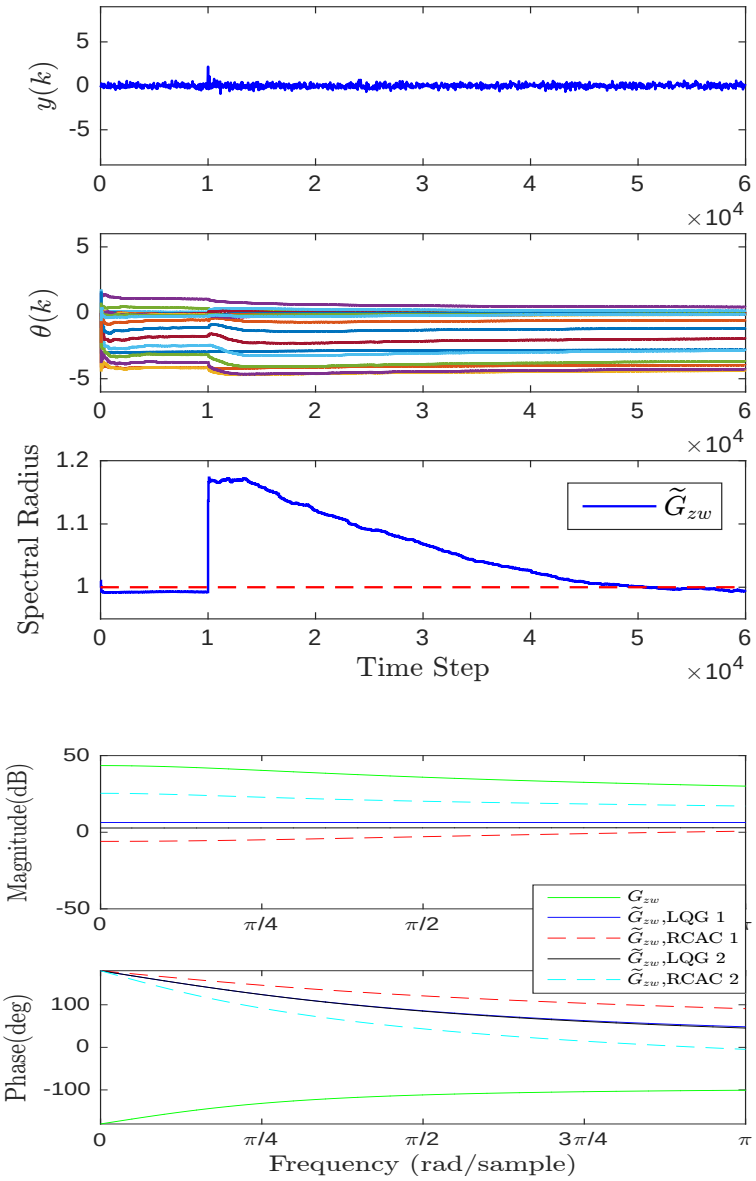

Figure 5.5: Example 5.5: Severely limited gain margin for the adaptive standard problem [1]. At step $k = 10000$, the gain margin is 0.0034, and the nominal plant G is replaced by $1.1G$. If G_c is fixed to be $G_{c,10000}$, then the closed-loop system becomes unstable. However, under adaptation, the plant is restabilized.

has poor transient response compared to RCAC. At step $k = 3000$, an unmodeled 7-step time delay is inserted into the loop, which destabilizes both closed-loop systems. Under continued adaptation and a prolonged transient response, RCAC restabilizes the closed-loop system at time step $k = 11800$. ■

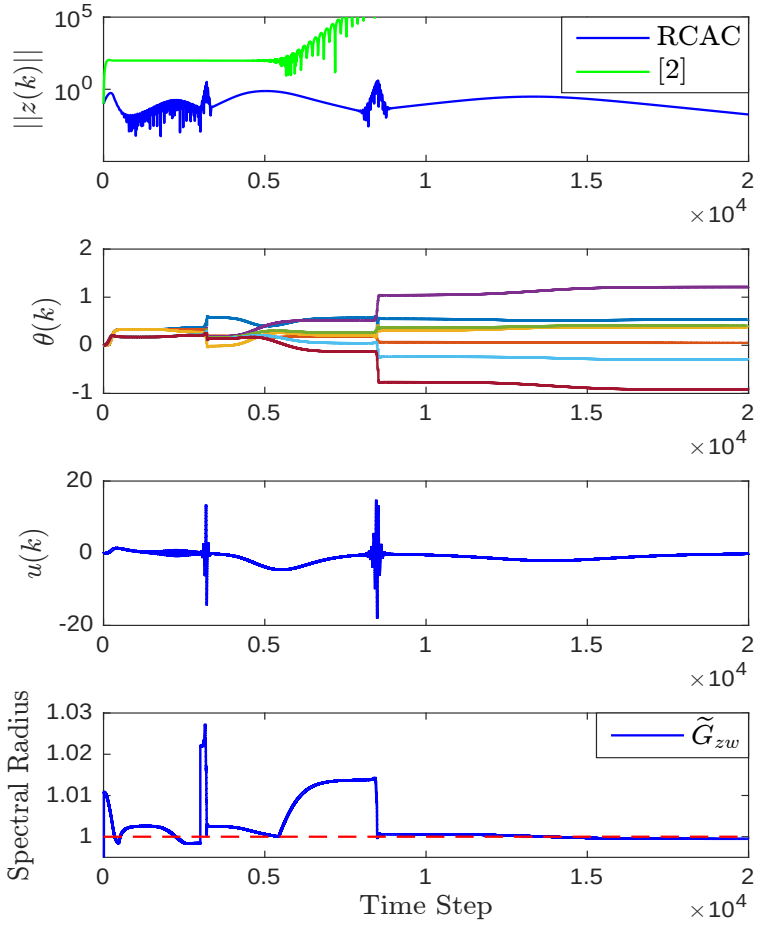

Figure 5.6: Example 5.6: Limited delay margin for the adaptive standard problem. Closed-loop responses for the initial condition $x(0) = [0.1\ 0.1\ 0.1]^{\mathrm{T}}$ for both the controller given by [2] and RCAC. Note that the controller given by [2], designed to achieve the maximum delay margin, has poor transient response compared to RCAC. At step $k = 3000$, a 7-step delay is introduced into the system, which destabilizes both closed-loop systems. However, RCAC re-adapts and restabilizes the closed-loop system.

Controller	ω_{mco} (rad/sec)	PM (deg)	DM (steps)
[2]	0.3708	129.12	6.07
RCAC	2.1834	38.83	0.31

Table 5.2: Margins for the controller from [2] and RCAC at step $k = 3000$.

5.3 Conclusions

In this chapter, we applied RCAC to a collection of examples involving plants that are practically impossible to control using fixed-gain controllers due to extremely small gain and phase margins. Plants of this type are viewed in [99] as potentially problematic for adaptive control as well. At convergence, the closed-loop systems possessed small gain or phase margin, as expected, and thus the insertion of additional gain or time delay caused instability. However, with continued adaptation using RCAC, it was shown that RCAC was able to re-adapt and restabilize the plant. The recoverable range of perturbation was assessed numerically. Future research will focus on deriving analytical bounds for recoverability.

CHAPTER 6

Adaptive Control Using Quasi-FIR Asymptotically Stable Controllers

6.1 Introduction

It is a well-known but unfortunate fact of feedback control that H_2-optimal and H_∞-optimal dynamic control laws are often unstable. Unstable controllers are undesirable for multiple reasons: they are difficult to start up; they are more susceptible to the adverse effects of saturation; and momentary disconnection from the plant due to delays or data loss can lead to divergence [100]. As discussed in [97, 101], some unstable plants can be stabilized only by unstable controllers; such plants are pathologically difficult to control but, fortunately, are rare in practice. We considered such a plant in Example 4.8, but such plants are outside the scope of this chapter. If the optimal controller is unstable, then all asymptotically stable controllers are necessarily suboptimal; the problem then is to determine the performance tradeoff due to the restriction to asymptotically stable controllers.

In some cases, it may be possible to obtain asymptotically stable H_2- and H_∞-suboptimal control laws by adjusting the weights of the cost function, but such techniques are ad hoc with no guarantee of success. In addition, by modifying the weights, the resulting controller is suboptimal for the original weights. More systematic tech-

niques have been developed [102–105], but these techniques add computational complexity to H_2 and H_∞ controller synthesis.

In this chapter, we focus on the problem of obtaining asymptotically stable controllers within the context of RCAC. As shown in [78], RCAC with full-order controllers mimics high-gain LQG controllers and can place poles based on the choice of the target model. Consequently, the adaptive controller may converge to an unstable controller. The goal of this chapter is to apply RCAC with a restricted class of controllers in order to avoid convergence to unstable controllers.

There are various ad hoc techniques that can be used to enforce asymptotic stability of the controller. For example, if the updated controller $G_{c,k}$ is unstable, then $G_{c,k}$ can be modified by replacing each unstable pole by its reflection inside the unit circle. Unfortunately, this requires computation at each step of all of the controller poles as well as the construction of the modified controller. More seriously, numerical experiments show that this approach can destabilize the closed-loop system. A more rigorous approach would be to update the controller subject to a stability constraint; however, this constraint is not convex and thus is computationally expensive.

The approach taken in this chapter is to adapt FIR or quasi-FIR control laws, that is, control laws all or most of whose poles are fixed at the origin. A related approach is developed in [106], where the motivation for sparse controllers is based on computational complexity and accuracy rather than controller stability. For a quasi-FIR controller comprising of the product of an FIR component and a low-order IIR component, the low-order IIR component provides the ability to adaptively develop an internal model or to facilitate pole placement. Although the IIR component can become unstable during adaptation, we reflect the unstable poles at each step in order to enforce controller stability.

We use qausi-FIR control laws for two objectives. First, we attempt to obtain near optimal controllers that are asymptotically stable in the case where the high-

authority LQG controller is unstable. Secondly, we use a quasi-FIR control law to perform command following for NMP plants without knowledge of the NMP zero.

6.2 Stochastic Disturbance Rejection

6.2.1 Quasi-FIR compensator

As an alternative to the IIR compensator (2.28), we consider the quasi-FIR compensator

$$u(k) = \sum_{i=1}^{2} P_i(k)u(k-i) + \sum_{i=1}^{n_c} Q_i(k)y(k-i). \tag{6.1}$$

The compensator (6.1) has at most two nonzero poles as well as $n_c - 2$ poles fixed at zero. At each step k, if either of the two free poles is unstable, then we reflect the pole to its reciprocal inside the unit disk. This technique relocates at most two poles, whereas, for the IIR controller, as many as n_c poles may need to be reflected within the unit disk. We use (6.1) to obtain asymptotically stable controllers in the case where the high-authority LQG controller is unstable.

6.2.2 Pole Reflection

In order to enforce asymptotic stability of the controller, we apply a reflection technique. In particular, if the updated controller $G_{c,k}$ is unstable, then $G_{c,k}$ is modified by replacing each unstable pole by its reciprocal inside the unit disk. For an IIR controller of order n_c, all of the poles may need to be reflected. However, in the next section we consider controllers all or most of whose poles are fixed inside the open unit disk. In this case, only a small number of controller poles may require reflection in order to enforce controller stability.

Example 6.1. Broadband Disturbance rejection for a NMP plant using an IIR controller. Consider the Lyapunov-stable, NMP plant

$$G(\mathbf{q}) = \frac{(\mathbf{q} - 0.8)(\mathbf{q} - 1.1)}{(\mathbf{q} - 0.5)(\mathbf{q}^2 - 1.9\mathbf{q} + 1)}, \tag{6.2}$$

and let w be zero-mean Gaussian white noise with standard deviation 0.01. For this plant, the high-authority LQG controller is unstable, with a pole at 1.0025. The H_2 cost of the LQG controller is 1.4798. Next, we apply RCAC with an IIR controller structure and the FIR target model (2.50) with $n_c = 5n$, $R_\theta = 0.5I_{l_\theta}$, and $R_u = 0$. The RCAC controller has an unstable pole at 1.002 and the H_2 cost is 1.4945. Figure 6.1 shows the closed-loop response and the closed-loop frequency response. Note that the closed-loop frequency response of the converged RCAC controller, which is unstable, approximates the closed-loop frequency response of the unstable high-authority LQG controller. ■

Example 6.2. Broadband Disturbance rejection for a minimum-phase plant using a quasi-FIR controller. Consider the Lyapunov-stable, minimum-phase plant

$$G(\mathbf{q}) = \frac{\mathbf{q}^2 - 1.52\mathbf{q} + 0.9025}{(\mathbf{q} - 0.85)(\mathbf{q}^2 - 1.8\mathbf{q} + 1)}, \tag{6.3}$$

and let w be zero-mean Gaussian white noise with standard deviation 0.01. For this plant, the high-authority LQG controller is unstable, with a pole at 1.13. The H_2 cost for the LQG controller is 1.7252. We apply RCAC with the quasi-FIR structure given by (6.1) and with the FIR target model (2.49) with $n_c = 50$, $R_\theta = 0.1I_{l_\theta}$, and $R_u = 0$. The RCAC controller is asymptotically stable, and the H_2 cost is 2.3717. Figure 6.2 shows the closed-loop response of z as well as the closed-loop frequency response. Note that the closed-loop frequency response of the converged RCAC controller, which is

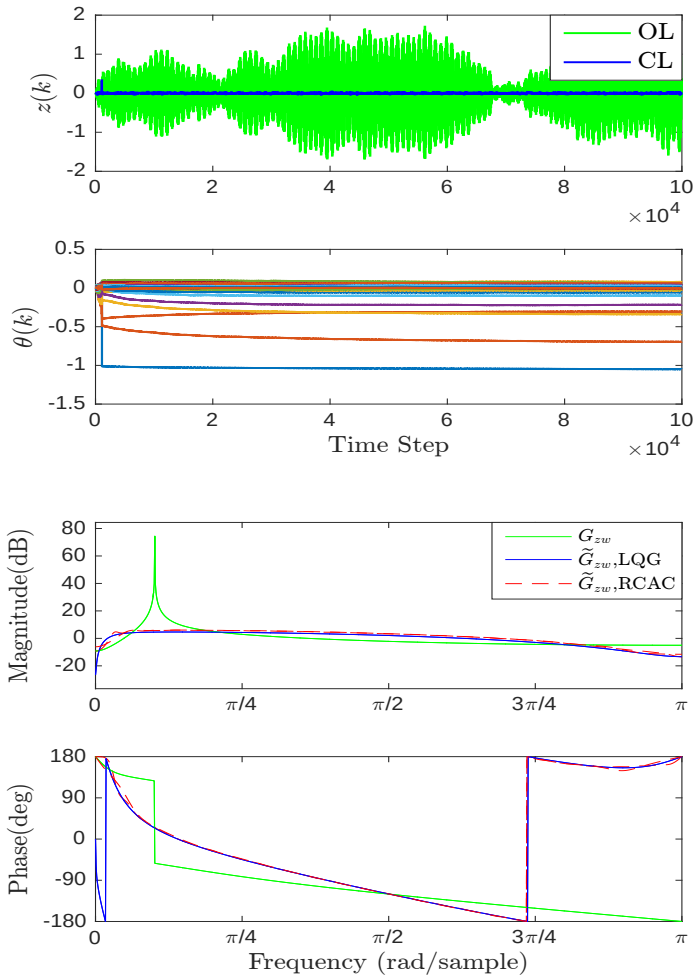

Figure 6.1: Example 6.1: Broadband disturbance rejection for the NMP plant (6.2) using the IIR controller structure (2.28). RCAC approximates the closed-loop frequency response of the high-authority LQG controller. The frequency-response plots are shown at step $k = 10^5$. However, RCAC converges to an unstable controller (not shown).

asymptotically stable, approximates the closed-loop frequency response of the unstable high-authority LQG controller. ■

Example 6.3. Broadband disturbance rejection for a NMP plant using a quasi-FIR controller. We reconsider the Lyapunov-stable, NMP plant (6.2), and apply RCAC with the quasi-FIR controller given by (6.1) and with the FIR target model (2.50) with $n_c = 50$, $R_\theta = 0.5 I_{l_\theta}$, and $R_u = 0$. The RCAC controller is asymptotically stable, and the H_2 cost is 1.4849, compared to the H_2 cost of 1.4798

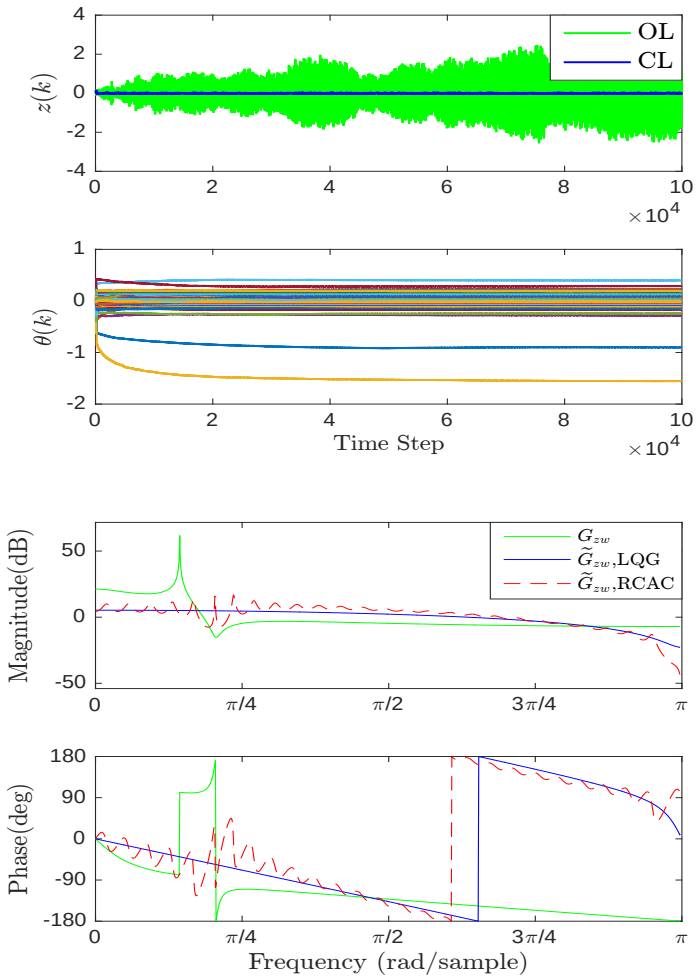

Figure 6.2: Example 6.2: Broadband disturbance rejection for the minimum-phase plant (6.3) using the quasi-FIR controller structure (6.1). RCAC approximates the closed-loop frequency response of the high-authority LQG controller. The frequency-response plots are shown at step $k = 10^5$.

of the unstable LQG controller. Figure 6.3 shows the closed-loop response and the closed-loop frequency response. Note that the closed-loop frequency response of the converged RCAC controller, which is asymptotically stable, approximates the closed-loop frequency response of the unstable high-authority LQG controller. ■

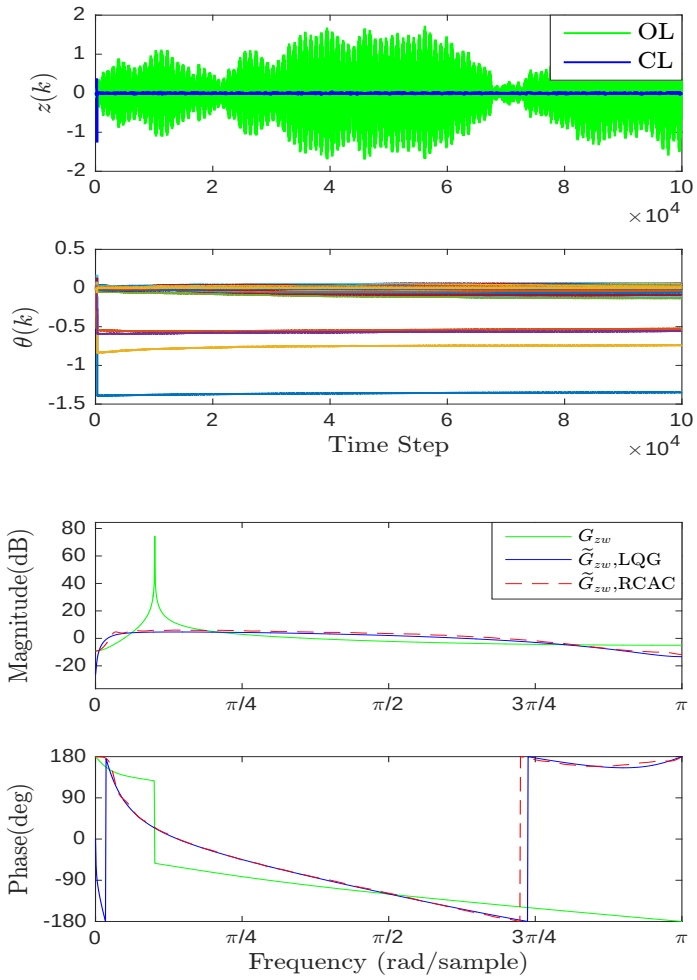

Figure 6.3: Example 6.3: Broadband disturbance rejection for the NMP plant (6.2) using the quasi-FIR controller structure (6.1). RCAC approximates the closed-loop frequency response of the high-authority LQG controller. The frequency-response plots are shown at step $k = 10^5$.

6.3 Command Following using Quasi-FIR Compensators

For command following, we use the quasi-FIR compensator with an FIR controller implemented in parallel with an integrator

$$u(k) = \sum_{i=1}^{n_c} Q_i(k)y(k-i) + K_I(k)\gamma(k), \tag{6.4}$$

where the integrator state satisfies

$$\gamma(k) = \gamma(k-1) + Fy(k), \tag{6.5}$$

$\gamma(k) \in \mathbb{R}^{l_\gamma}$ and $F \in \mathbb{R}^{l_\gamma \times l_y}$ selects components of $y(k)$. The motivation for (6.4) is to fix the poles of the compensator, in order to remove the possibility of unstable pole-zero cancellation. We use (6.4) for step command following for the adaptive servo problem.

Example 6.4. Step command following for a NMP plant using a quasi-FIR controller. Consider the Lyapunov-stable, NMP plant

$$G(\mathbf{q}) = \frac{(\mathbf{q}-1.1)(\mathbf{q}-1.2)}{(\mathbf{q}-0.99)(\mathbf{q}^2-1.8\mathbf{q}+1)}. \tag{6.6}$$

Let r be an alternating sequence of step commands with heights ± 1, $d = 0$, and let v be zero-mean Gaussian white noise with standard deviation 0.1. Applying RCAC with the IIR controller (2.28) results in an unstable controller (not shown). We apply RCAC with the quasi-FIR controller given by (6.4). Since (6.4) consists of an FIR portion and an integrator, there is no possibility of unstable pole-zero cancellation, and thus we use the FIR target model (2.49) with $n_{\mathrm{c}} = 10$, $R_\theta = 10^8 I_{l_\theta}$ and $R_u = 0$. Figure 6.4 shows the closed-loop response. Note that RCAC follows the sequence of step commands without knowledge of the NMP zeros of G. By using (6.4) for NMP plants with the FIR target model (2.49), this approach alleviates the need to know the NMP zeros of G_{zu}. ■

Example 6.5. Step command following for a MISO NMP plant using a

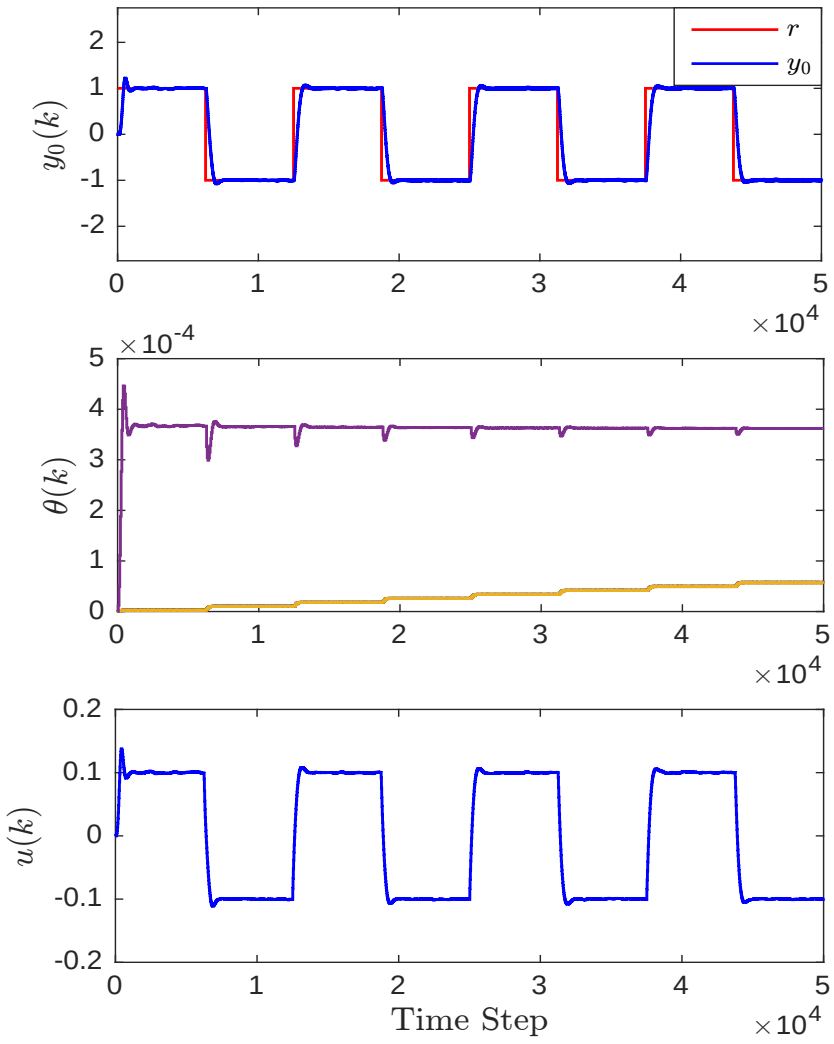

Figure 6.4: Example 6.4: Step command following for the NMP plant (6.6) using the quasi-FIR controller structure (6.4). RCAC follows the sequence of step commands without knowledge of the NMP zeros of G, and does not converge to an unstable controller.

quasi-FIR controller. Consider the asymptotically stable, NMP, MISO plant

$$G(\mathbf{q}) = \left[\begin{array}{cc} \frac{(\mathbf{q}-0.99)(\mathbf{q}^2+0.98)}{D(\mathbf{q})} & \frac{(\mathbf{q}-0.925)(\mathbf{q}-0.975)(\mathbf{q}-1.2)}{D(\mathbf{q})} \end{array} \right], \tag{6.7}$$

where $D(\mathbf{q}) = (\mathbf{q}-0.995)(\mathbf{q}-0.975)(\mathbf{q}^2-1.9\mathbf{q}+0.9125)$. Let r be an alternating sequence of step commands with heights ± 1, $v = 0$, and let d be zero-mean Gaussian white noise with standard deviation 2×10^{-6}. Applying RCAC with the IIR controller

(2.28) results in an unstable controller (not shown). We apply RCAC with the quasi-FIR controller given by (6.4). Since (6.4) consists of an FIR portion and an integrator, there is no possibility of unstable pole-zero cancellation, and thus we use the FIR target model (2.49) for both channels, with $n_c = 10$, $R_\theta = 10^{10} I_{l_\theta}$ and $R_u = 0$. Figure 6.5 shows the closed-loop response. Note that RCAC follows the sequence of step commands without knowledge of the NMP zeros of G. ■

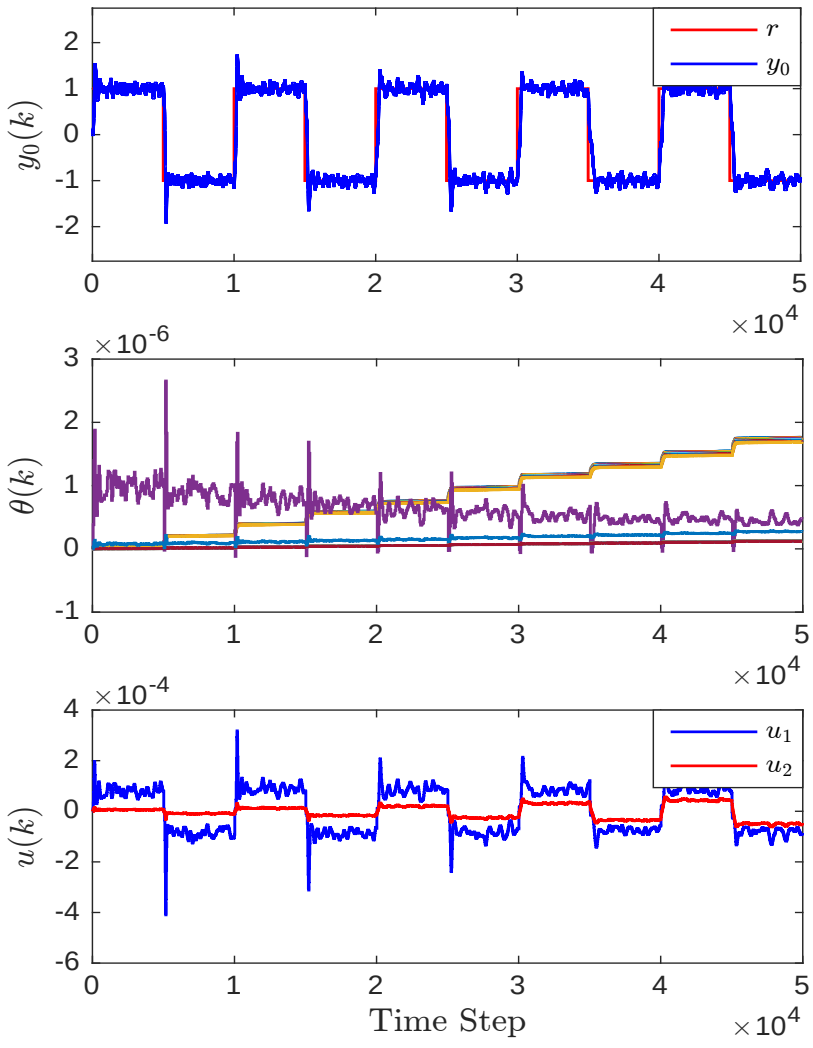

Figure 6.5: Example 6.5: Step command following for the MISO, NMP plant (6.7) using the quasi-FIR controller structure (6.4). RCAC follows the sequence of step commands without knowledge of the NMP zeros of G, and does not converge to an unstable controller.

6.4 Conclusions

In this chapter, we demonstrated that RCAC can be implemented with quasi-FIR compensators with a simple reflection technique to obtain asymptotically stable controllers. The rationale for applying quasi-FIR controllers is two fold. Firstly, only a small number of poles are unconstrained, and thus only a small number of controller poles may require reflection. Secondly, when applying an FIR controller in parallel with an integrator, all controller poles are fixed, and thus there is no need to constrain any controller poles.

We applied RCAC with quasi-FIR controllers to several examples to achieve H_2 cost near high-authority LQG, with asymptotically stable stabilization in cases where the high-authority LQG controller is unstable. This approach leads to the possibilty of using RCAC not as an adaptive control technique, but as a design tool for discrete control laws in cases where high-authority LQG controllers are unstable.

Next, we applied an FIR controller in parallel with an internal model to achieve command following without knowledge of the NMP zeros of the plant. Future work may include methods to apply RCAC for stochastic disturbance rejection and command following using (6.1), using constrained optimization to enforce stability and without knowledge of the NMP zeros of the plant, and also concurrent optimization of the denominator D_{f} of the target model and the controller $G_{\mathrm{c},k}$, in order to yield target pole locations that require stable controllers.

CHAPTER 7

Are All Full-Order Dynamic Compensators Observer-Based?

7.1 Introduction

Linear-quadratic-Gaussian (LQG) control theory states that the optimal compensator for a linear plant with white, Gaussian process and sensor noise and with suitable stabilizability and detectability assumptions is given by an observer-based compensator. The observer-based structure of the compensator reflects the *separation principle*, wherein an optimal state estimate is fed back by an optimal static full-state-feedback control law and where the observer and regulator gains are determined independently [107–109]. This result implies that every full-order dynamic compensator that is *not* observer-based must be suboptimal in the sense of LQG control.

7.2 Observer Based Compensation

To clarify the distinction between an observer-based compensator and a compensator of arbitrary structure, consider the SISO plant

$$\dot{x}(t) = Ax(t) + Bu(t), \tag{7.1}$$

$$y(t) = Cx(t), \tag{7.2}$$

where $x(t) \in \mathbb{R}^n$, $u(t) \in \mathbb{R}$, $y(t) \in \mathbb{R}$, $A \in \mathbb{R}^{n\times n}$, $B \in \mathbb{R}^{n\times 1}$, and $C \in \mathbb{R}^{1\times n}$. We assume that (A, B, C) is controllable and observable. We write a compensator in the form

$$\dot{x}_{\mathrm{c}}(t) = A_{\mathrm{c}}x_{\mathrm{c}}(t) + B_{\mathrm{c}}y(t), \tag{7.3}$$

$$u(t) = C_{\mathrm{c}}x_{\mathrm{c}}(t), \tag{7.4}$$

where the dimension n_{c} of x_{c} may be the same or different from the dimension n of the state of the plant (7.1), (7.2). To illustrate an observer-based compensator, let $F \in \mathbb{R}^{n\times 1}$ and consider the observer

$$\dot{\hat{x}}(t) = A\hat{x}(t) + Bu(t) + F\left[y(t) - \hat{y}(t)\right], \tag{7.5}$$

$$\hat{y}(t) = C\hat{x}(t), \tag{7.6}$$

where $\hat{x}(t) \in \mathbb{R}^n$. Note that (7.1) and (7.5) can be written as

$$\dot{x}(t) = (A - FC)x(t) + Bu(t) + Fy(t), \tag{7.7}$$

$$\dot{\hat{x}}(t) = (A - FC)\hat{x}(t) + Bu(t) + Fy(t). \tag{7.8}$$

Defining the error state

$$e(t) \triangleq x(t) - \hat{x}(t) \tag{7.9}$$

and subtracting (7.8) from (7.7) yields

$$\dot{e}(t) = (A - FC)e(t). \tag{7.10}$$

If $A - FC$ is asymptotically stable, then e converges to zero for all $x(0)$ and $\hat{x}(0)$. Note that, since $x(t)$ is not measured, $e(t)$ is unknown and thus (7.10) is used only for analysis.

Next, let $K \in \mathbb{R}^n$ and consider the observer-based feedback control law $u(t) = K\hat{x}(t)$ in (7.8). Then the observer-based compensator is

$$\dot{\hat{x}}(t) = (A + BK - FC)\hat{x}(t) + Fy(t), \tag{7.11}$$

$$u(t) = K\hat{x}(t). \tag{7.12}$$

Notice that (7.11), (7.12) is a full-order dynamic compensator of the form (7.3), (7.4) with

$$n_{\mathrm{c}} = n, \quad A_{\mathrm{c}} = A + BK - FC, \quad B_{\mathrm{c}} = F, \quad C_{\mathrm{c}} = K, \quad x_{\mathrm{c}}(t) = \hat{x}(t). \tag{7.13}$$

The only distinction between (7.3), (7.4) with $n_{\mathrm{c}} = n$ and (7.11), (7.12) is the fact that the dynamics matrix A_{c} in (7.3) has the observer-based form $A + BK - FC$ in (7.11). The structure of A_{c} suggests that observer-based compensators of the form (7.11), (7.12) comprise a subset of full-order compensators relative to the arbitrary structure (7.3), (7.4). LQG theory chooses an optimal compensator from this subset.

Comparing (7.3), (7.4) to (7.11), (7.12) motivates the question in the title of this

chapter, namely, are all full-order compensators observer-based? It is easy to show that the answer to this question is "no". In particular, note that the closed-loop system (7.1)–(7.4) is given by

$$\dot{\tilde{x}}(t) = \tilde{A}\tilde{x}(t), \tag{7.14}$$

where

$$\tilde{x}(t) \triangleq \begin{bmatrix} x(t) \\ x_{\mathrm{c}}(t) \end{bmatrix}, \quad \tilde{A} \triangleq \begin{bmatrix} A & BC_{\mathrm{c}} \\ B_{\mathrm{c}}C & A_{\mathrm{c}} \end{bmatrix}.$$

For the observer-based compensator, $\tilde{A}$ has the form

$$\tilde{A} = \begin{bmatrix} A & BK \\ FC & A + BK - FC \end{bmatrix}. \tag{7.15}$$

Using (7.12), (7.1) can be written as

$$\dot{x}(t) = (A + BK)x(t) - BKe(t). \tag{7.16}$$

Combining (7.10) and (7.16) yields

$$\dot{\tilde{x}}'(t) = \tilde{A}'\tilde{x}'(t), \tag{7.17}$$

where

$$\tilde{x}'(t) \triangleq \begin{bmatrix} x(t) \\ e(t) \end{bmatrix}, \quad \tilde{A}' \triangleq \tilde{S}\tilde{A}\tilde{S}^{-1} = \begin{bmatrix} A + BK & -BK \\ 0 & A - FC \end{bmatrix}, \quad \tilde{S} \triangleq \begin{bmatrix} I_n & 0 \\ I_n & -I_n \end{bmatrix}, \tag{7.18}$$

and $\tilde{A}$ is given by (7.15). Since $\tilde{A}$ and $\tilde{A}'$ are similar, they have the same eigenvalues. In addition, the eigenvalues of $\tilde{A}'$ consist of the eigenvalues of $A + BK$ and the

eigenvalues of $A - FC$. Since $A + BK$ is a real matrix, it follows that, if n is odd, then $A + BK$ has at least one real eigenvalue. The same statement can be made for $A - FC$. Consequently, if n is odd, then $\tilde{A}'$ and thus $\tilde{A}$ must have at least two real eigenvalues. This observation is made in [110, p. 43] in order to stress the distinction between observer-based controllers and dynamic compensators for pole placement that are not intended to estimate inaccessible states.

Now, consider the closed-loop system (7.14) consisting of (7.1)–(7.4), where (7.3), (7.4) is a full-order compensator. If n is odd and $\tilde{A}$ has no real eigenvalues, then the above discussion shows that (7.3), (7.4) cannot be an observer-based compensator. This leads to the following fundamental question: Is this the *only* situation where the full-order compensator is not observer-based in the sense that there does not exist a basis such that (7.3), (7.4) can be written in the form of (7.11), (7.12)? The main contribution of this chapter is to show that this is indeed the case.

To set the stage for the subsequent development, it is useful to recall that pole placement techniques can be used to assign the eigenvalues of $A + BK$ and $A - FC$. Therefore, if either

$$n \text{ is even} \tag{7.19}$$

or

$$n \text{ is odd, and } \tilde{A} \text{ has at least two real eigenvalues,} \tag{7.20}$$

then, for each full-order compensator (7.3), (7.4), there exists an observer-based compensator that replicates the closed-loop spectrum. However, this does not prove that (7.3), (7.4) is observer-based because we do not know whether or not the pole-placement compensator that replicates the closed-loop spectrum arising from (7.3), (7.4) is the *unique* full-order compensator with this property. The goal of this chapter

is thus to demonstrate uniqueness.

It is important to stress that the focus in this chapter is on uniqueness rather than existence. The existence of dynamic pole-placement controllers is extensively addressed in the literature. For example, sufficient conditions are given in [110] for the existence of a dynamic compensator of specified order that is able to place an arbitrary conjugate-symmetric set of closed-loop poles.

7.3 Analysis of the Sensitivity Function

In order to clarify the required uniqueness property, we consider the servo problem in Figure 7.1, where $G(s) \triangleq C(sI - A)^{-1}B = \frac{N(s)}{D(s)}$,

$$z(t) \triangleq r(t) - y(t), \tag{7.21}$$

$y(t) \in \mathbb{R}$ is the measurement, and $r(t) \in \mathbb{R}$ is the command. Note that D is monic and, since (A, B, C) is controllable and observable, D and N are coprime. The closed-loop

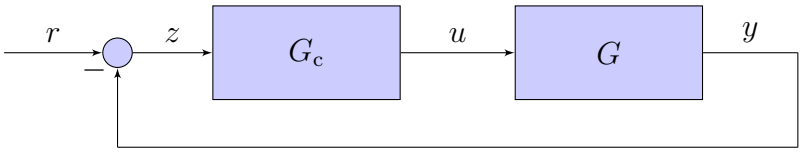

Figure 7.1: Transfer function representation of the servo problem with $G_d = G_u = G$.

transfer function from r to z is given by the sensitivity function

$$S \triangleq \frac{1}{1 + GG_{\mathrm{c}}} = \frac{DD_{\mathrm{c}}}{\tilde{D}}, \tag{7.22}$$

where $G_{\mathrm{c}} = \frac{N_{\mathrm{c}}}{D_{\mathrm{c}}}$ is a proper compensator of order $n_{\mathrm{c}} \geq 1$, and D_{c} is monic. The closed-loop characteristic polynomial is defined by

$$\tilde{D} \triangleq DD_{\mathrm{c}} + NN_{\mathrm{c}}. \tag{7.23}$$

It follows from (7.22) that G_c is given by

$$G_c = \frac{1-S}{SG}, \tag{7.24}$$

which shows that G_c is uniquely specified by S. Therefore, if two compensators G_{c1} and G_{c2} of arbitrary order give rise to the same sensitivity function S, then $G_{c1} = G_{c2}$. However, this does not show that, if two compensators G_{c1} and G_{c2} give rise to the same characteristic polynomial, then $G_{c1} = G_{c2}$. In the following section, we show that, if $\deg(N_{c1}) \leq \min\{n_c, n-1\}$ and $\deg(N_{c2}) \leq \min\{n_c, n-1\}$, then two compensator $G_{c1} = \frac{N_{c1}}{D_{c1}}$ and $G_{c2} = \frac{N_{c2}}{D_{c2}}$ that give rise to the same characteristic polynomial are equal. This fact then allows us to show that, if either (7.19) or (7.20) is satisfied, then every full-order compensator is observer-based. Before demonstrating this fact, we review pole placement using observer-based compensation.

7.4 Pole Placement Using Observer-Based Compensation

In this section, we review pole placement using observer-based compensation. We discuss the regulator and observer separately, and then present several examples. We also show that the observer-based compensator is independent of how the closed-loop poles are allocated to the regulator and the observer.

Designing the regulator

Let the characteristic polynomial of A be given by $p(s) = s^n + \alpha_{n-1}s^{n-1} + \cdots + \alpha_1 s + \alpha_0$. As shown in [111, pp. 309-311], since (A, B) is controllable, there exists a change of basis matrix $S_{\mathcal{C}} \in \mathbb{R}^{n\times n}$ such that

$$A + BK = S_{\mathcal{C}} \left(A_{\mathcal{C}} + B_{\mathcal{C}} K_{\mathcal{C}}\right) S_{\mathcal{C}}^{-1}, \tag{7.25}$$

where $K_{\mathcal{C}} \stackrel{\triangle}{=} K S_{\mathcal{C}}^{-1} = [K_{\mathcal{C},1} \ \cdots \ K_{\mathcal{C},n}]$,

$$A_{\mathcal{C}} \triangleq S_{\mathcal{C}} A S_{\mathcal{C}}^{-1} = \begin{bmatrix} 0 & 1 & 0 & \cdots & 0 \\ 0 & 0 & 1 & \cdots & 0 \\ \vdots & \vdots & \vdots & \ddots & \vdots \\ 0 & 0 & 0 & \cdots & 1 \\ -\alpha_0 & -\alpha_1 & -\alpha_2 & \cdots & -\alpha_{n-1} \end{bmatrix}, \quad B_{\mathcal{C}} \triangleq S_{\mathcal{C}} B = \begin{bmatrix} 0 \\ 0 \\ \vdots \\ 0 \\ 1 \end{bmatrix}, \tag{7.26}$$

and thus

$$A_{\mathcal{C}} + B_{\mathcal{C}} K_{\mathcal{C}} = \begin{bmatrix} 0 & 1 & 0 & \cdots & 0 \\ 0 & 0 & 1 & \cdots & 0 \\ \vdots & \vdots & \vdots & \ddots & \vdots \\ 0 & 0 & 0 & \cdots & 1 \\ -\alpha_0 + K_{\mathcal{C},1} & -\alpha_1 + K_{\mathcal{C},2} & -\alpha_2 + K_{\mathcal{C},3} & \cdots & -\alpha_{n-1} + K_{\mathcal{C},n} \end{bmatrix}. \tag{7.27}$$

Note that $A+BK$ and $A_{\mathcal{C}}+B_{\mathcal{C}}K_{\mathcal{C}}$ have the same eigenvalues, and that the eigenvalues of $A_{\mathcal{C}} + B_{\mathcal{C}}K_{\mathcal{C}}$ can be placed arbitrarily by the choice of $K_{\mathcal{C}}$. The regulator gain K can then be determined using $K = K_{\mathcal{C}} S_{\mathcal{C}}$. Finally, since $\mathcal{C}(A_{\mathcal{C}}, B_{\mathcal{C}}) = S_{\mathcal{C}}\mathcal{C}(A, B)$, it follows that $S_{\mathcal{C}} = \mathcal{C}(A_{\mathcal{C}}, B_{\mathcal{C}})\mathcal{C}(A, B)^{-1}$, where $\mathcal{C}(A, B)$ is the controllability matrix of the pair (A, B).

Designing the Observer

Let the characteristic polynomial of A be given by $p(s) = s^n + \alpha_{n-1}s^{n-1} + \cdots + \alpha_1 s + \alpha_0$. Since (A, C) is observable, there exists a change of basis matrix $S_{\mathcal{O}} \in \mathbb{R}^{n\times n}$ such that

$$A - FC = S_{\mathcal{O}}^{-1} \left(A_{\mathcal{O}} - F_{\mathcal{O}} C_{\mathcal{O}}\right) S_{\mathcal{O}}, \tag{7.28}$$

where $F_{\mathcal{O}} \triangleq S_{\mathcal{O}} F = \begin{bmatrix} F_{\mathcal{O},1} & \cdots & F_{\mathcal{O},n} \end{bmatrix}^{\mathrm{T}}$,

$$A_{\mathcal{O}} = S_{\mathcal{O}} A S_{\mathcal{O}}^{-1} = \begin{bmatrix} 0 & 0 & \cdots & 0 & -\alpha_0 \\ 1 & 0 & \cdots & 0 & -\alpha_1 \\ 0 & 1 & \cdots & 0 & -\alpha_2 \\ \vdots & \vdots & \ddots & & \vdots \\ 0 & 0 & \cdots & 1 & -\alpha_{n-1} \end{bmatrix}, \quad C_{\mathcal{O}} = C S_{\mathcal{O}}^{-1} = \begin{bmatrix} 0 & 0 & \cdots & 0 & 1 \end{bmatrix}, \tag{7.29}$$

and thus

$$A_{\mathcal{O}} - F_{\mathcal{O}} C_{\mathcal{O}} = \begin{bmatrix} 0 & 0 & \cdots & 0 & -\alpha_0 - F_{\mathcal{O},1} \\ 1 & 0 & \cdots & 0 & -\alpha_1 - F_{\mathcal{O},2} \\ 0 & 1 & \cdots & 0 & -\alpha_2 - F_{\mathcal{O},3} \\ \vdots & \vdots & \ddots & & \vdots \\ 0 & 0 & \cdots & 1 & -\alpha_{n-1} - F_{\mathcal{O},n} \end{bmatrix}. \tag{7.30}$$

Note that $A - FC$ and $A_{\mathcal{O}} - F_{\mathcal{O}} C_{\mathcal{O}}$ have the same eigenvalues, and that the eigenvalues of $A_{\mathcal{O}} - F_{\mathcal{O}} C_{\mathcal{O}}$ can be placed arbitrarily by the choice of $F_{\mathcal{O}}$. The observer gain F can then be determined using $F = S_{\mathcal{O}}^{-1} F_{\mathcal{O}}$. Finally, since $\mathcal{O}(A_{\mathcal{O}}, C_{\mathcal{O}}) = \mathcal{O}(A, C) S_{\mathcal{O}}^{-1}$, it follows that $S_{\mathcal{O}} = \mathcal{O}(A_{\mathcal{O}}, C_{\mathcal{O}})^{-1} \mathcal{O}(A, C)$, where $\mathcal{O}(A, C)$ is the observability matrix of the pair (A, C).

Example 7.1. Let

$$A = \begin{bmatrix} -1 & 4 \\ 0 & -3 \end{bmatrix}, \quad B = \begin{bmatrix} 0 \\ 1 \end{bmatrix}, \quad C = \begin{bmatrix} 1 & 0 \end{bmatrix}.$$

We assign the eigenvalues -5 and -4 to $A + BK$ and the eigenvalues -2 and -6 to $A - FC$. Solving (7.27) and (7.30) for K and F yields $K = \begin{bmatrix} -3 & -5 \end{bmatrix}$ and $F = \begin{bmatrix} 4 & -0.75 \end{bmatrix}^{\mathrm{T}}$. The transfer function representation of the observer-based compensator is

$$G_{\mathrm{c}}(s) = \frac{8.26s + 23.25}{s^2 + 13s + 49}. \tag{7.31}$$

As a check, we use the realization

$$A_{\mathrm{c}} = \begin{bmatrix} -5 & 4 \\ -2.25 & -8 \end{bmatrix}, \quad B_{\mathrm{c}} = \begin{bmatrix} 4 \\ -0.75 \end{bmatrix}, \quad C_{\mathrm{c}} = [-3 \quad -5]$$

of $G_{\mathrm{c}}(s)$ to find $\tilde{A}$. The closed-loop eigenvalues are given by the eigenvalues of

$$\tilde{A} = \begin{bmatrix} -1 & 4 & 0 & 0 \\ 0 & -3 & -3 & -5 \\ 4 & 0 & -5 & 4 \\ -0.75 & 0 & -2.25 & -8 \end{bmatrix},$$

which are the desired values $-2, -4, -5, -6$. ■

Proposition 1. Let $\tilde{D}$ be a monic polynomial of degree $2n$ with real coefficients, and assume that either n is even or both n is odd and $\tilde{D}$ has at least two real roots. Furthermore, let (7.11), (7.12) be an observer-based compensator such that the eigenvalues of $\tilde{A}$ are given by the roots of $\tilde{D}$. Then, G_{c} corresponding to (7.11), (7.12) is independent of how the poles are allocated to the regulator and observer.

The proof of Proposition 1 is presented after Proposition 2.

Proposition 1 shows that the same observer-based compensator is obtained regardless of how the desired closed-loop poles are allocated between the regulator and observer dynamics as long as a pair of complex poles is not separated between the observer and the regulator. We illustrate this result by revisiting Example 7.1.

Example 7.2. We reconsider Example 7.1, but we now assign the eigenvalues -5 and -6 to $A + BK$ and the eigenvalues -2 and -4 to $A - FC$. Solving (7.27) and (7.30) for K and F yields $K = [-5 \quad -7]$ and $F = [2 \quad -0.25]^{\mathrm{T}}$. The transfer function representation of the resulting observer-based compensator is again (7.31), as guaranteed by Proposition 1. ■

7.4.1 Uniqueness of the Compensator Based on Only the Closed-Loop Poles

Given $\tilde{D}$, the objective of pole placement design is to find a proper dynamic compensator $G_{\rm c}$ that assigns the $n + n_{\rm c}$ closed-loop poles. In this section, we present sufficient conditions for uniqueness of $G_{\rm c}$ based on only $\tilde{D}$. Pole placement using dynamic compensators is considered in [110].

Lemma 1. Let a, b, p, and q be polynomials such that $\deg(a) \leq \deg(b)$, $\deg(p) < \deg(q)$, q is monic, $p \neq 0$, and p and q are coprime. Then $bq + ap = 0$ if and only if $a = b = 0$.

Proof. Sufficiency is immediate. To prove necessity, suppose that $bq + ap = 0$, $a \neq 0$, and $b = 0$. Then $ap = 0$. However, since $p \neq 0$, it follows that $a = 0$, which is a contradiction. Next, suppose that $bq + ap = 0$, $a = 0$, and $b \neq 0$. Then $bq = 0$, However, since q is monic, it follows that $b = 0$, which is a contradiction. Finally, suppose that $bq + ap = 0$, $a \neq 0$, and $b \neq 0$. Then $\deg(ap) = \deg(bq)$. However, since $\deg(a) \leq \deg(b)$ and $\deg(p) < \deg(q)$, it follows that $\deg(ap) < \deg(bq)$, which is a contradiction. □

Proposition 2. Let $\tilde{D}$ be given by (7.23), where $\deg(\tilde{D}) = n + n_{\rm c}$, and let $\deg(N_{\rm c}) \leq \min\{n_{\rm c}, n-1\}$. Then, $N_{\rm c}$ and $D_{\rm c}$ are uniquely determined.

Proof. Let $G_{\rm c1} = \frac{N_{\rm c1}}{D_{\rm c1}}$ and $G_{\rm c2} = \frac{N_{\rm c2}}{D_{\rm c2}}$ be such that $\deg(D_{\rm c1}) = \deg(D_{\rm c2}) = n_{\rm c}$, $m_{\rm c1} \stackrel{\triangle}{=} \deg(N_{\rm c1}) \leq \min\{n_{\rm c}, n-1\}$, $m_{\rm c2} \stackrel{\triangle}{=} \deg(N_{\rm c2}) \leq \min\{n_{\rm c}, n-1\}$, and $\tilde{D} = DD_{\rm c1} + NN_{\rm c1} = DD_{\rm c2} + NN_{\rm c2}$. Define $a \stackrel{\triangle}{=} N_{\rm c1} - N_{\rm c2}$, $b \stackrel{\triangle}{=} D_{\rm c1} - D_{\rm c2}$, $p \stackrel{\triangle}{=} N$, and $q \stackrel{\triangle}{=} D$. Then $\deg(a) \leq \max\{m_{\rm c1}, m_{\rm c2}\}$, $\deg(b) \leq n_{\rm c}$, and $\deg(p) < \deg(q)$. Suppose that $\deg(a) > \deg(b)$. Then $N_{\rm c1} - N_{\rm c2} \neq 0$ and $\frac{N}{D} = -\frac{b}{a} = -\frac{D_{\rm c1} - D_{\rm c2}}{N_{\rm c1} - N_{\rm c2}}$. Since $\deg(D) = n$, it follows that $\deg(a) = \deg(N_{\rm c1} - N_{\rm c2}) \geq n$. Hence, $n \leq \deg(a) \leq \max\{m_{\rm c1}, m_{\rm c2}\} \leq \min\{n_{\rm c}, n-1\} \leq n-1$, which is a contradiction. Therefore, $\deg(a) \leq \deg(b)$. Lemma 1 thus implies that $N_{\rm c1} - N_{\rm c2} = D_{\rm c1} - D_{\rm c2} = 0$. Therefore,

$G_{c1} = G_{c2}$, and thus N_c and D_c are uniquely determined. □

We now use Proposition 2 to prove Proposition 1.

Proof of Proposition 1. For the observer-based compensator (7.11), (7.12), $\deg(N_c) = n-1$ and $n_c = n$. Since $\tilde{D}$ is monic, Proposition 2 implies that there exist unique polynomials N_c and D_c satisfying (7.23). Hence G_c is uniquely determined and is independent of how the poles are allocated to the regulator and observer. □

Although Proposition 2 provides only sufficient conditions for uniqueness, the following examples show that uniqueness can fail if these conditions are not satisfied.

Example 7.3. Let $G(s) = \frac{1}{s+2}$, and consider $G_c(s) = \frac{-s-1}{s+1}$ and $G_c(s) = \frac{-2s-3}{s+2}$. Note that $n = 1$, $n_c = 1$, and $\deg(N_c) = 1$, and thus the assumption $\deg(N_c) \leq \min\{n_c, n-1\}$ of Proposition 2 is not satisfied. For both compensators, $\tilde{D}(s) = s^2 + 2s + 1$. ■

Example 7.4. Let $G(s) = \frac{1}{s+2}$, and consider $G_c(s) = \frac{-3s-1}{s^2+2s+1}$ and $G_c(s) = \frac{-4s-3}{s^2+2s+2}$. Note that $n = 1$, $n_c = 2$, and $\deg(N_c) = 1$, and thus the assumption $\deg(N_c) \leq \min\{n_c, n-1\}$ of Proposition 2 is not satisfied. For both compensators, $\tilde{D}(s) = s^3 + 4s^2 + 2s + 1$. ■

We now state the main result, which answers the question posed in the title of this chapter.

Theorem 1. Let $G_c = N_c/D_c$ be a full-order strictly proper compensator. Then, G_c is observer-based if and only if either *i*) n is even or *ii*) n is odd and $\tilde{D} = DD_c + NN_c$ has at least two real roots.

Proof. To prove necessity, note that, since $\deg(D_c) = n$ and $\deg(N_c) \leq n-1$, Proposition 2 implies that N_c and D_c are the only polynomials that satisfy (7.23). Therefore, G_c is the unique observer-based compensator such that $\tilde{D} \triangleq DD_c + NN_c$. Since G_c is an observer-based compensator, it follows that n of the $2n$ closed-loop

eigenvalues are eigenvalues of the observer dynamics, while the remaining n closed-loop eigenvalues are eigenvalues of the regulator dynamics. Hence, in the case where n is odd, it follows that $\tilde{D}$ has at least two real roots.

Conversely, since either n is even or both n is odd and $\tilde{D}$ has at least two real roots, Proposition 2 implies that there exists a unique compensator $G_{\mathrm{c,obc}}$ with closed-loop poles given by the roots of $\tilde{D}$ and, in addition, $G_{\mathrm{c,obc}}$ is observer-based. □

7.5 Pole Placement Without Observer-Based Compensation

Theorem 1 shows that an observer-based compensator cannot be used in all cases to assign the closed-loop poles. For example, if n is odd, $n_{\mathrm{c}} = n$, and $\tilde{D}$ has no real roots, then the closed-loop eigenvalues cannot be allocated to an observer and a regulator, and thus no observer-based compensator that assigns the desired poles exists. However, by using a dynamic compensator, it is nevertheless possible to assign the desired closed-loop spectrum, albeit with a compensator that is not observer-based. This section thus concerns existence and uniqueness of a pole placement dynamic compensator in cases where an observer-based compensator does not exist. An algorithm based on the Sylvester resultant for designing pole-placement dynamic compensators is given in [112].

Let

$$N(s) = N_m s^m + \cdots + N_1 s + N_0, \tag{7.32}$$

$$D(s) = s^n + D_{n-1} s^{n-1} + \cdots + D_1 s + D_0, \tag{7.33}$$

$$N_{\mathrm{c}}(s) = N_{\mathrm{c},\hat{m}_{\mathrm{c}}} s^{\hat{m}_{\mathrm{c}}} + \cdots + N_{\mathrm{c},1} s + N_{\mathrm{c},0}, \tag{7.34}$$

$$D_{\mathrm{c}}(s) = s^{n_{\mathrm{c}}} + D_{\mathrm{c},n_{\mathrm{c}}-1} s^{n_{\mathrm{c}}-1} + \cdots + D_{\mathrm{c},1} s + D_{\mathrm{c},0}, \tag{7.35}$$

$$\tilde{D}(s) = s^{n+n_{\mathrm{c}}} + \tilde{D}_{n+n_{\mathrm{c}}-1} s^{n+n_{\mathrm{c}}-1} + \cdots + \tilde{D}_1 s + \tilde{D}_0, \tag{7.36}$$

where $\hat{m}_{\mathrm{c}} \leq n_{\mathrm{c}}$. Note that $N_{\mathrm{c},\hat{m}_{\mathrm{c}}}$ may or may not be zero, and thus (7.34) implies

that $m_{\rm c} \triangleq \deg(N_{\rm c}) \leq \hat{m}_{\rm c}$. Substituting (7.32)–(7.36) into (7.23) and matching like powers of s yields the linear system of equations

$$M \begin{bmatrix} D_{{\rm c},n_{\rm c}-1} \\ \vdots \\ D_{{\rm c},0} \\ N_{{\rm c},\hat{m}_{\rm c}} \\ \vdots \\ N_{{\rm c},0} \end{bmatrix} = \begin{bmatrix} \tilde{D}_{n+n_{\rm c}-1} - D_{n-1} \\ \vdots \\ \tilde{D}_{n_{\rm c}} - D_0 \\ \tilde{D}_{n_{\rm c}-1} \\ \vdots \\ \tilde{D}_0 \end{bmatrix}, \tag{7.37}$$

where $M \in \mathbb{R}^{(n+n_{\rm c})\times(\hat{m}_{\rm c}+n_{\rm c}+1)}$ is defined by

$$M \triangleq \begin{bmatrix} 1 & 0 & 0 & \cdots & \cdots & \cdots & \cdots & 0 & \cdots & \cdots & 0 \\ D_{n-1} & 1 & 0 & \cdots & \cdots & \cdots & \cdots & \vdots & \cdots & \cdots & \vdots \\ \vdots & D_{n-1} & \ddots & \ddots & \ddots & \ddots & \vdots & 0 & \cdots & \cdots & 0 \\ \vdots & \vdots & \ddots & \ddots & \ddots & \ddots & \vdots & N_m & 0 & \vdots & \vdots \\ \vdots & \vdots & \ddots & \ddots & \ddots & \ddots & \vdots & N_{m-1} & N_m & \ddots & \vdots \\ D_1 & \vdots & \ddots & \ddots & \ddots & \ddots & 0 & \vdots & N_{m-1} & \ddots & 0 \\ D_0 & D_1 & \ddots & \ddots & \ddots & \ddots & 1 & \vdots & \vdots & \ddots & N_m \\ 0 & D_0 & \ddots & \ddots & \ddots & \ddots & D_{n-1} & \vdots & \vdots & \ddots & N_{m-1} \\ \vdots & 0 & \ddots & \ddots & \ddots & \ddots & \vdots & N_1 & \vdots & \ddots & \vdots \\ \vdots & \vdots & \ddots & \ddots & \ddots & \ddots & \vdots & N_0 & N_1 & \ddots & \vdots \\ \vdots & \vdots & \ddots & \ddots & \ddots & \ddots & \vdots & 0 & N_0 & \ddots & \vdots \\ \vdots & \vdots & \ddots & \ddots & \ddots & \ddots & D_1 & \vdots & \vdots & \ddots & N_1 \\ 0 & 0 & \cdots & \cdots & \cdots & \cdots & D_0 & 0 & \cdots & \cdots & N_0 \end{bmatrix}. \tag{7.38}$$

The matrix M is constructed by listing the coefficients of D from 1 to D_0 starting at the top of the first column. In the second column, the coefficients of D are shifted downward by one row; $n_{\rm c}$ columns are constructed this way. Next, in column $n_{\rm c}+1$, the coefficients of N from N_m to N_0 are listed starting after $n+n_{\rm c}-m-\hat{m}_{\rm c}-1$ zeros. In the next column, the coefficients of N are shifted downward by one row;

$\hat{m}_c + 1$ columns are constructed this way. The matrix M thus has $n + n_c$ rows and $\hat{m}_c + n_c + 1$ columns. Hence M is square if and only if $\hat{m}_c = n - 1$. Therefore, M can be made square by choosing $\hat{m}_c = n - 1$ if and only if $m_c \leq n - 1$. Since $\hat{m}_c \leq n_c$, if M is square, then $n_c \geq n - 1$. Consequently, M can be made square if and only if $m_c \leq n - 1 \leq n_c$.

The following result relates M defined by (7.38) with the Sylvester resultants $\mathcal{M}_1$ and $\mathcal{M}_2$ defined by B.1 and B.2, respectively. Note that both Sylvester resultants are square.

Proposition 3. $M = \mathcal{M}_1(D, N)$ if and only if $\hat{m}_c = n - 1$ and $n_c \leq n$.

Proof. Suppose that $M = \mathcal{M}_1(D, N)$. Then M is square, and thus $\hat{m}_c = n - 1$. Hence, $\mathcal{M}_1(D, N) = M \in \mathbb{R}^{(n+n_c)\times(n+n_c)}$. Since $n = \deg(D)$, it follows from the construction of $\mathcal{M}_1(D, N)$ in Theorem A1 (note that $l \leq k$ in B.1) that $n_c \leq n$. Conversely, suppose that $\hat{m}_c = n - 1$ and $n_c \leq n$. Then M is square, $M \in \mathbb{R}^{(n+n_c)\times(n+n_c)}$, and $m \leq n - 1 = \hat{m}_c \leq n_c$. Therefore, $M = \mathcal{M}_1(D, N)$. □

Proposition 4. $M = \mathcal{M}_2(D, N)$ if and only if $\hat{m}_c = n - 1$ and $n_c = n$.

Proof. Suppose that $M = \mathcal{M}_2(D, N)$. Then M is square, and thus $\hat{m}_c = n - 1$. Hence, $M \in \mathbb{R}^{(n+n_c)\times(n+n_c)}$. Furthermore, $\mathcal{M}_2(D, N) \in \mathbb{R}^{2n\times 2n}$. Therefore, $n_c = n$. Conversely, suppose that $\hat{m}_c = n - 1$ and $n_c = n$. Then M is square, $M \in \mathbb{R}^{2n\times 2n}$, and $m < n$. Therefore, $M = \mathcal{M}_2(D, N)$. □

Since $\hat{m}_c \leq n - 1$, the above discussion shows that M is a Sylvester resultant if and only if $\hat{m}_c = n-1$ and $n-1 \leq n_c \leq n$. The case where $m_c = n-1$ and $n_c = n-1$ is discussed in [113]. These cases are summarized in Table 7.1.

Proposition 5. Assume that either $M = \mathcal{M}_1(D, N)$ or $M = \mathcal{M}_2(D, N)$. Then there exist unique N_c and D_c satisfying (7.37).

Proof. Since N and D are coprime, Theorem A1 and Theorem A2 state that $\mathcal{M}_1(D, N)$ and $\mathcal{M}_2(D, N)$ are nonsingular. It thus follows that there exist unique N_c

	$n_c = n-1$	$n_c = n$
$\deg(N_c)$	$\leq n-1$	$\leq n-1$
$\deg(D_c)$	$n-1$	n
$\deg(\tilde{D})$	$2n-1$	$2n$

Table 7.1: Cases $n_c = n-1$ and $n_c = n$. Note that, in the case $n_c = n-1$, G_c may be exactly proper or strictly proper, whereas, in the case $n_c = n$, G_c must be strictly proper.

and D_c satisfying (7.37). □

In [112, p. 182], necessary and sufficient conditions for the existence and uniqueness of N_c and D_c are given for the case where $n_c = n-1$, and, in [112, p. 182], sufficient conditions for existence are given in the case where $n_c > n-1$. The results in this chapter complement the results given in [112] by providing sufficient conditions for uniqueness in the case where $n_c = n$ and $\deg(N_c) \leq n-1$.

We now reconsider Example 7.1, which considers pole placement using an observer-based compensator. However, instead of designing an observer-based compensator with specified observer and regulator poles, we apply Proposition 5 by solving (7.37) to determine a compensator that places all $2n$ poles directly. Theorem 1 implies that there exists a unique nth-order compensator that places the closed-loop poles, and thus we expect to obtain the same compensator obtained in Example 1.

Example 7.5. We reconsider Example 7.1, and place the poles at $-6, -5, -4$, and -2 without observer-based compensation. Solving (7.37) for N_c and D_c yields $N_c(s) = 8.26s + 23.25$ and $D_c(s) = s^2 + 13s + 49$. Note that G_c is precisely the observer-based compensator obtained in Example 7.1. ■

We now consider an example where pole placement using an observer-based compensator is impossible. The example takes advantage of Proposition 5.

Example 7.6. Consider the state space equations for a DC motor, where

$$x \triangleq \begin{bmatrix} \theta \\ \dot{\theta} \\ i \end{bmatrix}, \quad A = \begin{bmatrix} 0 & 1 & 0 \\ 0 & -2 & 0.85 \\ 0 & -3 & -1 \end{bmatrix}, \quad B = \begin{bmatrix} 0 \\ 0 \\ 1 \end{bmatrix}, \quad C = \begin{bmatrix} 1 & 0 & 0 \end{bmatrix}.$$

We assign the closed-loop poles to $-0.5 \pm 0.1\jmath, -1 \pm 0.5\jmath, -2 \pm \jmath$. Solving (7.37) for N_{c} and D_{c} yields $N_{\mathrm{c}}(s) = 5.585s^2 + 8.034s + 1.912$ and $D_{\mathrm{c}}(s) = s^3 + 4s^2 + 3.96s + 0.73$. However, since three pairs of complex poles cannot be allocated separately to the regulator and observer dynamics, it is impossible to design an observer-based compensator that yields the desired closed-loop poles. Hence, $G_{\mathrm{c}}(s) = \frac{5.585s^2+8.034s+1.912}{s^3+4s^2+3.96s+0.73}$ is not observer-based and therefore must be suboptimal in the sense of LQG control.■

7.6 Conclusions

A full-order dynamic compensator is observer-based if, in some basis, it has the structure of an observer followed by state-estimate feedback. This chapter shows that almost all full-order compensators are in fact observer-based. The essential idea of the proof is that the observer-based compensator that achieves the desired spectrum is unique. An exception to this fact, however, is the case where the plant order is odd and the closed-loop spectrum has no real eigenvalues. In this case, the closed-loop spectra cannot be partitioned into conjugate-symmetric regulator and observer spectra, and therefore the compensator is not observer-based. All such compensators are, of course, suboptimal in the sense of LQG control.

CHAPTER 8

Parameter Estimation using Retrospective Cost Model Refinement

8.1 Introduction

In many modeling and control applications, the structure of the model is known, but the parameters may be uncertain. Within the context of system identification, models of this type are called *white box models*. In contrast, models whose structure is either partially or fully unknown are called *grey-box* and *black-box models*, respectively.

Parameter-estimation is related to, but distinct from, state estimation, where states evolve due to external inputs and their interaction with other states. In contrast, an unknown parameter may either be constant or time-varying in a pre-specified manner that is independent of initial conditions and outputs. Although a constant or time-varying parameter is not technically a state, it can be modeled as a state by assigning it fictitious dynamics and stochastic forcing. In continuous time, these dynamics are $\dot{x} = w$, whereas, in discrete time, these dynamics are $x(k+1) = x(k) + w(k)$, where w is the external forcing. For a system with linear dynamics, the resulting state estimation problem is nonlinear due to the multiplication between "real" and "fictitious" states.

State-estimation techniques are widely used for parameter estimation [114–116].

Among the earliest works is the paper [117], which analyzes the accuracy of the extended Kalman filter within the context of linear dynamics. Convergence analysis of the extended Kalman filter is provided in [118].

Beyond the extended Kalman filter, nonlinear estimation techniques have been developed based on a wide variety of techniques, including stochastic ensembles [119–121], deterministic ensembles [122, 123], Gaussian mixtures [124], density estimators [125], Fokker-Planck solutions [126], moving horizon techniques [127], and adaptive estimators [128, 129]. Each of these techniques can potentially be applied to parameter estimation. The goal of this chapter is to compare these established parameter estimation techniques to RCMR.

With this plethora of techniques available, it is of interest to evaluate the relative accuracy of these methods for parameter estimation. In this chapter, we apply several nonlinear estimation techniques to two examples, namely, a mass-spring structure and linearized aircraft dynamics. These low-order examples are chosen to provide a transparent setting for numerical studies. The methods we consider are the extended Kalman filter [116–118], the unscented Kalman filter [115], and RCMR. We consider parameter estimation for both constant and time-varying parameters, and we investigate the effects of sensor noise.

8.2 Problem Statement

Consider the multi-input, multi-output discrete-time system

$$x(k+1) = A(\kappa(k))x(k) + Bw(k), \tag{8.1}$$

$$y(k) = Cx(k) + v(k), \tag{8.2}$$

where $x(k) \in \mathbb{R}^n$ is the unknown state, $w(k) \in \mathbb{R}^m$ is an unknown input, $y(k) \in \mathbb{R}^p$ is the output, $v(k)$ is sensor noise, $\kappa(k) \in \mathbb{R}$ is an uncertain possibly time-varying

parameter, and $A(\kappa(k)) \in \mathbb{R}^{n\times n}$, $B \in \mathbb{R}^{n\times m}$, and $C \in \mathbb{R}^{p\times n}$. The goal is to estimate $\kappa(k)$. For simplicity in comparing estimation algorithms, we consider only the case where a single entry of $A(\kappa(k))$ is uncertain.

8.3 Parameter Identification Algorithms

To estimate the unknown parameter in (8.1), we use three algorithms, namely, the extended Kalman filter (EKF), the unscented Kalman filter (UKF), and retrospective cost model refinement (RCMR). For the Kalman filter approaches, we treat $\kappa(k)$ as an unknown state, and we augment the state vector to include $\kappa(k)$. This causes the augmented system to become nonlinear in $\kappa(k)$. For RCMR, we model the unknown parameter as an unknown subsystem. In this section, we briefly describe the EKF and UKF. In the following section, we describe RCMR.

8.3.1 Extended Kalman Filter

For nonlinear systems, the EKF uses a Jacobian of the dynamics for state estimation. Therefore, the EKF requires that the dynamics be differentiable functions. Consider the nonlinear dynamics given below

$$x(k) = f(x(k-1)) + w(k), \tag{8.3}$$

$$y(k) = h(x(k)) + v(k), \tag{8.4}$$

where w has covariance $Q(k) \in \mathbb{R}^{m\times m}$ and v has covariance $R(k) \in \mathbb{R}^{p\times p}$. The state estimate is given by

$$\hat{x}(k) = f(\hat{x}(k-1)) + K(k)\tilde{y}(k), \tag{8.5}$$

where $\tilde{y}(k) = y(k) - h(f(\hat{x}(k-1)))$, and $K(k)$ and $P(k)$ satisfy

$$\begin{aligned} K(k) =& (\hat{A}(k-1)P(k-1)\hat{A}^{\mathrm{T}}(k-1) + Q(k)) \\ & \cdot \hat{C}^{\mathrm{T}}(k)(\hat{C}(k)(\hat{A}(k-1)P(k-1)\hat{A}^{\mathrm{T}}(k-1) + Q(k))\hat{C}^{\mathrm{T}}(k) + R(k))^{-1} \quad (8.6) \\ P(k) =& (I - K(k)\hat{C}(k))(\hat{A}(k-1)P(k-1)\hat{A}^{\mathrm{T}}(k-1) + Q(k)), \quad (8.7) \end{aligned}$$

where

$$\hat{A}(k) \triangleq \left.\frac{\partial f}{\partial x}\right|_{\hat{x}(k-1)}, \quad \hat{C}(k) \triangleq \left.\frac{\partial h}{\partial x}\right|_{\hat{x}(k-1)}. \quad (8.8)$$

8.3.2 Unscented Kalman Filter

The UKF approach to state estimation of nonlinear systems is developed in [122]. UKF does not use the Jacobian of the dynamics or a factorization of the dynamics to propagate a pseudo error covariance. The starting point for UKF is a set of sample points, that is, a collection of state estimates that capture the initial probability distribution of the state. Let $P \in \mathbb{R}^{n\times n}$ be positive semidefinite. The unscented transformation provides $2n+1$ ensembles $X_i \in \mathbb{R}^n$ and corresponding weights $\gamma_{x,i}$ and $\gamma_{y,i}$, for $i = 0, 1, \ldots, 2n$, such that the weighted mean and weighted variance of the ensembles are x and P, respectively. Specifically, let $S \in \mathbb{R}^{n\times n}$ satisfy

$$SS^{\mathrm{T}} = P, \quad (8.9)$$

and, for all $i = 1, \ldots, n$, let S_i denote the ith column of S. For $\alpha > 0$, the unscented transformation $X = \Psi(x, S, \alpha) \in \mathbb{R}^{n\times(2n+1)}$ of x with covariance $P = SS^{\mathrm{T}}$ is defined

by

$$X \triangleq \begin{cases} x, & i = 0, \\ x + \sqrt{\alpha} S_i, & i = 1, \ldots, n, \\ x - \sqrt{\alpha} S_{i-n} & i = n+1, \ldots, 2n. \end{cases} \tag{8.10}$$

The parameter α determines the spread of the ensembles around x. Next, define the weights $\gamma_i \in \mathbb{R}$ by

$$\gamma_0 \triangleq \frac{\alpha - n}{n}, \quad \gamma_i \triangleq \frac{1}{2\alpha}, \quad i = 1, \ldots, 2n, \tag{8.11}$$

Then,

$$\sum_{i=0}^{2n} \gamma_i X_i = x, \quad \sum_{i=0}^{2n} \gamma_i (X_i - x)(X_i - x)^{\mathrm{T}} = P. \tag{8.12}$$

The unscented transformation (8.9)-(8.12) is the scaled unscented transformation given in [130]. This technique ensures that the distance between x and the sample point X_i does not increase as n increases.

UKF uses the unscented transformation to approximate the error covariance and estimate the state $x_k = x(k)$. Letting x_0^- be an initial estimate of x_0 with error covariance P_0^-, the data assimilation step of UKF is given by

$$x_k^+ = x_k^- + K_F(Y_k - y_k^-), \tag{8.13}$$

$$y_k^- = C_k x_k^-, \tag{8.14}$$

$$X_k^+ = \Psi(x_k^+, S_k^+, \alpha), \tag{8.15}$$

$$P_k^+ = P_k^- - K_k P_{yy,k} K_k^{\mathrm{T}}, \tag{8.16}$$

where

$$K_k = P_{xy,k} P_{yy,k}^{-1}, \tag{8.17}$$

$$P_{xy,k} = \sum_{i=0}^{2n} \gamma_i (X_{i,k}^- - x_k^-)(Y_{i,k}^- - y_k^-)^{\mathrm{T}}, \tag{8.18}$$

$$P_{yy,k} = \sum_{i=0}^{2n} \gamma_i (Y_{i,k}^- - y_k^-)(Y_{i,k}^- - y_k^-)^{\mathrm{T}} + R_k, \tag{8.19}$$

$$Y_{i,k}^- = h(X_{i,k}^-, k), i = 0, \ldots, 2n, \tag{8.20}$$

where $h(X_{i,k}^-, k)$ maps the input to the output and $S_k^+ \in \mathbb{R}^{n \times n}$ satisfies

$$S_k^+ (S_k^+)^{\mathrm{T}} = P_k^+. \tag{8.21}$$

The forecast step of UKF is given by

$$X_{i,k+1}^- = f(X_{i,k}^+, u_k, k), i = 0, \ldots, 2n, \tag{8.22}$$

$$x_{k+1}^- = \sum_{1=0}^{2n} \gamma_i X_{i,k+1}^-, \tag{8.23}$$

$$P_{k+1}^- = \sum_{1=0}^{2n} \gamma_i (X_{i,k+1}^- - x_{k+1}^-)(X_{i,k+1}^- - x_{k+1}^-)^{\mathrm{T}} = Q_k, \tag{8.24}$$

where $f(X_{i,k}^+, u_k, k)$ represents the dynamics of the nonlinear system. If the dynamics are linear, then UKF is equivalent to the Kalman filter. Furthermore, in the linear case, P_k^+ and P_k^- are the covariances of the errors $x_k - x_k^+$ and $x_k - x_k^-$, respectively. However, in the nonlinear case, P_k^+ and P_k^- are pseudo-error covariances.

At each time step k, the ensemble X_k^+ is constructed using the unscented transformation based on a square root S_k^+ of P_k^+ satisfying (8.21). However, the factor S_k^+ satisfying (8.21) is not unique. For example, the singular value decomposition or the Cholesky factorization can be used to obtain a square root of the pseudo-error co-

variance P_k^+ . Moreover, if $S_k^+ = \hat{S}_k^+$ satisfies (8.21), then, for any orthogonal matrix $U \in \mathbb{R}^{n\times n}$, the matrix $S_k^+ = \hat{S}_k^+ U$ also satisfies (8.21). For linear dynamics, UKF is equivalent to the Kalman filter, and the performance of UKF does not depend on the choice of S_k^+. However, for nonlinear dynamics, the performance of UKF depends on the choice of S_k^+, although simulation results indicate that the performance of UKF is similar for different choices of S_k^+.

8.4 Retrospective Cost Model Refinement

Consider the MIMO discrete-time main system

$$x(k+1) = A_0 x(k) + D_1 w(k) + Bu(k), \tag{8.25}$$

$$y_0(k) = E_1 x(k) + v(k), \tag{8.26}$$

$$y(k) = C_0 x(k), \tag{8.27}$$

where $x(k) \in \mathbb{R}^n$, $y(k) \in \mathbb{R}^{l_y}$, $y_0(k) \in \mathbb{R}^{l_{y_0}}$, $u(k) \in \mathbb{R}^{l_u}$, $w(k) \in \mathbb{R}^{l_w}$, $v(k) \in \mathbb{R}^{l_{y_0}}$, and $k \geq 0$. We assume that the excitation signal $w(k)$ is known and $v(k)$ denotes sensor noise. The main system (8.25)–(8.27) is interconnected with the unknown subsystem modeled by

$$u(k) = G_{\mathrm{s}}(\mathbf{q}) y_0(k). \tag{8.28}$$

The system (8.25)–(8.28) represents the true system. The dynamics of the true system can also be expressed as

$$x(k+1) = (A + B\kappa E_1)x(k) + D_1 w(k). \tag{8.29}$$

where κ is the unknown parameter.

Next, we assume a model of the main system of the form

$$\hat{x}(k+1) = \hat{A}\hat{x}(k) + \hat{D}_1 w(k) + \hat{B}\hat{u}(k), \tag{8.30}$$

$$\hat{y}_0(k) = \hat{E}_1\hat{x}(k), \tag{8.31}$$

$$\hat{y}(k) = \hat{C}\hat{x}(k), \tag{8.32}$$

where $\hat{x}(k) \in \mathbb{R}^n$, $\hat{y}(k) \in \mathbb{R}^{l_{\hat{y}}}$, $\hat{y}_0(k) \in \mathbb{R}^{l_{\hat{y}_0}}$, $\hat{u}(k) \in \mathbb{R}^{l_{\hat{u}}}$. The model of the main system is interconnected with the subsystem model

$$\hat{u}(k) = \hat{G}_{\mathrm{s}}(\mathbf{q})\hat{y}_0(k). \tag{8.33}$$

We choose $\hat{G}_s(\mathbf{q})$ to be an FIR first order approximation of $G_s(\mathbf{q})$. The goal is to estimate the subsystem model $\hat{G}_{\mathrm{s}}(\mathbf{q})$ by minimizing a cost function based on the performance variable

$$z(k) \stackrel{\triangle}{=} \hat{y}(k) - y(k) \in \mathbb{R}^{l_z}. \tag{8.34}$$

We estimate $\hat{G}_{\mathrm{s}}(\mathbf{q})$ by retrospectively reconstructing the signal $\hat{u}(k)$ that minimizes the performance at the current time step. The reconstruction of $\hat{u}(k)$ uses minimal modeling information about the true system (8.25)–(8.27), namely, a limited number of Markov parameters. We then use $\hat{u}(k)$ and $\hat{y}_0(k)$ to construct $\hat{G}_{\mathrm{s}}(\mathbf{q})$. Figure 8.1 illustrates the model-refinement architecture.

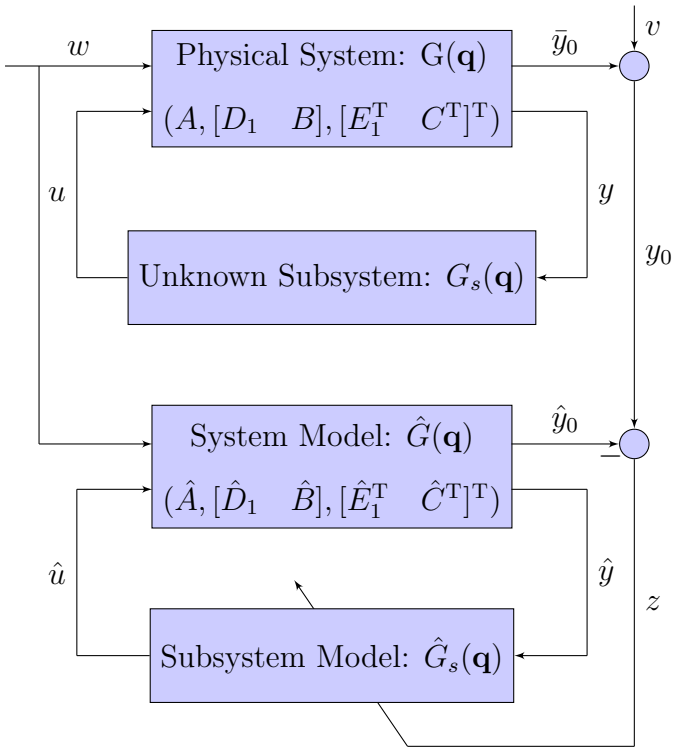

Figure 8.1: Model refinement architecture.

We begin by defining Markov parameters of the main system model $\hat{G}(\mathbf{q})$. For $i \geq 1$, let

$$H_i \triangleq \hat{C}\hat{A}^{i-1}\hat{B}. \tag{8.35}$$

Let r be a positive integer. Then, for all $k \geq r$,

$$\hat{x}(k) = \hat{A}^r\hat{x}(k-r) + \sum_{i=1}^{r}\hat{A}^{i-1}\hat{D}_1 w(k-i) + \sum_{i=1}^{r}\hat{A}^{i-1}\hat{B}\hat{u}(k-i), \tag{8.36}$$

and thus

$$z(k) = \hat{C}\hat{A}^r\hat{x}(k-r) + \sum_{i=1}^{r}\hat{C}\hat{A}^{i-1}\hat{D}_1 w(k-i) - y(k) + \bar{\mathcal{H}}\bar{U}(k-1), \tag{8.37}$$

where $\bar{\mathcal{H}} \triangleq \left[\begin{array}{ccc} H_1 & \cdots & H_r \end{array} \right] \in \mathbb{R}^{l_z \times r l_{\hat{u}}}$, and $\bar{U}(k-1) \triangleq \left[\begin{array}{ccc} \hat{u}^{\mathrm{T}}(k-1) & \cdots & \hat{u}^{\mathrm{T}}(k-r) \end{array} \right]^{\mathrm{T}}$.

Next, we rearrange the columns of $\bar{\mathcal{H}}$ and the components of $\bar{U}(k-1)$ and partition the resulting matrix and vector so that

$$\bar{\mathcal{H}}\bar{U}(k-1) = \mathcal{H}'U'(k-1) + \mathcal{H}U(k-1), \tag{8.38}$$

where $\mathcal{H}' \in \mathbb{R}^{l_z \times (r l_{\hat{u}} - l_U)}$, $\mathcal{H} \in \mathbb{R}^{l_z \times l_U}$, $U'(k-1) \in \mathbb{R}^{r l_{\hat{u}} - l_U}$, and $U(k-1) \in \mathbb{R}^{l_U}$. Then, we can rewrite (8.37) as

$$z(k) = \mathcal{S}(k) + \mathcal{H}U(k-1), \tag{8.39}$$

where

$$\mathcal{S}(k) \triangleq \hat{C}\hat{A}^r\hat{x}(k-r) + \sum_{i=1}^{r} \hat{C}\hat{A}^{i-1}\hat{D}_1 w(k-i) - y(k) + \mathcal{H}'U'(k-1). \tag{8.40}$$

For example, let $l_u = 1$, and $\bar{\mathcal{H}} = \left[\begin{array}{ccc} H_1 & H_2 & H_3 \end{array} \right]$. Then

$$\mathcal{H}' = \left[\begin{array}{cc} H_1 & H_2 \end{array} \right], \quad U'(k-1) = \left[\begin{array}{c} \hat{u}(k-1) \\ \\ \hat{u}(k-2) \end{array} \right],$$

and $\mathcal{H} = H_3, \quad U(k-1) = \hat{u}(k-3)$. Next, we rewrite (8.39) with a delay of k_j time steps, where $0 \leq k_1 \leq k_2 \leq \cdots \leq k_s$, in the form

$$z(k-k_j) = \mathcal{S}_j(k-k_j) + \mathcal{H}_j U_j(k-k_j-1), \tag{8.41}$$

where (8.40) becomes

$$\mathcal{S}_j(k-k_j) \stackrel{\triangle}{=} \hat{C}\hat{A}^r\hat{x}(k-k_j-r) + \sum_{i=1}^{r}\hat{C}\hat{A}^{i-1}\hat{D}_1 w(k-k_j-i) - y_0(k-k_j) + \mathcal{H}'_j U'_j(k-k_j-1) \quad (8.42)$$

and (8.38) becomes

$$\bar{\mathcal{H}}\bar{U}(k-k_j-1) = \mathcal{H}'_j U'_j(k-k_j-1) + \mathcal{H}_j U_j(k-k_j-1), \quad (8.43)$$

where $\mathcal{H}'_j \in \mathbb{R}^{l_z \times (rl_{\hat{u}} - l_{U_j})}$, $\mathcal{H}_j \in \mathbb{R}^{l_z \times l_{U_j}}$, $U'_j(k-k_j-1) \in \mathbb{R}^{rl_{\hat{u}} - l_{U_j}}$, and $U_j(k-k_j-1) \in \mathbb{R}^{l_{U_j}}$. Now, by stacking $z(k-k_1), \ldots, z(k-k_s)$, we define the *extended performance*

$$Z(k) \stackrel{\triangle}{=} \begin{bmatrix} z^{\mathrm{T}}(k-k_1) & \cdots & z^{\mathrm{T}}(k-k_s) \end{bmatrix}^{\mathrm{T}} \in \mathbb{R}^{sl_z}. \quad (8.44)$$

Therefore,

$$Z(k) \stackrel{\triangle}{=} \tilde{\mathcal{S}}(k) + \tilde{\mathcal{H}}\tilde{U}(k-1), \quad (8.45)$$

where $\tilde{\mathcal{S}}(k) \stackrel{\triangle}{=} \begin{bmatrix} \mathcal{S}^{\mathrm{T}}(k-k_1) \cdots \mathcal{S}^{\mathrm{T}}(k-k_s) \end{bmatrix}^{\mathrm{T}} \in \mathbb{R}^{sl_z}$, $\tilde{\mathcal{H}} \in \mathbb{R}^{sl_z \times l_{\tilde{U}}}$, and $\tilde{U}(k-1) \in \mathbb{R}^{l_{\tilde{U}}}$. The vector $\tilde{U}(k-1)$ is formed by stacking $U_1(k-k_1-1), \ldots, U_s(k-k_s-1)$ and removing repetitions of components. For example, with $k_1 = 0$ and $k_2 = 1$, stacking $U_1(k-1) = \begin{bmatrix} \hat{u}(k-1) \\ \hat{u}(k-2) \end{bmatrix}$ and $U_2(k-2) = \hat{u}(k-2)$ results in $\tilde{U}(k-1) = \begin{bmatrix} \hat{u}(k-1) \\ \hat{u}(k-2) \end{bmatrix}$. The coefficient matrix $\tilde{\mathcal{H}}$ consists of the entries of $\mathcal{H}_1, \ldots, \mathcal{H}_s$ arranged according to the structure of $\tilde{U}(k-1)$. Furthermore, we assume that the last entry of $\tilde{U}(k-1)$ is a component of $\hat{u}(k-r)$.

Next, we define the *retrospective performance*

$$\hat{z}(k-k_j) \triangleq \mathcal{S}_j(k-k_j) + \mathcal{H}_j U_j^*(k-k_j-1), \tag{8.46}$$

where the actual past subsystem outputs $U_j(k-k_j-1)$ in (8.41) are replaced by the retrospective subsystem outputs $U_j^*(k-k_j-1)$. The *extended retrospective performance* for (8.46), which is defined as

$$\hat{Z}(k) \triangleq \left[\begin{array}{ccc} \hat{z}^{\mathrm{T}}(k-k_1) & \cdots & \hat{z}^{\mathrm{T}}(k-k_s) \end{array} \right]^{\mathrm{T}} \in \mathbb{R}^{sl_z}, \tag{8.47}$$

is given by

$$\hat{Z}(k) = \tilde{\mathcal{S}}(k) + \tilde{\mathcal{H}}\tilde{U}^*(k-1), \tag{8.48}$$

where the components of $\tilde{U}^*(k-1) \in \mathbb{R}^{l_{\tilde{U}}}$ are components of $U_1^*(k-k_1-1), \ldots, U_s^*(k-k_s-1)$ ordered in the same way as the components of $\tilde{U}(k-1)$. Subtracting (8.45) from (8.48) yields

$$\hat{Z}(k) = Z(k) - \tilde{\mathcal{H}}\tilde{U}(k-1) + \tilde{\mathcal{H}}\tilde{U}^*(k-1). \tag{8.49}$$

Finally, we define the *retrospective cost function*

$$J(\tilde{U}^*(k-1), k) \triangleq \hat{Z}^{\mathrm{T}}(k) R(k) \hat{Z}(k), \tag{8.50}$$

where $R(k) \in \mathbb{R}^{sl_z \times sl_z}$ is a positive-definite performance weighting. The goal is to determine refined subsystem outputs $\tilde{U}^*(k-1)$ that would have provided better performance than the subsystem outputs $U(k)$ that were applied to the system. The refined subsystem outputs values $\tilde{U}^*(k-1)$ are subsequently used to update the subsystem estimate.

8.4.1 Cost Function Optimization with Adaptive Regularization

To ensure that (8.50) has a global minimizer, we consider the regularized cost

$$\bar{J}(\tilde{U}^*(k-1),k) \triangleq \hat{Z}^{\mathrm{T}}(k)R(k)\hat{Z}(k) + \eta(k)\tilde{U}^{*\mathrm{T}}(k-1)\tilde{U}^*(k-1), \tag{8.51}$$

where $\eta(k) = \bar{\eta}z^{\mathrm{T}}(k)z(k)$ and $\bar{\eta} \geq 0$. Substituting (8.49) into (8.51) yields

$$\bar{J}(\tilde{U}^*(k-1),k) = \tilde{U}^*(k-1)^{\mathrm{T}}\mathcal{A}(k)\tilde{U}^*(k-1) + \mathcal{B}(k)\tilde{U}^*(k-1) + \mathcal{C}(k), \tag{8.52}$$

where

$$\mathcal{A}(k) \triangleq \tilde{\mathcal{H}}^{\mathrm{T}}R(k)\tilde{\mathcal{H}} + \eta(k)I_{l_{\tilde{U}}}, \tag{8.53}$$

$$\mathcal{B}(k) \triangleq 2\tilde{\mathcal{H}}^{\mathrm{T}}R(k)[Z(k) - \tilde{\mathcal{H}}\tilde{U}(k-1)], \tag{8.54}$$

$$\mathcal{C}(k) \triangleq Z^{\mathrm{T}}(k)R(k)Z(k) - 2Z^{\mathrm{T}}(k)R(k)\tilde{\mathcal{H}}\tilde{U}(k-1) + \tilde{U}^{\mathrm{T}}(k-1)\tilde{\mathcal{H}}^{\mathrm{T}}R(k)\tilde{\mathcal{H}}\tilde{U}(k-1). \tag{8.55}$$

If either $\tilde{\mathcal{H}}$ has full column rank or $\eta(k) > 0$, then $\mathcal{A}(k)$ is positive definite. In this case, $\bar{J}(\tilde{U}^*(k-1),k)$ has the unique global minimizer

$$\tilde{U}^*(k-1) = -\frac{1}{2}\mathcal{A}^{-1}(k)\mathcal{B}(k). \tag{8.56}$$

8.4.2 Subsystem Modeling

The subsystem output $\hat{u}(k)$ is given by the strictly proper FIR time-series model of order n_{c} given by

$$\hat{u}(k) = \sum_{i=1}^{n_{\mathrm{c}}} N_i(k)\hat{y}(k-i), \tag{8.57}$$

where, for all $i = 1, \ldots, n_{\mathrm{c}}$, $N_i(k) \in \mathbb{R}^{l_{\hat{u}} \times l_{\hat{y}}}$. The subsystem output (8.57) can be expressed as $\hat{u}(k) = \theta(k)\phi(k-1)$, where $\theta(k) \in \mathbb{R}^{l_{\hat{u}} \times n_{\mathrm{c}} l_{\hat{y}}}$ and $\phi(k) \in \mathbb{R}^{n_{\mathrm{c}} l_{\hat{y}}}$,

$$\theta(k) \triangleq [N_1(k) \ \cdots \ N_{n_{\mathrm{c}}}(k)], \tag{8.58}$$

$$\phi(k-1) \triangleq \left[\hat{y}^{\mathrm{T}}(k-1) \ \cdots \ \hat{y}^{\mathrm{T}}(k-n_{\mathrm{c}})\right]^{\mathrm{T}}. \tag{8.59}$$

If $n_{\mathrm{c}} = 1$, then

$$\hat{u}(k) = \theta(k)\hat{y}(k-1) = N_1(k)\hat{y}(k-1). \tag{8.60}$$

Thus, $\theta(k)$ is the estimate of the uncertain parameter κ.

8.4.3 Recursive Least Squares Update

Let $d > 0$ such that $\tilde{U}^*(k-1)$ contains $u^*(k-d)$, and define the cost

$$\begin{aligned} J_{\mathrm{R}}(\theta(k)) \triangleq & \sum_{i=1}^{k} \lambda^{k-i} ||u^{*\mathrm{T}}(k-d) - \phi^{\mathrm{T}}(k-d-1)\theta^{\mathrm{T}}(k)||^2 \\ & + \lambda^k (\theta(k) - \theta(0)) P^{-1}(0) (\theta(k) - \theta(0))^{\mathrm{T}}, \end{aligned} \tag{8.61}$$

where $\phi(k-d)$ is given by (8.59), $\|\cdot\|$ is the Euclidean norm, and $\lambda(k) \in (0, 1]$ is the forgetting factor. Minimizing the cumulative cost function recursively yields

$$\theta^{\mathrm{T}}(k) = \theta^{\mathrm{T}}(k-1) + P(k)\phi(k-d-1) \cdot (u^*(k-d) - \phi^{\mathrm{T}}(k-d-1)\theta^{\mathrm{T}}(k-1)), \tag{8.62}$$

$$\begin{aligned} P(k) = & \lambda^{-1}(k)P(k-1) - \lambda^{-1}(k)P(k-1)\phi(k-d-1) \\ & \cdot [\phi^{\mathrm{T}}(k-d-1)P(k-1)\phi(k-d) + \lambda(k)]^{-1} \phi^{\mathrm{T}}(k-d-1)P(k-1). \end{aligned} \tag{8.63}$$

We initialize $P(0) = \beta I$, where $\beta > 0$.

8.5 Mass-Spring-Damper Example

Consider the mass-spring-damper system

$$m\ddot{q} + c\dot{q} + \kappa q = w, \tag{8.64}$$

$$y = \dot{q} + v, \tag{8.65}$$

where q and $\dot{q}$ are the position and velocity of the mass, respectively, $m = 1$, $c = 5$, and $\kappa = 10$ are the mass, damping, and spring constants, respectively, w is the force input, and v is white Gaussian sensor noise with mean μ_v and variance σ_v^2. The stiffness is assumed to be constant and uncertain. The state space representation of (8.65) is given by

$$\begin{bmatrix} \dot{q} \\ \ddot{q} \end{bmatrix} = \begin{bmatrix} 0 & 1 \\ -\frac{\kappa}{m} & -\frac{c}{m} \end{bmatrix} \begin{bmatrix} q \\ \dot{q} \end{bmatrix} + \begin{bmatrix} 0 \\ \frac{1}{m} \end{bmatrix} w, \tag{8.66}$$

$$y = \begin{bmatrix} 0 & 1 \end{bmatrix} \begin{bmatrix} q \\ \dot{q} \end{bmatrix} + v. \tag{8.67}$$

Euler discretization of (8.66) and (8.67) with sampling period $h = 0.1$ yields

$$\begin{bmatrix} x_1(k+1) \\ x_2(k+1) \end{bmatrix} = \begin{bmatrix} 1 & h \\ -\frac{\kappa h}{m} & 1 - \frac{ch}{m} \end{bmatrix} \begin{bmatrix} x_1(k) \\ x_2(k) \end{bmatrix} + \begin{bmatrix} 0 \\ \frac{h}{m} \end{bmatrix} w(k), \tag{8.68}$$

$$y(k) = \begin{bmatrix} 0 & 1 \end{bmatrix} \begin{bmatrix} x_1(k) \\ x_2(k) \end{bmatrix} + v(k), \tag{8.69}$$

where $x_1(k) \triangleq q(kh)$ and $x_2(k) \triangleq \dot{q}(kh)$. For each algorithm, we use $\hat{\kappa}(0) = 0$, $\hat{x}_1(0) = 0.1$ and $\hat{x}_2(0) = 0.01$. For EKF, we use $R = \sigma_v^2$ and $Q = \text{diag}([0.1, 0.1, 5000])$, for UKF, we use $R = \sigma_v^2$ and $Q = \text{diag}([0.1, 0.1, 200])$, and, for RCMR, we use $\beta = 0.42$, $\lambda = 1$, and $\tilde{\mathcal{H}} = [H_1 \quad H_2]$, unless otherwise specified.

Example 8.1. Estimation of a constant parameter. We first consider the case where there is no sensor noise. Figure 8.2 shows that all algorithms estimate the unknown parameter with roughly the same accuracy.

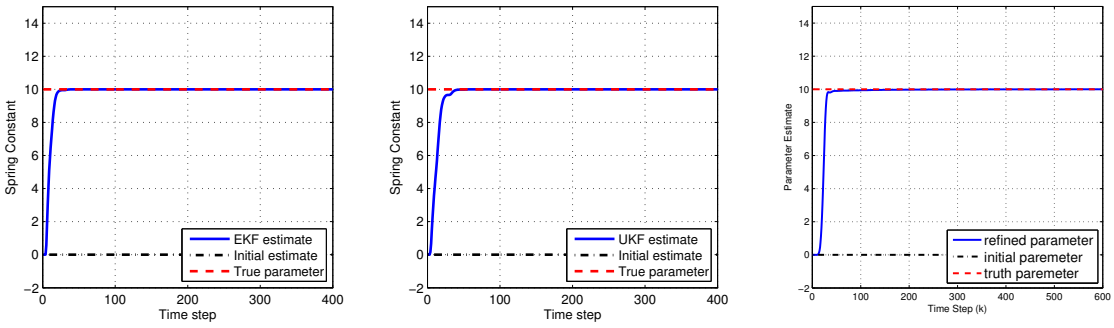

(a) (b) (c)

Figure 8.2: Example 8.1: Estimation of a constant parameter. Estimates of κ with $v = 0$. (a) EKF, (b) UKF, (c) RCMR. All algorithms estimate the unknown parameter with roughly the same accuracy.

Next, we consider the case where v is Gaussian white noise with $\mu_v = 10^{-3}$ and $\sigma_v^2 = 10^{-5}$. Figure 8.3 shows that EKF, UKF, and RCMR yield estimates of κ. Note that, EKF and UKF require estimates of the noise covariance, and RCMR does not. However, the RCMR estimate is the least corrupted by the sensor noise. ■

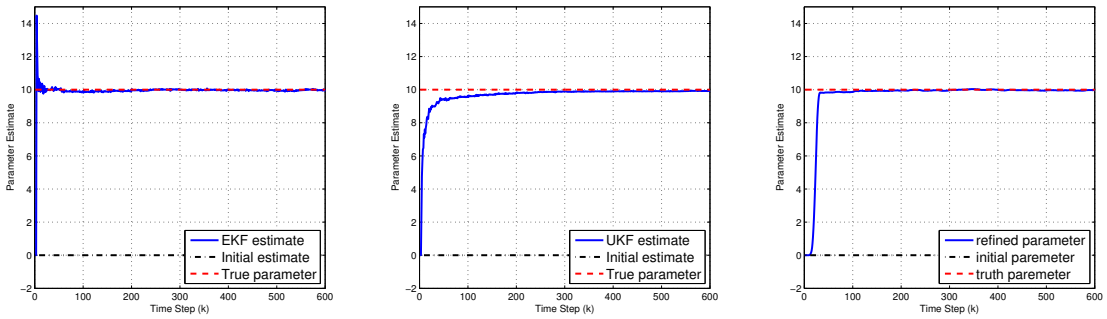

(a) (b) (c)

Figure 8.3: Example 8.1: Estimation of a constant parameter. Estimates of κ with $\mu_v = 10^{-3}$ and $\sigma_v^2 = 10^{-5}$. (a) EKF, (b) UKF, (c) RCMR. The RCMR estimate is the least corrupted by the sensor noise.

We now consider the case where κ is time varying. Specifically,

$$\kappa = \begin{cases} 10, & k < 200, \\ 10 + (k - 200)/20, & 200 \leq k \leq 400, \\ 20, & k > 400. \end{cases}$$

For each algorithm, we use $\hat{\kappa}(0) = 0$, $\hat{x}_1(0) = 0.1$ and $\hat{x}_2(0) = 0.01$. For EKF, we use $R = \sigma_v^2$ and $Q = \text{diag}([0.1, 0.1, 5000])$, for UKF, we use $R = \sigma_v^2$ and $Q = \text{diag}([0.1, 0.1, 200])$, and, for RCMR, we use $\beta = 0.3$, $\lambda = 0.985$, $\bar{\eta} = 0$, and $\tilde{\mathcal{H}} = [H_1 \ H_2]$, unless otherwise specified.

Example 8.2. Estimation of a time-varying parameter. We first consider the case where there is no sensor noise. Figure 8.4 shows that all algorithms identify the unknown parameter with roughly the same accuracy. However, RCMR is slower in tracking the shift in the parameter.

Next, we consider the case where v is Gaussian white noise with $\mu_v = 10^{-3}$ and $\sigma_v^2 = 10^{-5}$. Figure 8.5 shows that RCMR yields an estimate of κ with smaller error than EKF and UKF, and is the least corrupted by the sensor noise. ■

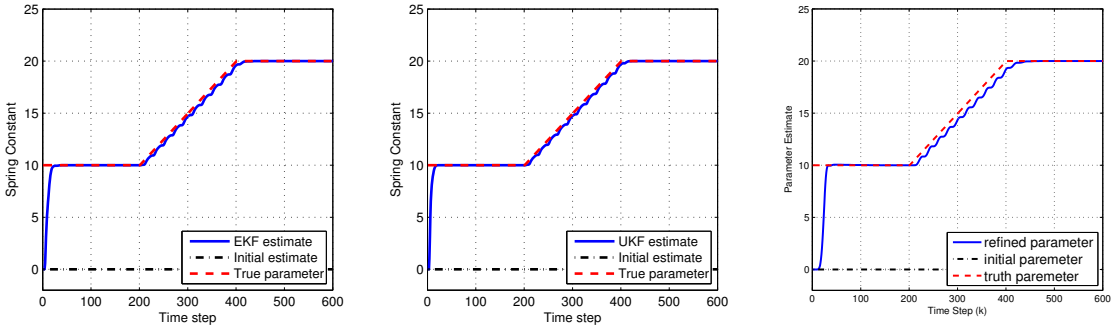

(a) (b) (c)

Figure 8.4: Example 8.2: Estimation of a time-varying parameter. Estimates of κ with $\mu_v = 0$ and $\sigma_v^2 = 0$. (a) EKF, (b) UKF, (c) RCMR. All algorithms identify the unknown parameter with roughly the same accuracy. However, RCMR is slower in tracking the shift in the parameter.

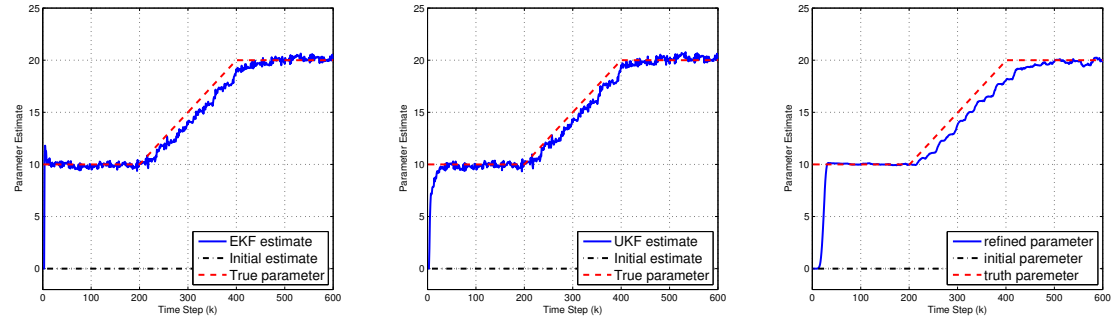

(a) (b) (c)

Figure 8.5: Example 8.2: Estimation of a time-varying parameter. Estimates of κ with $\mu_v = 10^{-3}$ and $\sigma_v^2 = 10^{-5}$. (a) EKF, (b) UKF, (c) RCMR. RCMR yields an estimate of κ with smaller error than EKF and UKF, and is the least corrupted by the sensor noise.

8.6 Estimation of a Repeated Parameter

We next consider the case where one unknown parameter appears in multiple locations within the model. Consider the continuous-time system

$$\dot{x} = A_c x + D_c w, \tag{8.70}$$

where a parameter α in A_c and D_c is uncertain. Let $\alpha = \hat{\alpha} + \Delta\alpha$, where $\hat{\alpha}$ is the initial estimate of α. The system model can be written approximately as

$$\dot{x} = (A_c + \frac{\partial A_c}{\partial \alpha}\bigg|_{\alpha=\hat{\alpha}} \Delta\alpha)x + (D_c + \frac{\partial D_c}{\partial \alpha}\bigg|_{\alpha=\hat{\alpha}} \Delta\alpha)w. \tag{8.71}$$

Discretizing (8.71) with sampling period h yields

$$\begin{aligned} x(k+1) &= (I + A_c h + \frac{\partial A_c}{\partial \alpha}\bigg|_{\alpha=\hat{\alpha}} \Delta\alpha h)x(k) + (D_c h + \frac{\partial D_c}{\partial \alpha}\bigg|_{\alpha=\hat{\alpha}} \Delta\alpha h)w(k) \\ &= (A + \frac{\partial A_c}{\partial \alpha}\bigg|_{\alpha=\hat{\alpha}} \Delta\alpha h)x(k) + (D_1 + \frac{\partial D_c}{\partial \alpha}\bigg|_{\alpha=\hat{\alpha}} \Delta\alpha h)w(k). \end{aligned} \tag{8.72}$$

We use (8.72) as the true system model with uncertain parameter $\Delta\alpha$. Since our goal is to estimate $\Delta\alpha$, we rewrite (8.72)

$$x(k+1) = Ax + \begin{bmatrix} D_1 & \frac{\partial A_c}{\partial \alpha}\Big|_{\alpha=\hat{\alpha}} h & \frac{\partial D_c}{\partial \alpha}\Big|_{\alpha=\hat{\alpha}} h \end{bmatrix} \begin{bmatrix} w(k) \\ \Delta\alpha x(k) \\ \Delta\alpha w(k) \end{bmatrix}. \tag{8.73}$$

Next, let

$$\hat{B} = \begin{bmatrix} \frac{\partial A_c}{\partial \alpha}\Big|_{\alpha=\hat{\alpha}} h & \frac{\partial D_c}{\partial \alpha}\Big|_{\alpha=\hat{\alpha}} h \end{bmatrix}, \tag{8.74}$$

$$\hat{y}(k) = \begin{bmatrix} \hat{x}(k) \\ w(k) \end{bmatrix}, \tag{8.75}$$

$$\Delta\alpha(k) = \hat{G}_s(q) = \theta(k), \tag{8.76}$$

$$\hat{u}(k) = \Delta\alpha(k)\hat{y}(k). \tag{8.77}$$

Note that (8.77) shows that $\hat{u}(k)$ is a function of $\hat{y}(k)$. We define

$$\hat{Y}(k) \triangleq \begin{bmatrix} \hat{y}^{\mathrm{T}}(k-k_1) & \cdots & \hat{y}^{\mathrm{T}}(k-k_s) \end{bmatrix}^{\mathrm{T}} \in \mathbb{R}^{sl_y}. \tag{8.78}$$

Using (8.73)–(8.78), (8.52)-(8.56) can be written as

$$\bar{J}(\Delta\alpha^*(k-1),k) = \mathcal{A}(k)\Delta\alpha^{*2}(k-1) + \mathcal{B}(k)\Delta\alpha^*(k-1) + \mathcal{C}(k), \tag{8.79}$$

where

$$\mathcal{A}(k) \triangleq \hat{Y}(k-1)^T[\tilde{\mathcal{H}}^{\mathrm{T}}R(k)\tilde{\mathcal{H}} + \eta(k)I_{l_{\tilde{U}}}]\hat{Y}(k-1), \tag{8.80}$$

$$\mathcal{B}(k) \triangleq 2\tilde{\mathcal{H}}^{\mathrm{T}}R(k)[Z(k) - \tilde{\mathcal{H}}\tilde{U}(k-1)]\hat{Y}(k-1), \tag{8.81}$$

$$\begin{aligned}\mathcal{C}(k) \triangleq & Z^{\mathrm{T}}(k)R(k)Z(k) - 2Z^{\mathrm{T}}(k)R(k)\tilde{\mathcal{H}}\tilde{U}(k-1) \\ & + \tilde{U}^{\mathrm{T}}(k-1)\tilde{\mathcal{H}}^{\mathrm{T}}R(k)\tilde{\mathcal{H}}\tilde{U}(k-1),\end{aligned} \tag{8.82}$$

$$\tilde{U}^*(k-1) = \Delta\alpha^*(k-1)\hat{Y}(k-1) = -\frac{1}{2}\mathcal{A}^{-1}(k)\mathcal{B}(k)\hat{Y}(k-1). \tag{8.83}$$

We use one parameter in $\tilde{U}^*(k-1)$ and the corresponding parameter in $\tilde{Y}(k-1)$ to compute the recursive least squares update. In the next section we use the same mass-spring system to illustrate the algorithm.

Example 8.3. Mass estimation using RCMR. Consider the mass-spring-damper structure where $A_c = \begin{bmatrix} 0 & 1 \\ -\frac{\kappa}{m} & -\frac{c}{m} \end{bmatrix}$, $D_c = \begin{bmatrix} 0 \\ \frac{1}{m} \end{bmatrix}$, and $E_c = \begin{bmatrix} 0 & 1 \end{bmatrix}$. In this example we assume that the parameter m is unknown. We demonstrate the algorithm by choosing $\kappa = 30$ and $c = 5$, and we assume that $m = 0.9$. We use an initial estimate is $\hat{m}(0) = 1$, so that $\Delta m(0) = -0.1$.

From (8.74), we obtain

$$\hat{B} = \begin{bmatrix} 0 & 0 & 0 \\ \\ 3 & 0.5 & -0.1 \end{bmatrix}, \tag{8.84}$$

We choose $P(0) = 1$, $\lambda = 1$, $\bar{\eta} = 0$, $\mu = 0$, $\sigma_v^2 = 0$ and $\tilde{\mathcal{H}} = \begin{bmatrix} H_1 & H_2 \end{bmatrix}$, which are the first and second Markov parameters of $\hat{G}$. We choose the ramp input $w(k) = 0.1k$ and the initial state $\begin{bmatrix} \hat{x}_1(0) \\ \\ \hat{x}_2(0) \end{bmatrix} = \begin{bmatrix} x_1(0) \\ \\ x_2(0) \end{bmatrix} = \begin{bmatrix} 0 \\ \\ 0 \end{bmatrix}$. RCMR is turned on at $k = 100$ steps. Figure 8.6 shows the performance z and the estimate $\hat{m}$. RCMR yields an estimate of the mass, and the performance z approaches zero asymptotically.

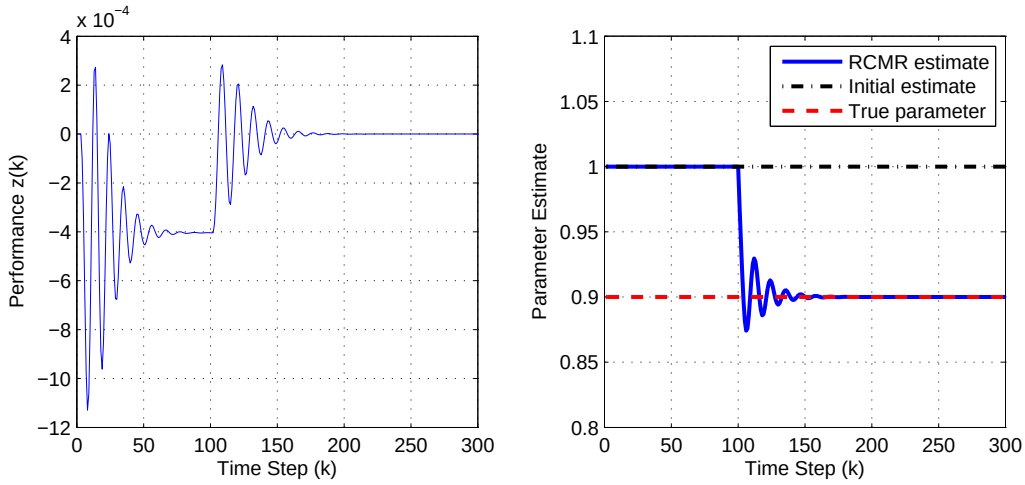

Figure 8.6: Example 8.3: Mass estimation using RCMR. The performance z and the estimate $\hat{m}$. RCMR yields an estimate of the mass, and the performance z approaches zero asymptotically.

We next consider the effect of zero-mean Gaussian white noise sensor noise. Figure 8.7 shows the estimation performance for several values of σ_v^2. As σ_v^2 increases, the accuracy of the estimate is degraded. ■

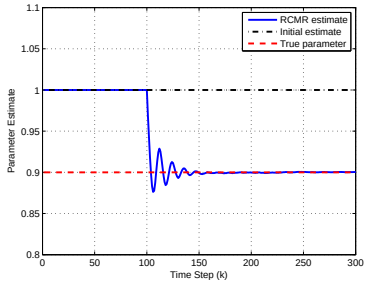

(a) $\sigma_v^2 = 1 \times 10^{-10}$

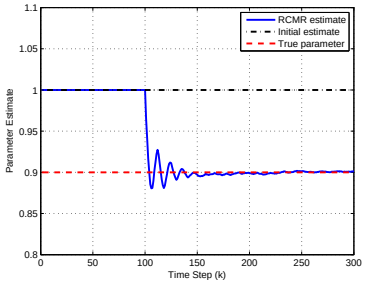

(b) $\sigma_v^2 = 1 \times 10^{-9}$

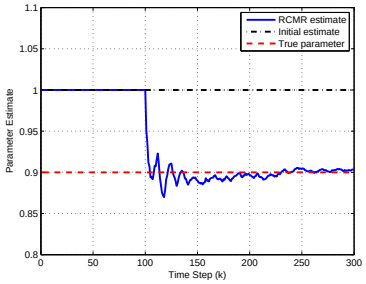

(c) $\sigma_v^2 = 1 \times 10^{-8}$

Figure 8.7: Example 8.3: Mass estimation using RCMR. The estimate $\hat{m}$ of m for various values of σ_v^2. As σ_v^2 increases, the accuracy of the estimate is degraded.

8.7 Estimation of Linearized Aircraft Dynamics in the Presence of Modeling Errors

In this section we consider an example where entries of A and B that are not being estimated have modeling errors. We consider a discretized model of a hypersonic aircraft, where $x = \begin{bmatrix} \beta & P & R & \phi \end{bmatrix}^{\mathrm{T}}$. The true system model is obtained by Euler discretization of the continuous-time plant (3.1)–(3.2) with $h = 0.001$. The discrete-time matrices are given by

$$A_{\text{true}} = \begin{bmatrix} 0.9999 & 0.000269 & -0.000963 & -0.000039 \\ A_{2,1} & 1.00021 & 0.000099 & 0 \\ 0.00041 & 0.000037 & 0.9973 & 0 \\ 0 & 0.00100 & -0.00042 & 1.0000 \end{bmatrix}, B_{\text{true}} = \begin{bmatrix} 0 \\ 0.002519 \\ -0.0000665 \\ 0 \end{bmatrix}, \tag{8.85}$$

$$C_{\text{true}} = \begin{bmatrix} 0 & 1 & 0 & 0 \end{bmatrix}, \tag{8.86}$$

where

$$A_{2,1} = \begin{cases} -0.02560 & k < 25000, \\ -0.02560 - 1.6640 \times 10^{-6} k & 25000 \leq k \leq 75000, \\ -0.1088 & k > 75000. \end{cases} \tag{8.87}$$

However, aside from $A_{2,1}$, we assume that the $(3,1)$ entry of A and the $(3,1)$ component of B are erroneous and are given by

$$A_{\text{model}} = \begin{bmatrix} 0.9999 & 0.000269 & -0.000963 & -0.000039 \\ \hat{A}_{2,1} & 1.00021 & 0.000099 & 0 \\ 0.000616 & 0.000037 & 0.9973 & 0 \\ 0 & 0.00100 & -0.00042 & 1.0000 \end{bmatrix}, B_{\text{model}} = \begin{bmatrix} 0 \\ 0.002519 \\ -0.0000222 \\ 0 \end{bmatrix}, \tag{8.88}$$

$$C_{\text{model}} = \begin{bmatrix} 0 & 1 & 0 & 0 \end{bmatrix}. \tag{8.89}$$

The goal is to thus estimate $A_{2,1}$, despite A_{model} and B_{model} having erroneous entries.

In all subsequent examples, the input signal w is zero-mean Gaussian white noise with $\sigma_w^2 = 0.001$, the initial estimate is $\hat{A}_{2,1}(0) = -0.02560$, and the initial conditions are $x(0) = 0$. The examples below consider parameter estimation for each algorithim under various scenarios of noise and bias in the measurement.

In all cases, we set, $\beta = 1$ and $\bar{\eta} = 0$. We do not compare UKF since it was found to be difficult to tune for this example. In fact, considerable retuning was required for each case when using EKF.

Example 8.4. Estimation of aircraft dynamics using EKF and RCMR. We first consider the case where $v = 0$. We choose $\lambda = 0.97$ for this case. Figure 8.8 shows the accuracy of EKF and RCMR. Both algorithms yield estimates of $A_{2,1}$.

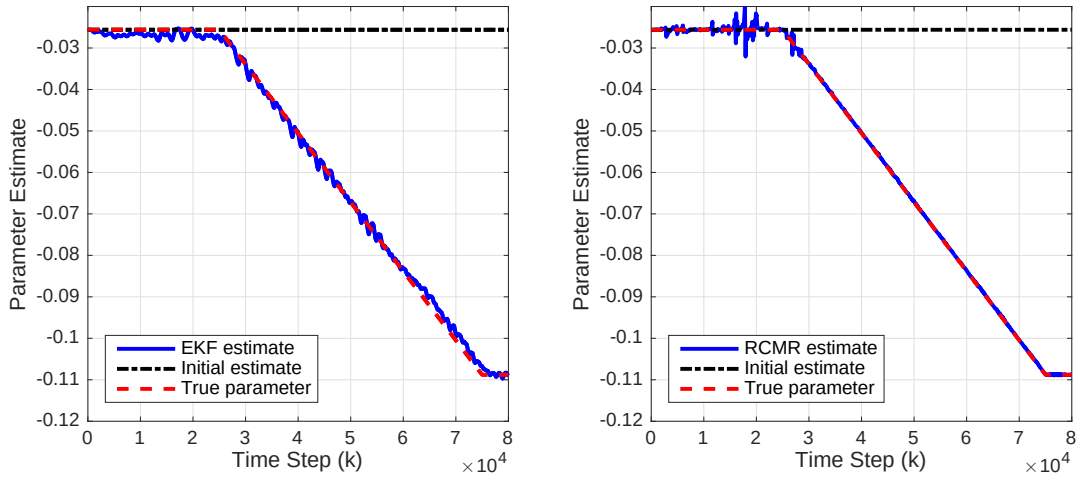

(a) (b)

Figure 8.8: Example 8.4: Estimation of aircraft dynamics using EKF and RCMR with $v = 0$. (a) EKF, (b) RCMR. Both algorithms yield estimates of $A_{2,1}$.

Next, we consider the case where zero-mean Gaussian white sensor noise is present. We assume $\sigma_v^2 = 1 \times 10^{-8}$ and choose $\lambda = 0.97$. Figure 8.9 shows the accuracy of EKF and RCMR for the hypersonic aircraft in this case. Both algorithms yield estimates of $A_{2,1}$, however RCMR is slower in tracking the shift in the parameter.

Next, we consider the case where biased sensor noise is present. We assume $\mu_v = 1 \times 10^{-2}$, $\sigma_v^2 = 0$ and choose $\lambda = 0.97$. Figure 8.10 shows the accuracy of RCMR. Note that EKF is not able to estimate the parameter correctly despite considerable tuning effort. Note that we do not attempt to measure the measurement bias when using the EKF. ■

Example 8.5. Estimation of aircraft dynamics using RCMR in the present of nonzero-mean sensor noise. We now consider the case of nonzero-mean Gaussian white sensor noise. We assume $\mu_v = 1 \times 10^{-2}$, $\sigma_v^2 = 1 \times 10^{-8}$ and choose $\lambda = 0.995$

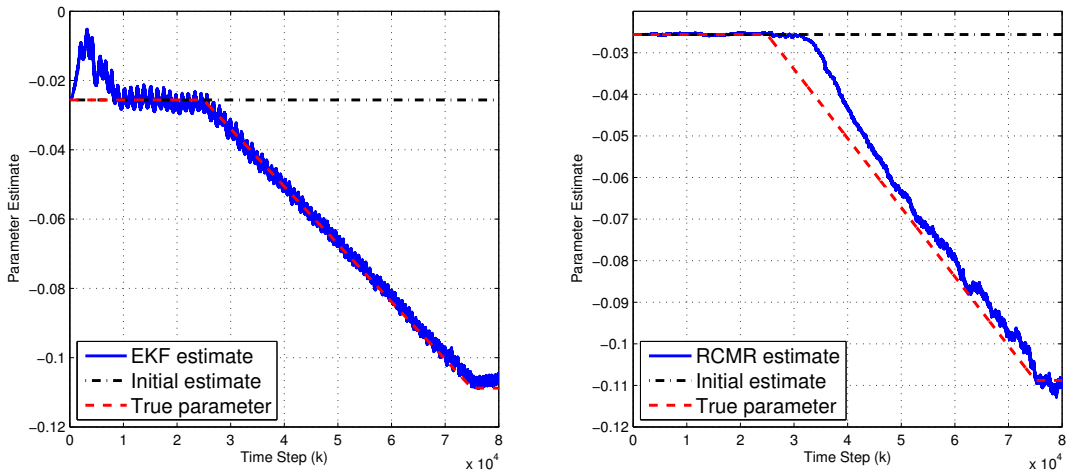

(a) (b)

Figure 8.9: Example 8.4: Estimation of aircraft dynamics using EKF and RCMR with $\sigma_v^2 = 1\times10^{-8}$. (a) EKF, (b) RCMR. Both algorithms yield estimates of $A_{2,1}$, however RCMR is slower in tracking the shift in the parameter.

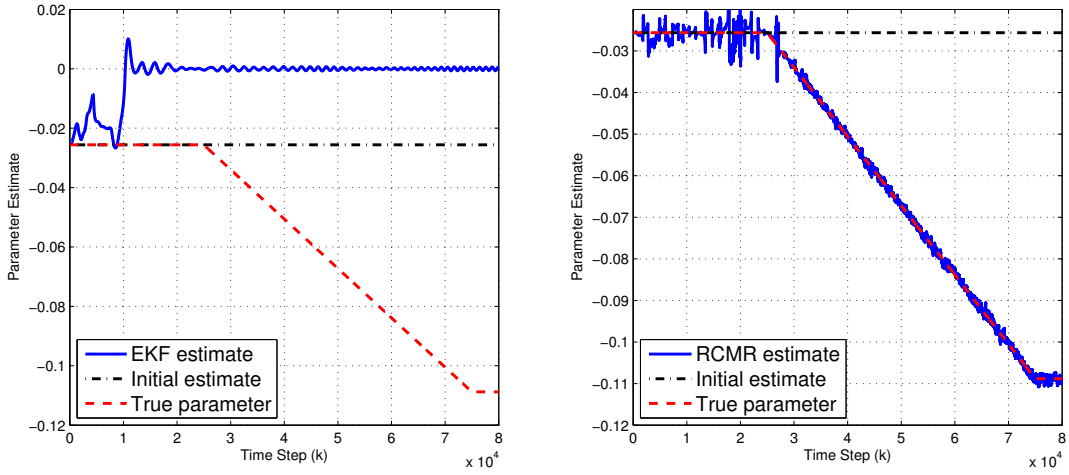

(a) (b)

Figure 8.10: Example 8.4: Estimation of aircraft dynamics using EKF and RCMR with $\mu_v = 1\times10^{-2}$ and $\sigma_v^2 = 0$. (a) EKF, (b) RCMR. Note that EKF is not able to estimate the parameter correctly despite considerable tuning effort. Note that we do not attempt to measure the measurement bias when using the EKF.

for this case. Figure 8.11 shows the estimate accuracy of RCMR for the hypersonic aircraft in this case. RCMR yields an estimate of $A_{2,1}$, but the estimate is corrupted by the sensor noise. ■

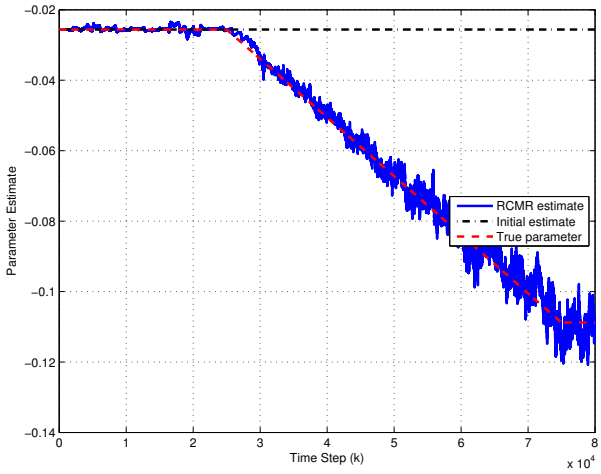

Figure 8.11: Example 8.5: Estimation of aircraft dynamics using RCMR with $\mu_v = 1 \times 10^{-2}$ and $\sigma_v^2 = 1 \times 10^{-8}$. RCMR yields an estimate of $A_{2,1}$, but the estimate is corrupted by the sensor noise.

8.8 Step Command Following with Forward-Propagating Riccati-Based Control with identification using RCMR

In this section we use RCMR to provide parameter estimates for a forward-propogating Riccati-based controller. We perform step command following for the lateral aircraft dynamics model discussed in Chapter 3. We consider both full-state feedback and output feedback. We first present forward-propogating Riccati-based control.

8.8.1 Full-State Feedback

Consider the discrete-time system

$$x(k+1) = A(k)x(k) + B(k)u(k). \tag{8.90}$$

We add an additional state representing the integral of the error in the form

$$\begin{bmatrix} x(k+1) \\ \gamma(k+1) \end{bmatrix} = \begin{bmatrix} A(k) & 0 \\ -C(k) & 1 \end{bmatrix} \begin{bmatrix} x(k) \\ \gamma(k) \end{bmatrix} + \begin{bmatrix} B(k) \\ 0 \end{bmatrix} u(k) + \begin{bmatrix} 0 \\ 1 \end{bmatrix} r, \tag{8.91}$$

where γ represents the integrator output, that is

$$\gamma(k+1) = \gamma(k) + r(k) - Cx(k), \tag{8.92}$$

where $C(k) = \begin{bmatrix} 0 & 0 & 0 & 1 \end{bmatrix}$ and r is a step command in ϕ. We thus obtain the augmented system

$$x_{\mathrm{a}}(k+1) = A_{\mathrm{a}}(k)x_{\mathrm{a}}(k) + B_{\mathrm{a}}(k)u(k) + \begin{bmatrix} 0 \\ 1 \end{bmatrix} r \tag{8.93}$$

where $x_{\mathrm{a}}(k) = \begin{bmatrix} x(k) & \gamma(k) \end{bmatrix}^{\mathrm{T}}$, and

$$A_{\mathrm{a}}(k) = \begin{bmatrix} A(k) & 0 \\ -C(k) & 1 \end{bmatrix}, B_{\mathrm{a}}(k) = \begin{bmatrix} B(k) \\ 0 \end{bmatrix}$$

The LQR control law is given by

$$u(k) = K(k)x_{\mathrm{a}}(k), \tag{8.94}$$

where

$$K = -(R_2 + B_{\mathrm{a}}^{\mathrm{T}} P B_{\mathrm{a}})^{-1} B_{\mathrm{a}}^{\mathrm{T}} P A_{\mathrm{a}}, \tag{8.95}$$

where the argument k has been dropped. We update P by using the forward-propagating Riccati equation

$$P(k+1) = A_{\mathrm{a}}^{\mathrm{T}} P(k) A_{\mathrm{a}} + R_1 - A_{\mathrm{a}}^{\mathrm{T}} P(k) B_{\mathrm{a}} (R_2 + B_{\mathrm{a}}^{\mathrm{T}} P(k) B_{\mathrm{a}})^{-1} B_{\mathrm{a}}^{\mathrm{T}} P(k) A_{\mathrm{a}}. \tag{8.96}$$

Equations (8.95) and (8.96) give the FPR regulator.

8.8.2 Output Feedback

In the case of output feedback, we consider an observer-based compensator of the form

$$x_{\mathrm{c}}(k+1) = [A_{\mathrm{a}}(k) + B_{\mathrm{a}}(k) K(k) - F(k) C_{\mathrm{a}}(k)]\, x_{\mathrm{c}}(k) + B_{\mathrm{c}}(k) y(k), \tag{8.97}$$

$$u(k) = C_{\mathrm{c}}(k) x_{\mathrm{c}}(k). \tag{8.98}$$

where

$$C_{\mathrm{a}} = \begin{bmatrix} 0 & 0 & 0 & 1 & 0 \end{bmatrix}$$

The regulator gain $K(k)$ is the full-state-feedback gain (8.95), and the observer gain $F(k)$ is given by

$$F(k) = A_{\mathrm{a}} Q(k) C_{\mathrm{a}}^{\mathrm{T}} (C_{\mathrm{a}} Q(k) C_{\mathrm{a}}^{\mathrm{T}} + V_2)^{-1}, \tag{8.99}$$

where $Q(k)$ is obtained by the dual equation

$$Q(k+1) = A_{\mathrm{a}}Q(k)A_{\mathrm{a}}^{\mathrm{T}} + V_1 - A_{\mathrm{a}}Q(k)C_{\mathrm{a}}^{\mathrm{T}}(C_{\mathrm{a}}Q(k)C_{\mathrm{a}}^{\mathrm{T}} + V_2)^{-1}C_{\mathrm{a}}Q(k)A_{\mathrm{a}}^{\mathrm{T}} \tag{8.100}$$

Equations (8.99) and (8.100) give the FPR Estimator. The structure of the observer-based compensator (8.97), (8.98) represents a regulator/observer structure. The closed-loop system with the observer-based dynamic compensator is given by

$$\tilde{x}(k+1) = \tilde{A}(k)\tilde{x}(k), \tag{8.101}$$

where

$$\tilde{x}(k) \triangleq \begin{bmatrix} x_{\mathrm{a}}(k) \\ \\ x_{\mathrm{c}}(k) \end{bmatrix}, \quad \tilde{A} \triangleq \begin{bmatrix} A_{\mathrm{a}} & B_{\mathrm{a}}K \\ \\ FC_{\mathrm{a}} & A + BK - FC_{\mathrm{a}} \end{bmatrix}. \tag{8.102}$$

We now use the RCMR estimate to update the plant dynamics for the FPR regulator and estimator. RCMR is turned on after 10 sec. In all cases where identification is available, RCMR provides an estimate of only $A_{2,1}$. In all examples in this section, the transition to off-nominal takes place over one time step, that is, 0.01 sec. The controller and observer both use incorrect modeling data for B, where we use a weighted average of the nominal and off-nominal plants. For A, the compensator uses the nominal system for all entries apart from $A_{2,1}$.

Example 8.6. Step-command following with full-state feedback. We first consider full-state feedback. Figure 8.12 shows step command following when using full-state feedback, and Figure 8.13 shows the parameter estimate in this case. The controller is able to follow the command after the transition to off-nominal conditions, after an inital deviation. RCMR is not able to converge to the true parameter due to modeling errors in the main system model, and the lack of persistent excitation.

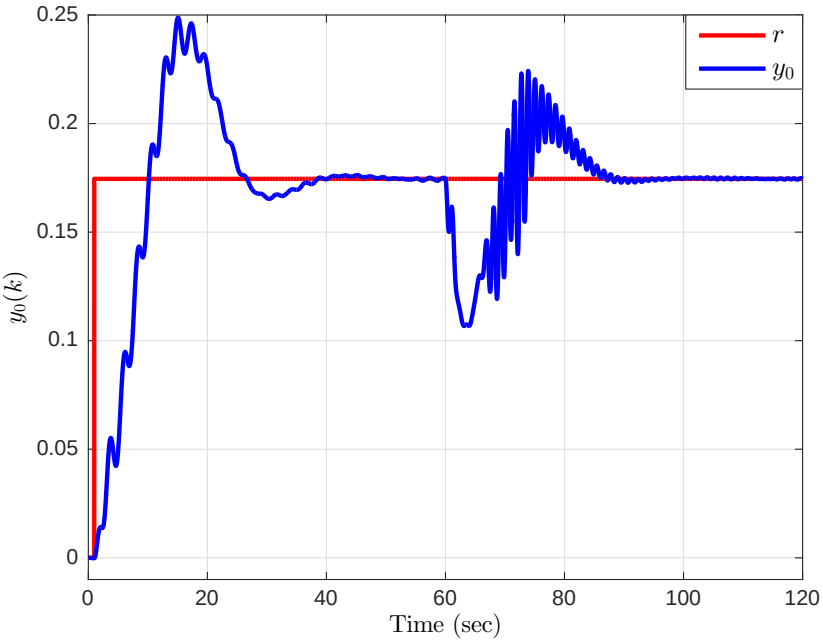

Figure 8.12: Example 8.6: Step-command following with full-state feedback with the RCMR estimate available. The controller is able to follow the command after the transition to off-nominal conditions, after an inital deviation.

The FPR tuning parameters are $P(0) = 0$, $R_1 = I_5$, and $R_2 = 10$. The RCMR tuning parameters are $l_y = l_z = l_u = 4$, $n_c = 1$, $\bar{\eta} = 0$, $\beta = 2 \times 10^5$, and $\lambda = 1$. ■

Example 8.7. Step-command following with output feedback. Next, we consider output feedback, where the RCMR estimate is available for the FPR estimator. RCMR is turned on after 10 sec. RCMR is also using the state estimates provided by the state observer. Figure 8.14 shows step command following with the RCMR estimate available. After the transition, the controller is able to follow the step command after an initial deviation. Note that the deviation is more severe than when using full-state feedback . Figure 8.15 shows the parameter estimate provided by RCMR. Figure 8.16 shows the observer error in this case. Notice that, after the transition to off-nominal conditions at 60 sec, the observer is able to drive to observer error back to zero, after an initial deviation.

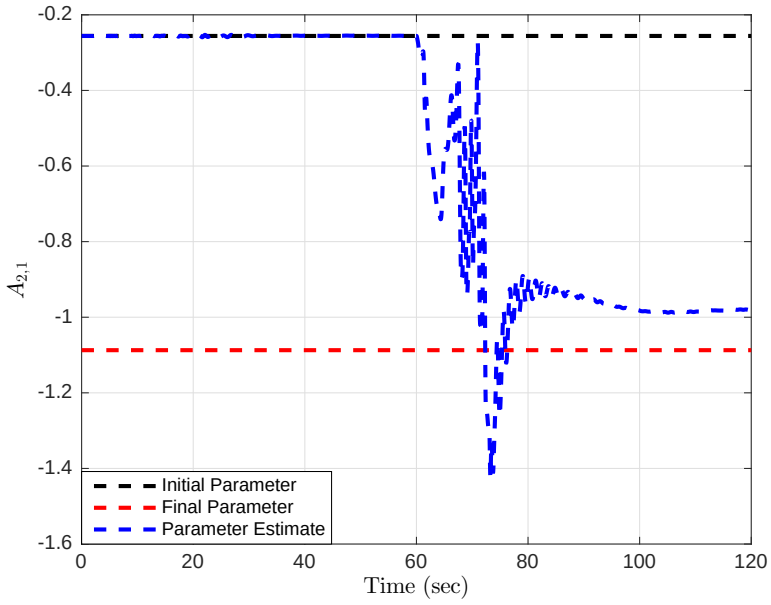

Figure 8.13: Example 8.6: Step-command following with full-state feedback. The RCMR parameter estimate does not converge to the right value due to modeling errors and the lack of persistent excitation.

The FPR regulator tuning parameters are $P(0) = 0$, $R_1 = I_5$, and $R_2 = 100$. The observer tuning parameters are $P_0 = I_5$, $V_1 = I_5$, and $V_2 = 1$. The RCMR tuning parameters are $l_y = l_z = l_u = 4$, $n_c = 1$, $\bar{\eta} = 0$, $\beta = 2$, and $\lambda = 1$. ■

8.9 Conclusions

The goal of this chapter was to compare the accuracy of established techniques for parameter estimation with RCMR, and present an online estimation and control technique. A plethora of techniques exists for nonlinear estimation, and all of these algorithms are candidates for parameter estimation. In this chapter we compared two nonlinear estimation algorithms with RCMR, which is not an estimation technique but rather is intended for subsystem identification, of which parameter estimation is a special case. The results suggest that RCMR is less sensitive to sensor noise, par-

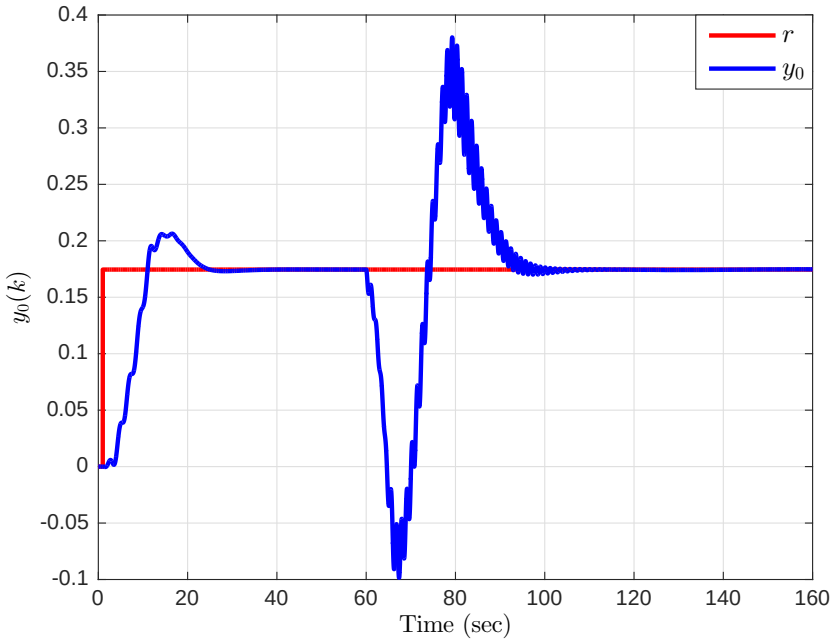

Figure 8.14: Example 8.7: Step-command following with output feedback with the RCMR estimate available. The controller is able to follow the command after the transition to off-nominal conditions, after a deviation during which RCMR estimates are improving.

ticularly, biased measurements. No attempt was made to estimate the measurement bias. Since RCMR does not involve an ensemble of models, it is computationally efficient compared to UKF. However, unlike EKF and UKF, RCMR does not provide an error probability distribution for the parameter estimates. Next, we used RCMR to provide parameter estimates to a forward propogating Riccati based controller, for command following for an aircraft lateral dynamics model with a transition to NMP dynamics.

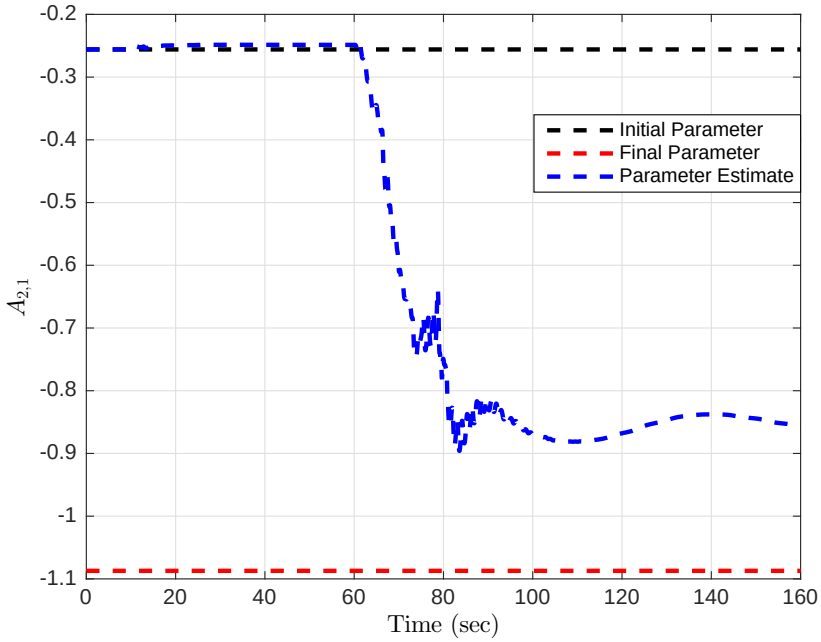

Figure 8.15: Example 8.7: Step-command following with full-state feedback. The RCMR parameter estimate does not converge to the right value due to modeling errors and the lack of persistent excitation.

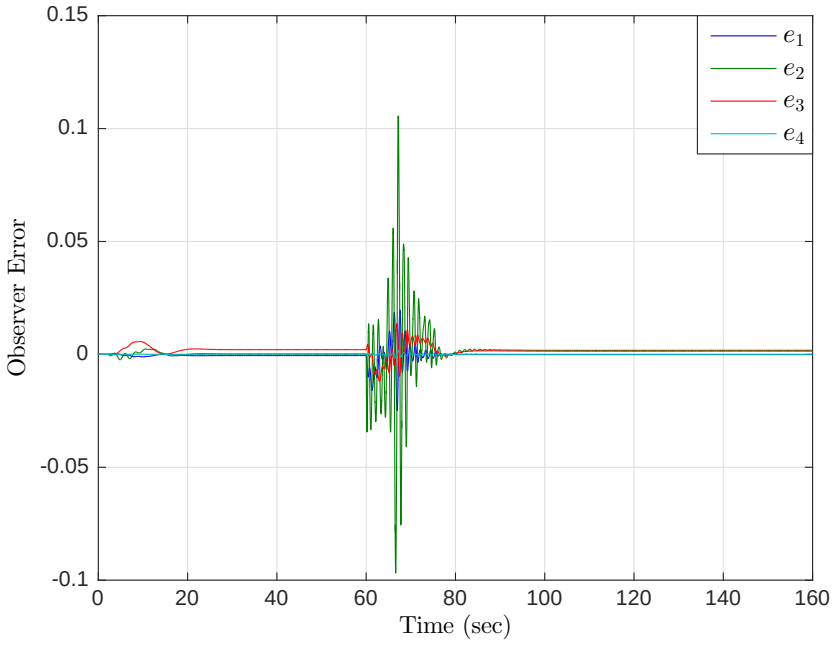

Figure 8.16: Example 8.7: Step-command following with full-state feedback. Observer error with the RCMR estimate available. The observer drives the observer error back to zero after a transient during the transition to off-nominal conditions.

CHAPTER 9

Conclusions and Future Work

9.1 Conclusions

Retrospective cost adaptive control (RCAC) is a direct adaptive control technique that is applicable to stable or unstable, minimum-phase or NMP, linear or nonlinear systems, for stabilization, command following, or disturbance rejection problems. RCAC requires minimal modeling information, as demonstrated in this dissertation. This dissertation expands on the development of RCAC, and explores several new applications for RCAC, including feedforward control, adaptive pole placement, adaptive PID control, and compares the H_2 cost and closed-loop frequency response of RCAC with discrete time LQG control.

In past work, RCAC was viewed as retrospective optimization of a dynamic compensator utilizing past performance data and control effort. The filter G_{f} was viewed as an FIR approximation of the transfer function G_{zu} from the control input u to the performance variable z. A key contribution of this dissertation was the demonstration that retrospective cost optimization updates the controller coefficients to minimize the residual of the fit between z and the output of the target model G_{f} with input $\tilde{u}$. Doing so matches the intercalated closed-loop transfer function $\widetilde{G}_{z\tilde{u}}$ to G_{f} , thus leading to the interpretation of G_{f} as a target model for $\widetilde{G}_{z\tilde{u}}$. It was shown that $\widetilde{G}_{z\tilde{u}}$ is the transfer function from the virtual external controller perturbation $\tilde{u}$ to the

performance variable z. The special nature of $\widetilde{G}_{z\tilde{u}}$ is due to the fact that $\tilde{u}$ enters the feedback loop through intercalated injection, which means that $\tilde{u}$ is injected internally to the controller as opposed to simply being added to the control input.

The target model G_{f} is selected by the user, and the choice of G_{f} is guided by its role in the controller adaptation. In particular, since RCAC tends to match $\widetilde{G}_{z\tilde{u}}$ to the target model and, since the target model possesses the NMP zeros of G_{zu}, the NMP zeros must be reproduced in the target model; otherwise, RCAC may cancel them, resulting in a hidden instability. This modeling information, along with the relative degree of G_{zu} and its leading numerator coefficient, constitutes the basic modeling information required by RCAC. These statements apply to the case where G_{zu} is SISO.

We applied RCAC to problems that are difficult or even impossible for fixed gain controllers, including plants with transitions from minimum phase to NMP dynamics, as well as plants with erroneous modeling information or unmodeled dynamics, plants with limited achievable stability margins. It was shown that RCAC can readapt to destabilizing perturbations, and can restabilize the closed-loop system. We use quasi-FIR control laws to achieve near optimal control for plants which yield unstable high-authority LQG controllers, as well as for command following for NMP plants without knowledge of the NMP zero.

Next, we considered the question, "Are all full-order compensators observer-based?" It was shown that apart from the case where n is odd and the closed-loop spectrum does not contain at least one real root, all full order compensators are observer-based. Next, it was shown that since the LQG solution requires separation, all such compensators are thus inherently sub-optimal. This question helps to understand the closed-loop pole locations arising from full-order RCAC compensators.

Finally, we used retrospective cost model refinement (RCMR) to demonstrate parameter estimation for several examples, and compare RCMR to established es-

timation techniques, namely the extended Kalman filter and the unscented Kalman filter. We then used RCMR for indirect adaptive control, performing closed-loop identification under conditions where persistent excitation is infeasible. RCMR was used to provide estimates of time-varying parameters to a forward propagating Riccati based controller.

9.2 Future Work

9.2.1 Extensions to MIMO G_{zu}

Although RCAC was presented in the case where G_{zu} is a MIMO transfer function, the construction of the target model G_{f} was confined to the case where the control and performance variable are scalar signals. In this case, it is easy to incorporate the NMP zeros of G_{zu} in the target model. By comparison, the case of MIMO G_{zu} is much more challenging. In this case, the target model G_{f} would need to be constructed so as to prevent the possibility of hidden cancellation of transmission zeros. In principle, this is not difficult since transmission zeros are well understood in terms of the Smith-McMillan form [131–133]. However, the minimal modeling information required to determine the relevant zero directions remains to be determined. In addition, construction of the Smith-McMillan form depends on symbolic computation, which can be numerically sensitive. An added challenge is the fact, as shown in [41], that RCAC tends to square non-square plants, which may introduce squaring zeros that are NMP.

9.2.2 Controller Stability

As shown in this dissertation, as a consequence of optimality, LQG may produce unstable controllers in cases where an unstable controller is not required for closed-loop stability. Since RCAC tends to match LQG, it is not surprising that RCAC may

produce unstable controllers in cases where an asymptotically stable controller may produce near-optimal performance. It is therefore of interest to develop extensions of RCAC that enforce controller stability during adaptation without losing closed-loop stability. One such method is to choose target pole locations that may be achieved by stable controllers. However, since computing such pole locations requires knowledge of the denominator and numerator of G_{yu}, it is not a desirable solution. An alternative method may be to optimize the retrospective cost function with respect to not just $\hat{\theta}$ but also the denominator D_{f} of the target model. By defining an alternative retrospective performance variable, with two FIR filters instead of one IIR filter, it can be shown that this optimization problem is convex in $\hat{\theta}$ and D_{f}, and tends to yield stable controllers.

9.2.3 Dual Retrospective Cost Adaptive Control

It is a fundamental tenet of feedback control that poles can be moved but zeros cannot, at least not by using linear time-invariant feedback. Consequently, NMP zeros, which cannot be canceled, present one of the key impediments to feedback control [98]. Not surprisingly, NMP zeros pose one of the key impediments to adaptive control. For example, the positive real conditions that are invoked in classical adaptive control techniques [4, 68, 134–137] cannot be satisfied for NMP plants. In the case of RCAC, the locations of the NMP zeros are included in the basic modeling information used to construct the target model G_{f}.

The analysis in this dissertation suggests a novel way forward. In particular, the virtual external control perturbation $\tilde{u}$ is the input to $\widetilde{G}_{z\tilde{u},k}$, whose zeros include the zeros required to construct G_{f}. This suggests the possibility of identifying $\widetilde{G}_{z\tilde{u},k}$ during controller adaptation and using the estimates of the zeros of $\widetilde{G}_{z\tilde{u},k}$ to update G_{f} during adaptation. In effect, identification and adaptation are performed concurrently, where the adaptation drives the identification through the virtual external

control perturbation $\tilde{u}$, while the identification provides the modeling information to the controller adaptation that is required to avoid cancellation of NMP zeros.

This approach–concurrent identification and adaptation where the identification signal is the virtual external control perturbation $\tilde{u}$ with intercalated injection–can be viewed as a form of dual control. As discussed in [138–140], dual control is a fundamental and longstanding problem in feedback control. In the spirit of dual control, it is possible to exploit the immovability of the plant zeros by using the virtual external control perturbation $\tilde{u}$ to estimate their locations, which remain fixed (viewed as "instantaneous zeros") despite the time-dependent adaptation. In the case of MIMO G_{zu}, this approach can potentially overcome difficulties associated with zero directions and the construction of the Smith-McMillan form.

APPENDICES

APPENDIX A

Discrete-Time LQG Control

Discrete-time LQG is not as widely used as the continuous-time version [A1, A2]; the relevant equations for discrete-time LQG can be found in [131, p. 878], and a complete derivation in a more general context is given in [A3]. Solutions of the discrete-time Riccati equations are discussed in [A4]. Here we focus on the high-authority LQG solution.

For the standard problem (2.1)–(2.3), define

$$R_1 \triangleq E_1^{\mathrm{T}} E_1 \in \mathbb{R}^{n\times n}, \quad R_{12} \triangleq E_1^{\mathrm{T}} E_2 \in \mathbb{R}^{n\times l_u}, \quad R_2 \triangleq E_2^{\mathrm{T}} E_2 \in \mathbb{R}^{l_u\times l_u}, \tag{A.1}$$

$$V_1 \triangleq D_1 D_1^{\mathrm{T}} \in \mathbb{R}^{n\times n}, \quad V_{12} \triangleq D_1 D_2^{\mathrm{T}} \in \mathbb{R}^{n\times l_y}, \quad V_2 \triangleq D_2 D_2^{\mathrm{T}} \in \mathbb{R}^{l_y\times l_y}. \tag{A.2}$$

Assuming that w is zero-mean Gaussian white noise with covariance I_{l_w}, the n^{th}-order strictly proper LQG controller $G_{\mathrm{c}} \sim \left[\begin{array}{c|c} A_{\mathrm{c}} & B_{\mathrm{c}} \\ \hline C_{\mathrm{c}} & 0 \end{array}\right]$ minimizes

$$J(A_{\mathrm{c}}, B_{\mathrm{c}}, C_{\mathrm{c}}) \triangleq \lim_{k\to\infty} \mathbb{E}\left[\frac{1}{k}\sum_{i=0}^{k} z^{\mathrm{T}}(i) z(i)\right], \tag{A.3}$$

and is given by

$$A_{\mathrm{c}} = A + BC_{\mathrm{c}} - B_{\mathrm{c}}C - B_{\mathrm{c}}D_0C_{\mathrm{c}}, \tag{A.4}$$

$$B_{\mathrm{c}} = (AQC^{\mathrm{T}} + V_{12})(V_2 + CQC^{\mathrm{T}})^{-1}, \tag{A.5}$$

$$C_{\mathrm{c}} = -(R_2 + B^{\mathrm{T}}PB)^{-1}(R_{12}^{\mathrm{T}} + B^{\mathrm{T}}PA), \tag{A.6}$$

where the positive-semidefinite matrices $P \in \mathbb{R}^{n\times n}$ and $Q \in \mathbb{R}^{n\times n}$ are solutions of the discrete-time algebraic Riccati equations

$$P = \hat{A}_{\mathrm{R}}^{\mathrm{T}}P\hat{A}_{\mathrm{R}} - \hat{A}_{\mathrm{R}}^{\mathrm{T}}PB(R_2 + B^{\mathrm{T}}PB)^{-1}B^{\mathrm{T}}P\hat{A}_{\mathrm{R}} + \hat{R}_1, \tag{A.7}$$

$$Q = \hat{A}_{\mathrm{E}}Q\hat{A}_{\mathrm{E}}^{\mathrm{T}} - \hat{A}_{\mathrm{E}}QC^{\mathrm{T}}(V_2 + CQC^{\mathrm{T}})^{-1}CQ\hat{A}_{\mathrm{E}}^{\mathrm{T}} + \hat{V}_1, \tag{A.8}$$

where

$$\hat{A}_{\mathrm{R}} \triangleq A - BR_2^{-1}R_{12}^{\mathrm{T}}, \quad \hat{R}_1 \triangleq R_1 - R_{12}R_2^{-1}R_{12}^{\mathrm{T}}, \tag{A.9}$$

$$\hat{A}_{\mathrm{E}} \triangleq A - V_{12}V_2^{-1}C, \quad \hat{V}_1 \triangleq V_1 - V_{12}V_2^{-1}V_{12}^{\mathrm{T}}. \tag{A.10}$$

The eigenvalues of the closed-loop system are given by

$$\mathrm{mspec}(\widetilde{A}) = \mathrm{mspec}(A + BC_{\mathrm{c}}) \cup \mathrm{mspec}(A - B_{\mathrm{c}}C), \tag{A.11}$$

where

$$\widetilde{A} \triangleq \begin{bmatrix} A & BC_{\mathrm{c}} \\ B_{\mathrm{c}}C & A_{\mathrm{c}} + B_{\mathrm{c}}D_0C_{\mathrm{c}} \end{bmatrix} \tag{A.12}$$

and "mspec" denotes the spectrum of a matrix including eigenvalue multiplicity. Under the assumptions

i) (A, B) is stabilizable.

ii) $(\hat{A}_{\mathrm{R}}, \hat{R}_1)$ has no unobservable eigenvalues on the unit circle.

iii) (A, C) is detectable.

iv) $(\hat{A}_{\mathrm{E}}, \hat{V}_1)$ has no uncontrollable eigenvalues on the unit circle.

it follows that (A.7) and (A.8) have unique positive-semidefinite solutions P and Q, and, furthermore, $\widetilde{A}$ is asymptotically stable.

Note that the LQG controller is independent of E_0. This is due to the fact that, since LQG is based on the assumption that w is zero-mean Gaussian white noise, the contribution of $E_0 w$ to $J(A_{\mathrm{c}}, B_{\mathrm{c}}, C_{\mathrm{c}})$ is not affected by the choice of A_{c}, B_{c}, and C_{c}. However, for the servo problem shown in Figure 2.3, E_0 is not zero, and the command r, which is a component of w, is not Gaussian white noise. Likewise, in some applications, the disturbance d in the servo problem is not Gaussian white noise, and thus the exogenous signal w in the standard problem is not Gaussian white noise. Therefore, in these cases the LQG controller is not necessarily optimal. Nevertheless, for comparison with RCAC, we use the LQG controller in these cases without modification. In examples 4.1–4.3, we compare the closed-loop frequency response and H_2 cost of RCAC to high-authority LQG.

Properties of Discrete-Time High-Authority LQG

In this section, we review properties of high-authority LQG, that is, the case where $R_2 = 0$ and $V_2 = 0$. In this case, $\hat{A}_{\mathrm{R}} = A$, $\hat{R}_1 = R_1$, $\hat{A}_{\mathrm{E}} = A$, and $\hat{V}_1 = V_1$. The properties of discrete-time high-authority LQG are analogous to the properties of continuous-time high-authority LQG given in [A1, pp. 281–289].

For simplicity, we assume that y, z, u, and w are scalar signals. We consider the

factorizations of the numerators N_{zu} and N_{yw} of G_{zu} and G_{yw}, respectively, given by

$$N_{zu} = H_{\mathrm{d}_{zu}} N_{zu,\mathrm{s}} N_{zu,\mathrm{u}}, \tag{A.13}$$

$$N_{yw} = H_{\mathrm{d}_{yw}} N_{yw,\mathrm{s}} N_{yw,\mathrm{u}}, \tag{A.14}$$

where $\mathrm{d}_{zu} \geq 0$ is the relative degree of G_{zu}, $H_{\mathrm{d}_{zu}}$ is the first nonzero Markov parameter of G_{zu}, $\mathrm{d}_{yw} \geq 0$ is the relative degree of G_{yw}, $H_{\mathrm{d}_{yw}}$ is the first nonzero Markov parameter of G_{yw}, the roots of the monic polynomials $N_{zu,\mathrm{s}}$ and $N_{yw,\mathrm{s}}$ are the minimum-phase zeros of G_{zu} and G_{yw}, respectively, and the roots of the monic polynomials $N_{zu,\mathrm{u}}$ and $N_{yw,\mathrm{u}}$ are the NMP zeros of G_{zu} and G_{yw}, respectively. Note that $H_{\mathrm{d}_{zu}}$ is the leading nonzero coefficient of N_{zu}, and $H_{\mathrm{d}_{yw}}$ is the leading nonzero coefficient of N_{yw}. With this notation it follows that

$$\mathrm{mspec}(A + BC_{\mathrm{c}}) = \mathrm{mzeros}(\mathbf{z}^{\mathrm{d}_{zu}} N_{zu,\mathrm{s}}(\mathbf{z}) N_{zu,\mathrm{u}}(\mathbf{z}^{-1})), \tag{A.15}$$

$$\mathrm{mspec}(A - B_{\mathrm{c}}C) = \mathrm{mzeros}(\mathbf{z}^{\mathrm{d}_{yw}} N_{yw,\mathrm{s}}(\mathbf{z}) N_{yw,\mathrm{u}}(\mathbf{z}^{-1})), \tag{A.16}$$

where mzeros denotes the multiset of zeros of a rational function including multiplicity. Note that the zeros of $N_{zu,\mathrm{u}}(\mathbf{z}^{-1})$ are the reflections across the unit circle (that is, the reciprocals) of the NMP zeros of G_{zu}. For example, if $N_{zu,\mathrm{u}}(\mathbf{z}) = \mathbf{z} - 1.2$, then $N_{zu,\mathrm{u}}(\mathbf{z}^{-1}) = \frac{1-1.2\mathbf{z}}{\mathbf{z}}$. It follows from (A.15) and (A.16) that the closed-loop poles of high-authority LQG control are the zeros of

$$\widetilde{D}_{\mathrm{HA}}(\mathbf{z}) = \mathbf{z}^{\mathrm{d}_{zu}+\mathrm{d}_{yw}} N_{zu,\mathrm{s}}(\mathbf{z}) N_{zu,\mathrm{u}}(\mathbf{z}^{-1}) N_{yw,\mathrm{s}}(\mathbf{z}) N_{yw,\mathrm{u}}(\mathbf{z}^{-1}). \tag{A.17}$$

It thus follows from (A.11) that $\mathrm{mspec}(\widetilde{A}) = \mathrm{mzeros}(\widetilde{D}_{\mathrm{HA}})$. Similar observations are made for continuous-time systems in [A1] and for discrete-time systems in [39]. A surprising aspect of high-authority LQG control is the fact that the poles and zeros of G_{yu}, which is present in the feedback loop and thus determines the gain and

phase margins, do not affect the locations of the closed-loop poles. In the subsequent examples, we consider high-authority LQG control. For each example, w is zero-mean Gaussian white noise with standard deviation 1.

Example A.1. High-authority LQG control for the standard problem with $y \neq z$, with stochastic w not matched with u, and with minimum-phase G_{zu}, G_{zw}, G_{yu}, and G_{yw}. Consider the asymptotically stable, minimum-phase plant

$$A = \begin{bmatrix} 0.4 & 0.0958 & 0.1183 & 0.3162 \\ 0 & 0.81 & 1 & 0 \\ 0 & -0.1539 & 0.81 & 0.4813 \\ 0 & 0 & 0 & -0.5 \end{bmatrix}, \quad B = \begin{bmatrix} 0 \\ 0 \\ 0 \\ 1 \end{bmatrix}, \quad D_1 = \begin{bmatrix} -0.3807 \\ -0.2039 \\ 0.1771 \\ 0.8844 \end{bmatrix}, \tag{A.18}$$

$$C = [0.4456 \quad 0.0832 \quad -0.332 \quad -0.8272], \quad D_0 = 0, \quad D_2 = 0, \tag{A.19}$$

$$E_1 = [-0.274 \quad 0.2625 \quad 0.3241 \quad 0.8666], \quad E_0 = 0, \quad E_2 = 0. \tag{A.20}$$

The open-loop and closed-loop poles are shown in Figure A.1. Note that mspec($A+BC_c$) consists of the zeros of G_{zu} as well as 0 with multiplicity 1, while mspec($A-B_cC$) consists of the zeros of G_{yw} as well as 0 with multiplicity 1. This example illustrates (A.15) and (A.16), which relate the closed-loop spectrum to the zeros of G_{zu} and G_{yw}. ■

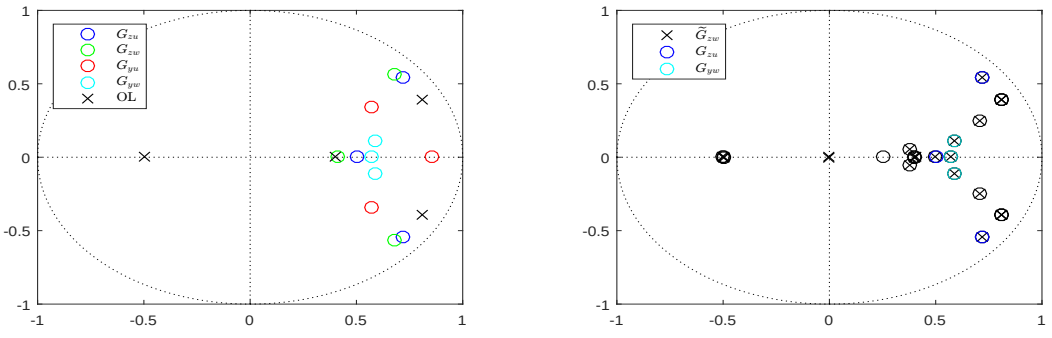

Figure A.1: Example A.1: High-authority discrete-time LQG control for the standard problem. The closed-loop transfer function $\widetilde{G}_{zw}$ has one pole at each zero of G_{zu} and G_{yw} as well as two poles at 0.

Example A.2. High-authority LQG control for the standard problem with $y \neq z$, with stochastic w not matched with u, and with NMP G_{zu}, G_{zw}, G_{yu}, and G_{yw}, all of which have different NMP zeros. Consider the asymptotically stable, NMP plant

$$A = \begin{bmatrix} 0.81 & 1 & 0 \\ -0.1539 & 0.81 & 0.6998 \\ 0 & 0 & 0.5 \end{bmatrix}, \quad B = \begin{bmatrix} 0 \\ 0 \\ 1 \end{bmatrix}, \quad D_1 = \begin{bmatrix} 0.1841 \\ 0.1074 \\ 0.9770 \end{bmatrix}, \tag{A.21}$$

$$C = [0.9280 \quad 0.1102 \quad 0.3558], \quad D_0 = 0, \quad D_2 = 0, \tag{A.22}$$

$$E_1 = [0.4531 \quad -0.3513 \quad 0.8193], \quad E_0 = 0, \quad E_2 = 0. \tag{A.23}$$

The open-loop and closed-loop poles are shown in Figure A.2. Note that mspec$(A + BC_c)$ consists of the reciprocals of the NMP zeros of G_{zu} as well as 0 with multiplicity 1, while mspec$(A - B_cC)$ consists of the reciprocals of the NMP zeros of G_{yw} as well as 0 with multiplicity 1. This example illustrates (A.15) and (A.16) in the case where both G_{yu} and G_{zw} are NMP. This example also shows that the NMP zeros of G_{zw} and G_{yu} have no effect on the closed-loop poles. ■

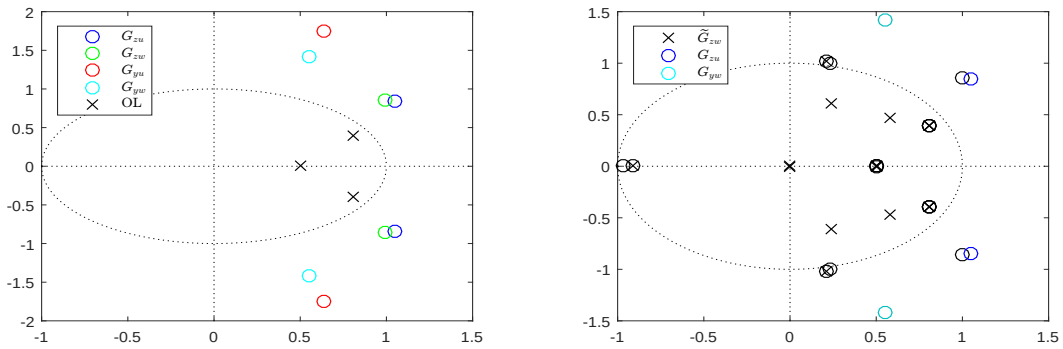

Figure A.2: Example LQGA.2: High-authority discrete-time LQG control for the standard problem. The closed-loop transfer function $\widetilde{G}_{zw}$ has one pole at the reciprocal of each NMP zero of G_{zu} and G_{yw} as well as two poles at 0.

Bibliography

[A1] H. Kwakernaak and R. Sivan, *Linear Optimal Control Systems*. Wiley, 1972.

[A2] K. Zhou, J. C. Doyle, and K. Glover, *Robust and Optimal Control*. Prentice Hall, 1996.

[A3] W. M. Haddad, V. Kapila, and E. G. Collins, Jr., *Optimality Conditions for Reduced-Order Modeling, Estimation, and Control for Discrete-Time Linear Periodic Plants*. J. Math. Sys. Est. Contr., vol. 6, pp. 437-460, 1996.

[A4] V. Ionescu, C. Oara, and M. Weiss, *Generalized Riccati Theory and Robust Control*. Wiley, 1999.

APPENDIX B

The Sylvester Resultant

The Sylvester resultant provides a necessary and sufficient condition for the coprimeness of two polynomials [B1, pp. 459-461], [B2, pp. 234-236], and [B3, pp. 140-142].

Theorem A1. Let k and l be nonnegative integers such that $k + l \geq 1$, let $a(s) = a_k s^k + a_{k-1} s^{k-1} + \cdots + a_1 s + a_0$ and $b(s) = b_l s^l + b_{l-1} s^{l-1} + \cdots + b_1 s + b_0$, and assume that $a_k \neq 0$ and $l \leq k$. Furthermore, define

$$\mathcal{M}_1(a,b) \triangleq \begin{bmatrix} a_k & 0 & \cdots & 0 & b_l & 0 & \cdots & 0 \\ a_{k-1} & a_k & \ddots & \vdots & b_{l-1} & b_l & \ddots & \vdots \\ \vdots & a_{k-1} & \ddots & 0 & \vdots & b_{l-1} & \ddots & \vdots \\ a_1 & \vdots & \ddots & a_k & b_1 & \vdots & \ddots & b_l \\ a_0 & a_1 & \ddots & a_{k-1} & b_0 & b_1 & \ddots & b_{l-1} \\ 0 & a_0 & \ddots & \vdots & 0 & b_0 & \ddots & \vdots \\ \vdots & 0 & \ddots & a_1 & \vdots & \vdots & \ddots & b_1 \\ 0 & \cdots & \cdots & a_0 & 0 & \cdots & \cdots & b_0 \end{bmatrix} \in \mathbb{R}^{(k+l)\times(k+l)}. \quad \text{(B.1)}$$

Then the number of common roots of a and b is $k+l-\operatorname{rank}(\mathcal{M}_1(a,b))$. Furthermore, a and b are coprime if and only if $\mathcal{M}_1(a,b)$ is nonsingular.

The Sylvester resultant $\mathcal{M}_1(a,b)$ is constructed by listing the coefficients of a from a_k to a_0 starting at the top of the first column. In the second column, the coefficients of a are shifted downward by one row; l columns are constructed this way. Next, list the coefficients of b from b_l to b_0 starting at the top of column $l+1$. In the next column, the coefficients of b are shifted downward by one row; k columns are constructed this way. The final matrix has $k+l$ rows and $k+l$ columns.

Note that in Theorem A1 b_l may be zero, and thus $\deg(b) \leq l \leq k = \deg(a)$. Therefore, since $l \leq k$, without loss of generality, $b(s)$ can be written with $k+l-1$ additional leading zeros of the form $b(s) = 0s^k + \cdots + 0s^{l+1} + b_l s^l + \cdots + b_0$, and Theorem A1 can be rewritten as follows.

Theorem A2. Let k be a nonnegative integer, let $a(s) = a_k s^k + a_{k-1}s^{k-1} + \cdots + a_1 s + a_0$, where $a_k \neq 0$, and $b(s) = b_k s^k + b_{k-1}s^{k-1} + \cdots + b_1 s + b_0$. Furthermore, define

$$\mathcal{M}_2(a,b) \triangleq \begin{bmatrix} a_k & 0 & \cdots & 0 & b_k & 0 & \cdots & 0 \\ a_{k-1} & a_k & \ddots & \vdots & b_{k-1} & b_k & \ddots & \vdots \\ \vdots & a_{k-1} & \ddots & 0 & \vdots & b_{k-1} & \ddots & \vdots \\ a_1 & \vdots & \ddots & a_k & b_1 & \vdots & \ddots & b_k \\ a_0 & a_1 & \ddots & a_{k-1} & b_0 & b_1 & \ddots & b_{k-1} \\ 0 & a_0 & \ddots & \vdots & 0 & b_0 & \ddots & \vdots \\ \vdots & 0 & \ddots & a_1 & \vdots & \vdots & \ddots & b_1 \\ 0 & \cdots & \cdots & a_0 & 0 & \cdots & \cdots & b_0 \end{bmatrix} \in \mathbb{R}^{2k \times 2k}. \tag{B.2}$$

Then the number of common roots of a and b is $2k - \operatorname{rank}(\mathcal{M}_2(a,b))$. Furthermore, a and b are coprime if and only if $\mathcal{M}_2(a,b)$ is nonsingular.

Note that in Theorem A2 b_k may be zero, and thus $\deg(b) \leq k$. $\mathcal{M}_1(a,b)$ appears in [S3], whereas $\mathcal{M}_2(a,b)$ appears in [S1] and [S2].

Example B.1. Let $a(s) = s + 1$ and $b(s) = s + 2$, which are coprime. Then, using B.1,

$$\mathcal{M}_1(a, b) = \begin{bmatrix} 1 & 1 \\ 1 & 2 \end{bmatrix},$$

which is nonsingular. ■

Example B.2. Let $a(s) = s + 1$ and $b(s) = (s + 1)(s + 2) = s^2 + 3s + 2$, which are not coprime. Then, using B.1,

$$\mathcal{M}_1(a, b) = \begin{bmatrix} 1 & 0 & 1 \\ 1 & 1 & 3 \\ 0 & 1 & 2 \end{bmatrix},$$

which has rank 2 and thus is singular. The number of common roots is $k + l - \text{rank}(\mathcal{M}_1(a, b)) = 1 + 2 - 2 = 1$. ■

Example B.3. Let $a(s) = s^3 + 2s^2 + 4s + 1$ and $b(s) = 6$. Since b is a constant and nonzero, it has no roots, and thus a and b are coprime. Furthermore, using B.1,

$$\mathcal{M}_1(a, b) = \begin{bmatrix} 6 & 0 & 0 \\ 0 & 6 & 0 \\ 0 & 0 & 6 \end{bmatrix},$$

which is nonsingular. ■

Example B.4. In in this example, we use B.2 instead of B.1. We add leading zeros to b in Example B.3 by writing $b(s) = 0s^3 + 0s^2 + 0s + 6$. Thus, using B.2,

$$\mathcal{M}_2(a,b) = \begin{bmatrix} 1 & 0 & 0 & 0 & 0 & 0 \\ 2 & 1 & 0 & 0 & 0 & 0 \\ 4 & 2 & 1 & 0 & 0 & 0 \\ 1 & 4 & 2 & 6 & 0 & 0 \\ 0 & 1 & 4 & 0 & 6 & 0 \\ 0 & 0 & 1 & 0 & 0 & 6 \end{bmatrix},$$

which is nonsingular. In fact, $\det(\mathcal{M}_2(a,b)) = 216$, as in Example B.3. ■

Example B.5. Let $a(s) = s^3 + 2s^2 + 4s + 1$ and $b(s) = 0s^3 + 0s^2 + 0s + 0$ so that b is the zero polynomial. Then, using B.2,

$$\mathcal{M}_2(a,b) = \begin{bmatrix} 1 & 0 & 0 & 0 & 0 & 0 \\ 2 & 1 & 0 & 0 & 0 & 0 \\ 4 & 2 & 1 & 0 & 0 & 0 \\ 1 & 4 & 2 & 0 & 0 & 0 \\ 0 & 1 & 4 & 0 & 0 & 0 \\ 0 & 0 & 1 & 0 & 0 & 0 \end{bmatrix}.$$

Since $\text{rank}(\mathcal{M}_2(a,b)) = 3$, Theorem A1 implies that the number of common roots of a and b is $2k - \text{rank}(\mathcal{M}_2(a,b)) = 6 - 3 = 3$, which shows that every root of a is also a root of b. ■

Bibliography

[B1] P. Lancaster and M. Tismenetsky, *The Theory of Matrices*, Academic Press, 1985.

[B2] W. A. Wolovich, *Linear Multivariable Systems*, Springer-Verlag, 1974.

[B3] T. Kailath, *Linear Systems*, Prentice Hall, 1980.

BIBLIOGRAPHY

BIBLIOGRAPHY

[1] J. C. Doyle, "Guaranteed Margins for LQG Regulators," *IEEE Trans. Autom. Control*, vol. 23, pp. 756–757, 1978.

[2] R. H. Middleton and D. E. Miller, "On the Achievable Delay Margin Using LTI Control for Unstable Plants," *IEEE Trans. Autom. Control*, vol. 52, no. 7, pp. 1194–1207, 2007.

[3] K. Narendra and A. Annaswamy, "A New Adaptive Law for Robust Adaptive Control Without Persistent Excitation," *IEEE Trans. Autom. Contr.*, vol. AC-32, pp. 134–145, 1987.

[4] P. A. Ioannou and J. Sun, *Robust Adaptive Control*. Prentice Hall, 1996.

[5] A. M. Annaswamy and J. Wong, "Adaptive Control in the Presence of Saturation Non-linearity," *Int. J. Adapt. Contr. Signal Proc.*, vol. 11, no. 1, pp. 3–19, 1997.

[6] K. S. Narendra and J. Balakrishnan, "Adaptive Control Using Multiple Models," *IEEE Trans. Autom. Control*, vol. 42, no. 2, pp. 171–187, 1997.

[7] G. Tao, *Adaptive Control Design and Analysis*. Wiley, 2003.

[8] N. T. Nguyen, K. S. Krishnakumar, and J. D. Boskovic, "An Optimal Control Modification to Model-Reference Adaptive Control for Fast Adaptation," in *Proc. AIAA Guid. Nav. Contr. Conf.*, Honolulu, HI, August 2008, AIAA-2008-7283.

[9] "Combined/Composite Model Reference Adaptive Control," in *Proc. AIAA Guid. Nav. Contr. Conf.*, Chicago, IL, August 2009, AIAA-2009-6065.

[10] N. Hovakimyan and C. Cao, L_1 *Adaptive Control Theory: Guaranteed Robustness with Fast Adaptation*. SIAM, 2010.

[11] G. Chowdhary, T. Yucelen, M. Mühlegg, and E. N. Johnson, "Concurrent Learning Adaptive Control of Linear Systems with Exponentially Convergent Bounds," *Int. J. Adapt. Contr. Signal Proc.*, vol. 27, no. 4, pp. 280–301, 2013.

[12] G. C. Goodwin, P. J. Ramadge, and P. E. Caines, "Discrete-Time Multivariable Adaptive Control," *IEEE Trans. Autom. Control*, vol. 25, pp. 449–456, 1980.

[13] K. J. Åström, "Direct Methods for Nonminimum Phase Systems," in *Proc. Conf. Dec. Contr.*, Albuquerque, NM, December 1980, pp. 611–615.

[14] G. C. Goodwin and K. S. Sin, "Adaptive Control of Nonminimum Phase Systems," *IEEE Trans. Autom. Contr.*, vol. 26, pp. 478–483, 1981.

[15] R. Johansson, "Parametric Models of Linear Multivariable Systems for Adaptive Control," *IEEE Trans. Autom. Contr.*, vol. 32, pp. 303–313, 1987.

[16] L. Praly, S. T. Hung, and D. S. Rhode, "Towards a Direct Adaptive Scheme for a Discrete-Time Control of a Minimum Phase Continuous-Time System," in *Proc. Conf. Dec. Contr.*, Fort Lauderdale, FL, December 1989, pp. 1188–1191.

[17] R. Venugopal, V. G. Rao, and D. S. Bernstein, "Lyapunov-Based Backward-Horizon Discrete-Time Adaptive Control," *Adaptive Contr. Sig. Proc.*, vol. 17, pp. 67–84, 2003.

[18] T. Hayakawa, W. M. Haddad, and A. Leonessa, "A Lyapunov-Based Adaptive Control Framework for Discrete-time Non-linear Systems with Exogenous Disturbances," *Int. J. Control*, vol. 77, pp. 250–263, 2004.

[19] S. Akhtar, R. Venugopal, and D. S. Bernstein, "Logarithmic Lyapunov Functions for Direct Adaptive Stabilization with Normalized Adaptive Laws," *Int. J. Contr.*, vol. 77, pp. 630–638, 2004.

[20] J. B. Hoagg, M. A. Santillo, and D. S. Bernstein, "Discrete-time Adaptive Command Following and Disturbance Rejection with Unknown Exogenous Dynamics," *IEEE Trans. Autom. Contr.*, vol. 53, pp. 912–928, 2008.

[21] C.-C. Cheng and S. H.-S. Fu, "On Trajectory-Dependent Direct Adaptive Control for a Class of Uncertain Linear Discrete-time Systems," *Int. J. Adapt. Contr. Signal Proc.*, vol. 23, pp. 1014–1030, 2009.

[22] C. Li and J. Lam, "Stabilization of Discrete-Time Nonlinear Uncertain Systems by Feedback Based on LS Algorithm," *SIAM J. Contr. Optim.*, vol. 51, pp. 1128–1151, 2013.

[23] M. Yu, J.-X. Xu, and D. Huang, "Discrete-Time Periodic Adaptive Control for Parametric Systems with Non-sector Nonlinearities," *Int. J. Adapt. Contr. Signal Proc.*, vol. 28, pp. 987–1001, 2014.

[24] C. E. Rohrs, L. Velavani, M. Athans, and G. Stein, "Robustness of Continuous-Time Adaptive Control Algorithms in the Presence of Unmodeled Dynamics," *IEEE Trans. Autom. Contr.*, vol. AC-30, pp. 881–889, 1985.

[25] K. J. Astrom, P. Hagander, and J. Sternby, "Zeros of Sampled Systems," *Automatica*, vol. 20, pp. 31–38, 1984.

[26] R. Venugopal and D. S. Bernstein, "Adaptive Disturbance Rejection Using ARMARKOV System Representations," *IEEE Trans. Contr. Sys. Tech.*, vol. 8, pp. 257–269, 2000.

[27] M. C. Campi, A. Lecchini, and S. M. Savaresi, "Virtual Reference Feedback Tuning (VRFT): A new Direct Approach to the Design of Feedback Controllers," in *Proc. Conf. Dec. Contr.*, Sydney, Australia, 2000, pp. 623–629.

[28] M. C. Campi and S. M. Savaresi, "Direct Nonlinear Control Design: The Virtual Reference Feedback Tuning (VRFT) Approach," *IEEE Trans. Autom. Control*, vol. 51, no. 1, pp. 14–27, 2006.

[29] Z. Hou and S. Jin, "A Novel Data-driven Control Approach for a Class of Discrete-time Nonlinear Systems," *IEEE Trans. Contr. Sys. Tech.*, vol. 19, no. 6, pp. 1549–1558, 2011.

[30] A. S. Bazanella, L. Campestrini, and D. Eckhard, *Data-Driven Controller Design: The H_2 Approach.* Springer, 2011.

[31] S. S. Ge, Z. Li, and H. Yang, "Data Driven Adaptive Predictive Control for Holonomic Constrained Under-actuated Biped Robots," *IEEE Trans. Contr. Sys. Tech.*, vol. 20, no. 3, pp. 787–795, 2012.

[32] Z. S. Hou and Z. Wang, "From Model-Based Control to Data-Driven Control: Survey, Classification and Perspective," *Infor. Sci.*, vol. 235, pp. 3–35, 2013.

[33] H. Sane and D. S. Bernstein, "Active Noise Control Using an Acoustic Servovalve," in *Proc. Amer. Contr. Conf.*, Philadelphia, PA, June 1998, pp. 2621–2625.

[34] H. Sane, R. Venugopal, and D. S. Bernstein, "Disturbance Rejection Using Self-Tuning ARMARKOV Adaptive Control with Simultaneous Identification," *IEEE Trans. Contr. Sys. Tech.*, vol. 19, pp. 101–106, 2001.

[35] S. L. Lacy, R. Venugopal, and D. S. Bernstein, "ARMARKOV Adaptive Control of Self-Excited Oscillations of a Ducted Flame," in *Proc. Conf. Dec. Contr.*, Tampa, FL, December 1998, pp. 4527–4528.

[36] M. A. Santillo and D. S. Bernstein, "Adaptive Control Based on Retrospective Cost Optimization," *J. Guid. Contr. Dyn.*, vol. 33, pp. 289–304, 2010.

[37] J. B. Hoagg and D. S. Bernstein, "Retrospective Cost Model Reference Adaptive Control for Nonminimum-Phase Systems," *J. Guid. Contr. Dyn.*, vol. 35, pp. 1767–1786, 2012.

[38] E. D. Sumer and D. S. Bernstein, "Robust Sampled-Data Adaptive Control of the Rohrs Counterexamples," in *Proc. Conf. Dec. Contr.*, Maui, HI, December 2012, pp. 7273–7278.

[39] E. D. Sumer, J. B. Hoagg, and D. S. Bernstein, "Broadband Disturbance Rejection Using Retrospective Cost Adaptive Control," in *Proc. Dyn. Sys. Contr. Conf.*, no. DSCC2012-MOVIC2012-8572, Fort Lauderdale, FL, October 2012, pp. 1–10.

[40] J. Yan and D. S. Bernstein, "Minimal Modeling Retrospective Cost Adaptive Control of Uncertain Hammerstein Systems Using Auxiliary Nonlinearities," *Int. J. Contr.*, vol. 87, pp. 483–505, 2014.

[41] E. D. Sumer and D. S. Bernstein, "On the Role of Subspace Zeros in Retrospective Cost Adaptive Control of Nonsquare Plants," *Int. J. Contr.*, vol. 88, pp. 295–323, 2015.

[42] M. Rizzo, M. A. Santillo, A. Padthe, J. B. Hoagg, S. Akhtar, D. S. Bernstein, and K. G. Powell, "CFD-Based Identification for Adaptive Flow Control Using ARMARKOV Disturbance Rejection," in *Proc. Amer. Contr. Conf.*, Minneapolis, MN, June 2006, pp. 3783–3788.

[43] Y.-C. Cho, J. B. Hoagg, D. S. Bernstein, and W. Shyy, "Retrospective Cost Adaptive Flow Control of Low-Reynolds Number Aerodynamics Using a Dielectric Barrier Discharge Actuator," in *Proc. 5th AIAA Flow Contr. Conf.*, Chicago, IL, August 2010, AIAA-2010-4841.

[44] M. Isaacs, J. B. Hoagg, A. V. Morozov, and D. S. Bernstein, "A Numerical Study on Controlling a Nonlinear Multilink Arm Using A Retrospective Cost Model Reference Adaptive Controller," in *Proc. Conf. Dec. Contr.*, Orlando, FL, December 2011, pp. 8008 – 8013.

[45] E. D. Sumer and D. S. Bernstein, "Adaptive Decentralized Noise and Vibration Control with Conflicting Performance Objectives," in *Proc. Dyn. Sys. Contr. Conf.*, no. DSCC2012-MOVIC2012-8580, Fort Lauderdale, FL, October 2012, pp. 1–10.

[46] ——, "Adaptive Control of Flexible Structures with Uncertain Dynamics and Uncertain Disturbance Spectra," in *Proc. AIAA Guid. Nav. Contr. Conf.*, Minneapolis, MN, August 2012, AIAA-2012-4437-323.

[47] A. K. Padthe, P. P. Friedmann, and D. S. Bernstein, "Retrospective Cost Adaptive Control for Helicopter Vibration Reduction," in *Proc. AHS 69th Annual Forum*, Phoenix, AZ, May 2013, AHS2013-000179.

[48] J. Yan, A. M. D'Amato, K. Butts, I. Kolmanovsky, and D. S. Bernstein, "Adaptive Control of the Air Flow System in a Diesel Engine," in *Proc. Dyn. Sys. Contr. Conf.*, no. DSCC2012-MOVIC2012-8597, Fort Lauderdale, FL, October 2012, pp. 1–9.

[49] M. J. Yu, Y. Rahman, E. M. Atkins, I. Kolmanovsky, and D. S. Bernstein, "Minimal Modeling Adaptive Control of the NASA Generic Transport Model with

Unknown Control-Surface Faults," in *Proc. AIAA Guid. Nav. Contr. Conf.*, Boston, MA, August 2013, AIAA-2013-4693.

[50] F. Sobolic and D. S. Bernstein, "Aerodynamic-free adaptive control of the NASA generic transport model," in *Proc. AIAA Guid. Nav. Contr. Conf.*

[51] M. J. Yu, J. Zhong, E. M. Atkins, I. V. Kolmanovsky, and D. S. Bernstein, "Trim-commanded adaptive control for waypoint-defined trajectory following," in *Proc. AIAA Guid. Nav. Contr. Conf.*, Boston, MA, August 2013, AIAA-2013-4999.

[52] Y. Rahman, K. Aljanaideh, E. D. Sumer, and D. S. Bernstein, "Adaptive Control of Aircraft Lateral Motion with an Unknown Transition to Nonminimum-Phase Dynamics," in *Proc. Amer. Contr. Conf.*, Portland, OR, June 2014, pp. 2359–2364.

[53] A. Ansari and D. S. Bernstein, "Adaptive Control of an Aircraft with Uncertain Nonminimum-Phase Dynamics," in *Proc. Amer. Contr. Conf.*, Chicago, IL, July 2015, pp. 844–849.

[54] M. Camblor, G. Cruz, S. Esteban, F. A. Leve, and D. S. Bernstein, "Retrospective Cost Adaptive Spacecraft Attitude Control Using Control Moment Gyros," in *Proc. Amer. Contr. Conf.*, Portland, OR, June 2014, pp. 2492–2497.

[55] S. Dai, T. Lee, and D. S. Bernstein, "Adaptive Control of a Quadrotor UAV Transporting a Cable-Suspended Load with Unknown Mass," in *Proc. Conf. Dec. Contr.*, Los Angeles, CA, December 2014, pp. 6149–6154.

[56] F. Sobolic and D. S. Bernstein, "An Inner-Loop/Outer-Loop Architecture for an Adaptive Missile Autopilot," in *Proc. Amer. Contr. Conf.*, Chicago, IL, July 2015, pp. 850–855.

[57] A. Goel, A. Xie, K. Duraisamy, and D. S. Bernstein, "Retrospective Cost Adaptive Thrust Control of a 1D Scramjet with Mach Number Disturbance," in *Proc. Amer. Contr. Conf.*, Chicago, IL, July 2015, pp. 5551–5556.

[58] M. A. Janaideh and D. S. Bernstein, "Adaptive Control of Hammerstein Systems with Unknown Prandtl-Ishlinskii Hysteresis," *Proc. IMechE Part 1: J. Sys. Contr. Eng.*, pp. 1–9, 2014.

[59] B. L. Pence, M. A. Santillo, and D. S. Bernstein, "Markov-Parameter-Based Adaptive Control of 3-Axis Angular Velocity in a 6DOF Stewart Platform," in *Proc. Amer. Contr. Conf.*, Seattle, WA, June 2008, pp. 4767–4772.

[60] M. A. Santillo, A. M. D'Amato, and D. S. Bernstein, "System Identification Using a Retrospective Correction Filter for Adaptive Feedback Model Updating," in *Proc. Amer. Contr. Conf.*, St. Louis, MO, June 2009, pp. 4392–4397.

[61] A. M. D'Amato and D. S. Bernstein, "Linear Fractional Transformation Identification Using Retrospective Cost Optimization," in *Proc. SYSID*, Saint-Malo, France, July 2009, pp. 450–455.

[62] A. M. D'Amato, A. R. Wu, K. S. Mitchell, S. L. Kukreja, and D. S. Bernstein, "Damage Localization for Structural Health Monitoring Using Retrospective Cost Model Refinement," in *Proc. AIAA SDM Conf.*, Orlando, FL, April 2010, AIAA-2010-2628.

[63] A. M. D'Amato, A. J. Ridley, and D. S. Bernstein, "Retrospective-Cost-Based Adaptive Model Refinement for the Ionosphere and Thermosphere," *Statistical Analysis and Data Mining*, vol. 4, pp. 446–458, 2011.

[64] Y. Rahman, J. Zhong, A. Morozov, and D. S. Bernstein, "On the Accuracy of State Estimators for Constant and Time-Varying Parameter Estimation," in *Proc. AIAA Guid. Nav. Contr. Conf.*, Boston, MA, August 2013, AIAA-2012-5192.

[65] J. Zhong, J. Yan, Y. Rahman, C. Wang, and D. S. Bernstein, "Retrospective Cost Model Refinement for On-line Estimation of Constant and Time-Varying Flight Parameters," in *Proc. AIAA Guid. Nav. Contr. Conf.*, Boston, MA, August 2013, AIAA-2012-5193.

[66] E. D. Sumer and D. S. Bernstein, "Retrospective Cost Adaptive Control with Error-Dependent Regularization for MIMO Systems with Uncertain Nonminimum-Phase Transmission Zeros," in *Proc. AIAA Guid. Nav. Contr. Conf.*, Minneapolis, MN, August 2012, AIAA-2012-4670-123.

[67] K. J. Astrom and B. Wittenmark, *Adaptive Control*, 2nd ed. Addison-Wesley, 1995.

[68] G. C. Goodwin and K. S. Sin, *Adaptive Filtering, Prediction, and Control*. Prentice Hall, 1984.

[69] B. Teixeira, "Kalman Filters," *IEEE Contr. Sys. Mag.*, vol. 28, no. 2, pp. 16–18, 2008.

[70] K. J. Åström and T. Hägglund, *Advanced PID Control*. ISA-The Instrumentation, Systems and Automation Society, 2006.

[71] A. O'Dwyer, *Handbook of PI and PID Controller Tuning Rules*. Imperial College Press, 2009, vol. 57.

[72] Y. Li, K. A. Ang, and G. C. Chong, "PID Control System Analysis and Design: Problems, Remedies, and Future Directions," *IEEE Contr. Sys. Mag.*, vol. 26, no. 1, pp. 32–41, 2006.

[73] V. Bobál, J. Böhm, J. Fessl, and J. Machácek, *Digital Self-tuning Controllers: Algorithms, Implementation and Applications*. Springer, 2006.

[74] D. S. Bernstein and A. N. Michel, "A Chronological Bibliography on Saturating Actuators," *Int. J. Robust Nonlinear Contr.*, vol. 5, pp. 375–580, 1995.

[75] N. Kapoor, A. R. Teel, and P. Daoutidis, "An Anti-windup Design for Linear Systems with Input Saturation," *Automatica*, vol. 34, pp. 559–574, 1998.

[76] P. Hippe, *Windup in Control: Its Effects and Their Prevention.* Princeton University Press, 2011.

[77] L. Zaccarian and A. R. Teel, *Modern Anti-windup Synthesis: Control Augmentation for Actuator Saturation.* Springer, 2006.

[78] Y. Rahman, A. Xie, J. B. Hoagg, and D. S. Bernstein, "A Tutorial and Overview of Retrospective Cost Adaptive Control," in *Proc. Amer. Contr. Conf.*, Boston, MA, July 2016, pp. 3386–3409.

[79] J. B. Hoagg and D. S. Bernstein, "Nonminimum-Phase Zeros: Much to Do about Nothing," *IEEE Contr. Sys. Mag.*, vol. 27, no. June, pp. 45–57, 2007.

[80] B. R. Holt and M. Morari, "Design of resilient processing plants-vi. the effect of right-half-plane zeros on dynamic resilience," *Chem. Eng. Sci.*, vol. 40, pp. 59–74, 1985.

[81] D. P. Looze and J. S. Freudenberg, "Limitations of feedback properties imposed by open-loop right half plane poles," *IEEE Trans. Autom. Control*, vol. 36, pp. 736–739, 1991.

[82] H. K. Khalil, "Adaptive output feedback control of nonlinear systems represented by input-output models," *Automatic Control*, vol. 41, pp. 177–188, 1996.

[83] B. M. Mirkin and P. O. Gutman, "Decentralized output-feedback mrac of linear state delay systems," *Automatic Control*, vol. 48, pp. 1613–1619, 2003.

[84] M. Bodson and J. E. Groszkiewicz, "Multivariable adaptive algorithms for reconfigurable flight control," *Control Systems Technology*, vol. 5, pp. 217–229, 1997.

[85] J. Yan, J. B. Hoagg, R. E. Hindman, and D. S. Bernstein, "Longitudinal Aircraft Dynamics and the Instantaneous Acceleration Center of Rotation: The Case of the Vanishing Zeros," *IEEE Contr. Sys. Mag.*, vol. 30, pp. 68–92, 2011.

[86] E. H. Maslen, "Positive real zeros in flexible beams," *Shock and Vibration Digest*, vol. 2, pp. 429–435, 1995.

[87] D. K. Miu, *Mechatronics: Electromechanics and Contromechanics.* New York: Springer Verlag, 1993.

[88] A. V. Morozov, J. B. Hoagg, and D. S. Bernstein, "Retrospective adaptive control of a planar multilink arm with nonminimum-phase zeros," in *Proc. Conf. Dec. Contr.*, Atlanta, GA, December 2010, pp. 3706–3711.

[89] J. B. Hoagg and D. Bernstein, "Retrospective Cost Model Reference Adaptive Control for Nonminimum-Phase Systems," *AIAA J. Guid. Contr. Dyn.*, vol. 35, pp. 1767–1786, 2012.

[90] A. Morozov, A. M. D'Amato, J. B. Hoagg, and D. S. Bernstein, "Retrospective cost adaptive control for nonminimum-phase systems with uncertain nonminimum-phase zeros using convex optimization," in *Proc. Amer. Contr. Conf.*, San Francisco, CA, June 2011, pp. 1188–1193.

[91] M. A. Bolender and D. B. Doman, "Flight path angle dynamics of airbreathing hypersonic vehicles," in *Proc. AIAA Guid. Nav. Contr. Conf.*, Keystone, CO, August 2006, aIAA-2006-6692.

[92] B. Xu, D. Wang, F. Sun, and Z. Shi, "Direct neural control of hypersonic flight vehicles with prediction model in discrete time," *Neurocomputing*, vol. 115, pp. 39–48, 2013.

[93] Q. Wei and X. Huang, "Lateral stability analysis of hypersonic vehicle under pressure fluctuation by solving mathieu differential equation," *arXiv*, p. arXiv:1204.2490, 2012.

[94] M. Kamrunnahar, B. Huang, and D. B. Fisher, "Estimation of Markov Parameters and Time-delay/Interactor Matrix," *Chemical Engineering Science*, vol. 55, pp. 3353–3363, 1999.

[95] M. S. Fledderjohn, M. S. Holzel, H. Palanthandalam-Madapusi, R. J. Fuentes, and D. S. Bernstein, "A Comparison of Least Squares Algorithms for Estimating Markov Parameters," in *Proc. Amer. Contr. Conf.*, Baltimore, MD, June 2010, pp. 3735–3740.

[96] J. N. Juang, *Applied System Identification*. Upper Saddle River, NJ: Prentice Hall, 1993.

[97] M. Vidyasagar, *Control System Synthesis: A Factorization Approach*. MIT Press, 1985.

[98] M. M. Seron, J. H. Braslavsky, and G. C. Goodwin, *Fundamental Limitations in Filtering and Control*. Springer, 1997.

[99] B. D. O. Anderson and A. Dehghani, "Challenges of Adaptive Control–Past, Permanent and Future," *Ann. Rev. in Contr.*, vol. 32, pp. 123–135, 2008.

[100] D. G. MacMartin and J. P. How, "Implementation and Prevention of Unstable Optimal Compensators," in *Proc. Amer. Contr. Conf.*, Baltimore, MD, June 1994, pp. 2190–2195.

[101] P. Dorato, *Analytic Feedback System Design: An Interpolation Approach*. Brooks/Cole, 1999.

[102] Y. Halevi, "Stable LQG Controllers," *IEEE Trans. Autom. Control*, vol. 39, no. 10, pp. 2104–2106, 1994.

[103] C. Ganesh and J. B. Pearson, "H_2-Optimization with Stable Controllers," *Automatica*, vol. 25, no. 4, pp. 629–634, 1989.

[104] D. U. Campos-Delgado and K. Zhou, "H_∞ Strong Stabilization," *IEEE Trans. Autom. Control*, vol. 46, no. 12, pp. 1968–1972, 2001.

[105] A. A. Saif, D. Gu, and I. Postlethwaite, "Strong Stabilization of MIMO Systems via H_∞ Optimization," *Systems & Control Letters*, vol. 32, no. 2, pp. 111–120, 1997.

[106] S. Formentin and A. Karimi, "Direct Data-Driven Design of Sparse Controllers," in *Proc. Amer. Contr. Conf.*, Washington, DC, June 2013, pp. 3099–3104.

[107] H. Kwakernaak and R. Sivan, *Linear Optimal Control Systems*. John Wiley & Sons, 1972.

[108] G. E. Dullerud and F. Paganini, *A Course in Robust Control Theory: A Convex Approach*. Springer, 2000.

[109] B. D. O. Anderson and J. B. Moore, *Optimal Control: Linear Quadratic Methods*. Prentice Hall, 1990.

[110] F. M. Brasch Jr and J. B. Pearson, "Pole placement using dynamic compensators," *IEEE Trans. Autom. Contr.*, vol. 15, no. 1, pp. 34–43, 1970.

[111] D. S. Bernstein, *Matrix Mathematics*, 2nd ed. Princeton, 2009.

[112] G. C. Goodwin, S. F. Graebe, and M. E. Salgado, *Control System Design*. Prentice Hall, 2001.

[113] C. Chen, *Linear System Theory and Design*. Oxford, 1999.

[114] H. Moradkhani, S. Sorooshian, H. V. Gupta, and P. R. Houser, "Dual state-parameter estimation of hydrological models using ensemble kalman filter," *Advances in Water Resources*, vol. 28, pp. 135–147, 2005.

[115] R. V. D. Merwe and E. A. Wan, "The square-root unscented kalman filter for state and parameter-estimation," in *Acoustics, Speech, and Signal Processing*, Beaverton, OR, May 2001, pp. 3461–3464.

[116] T. Lefebvre, H. Bruyninckx, and J. D. Schutter, "Kalman filters for non-linear systems: a comparison of performance," *International Journal of Control*, vol. 77, no. 7, 2004.

[117] L. Ljung, "Asymptotic behavior of the extended kalman filter as a parameter estimator for linear systems," *IEEE Trans. Autom. Control*, vol. 24, pp. 36–50, 1979.

[118] J. W. Grizzle and Y. Song, "The extended kalman filter as a local asymptotic observer for nonlinear discrete-time systems," *Journal of Mathematical Systems, Estimation and Control*, vol. 5, pp. 59–78, 1995.

[119] J. L. Anderson, "An ensemble adjustment kalman filter for data assimilation," *Monthly Weather Review*, vol. 129, pp. 2884–2903, 2001.

[120] G. Evensen, "Sequential data assimilation with a nonlinear quasi-geostrophic model using monte carlo methods to forecast error statistics," *Journal of Geophysical Research*, vol. 99, pp. 10 143–10 162, 1994.

[121] D. Crisan and A. Doucet, "A survey of convergence results on particle filtering methods for practitioners," *IEEE Transactions on Signal Processing*, vol. 50, pp. 736–746, 2002.

[122] S. J. Julier and J. K. Uhlmann, "Unscented filtering and nonlinear estimation," *Proceedings of the IEEE*, vol. 92, pp. 401–422, 2004.

[123] S. Thrun, W. Burgard, and D. Fox, *Probabilistic Robotics*. MIT Press, 2005.

[124] H. W. Sorenson and D. L. Alspach, "Recursive bayesian estimation using gaussian sums," *Automatica*, vol. 7, pp. 465–479, 1971.

[125] U. D. Hanebeck, K. Briechle, and A. Rauh, "Progressive bayes: A new framework for nonlinear state estimation," *Proceedings of SPIE*, vol. 5099, pp. 256–267, 2003.

[126] M. Kumar, P. Singla, S. Chakravorty, and J. Junkins, "The partition of unity finite element approach to the stationary fokker-planck equation," in *AIAA/AAS Astrodynamics Specialist Conference and Exhibit*, Keystone, CO, August 2006, aIAA-2006-6285.

[127] C. V. Rao, J. Rawlings, and D. Q. Mayne, "Constrained state estimation for nonlinear discrete-time systems: Stability and moving horizon approximations," *IEEE Transactions on Automatic Control*, vol. 48, pp. 246–258, 2003.

[128] A. M. D'Amato, J. Springmann, A. A. Ali, J. W. Cutler, A. J. Ridley, and D. S. Bernstein, "Adaptive state estimation for nonminimum-phase systems with uncertain harmonic inputs," Portland, OR, August 2011, aIAA-2011-6315.

[129] K. Agarwal, A. A. Ali, A. M. D'Amato, A. J. Ridley, and D. S. Bernstein, "Retrospective-cost-based adaptive state estimation and input reconstruction for the global ionosphere-thermosphere model," Minneapolis, MN, August 2012, aIAA-2012-4601-996.

[130] S. J. Julier, "The scaled unscented transformation," Anchorage, May 2002, pp. 4555–4559.

[131] D. S. Bernstein, *Matrix Mathematics*, 2nd ed. Princeton, 2009.

[132] J. Tokarzewski, *Finite Zeros in Discrete Time Control Systems*. Springer, 2006.

[133] A. I. G. Vardulakis, *Linear Multivariable Control: Algebraic Analysis and Synthesis Methods*. Wiley, 1991.

[134] S. Sastry and M. Bodson, *Adaptive Control: Stability, Convergence, and Robustness*. Prentice Hall, 1989.

[135] K. Narendra and A. Annaswamy, *Stable Adaptive Systems*. Prentice Hall, 1989.

[136] E. Mosca, *Optimal, Predictive, and Adaptive Control*. Prentice Hall, 1995.

[137] M. Sanchez and J. Manuel, *Adaptive Predictive Control: From the Concepts to Plant Optimization*. Prentice Hall, 1996.

[138] K. J. Astrom and P. R. Kumar, "Control: A Perspective," *Automatica*, vol. 50, no. 1, pp. 3–43, 2014.

[139] N. M. Filatov and H. Unbehauen, *Adaptive Dual Control: Theory and Applications*. Springer, 2004.

[140] A. A. Feldbaum, "Dual Control Theory, Parts I and II," *Autom. Rem. Contr.*, vol. 21, pp. 874–880,1033–1039, 1961.